THEORETICAL STUDIES ON MOLECULAR ADSORPTION AND SELECTIVE HYDROGENATION CATALYSTS

Crisa Vargas Fuentes

THEORETICAL STUDIES ON MOLECULAR ADSORPTION AND SELECTIVE HYDROGENATION CATALYSTS

DOCTORAL THESIS

Crisa Vargas Fuentes

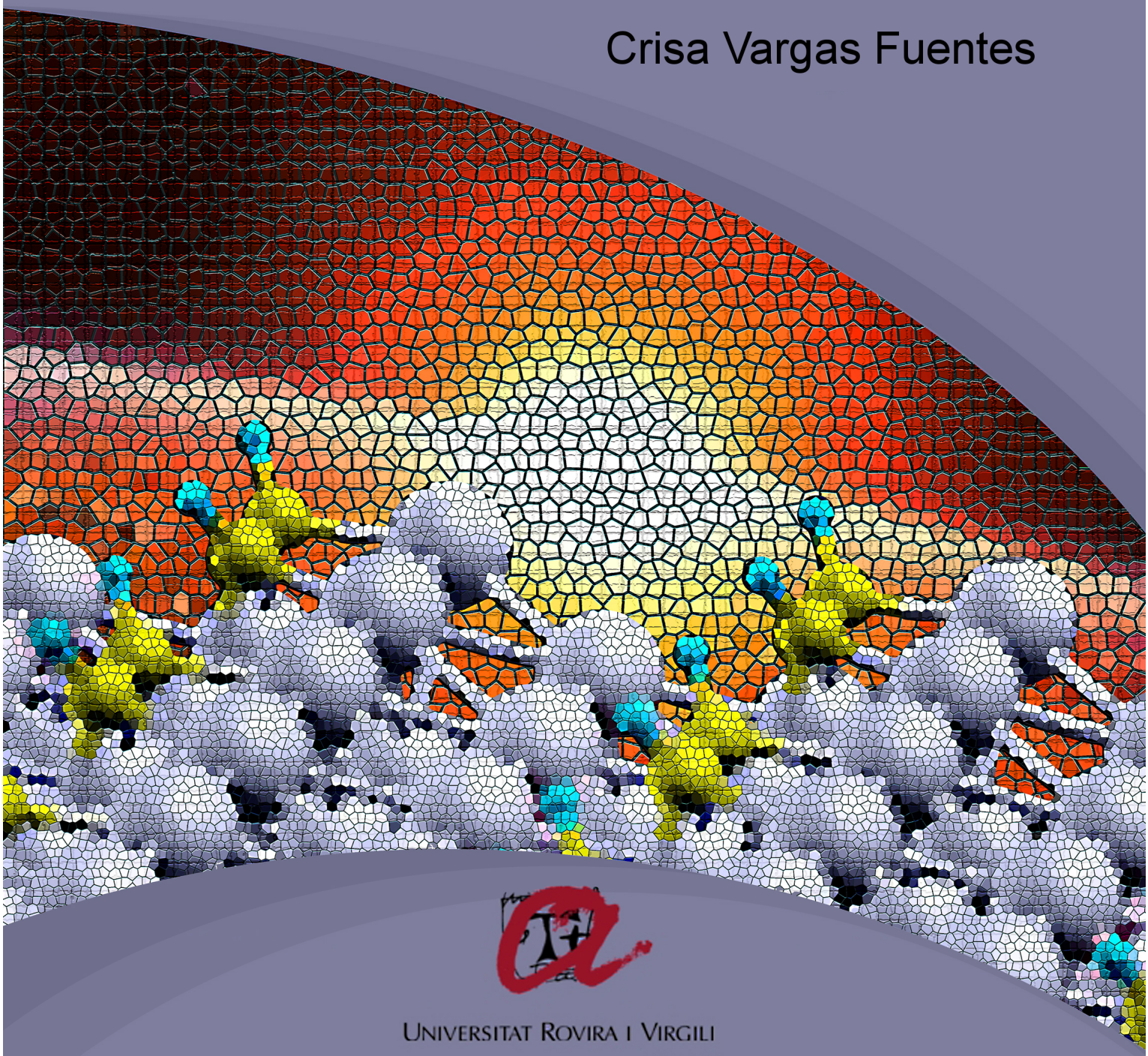

UNIVERSITAT ROVIRA I VIRGILI

2013

UNIVERSITAT ROVIRA I VIRGILI
THEORETICAL STUDIES ON MOLECULAR ADSORPTION AND SELECTIVE HYDROGENATION CATALYSTS
Crisa Vargas Fuentes

UNIVERSITAT ROVIRA I VIRGILI
THEORETICAL STUDIES ON MOLECULAR ADSORPTION AND SELECTIVE HYDROGENATION CATALYSTS
Crisa Vargas Fuentes

Crisa Vargas Fuentes

THEORETICAL STUDIES ON MOLECULAR ADSORPTION AND SELECTIVE HYDROGENATION CATALYSTS

DOCTORAL THESIS

Supervised by Dr. Núria López Alonso

Departament de Química Física i Inorgànica

UNIVERSITAT ROVIRA I VIRGILI

TARRAGONA
2013

UNIVERSITAT ROVIRA I VIRGILI
THEORETICAL STUDIES ON MOLECULAR ADSORPTION AND SELECTIVE HYDROGENATION CATALYSTS
Crisa Vargas Fuentes

Institut Català d'Investigació Química
Avgda. Països Catalans, 16
43007 Tarragona (Spain)

NÚRIA LÓPEZ ALONSO, group leader at the Institute of Chemical Research of Catalonia, associate professor of Physical Chemistry at the Rovira i Virgili University and research supervisor for Crisa Vargas Fuentes,

I hereby CERTIFY by signing below that the research and writing embodied in the present thesis entitled "Molecular Adsorption And Selective Hydrogenation Reactions from a Theoretical Point of View" have been carried out at the Institute of Chemical Research of Catalonia and that it fulfils all the necessary requirements.

Tarragona, 25th September 2013

Dr. Núria López

UNIVERSITAT ROVIRA I VIRGILI
THEORETICAL STUDIES ON MOLECULAR ADSORPTION AND SELECTIVE HYDROGENATION CATALYSTS
Crisa Vargas Fuentes

Acknowledgments

Tengo mucho que agradecer a la Dra. Núria López, la directora de mi tesis, ya que sin sus enseñanzas nada de esto habría sido posible. Tampoco lo hubiera sido sin el apoyo económico y logístico del Institut Català d'Investigació Química y el Ministerio de Economía y Competitividad, así como los proyectos asociados a él, CTQ2009-07553/BQU y CTQ2012-33826.

Me gustaría agradecer de una forma muy especial la enorme ayuda que me ha proporcionado en multitud de aspectos, tanto laborales como personales, una de las personas más maravillosas con las que me he topado a lo largo de mi vida, Núria Vendrell. No cambies nunca.

No pueden faltar en estas líneas nombres como Maria Besora, Gerard, Neyvis, Pere, Carles, Feliu, Martín, Rodrigo, Jesús, Chunhui Liu, Torstein, Fernando, Luca, David y, muy especialmente, mi amiga Mónica, por todos los buenos consejos y enseñanzas que he recibido de ellos. Gracias a todos los compañeros que han pasado por el laboratorio teórico y el ICIQ entero durante estos cuatro años, tanto en el área de la investigación, como en admistración, limpieza, mantenimiento y catering. Siguiendo con el ICIQ, he de decir que es fácil empezar la jornada con ganas cada día cuando tienes a una amiga esperándote en recepción con una sonrisa y siempre algo interesante que comentar. Te echaré de menos, María.

Tengo que quitarme el sombrero ante personas, ahora indispensables en mi vida, que me han dado ánimos cuando más lo necesitaba y que me han mostrado cómo ver cada acontecimiento desde perspectivas diferentes. Gracias, Oier, Richard, Adrià y Luís; y por hacer de mi estancia en Tarragona una experiencia inolvidable y potenciar mi crecimiento como persona a muchos niveles, he de agradecer a mis amigos: Maribel, Mari, Almu, Lucía, Anna, Carmen, Jose, Miguel, Jessi, Montse Fibla, Agus, Montse Cerrato, Lluís, Papabet, Ricard y

su estupenda familia, Vicky, Vero, Ramón, Zeus, Jordi, Judit, Fer, Loli, Fran, Janine, Silvia, Kurt y los boys, Mamen, Colibrí, Èlia, Pepe, Lau, Ángel y en algn momento hay que parar, pero de verdad que muchas gracias a todos por estar ahí. Me encanta Tarragona y su gente.

Estos últimos meses deberían haber sido realmente estresantes, pero la verdad es que no ha sido así gracias a tí. Tu apoyo, buen humor, cariño, imaginación, entusiasmo y amor me hacen muy feliz. Gracias por estar a mi lado, Salva.

A los que va dedicada esta tesis, mi familia: Dani, Laura, Silvia, Rafa, Sonia, papá y mamá por su apoyo incondicional y su amor infinito. Todo lo que soy es gracias a vosotros. Os quiero con locura.

Por ayudarme en lo que, sin duda ha sido la etapa más dura de estos cuatro años, muchas gracias por no dejarme sola en aquellos momentos, Marta Santiago, eres una persona excepcional y te mereces todo lo mejor. Finalmente, quisiera dedicar unas palabras de despedida a mi compañero en la primera etapa de esta tesis, una persona excepcional y un gran amigo al que tengo mucho que agradecer. Gracias por enseñarme con tanta paciencia cuando no sabía nada, por tus truquitos y teorías para aprender más rápido. Gracias por tus recomendaciones nutricionales y culinarias. Por tus montones y montones de correos electrónicos de tertulias, ideas y puestas al día. Gracias por acogerme en Zúrich, por recogerme en el aeropuerto, por ofrecerme tu casa. Por conseguirme una bici, por presentarme a tus amigos. Por prepararme la cena cada día, por dejarme bombones en el buzón. Gracias por esa cita dominguera para contarme el fin de semana en la montaña con un cafelito, aunque nunca pudieras acudir a ella. Me alegro mucho de haberte conocido. Muchas gracias por todo.

Gracias a todos.

El trabajo desarrollado en esta tesis doctoral ha sido posible gracias a la financiación del Institut Català d'Investigació Química (ICIQ) y del Ministerio de Economía y Competitividad (MEC), y se ha desarrollado en el marco del proyecto CTQ2009-07553 asociado a la beca FPI BES-2010-039809.

UNIVERSITAT ROVIRA I VIRGILI
THEORETICAL STUDIES ON MOLECULAR ADSORPTION AND SELECTIVE HYDROGENATION CATALYSTS
Crisa Vargas Fuentes

A mis padres y a mis hermanos,

Los ordenadores son inútiles.
Sólo pueden darte respuestas

Pablo Picasso, Andalucian artist

UNIVERSITAT ROVIRA I VIRGILI
THEORETICAL STUDIES ON MOLECULAR ADSORPTION AND SELECTIVE HYDROGENATION CATALYSTS
Crisa Vargas Fuentes

Contents

UNIVERSITAT ROVIRA I VIRGILI
THEORETICAL STUDIES ON MOLECULAR ADSORPTION AND SELECTIVE HYDROGENATION CATALYSTS
Crisa Vargas Fuentes

Part I

Introduction

UNIVERSITAT ROVIRA I VIRGILI
THEORETICAL STUDIES ON MOLECULAR ADSORPTION AND SELECTIVE HYDROGENATION CATALYSTS
Crisa Vargas Fuentes

Chapter 1

Chemical framework

1.1 Catalysis

Catalysis is a chemical phenomenum through which a compound that is not a reactant makes the reaction go faster. Sometimes, the speed reached can be several orders of magnitude larger than the one without the catalyst. This becomes enormously significant when refers, for example, to processes that are essencial for life, since without the organic catalysts or enzymes the amount of time needed for carrying out basic metabolic reactions would be so long that life could not be possible. But catalytic materials can also be man made. In that case, they can accelerate reactions that are suitable to transform raw materials found in nature to others that can be intensively used by human kind to improve their life standards.

As can be seen in Figure 1.1, a catalyst reaches its target by binding the reacting molecules and by allowing them to react to products. The new molecules move away from the catalyst, forcing it to recover its original shape and to be ready to bind other reacting molecules. This periodic performance is known as the catalytic cycle.

We can understand easily why this acceleration happens looking at the energy diagram also in Figure 1.1. The comparison between the uncatalysed and catalysed process shows that the energy requirements to carry out the catalytic reaction is much lower than that needed to perform the non-catalytic reaction. Although the catalytic path is obviously more complex, it is also energetically much more favourable.

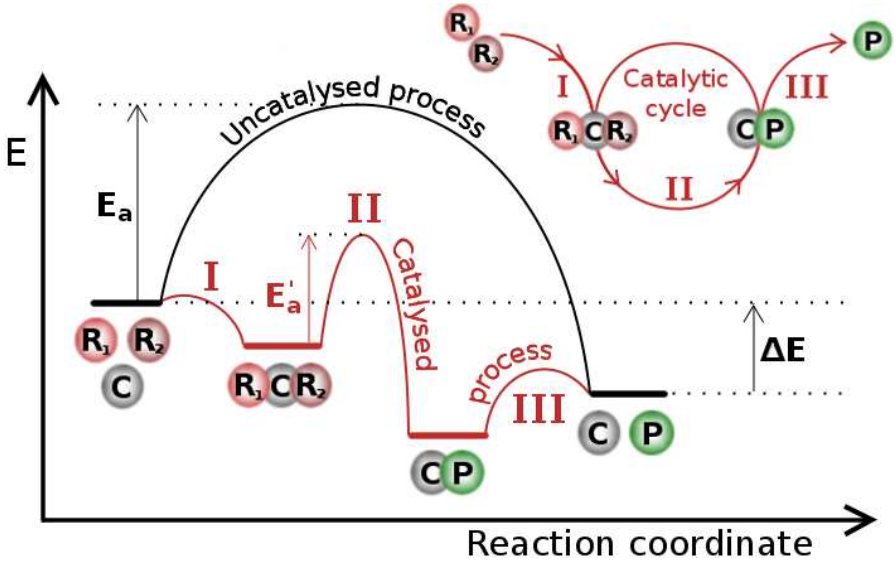

Figure 1.1: The catalytic cycle is basically divided in three steps. I: reactant molecules, R_1 and R_2, bind to the catalyst, C, II: reaction, and III: separation between the catalyst and the product, P. In the energy diagram of the uncatalysed and the catalysed processes, the activation barrier of the latter is much lower than that of the former, $E'_a < E_a$.

For the uncatalysed process, the figure is simply a way to visualize the reaction: it proceeds when the reactants, R_1 and R_2, collide with sufficient energy to overcome the activation barrier, E_{a}. The change in energy between the reactants and the product, P, is ΔE. The catalysed process starts by bonding of the reactants to the catalyst, C, in a spontaneous reaction. There then follows the reaction between R_1 and R_2 while they are still bound to the catalyst. This step is associated with an activation energy, E'_a; however, it is significantly lower than that for the uncatalysed reaction. Finally, the product separates from the catalyst. It's advisable to notice that the change in the formation energy for the catalytic reaction equals that of the uncatalysed reaction. Hence, the catalyst does not affect the equilibrium constant for the overall reaction of $R_1 + R_2$ to P. Thus, if a reaction is thermodynamically unfavourable, a catalyst cannot change this situation. A catalyst changes the kinetics but not the thermodynamics.

Catalysis is involved in multiple manufacturing processes including the production of fertilizers for agriculture, fuels for transport and fine chemicals for pharmaceutical purpouses. The largest fraction of catalysis is performed in different phases, then catalysts are called heterogeneous catalysis. By far, they constitute the major part of the catalytic materials employed in industry and the study of some of their properties will constitute most of the present work.

1.2 Properties and structures of the transition metals

The 38 elements in groups 3 through 12 of the periodic system are called transition metals. As with all metals, the transition elements are both ductile and malleable, and conduct electricity and heat. The interesting thing about transition metals is that their valence electrons are present in more than one shell. This is the reason why they often exhibit several common oxidation states. The general reactivity and electropositivity of these metals increases down the group. Most of them tarnish in air and burn to give the oxides relative quite easlily. They react with halogens at room temperature and with most non-metals on warming. They reduce water with evolution of hydrogen, particularly if finely divided or heated, and all dissolve in dilute acid. Strong acids produce soluble salts whereas weak acids produce sparingly soluble or insoluble salts.

The most important metals for catalysis are those of the groups 8-11 of the periodic system. Three crystal structures are important in these cases, hexagonally close-packed (*hcp*: Co, Ru, Os), face-centered cubic (*fcc*: Ni, Cu, Rh, Pd, Ag, Ir, Pt, Au) and body-centered cubic (*bcc*: Fe). See Figure 1.2. The unit cells contain 6, 4 and 2 atoms for the *hcp*, *fcc* and *bcc* structures, respectively. If the lattices are viewed as close-packed spheres, the *fcc* lattice has the highest density, showing about 26% empty space, and it is also the more stable structure of all the metals that will be studied in the present work. Each atom in the bulk has 12 nearest neighbours, or in other words, any atom has a coordination number of 12. Before discussing the surfaces that the metals expose, a few useful details concerning crystallography will be mentioned.

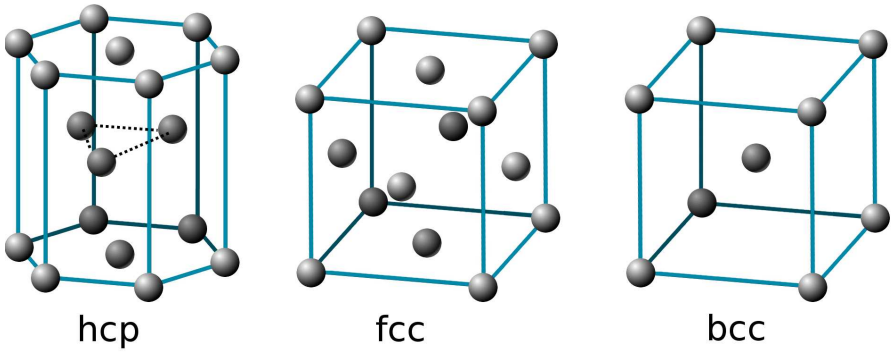

Figure 1.2: Unit cells of the face-centered cubic (*fcc*), body-centered cubic (*bcc*), and hexagonally closed packed (*hcp*) lattices.

1.2.1 Crystallography

The structure and geometry of a surface play a dominant role with respect to its reactivity in adsorption and catalysis. It is therefore always necessary to specify which structure we are dealing with and, hence, it is important to have a notation that describes the various surfaces in a unique manner. Surface crystallography is simply the two-dimensional analogue of bulk crystallography, in which we consider the structure of the different planes where the atoms in the three-dimensional crystal reside. A crystal surface is described by a vector normal to it, given by $\overrightarrow{v} = (v_x, v_y, v_z) = (hkl)$. The surface is then indicated by the set h, k, and l between parentheses (hkl), often in combination with the metals, such as in Cu(100) or Pt(111). For a (100) surface, the atoms reside in a plane parallel to the y-z-plane. [1]

The three basal planes of cubic crystals are (100), (110) and (111). The respective cross sections are shown in Figure 1.3. The positions of the surface atoms that appear by applying these cuts on the *fcc* unit cells are shown in Figure 1.4. An important parameter for surface reactivity is the density of atoms in the surface. The general rule of thumb is that the more open the surface, the more reactive it is. Note that (110) is the most open basal plane of an *fcc* crystal, whereas (111) exhibits the closest packing. For bcc crystals the order is the opposite, *i.e.*, (111) is the most open and (110) the most dense.

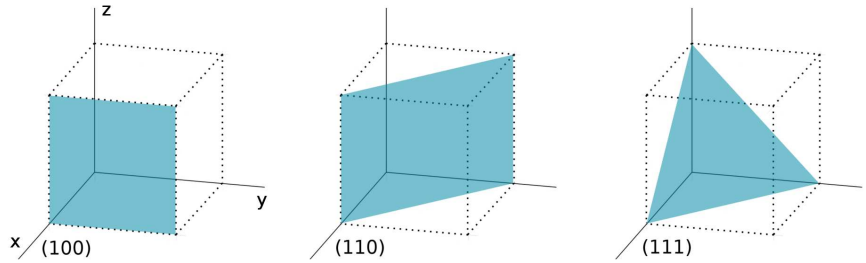

Figure 1.3: Basal planes formed by cutting the unit cells of simple crystal structures.

The reactivity of a surface depends on the number of unsaturated bonds. An unsaturated bond being what is left from a former bond with a neighbouring metal atom that had to be broken to create the surface. Thus we need to know the number of missing neighbours of an atom in each surface plane. One can infer from Figure 1.4 that an atom in the *fcc* (111) surface has 6 neighbours in the surface and three below, but in the surface it misses the three neighbours above that were presented in the bulk coordination. An atom in the *fcc* (100) surface, on the other hand, has four neighbours in the surface, four below, and misses four above the surface. Hence, an atom in the *fcc* (100) surface has one more unsaturated bond than an atom in the *fcc* (111) surface and is, therefore, slightly more prone to bind other compounds. Using the same reasoning, it is obvious that atoms at monoatomic steps are much more reactive than the atoms in the terraces. In fact, it is known that such sites may enhance the reactivity by many orders of magnitude. [2]

1.2.2 Wulff construction

At the end of 19^{th} century, Gibbs [3] proposed that a droplet of crystal will arrange itself such that its Gibbs free energy is minimized by assuming a configuration of low Surface energy. He defined the quantity

$$\triangle G_i = \sum_j \gamma_j O_j$$

where γ_j repersents the surface free energy per unit area of the j^{th} crystal face or surface free energy density, and O_j is the area of said face. $\triangle G_i$ represents the difference in energy between a real crystal composed of i molecules with a surface, and a similar configuration

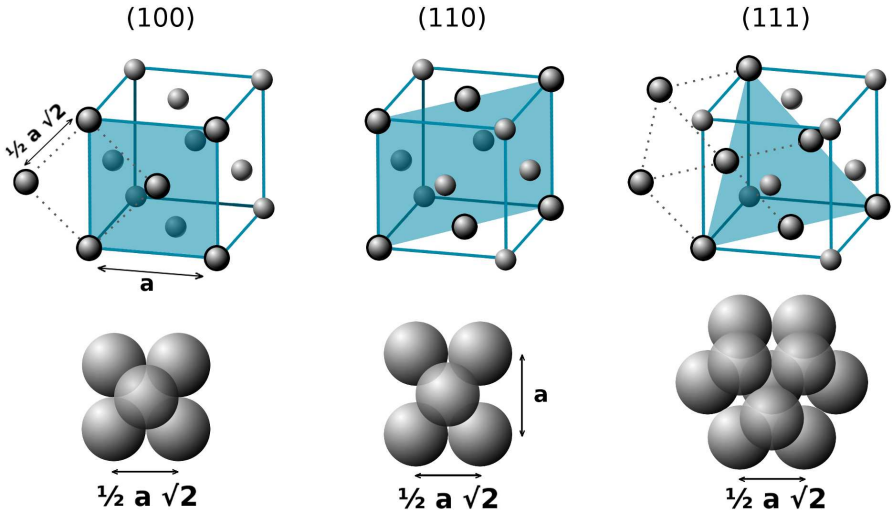

Figure 1.4: Some crystallographic surfaces of the *fcc* lattice. In each structure, the spheres surrounded by black circumferences are coplanar. The transparent spheres indicate atoms in the second layer. Interatomic distances are given in terms of the lattice constant a.

of i molecules located inside an infinitely large crystal. This quantity is therefore the energy associated with the surface. The equilibrium shape of the crystal will then be that which minimizes the value of $\triangle G_i$.

The Wulff construction [4] is a well-known method of calculating the shape that minimizes the total surface free energy of a fixed volume of a material in a particular environment, and can be an important contributor in determining the physical properties of a material. [5] It was formulated without proving at the beginning of the past century as follows: *"for an equilibrium crystal there is a point in the interior such that its perpendicular distance h_i from the i^{th} face is proportional to the surface energy, γ_j"*. Finally, more than half a century later, Herring [6, 7] gave a proof of the theorem and a method for determining the equilibrium shape of a crystal, which consists of two main exercises. To begin, the surface energy for each surface is plotted in a polar graph, as can be seen in the right part of Figure 1.5. This is known as the γ-plot and is usually denoted as $\gamma(hkl)$, given as a scalar function of the interfacial orientation or surface normal, (hkl). The second part is the Wulff construction itself, in which the gamma plot is used to determine graphically

which crystal faces will be present, that are known to be the ones with the lowest surface energies. When $\gamma(hkl)$ is very anisotropic, the Wulff shape can exhibit a faceted morphology composed only of planes, edges and corners. As mentionated before, the construction relies on Wulff's assumption that the distance from the surface of a specific plane to the center of the crystallite is proportional to the surface energy. Thus, if we have a surface plane of small surface energy, its distance from the center of the crystallite will be small and this plane will then cut of all others and dominate the polyhedron. It can be determined graphically by drawing lines from the origin to every point on the γ-plot. For every orientation, (hkl), where it intersects γ-plot a plane is defined that is perpendicular to (hkl) and located a distance γ_{hkl} from the origin. The inner envelope of these planes forms the equilibrium shape of the crystal, that is given by the Wulff construction and can be seen in Figure 1.5.

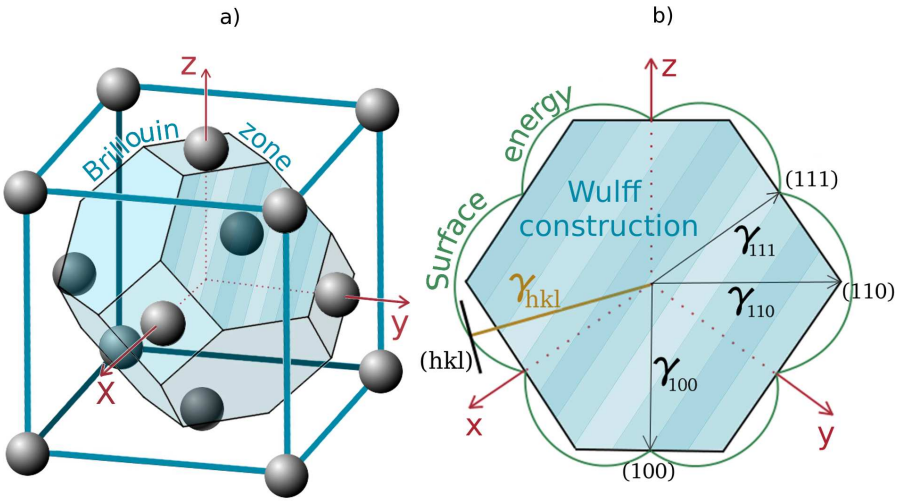

Figure 1.5: a) Brillouin zone of a *fcc* structure. b) Wulff construction of a two-dimensional *fcc* crystal where the surface energy in polar coordinates or γ-plot has the following order $\gamma_{111} < \gamma_{100} < \gamma_{110}$. γ_{hkl} is a generic surface free energy density radial vector and (hkl) its respective normal Wulff plane. As such plane does not fit inside the γ-plot, it does not become part of the Wulff construction.

For metals, close-packed surfaces such as the (111) and (100) facets have, in general, the smallest surface free energy and therefore these surfaces dominate on small particles. However, in supported catalysts particles are not free, as they would immediately minimize their free energy by merging to form large agglomerates. The oxide support hinders this process. The shape of the particle is to some extend also determined by the energy associated with the interface between the metal particle and the oxide surface, leading to an extra parameter that can control the wetting phenomena. [8] In Figure 1.6, two atomic-resolution images of a crystalline nanosize Pd cluster supported on Al_2O_3 can be seen. The atomic arrangement of the top layer facet is seen to be that of a (111) layer. [9] Furthermore, a crystal typically grows in a non-equilibrium situation and its final shape is influenced by many factors contributing to the kinetics of growth. It is actually not easy to bring a crystal into equilibrium. Therefore, the Wulff construction is a very useful tool as a starting point in the study of the equilibrium shape of crystals, but the experimental conditions have to be also taken into account as the geometry of the final structure will be a function of the nature of the crystal and its surroundings.

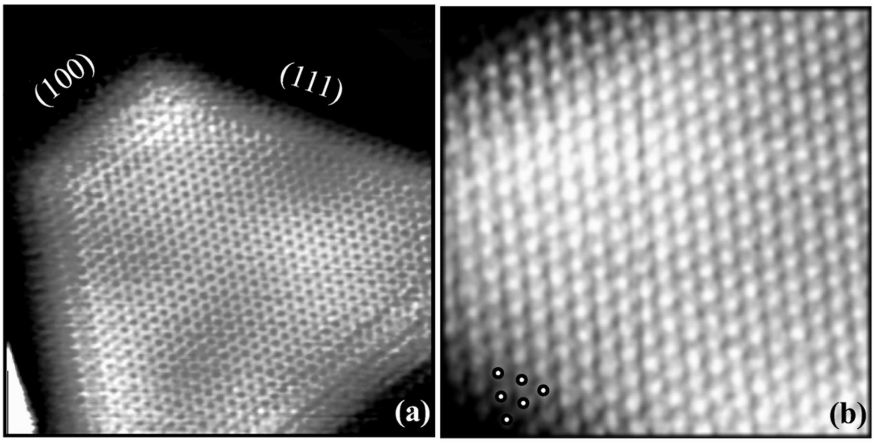

Figure 1.6: Atomic-resolution images of crystalline nanosize Pd clusters. (a) $95 \times 95\text{Å}^2$. (b) $45 \times 45\text{Å}^2$. The resolution is kept a few layers down the sides, allowing identification of the side facets. The dots indicate atomic positions consistent with a (111) facet. [9]

Table 1.1: Comparison between the two regimes of adsorption on surfaces

Regime for bond	BE	Force
Chemisorption	$> 100\ kJ/mol$	- Covalent - Ionic
Physisorption	$< 100\ kJ/mol$	- Polarization - vdW

1.3 Theory of adsorption

1.3.1 Chemisorption and physisorption

When an atom or molecule approaches a reactive surface it feels the potential energy set up by the atoms in the solid. The study of the adsorption of organic molecules on metal surfaces is crucial to understand the chemical and physical properties that control their potential applications in catalysis and nanotechnology. [1] Text books split adsorption into two regions: the long-distance behaviour, where physisorption is responsible for the bond, and a short-distance one where chemical bonds are possible and that implies a large rearrangement of the electron distribution and even geometric rearrangements, [10, 11] as explained in Figure 1.7 and Table 1.1. The physisorption is a weak interaction, a chemical bond is not formed, then the bond energy is less than 100 kJ/mol, and the interaction is due to polarization or van der Waals forces. This problem has not been well treated in the DFT functionals so far, although promising extensions are being developed. [12] When molecules or atoms form a chemical bond with the surface upon adsorption we call this chemisorption and the bond is correctly reproduced by DFT.

1.3.2 Dispersion forces

Importance of van der Waals contribution to molecular adsorption

van der Waals forces are a kind of physisorption that take place between non-polar molecules, where the formation of instantaneous dipoles are possible. Despite these so called dispersion or London forces are much weaker than the ones due to chemisorption mentioned in the previous Section (1.3.1), the sum of a large amount of these contributions sometimes may be the difference between a non-reacting material and a successful catalyst.

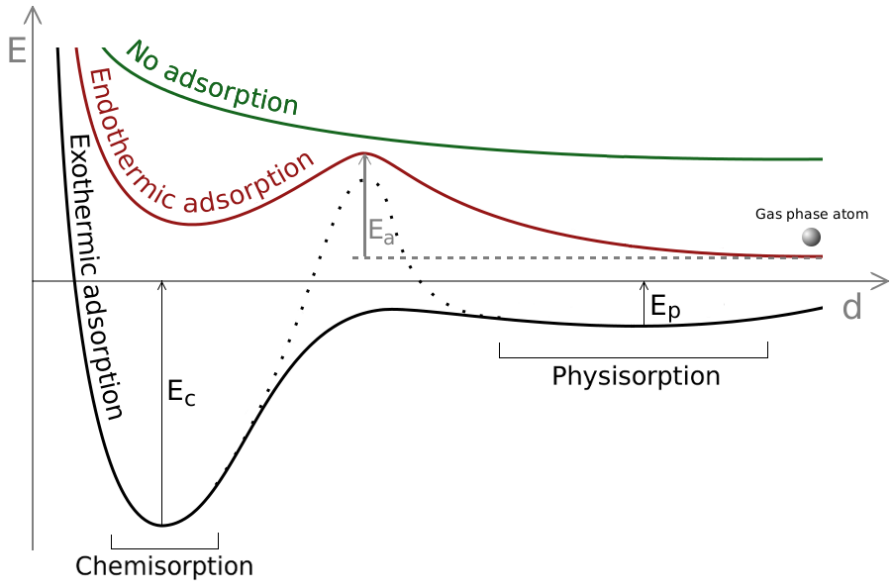

Figure 1.7: Difference between physisorption and chemisorption. While the former is a weak interaction and make long range bonding, the latter is a strong interaction and makes short range bonding, involving orbital overlap and possibly change transfer. E_c and E_p are the corresponding energies for the chemisorbed and physisorbed states. E_a is the activation energy. The black line: exothermic adsorption, red line: endothermic adsorption and green line: no adsorption.

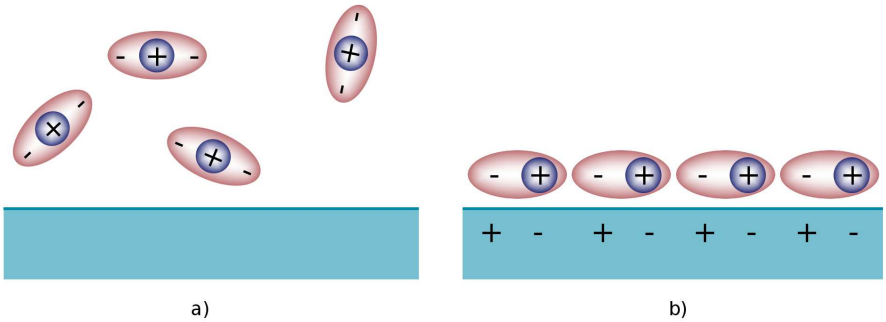

Figure 1.8: Schematic representation of molecules that do not feel attraction to the surface by themselves. a) No van der Waals interactions are taken place. b) van der Waals forces between them favour also the adsorption to the surface.

As a type of van der Waals interaction, the dispersion forces include electrostatic attraction between molecules or molecules and surfaces, thus they may be crucial in the study of heterogeneous reactions.

1.4 Surface reactivity

Gas-surface interactions and reactions on surfaces play a crucial role in many technologically important areas such as corrosion, adhesion, synthesis of new materials, electrochemistry and heterogeneous catalysis. [1] This section aims to describe the role of the catalyst and the interaction of gases with metal surfaces in terms of chemical bonding. Molecular orbital and band structure theory are the basic tools for this.

1.4.1 Heterogeneous Catalysis

Catalysts come in a multitude of forms, varying from atoms and molecules to large structures such as zeolites or enzymes. In addition, they may be employed in various surroundings: in liquids, gases or at the surface of solids. It is customary to distinguish the following three subdisciplines in catalysis: homogeneous, heterogeneous and bio-catalysis. The present work will be based on the second one. In heterogeneous catalysis, solids catalyze reactions of molecules in gas or solution. As solids -unless they are porous- are commonly impenetrable, catalytic reactions occur at the surface. To use the often expensive materials in an economical way, catalysts are usually nanometer-sized particles, supported on an inert, porous structure. [1]

The chemistry of surfaces and interfaces plays dominating roles in our lives. One of the challenges of modern physical chemistry is to understand macroscopic surface phenomena at the molecular level, as many of these phenomena might be used in innovative technologies relying on metal, semiconductor, and polymer surfaces to achieve controlled chemical bonding, adhesion, friction, electron and atom transport, solar energy conversion, and active selective catalysis. In the last two decades, theoretical simulation of surfaces, heterogeneous catalysis and the study of materials at molecular level have reached enough accuracy for these purposes. This together with the development of new computers has steered the field of theoretical simulation for the design of new and more efficient materials.

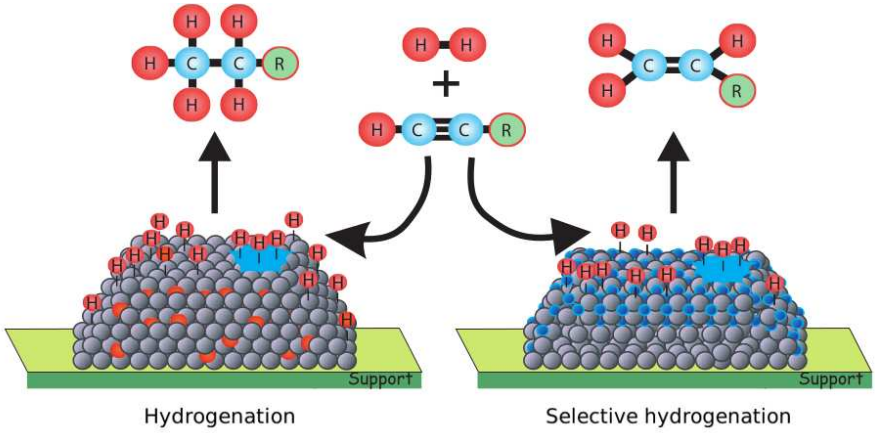

Figure 1.9: Figure based on Reference 13. Schematic representation of two catalysts operating in the selective and unselective alkyne hydrogenation regimes, respectively. [13]

1.4.2 Selective hydrogenation

The development of selective processes is the key for the research in the chemical industry in the twenty-first century. [14] Sharp reactions are a must to achieve eco-efficient alternatives to existing processes. A large fraction of reactions, in the production of bulk chemicals, fine chemicals, and pharmaceuticals, corresponds to selective hydrogenations. [15, 16] Hydrogenation reactions can involve a single unsaturated reactant that is the partially hydrogenated, multifunctionalized molecules, and/or complex mixtures presenting more than a single active species where onle one of the reactants or functional groups should be partially hydrogenated. Selectivity can be classified in three different terms: [1]

(1) Selectivity to a reaction.

(2) Selectivity to a reactant.

(3) Selectivity to a product.

For partial alkyne hydrogenations, for example, all these selectivities are required: namely stopping the hydrogenation process at the thermodynamically metastable alkene (product selectivity), eliminating the competition of different substrates for the catalyst (reactant selectivity), and blocking oligomerization reactions (reaction

selectivity). The adsorption and selective hydrogenation of alkynes versus that os alkenes have been considered as a model reaction and have been subject to several theoretical studies. [17]

1.4.3 Promoters and poisons: the role of the co-catalyst

Three aspects need to be taken into account as shown in Figure 1.10 when studying the reactivity of metallic surfaces in the field of heterogeneous catalysis: the active metal itself, the promoter or co-catalyst and the molecular modifier.

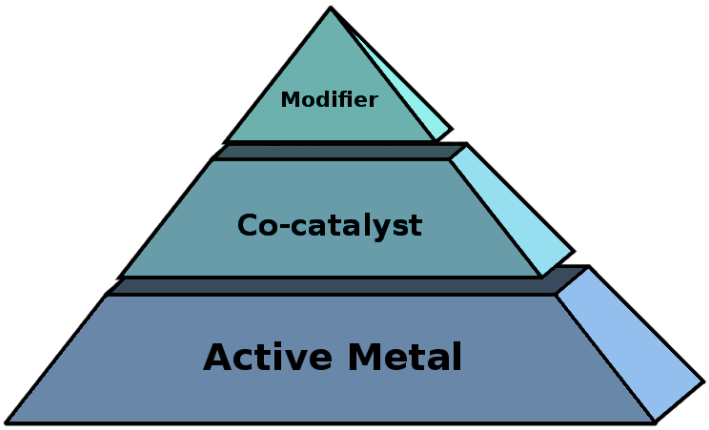

Figure 1.10: Schematic representation of the design strategy used in hydrogenation catalysts both for industrial and laboratory purposes. [18]

Although much has been done to investigate the nature and the properties of the unpromoted catalysts, little is known about the role of the co-catalysts. On most pure catalysts, all possible paths of a reaction may take place to a relevant extent. The role of the co-catalyst is then to reduce the amount of products obtained from those lateral paths and so let the desired path be unique: selectivity enhancement. The way this can be achieved has been traditionally discussed in two main terms:

- *Electronic or ligand effect,* due to the perturbations induced by the bonding of the promoter to the active species.
- *Geometric effect,* because of the dilution of the promoter in the surface and the avoidance of the reactant or any other of the species involved to adsorb en masse.

The study of selectivity represents the next frontier in heterogeneous catalysis. New materials with very specific properties are required to improve energy use and atom economy, two crucial elements to enhancing the sustainability of the industries. Selectivity represents a challenge from a theoretical point of view as the main reaction pathway and side reactions need to be considered and, in order to be truly representative, high accuracy for a large number of paths needs to be evaluated.

1.5 Descriptors

1.5.1 Scaling properties

Once all the data of a specific study are taken, a way to compare them and extract significant information is needed. In this point, descriptors become a powerful tool and, although scaling is a difficult issue for any analysis of chemical properties or molecular topology when disparate descriptors are involved, it can be solve defining a common scale to compare properties across the different data sets. [19]

One of the main aims of research in the field of heterogeneous catalysis is to find rules for the activity and selectivity of a given material that can act as a catalyst. Usually these rules are termed as structure-activity relationships and the final idea is to retrieve the activity (or selectivity) provided that the structure of the material is known. Therefore, these rules allow the design of new materials that can speed up the synthesis of new catalyst by avoiding the time and human resources consuming trial-and-error traditional way of preparing new catalytic materials.

Theoretical studies consitute an excellent way to address structure-activity relationships as systems are well defined and the accuracy obtained with the calculations is sufficient to represent the chemical phenomena. Calculations allow the systematic treatment of adsorption and reaction on different families of materials and thus proper parameters controlling them can be obtained. Such parameters are known as descriptors. Recently, several groups have started to investigate the activity of small molecules on model materials following this methodology. [21] These authors have determined for instance that the adsorption of AH_x fragments (A=O,S,N) linearly correlates with the adsorption energy of the central A atom. [21] The extension to larger molecules containing more than one non-hydrogen atom

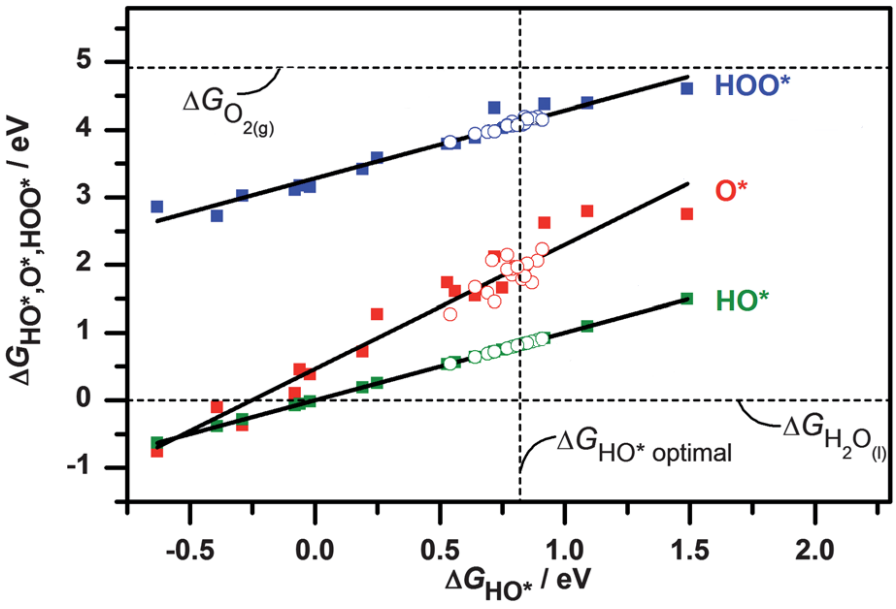

Figure 1.11: Plot of the computed free energies of adsorption for oxygen reduction reaction intermediates, OOH*, OH* and O* (denoted as $\triangle G_{OOH*}$, $\triangle G_{OH*}$ and $\triangle G_{O*}$, respectively), as a function of $\triangle G_{OH*}$, for (111), (100) and (211) pure metal surfaces (filled squares), as well as Pt overlayers on Pt-alloy surfaces (open circles). The plot illustrates that the adsorption energies scale linearly with each other providing the opportunity to use only a single descriptor to identify active surfaces towards the oxygen reduction. [20]

is necessary, but up to now only molecules containing two carbon atoms have been investigated, and still follow these correlations. [22] In the field of heterogeneous catalysis, the strategy to find a good descriptor is, first, exploring effects of (co)-adsorbed species on energy profile of our system, then identifying general trends and rules, and finally defining the new descriptor. In Figure 1.11 it can be seen that the adsorption energy of ethene and acetylene depends linearly with adsorption energy of methyl group. Such screening metals and alloys using CH_3 saves time when designing active catalyst.

UNIVERSITAT ROVIRA I VIRGILI
THEORETICAL STUDIES ON MOLECULAR ADSORPTION AND SELECTIVE HYDROGENATION CATALYSTS
Crisa Vargas Fuentes

Chapter 2

Theoretical background

Contents

In this Chapter, some of the most important theories and main tools related to first principles atomistic simulations in heterogeneous catalysis will be summarized. Density Functional Theory, DFT, created to investigate the ground state of many-body systems will be reviewed together with local-density, LDA, and generalized gradient approximations, GGA, used to describe the exchange-correlation energy. In addition, an overview of the latest approaches to van der Waals interactions in the theoretical study of heterogeneous catalysis will be presented. And finally, some practical aspects will be introduced: basis set, k-point sampling, pseudopotentials, supercells, and also chemical bonding at surfaces will be addressed.

2.1 Electronic structure calculations

In 1926, Erwin Schrödinger suggested an equation with the purpose of describing the state of any system

$$\widehat{H}\Psi = E\Psi \tag{2.1}$$

where Ψ represents the state, E stands for the energy and $\widehat{H}$ is the hamiltonian operator for the system, whose definition is

$$\widehat{H} \equiv \widehat{T} + \widehat{V}, \tag{2.2}$$

consisting of the sum of the kinetic and potential operators, $\widehat{T}$ and $\widehat{V}$, respectively. To know how the system evolves with time, the time-dependent Schrödinger equation must be solved

$$\widehat{H}\Psi(t) = i\hbar\frac{\partial\Psi(t)}{\partial t} \tag{2.3}$$

Due to its complexity, the complete Schrödinger equation can be analitically solved only for two-body systems. Therefore, in the case of many-body electronic structure calculations, approaches are needed. One of the most useful and handy is the Born-Oppenheimer approximation, [23] where the nuclei of the treated molecules or clusters are usually seen as fixed, generating a static external potential, V, in which the electrons are moving. A stationary electronic state is then described by a wavefunction, $\Psi_{elec}(\boldsymbol{r}_1,\ldots,\boldsymbol{r}_n)$, satisfying the many-electron stationary Schrödinger equation:

$$\widehat{H}_{elec}\Psi_{elec} = \left[\widehat{T} + \widehat{V} + \widehat{U}\right]\Psi = E_{elec}\Psi_{elec} \tag{2.4}$$

$$\widehat{T} \equiv \sum_{i}^{N} -\frac{\hbar^2}{2m}\nabla_i^2 \tag{2.5}$$

$$\widehat{V} \equiv \sum_{i}^{N} V(\mathbf{r}_i) \tag{2.6}$$

$$\widehat{U} \equiv \sum_{i<j} U(\mathbf{r}_i, \mathbf{r}_j) \tag{2.7}$$

where $\widehat{H}_{elec}$ is the electronic Hamiltonian, $\widehat{T}$, $\widehat{V}$ and $\widehat{U}$ are the operators for the kinetic energy, the external potential, and the electron-electron interaction, respectively. N is the total number of electrons. $\widehat{T}$ and $\widehat{U}$ are universal operators as they are the same for any system, while $\widehat{V}$ is system dependent or non-universal. The difference between a single-particle problem and the many-particle problem just arises from the interaction term, $\widehat{U}$. There are many methods to solve the many-body Schrödinger equation based on the expansion of the wavefunction in Slater determinants. The simplest one is the Hartree-Fock method and more sophisticated approaches are usually categorised as post-Hartree-Fock methods. However, the problem with these methods is the huge computational effort that they require, which makes it virtually impossible to apply them efficiently to large complex systems, in particular, those with metals. Instead, Density Functional Theory, DFT, provides an appealing alternative. All the calculations performed through these pages make use of DFT to solve the stationary Schrödinger equation.

2.2 Density Functional Theory

Density Functional Theory, DFT, is a quantum mechanics theory applied to find the ground state of many-body systems, such as atoms, molecules and condensed phases. As its name suggests, in DFT the key functional and more basic variable is the electronic density, $n(\boldsymbol{r})$, and is given by

$$n(\mathbf{r}) = N \int \mathrm{d}^3 r_2 \int \mathrm{d}^3 r_3 \ldots \int \mathrm{d}^3 r_N \Psi^*(\mathbf{r}, \mathbf{r}_2, \ldots, \mathbf{r}_N)\Psi(\mathbf{r}, \mathbf{r}_2, \ldots, \mathbf{r}_N) \tag{2.8}$$

It implies that DFT does without the many-body stationary wavefunction, Ψ ($\boldsymbol{r}_1$, $\boldsymbol{r}_2$, ..., $\boldsymbol{r}_\mathrm{n}$), which is dependent on 6N variables, whereas the electronic density is only a function of three variables and easier deal with both conceptually and practically, as can be directly mapped to experiments.

2.2.1 History

DFT basis are inspired in the Thomas-Fermi model and Dirac additions [24] of the ground-state properties of many-electron systems. Thomas and Fermi employed a statistical model to approximate the distribution of electrons in an atom. The mathematical basis postulated that electrons are distributed uniformly in phase

space with two electrons in every h^3 of volume, where h, the Planck constant, is a physical constant that is employed to describe the sizes of quanta. For each element of coordinate space volume, $d^3\boldsymbol{r}$, we can fill out a sphere, Fermi sphere, the radius called Fermi momentum, $\boldsymbol{p}_f$, and its volume is

$$V_{Fermi} = \frac{4}{3}\pi \mathbf{p}_f^3(\mathbf{r}) \tag{2.9}$$

making equal the number of electrons in coordinate space to that in phase space gives

$$n(\mathbf{r}) = \frac{\mathbf{p}_f^3}{3\pi^2} \tag{2.10}$$

solving for $\boldsymbol{p}_\mathrm{f}$ and substituting in the classical kinetic energy formula leads directly to a kinetic energy, $T_F(n)$, represented as a functional of the electron density,

$$T_F(n) = C_F \int n^{5/3}(\mathbf{r}) d^3\mathbf{r}. \tag{2.11}$$

As such, they were able to calculate the energy of an atom using this kinetic energy functional combined with the classical expressions for the nuclear-electron and electron-electron interactions, which can both also be represented in terms of the electron density.

Although this was an important first step, the accuracy of the Thomas-Fermi model is limited both because the resulting kinetic energy functional is only approximate and because the method does not include the exchange energy that arises from the Pauli principle. An exchange energy functional was added to the model by Paul Dirac in 1928. [24] However, the Thomas-Fermi-Dirac theory remained rather inaccurate for most applications. The largest source of error was in the representation of the kinetic energy, followed by the errors in the exchange energy, and due to the complete neglect of electron correlation. Edward Teller, [25] showed that Thomas-Fermi-Dirac theory cannot describe molecular bonding. This was overcome by improving the kinetic energy functional as done by Carl Friedrich in 1935,

$$T_W(n) = \frac{1}{8}\frac{\hbar^2}{m}\int \frac{|\nabla n(\mathbf{r})|^2}{n(\mathbf{r})} dr \tag{2.12}$$

In 1964, Pierre Hohenberg and Walter Kohn developed the existence of a one-to-one correspondence between the ground state electron density, $n_0(\boldsymbol{r})$, and the ground state wavefunction of a many-particle system, $\Psi_0(\boldsymbol{r}_1,\ldots,\boldsymbol{r}_N)$, *i.e.*, the Density Funcional Theory, and later on its practical application was proved by Kohn and Sham. [26] Hohenberg and Kohn demonstrated that the energy of a quantum mechanical system is a unique function of the electron density, $n(\boldsymbol{r})$, and that the correct ground-state density minimizes it. The original Hohenberg-Kohn theorems hold only for a non-degenerate ground state in the absence of magnetic field, although they have been generalised to the ground states of each symmetry. These details will be examined in the next section.

2.2.2 Derivation and formalism

As briefly seen above, Hohenberg and Kohn proved in 1964 that the Equation 2.8 can be reversed, [27] *i.e.*, to a given ground state density $n_0(\boldsymbol{r})$ it is in principle possible to obtain the corresponding ground state wavefunction $\Psi_0(\boldsymbol{r}_1, \ldots,\boldsymbol{r}_N)$. In other words, Ψ_0 is a unique functional of n_0, $\Psi_0{=}\Psi(n_0)$. This means that all other ground state observables are also functionals of n_0. In particular, the ground state energy, E_0, can be expressed as a functional of n_0:

$$E_0 = E(n_0) = \langle \Psi_0(n_0) \left| T(n_0) + V(n_0) + U(n_0) \right| \Psi_0(n_0) \rangle \qquad (2.13)$$

The functionals $T(n)$, $U(n)$, and $V(n)$ are equivalent to those operators of Equations 2.5 to 2.7, and in the same way $T(n)$ and $U(n)$ can be called universal functionals while $V(n)$ is non-universal, as it depends on the system under study, *i.e.*, its configuration. The state energy, $E(n)$, can be expressed as:

$$E(n) = T(n) + U(n) + \int V(\mathbf{r}) n(\mathbf{r}) d^3\mathbf{r} \qquad (2.14)$$

Having specified a system, V is known, a successful minimization of the energy functional with respect to $n(\boldsymbol{r})$ will yield the ground state density, $n_0(\boldsymbol{r})$, and thus other ground state observables. The variational problem of minimizing the energy functional, *E[n]*, can be solved by applying the Lagrangian method of undetermined multipliers, which was done by Kohn and Sham in 1965. [26] Hereby, one uses the fact that the functional in the equation above can be written as a fictitious density functional of a non-interacting system

$$E_{KS}[n] = \langle \Psi_{KS}(n) \left| T_{KS} + V_{KS} \right| \Psi_{KS}(n) \rangle \tag{2.15}$$

where T_{KS} denotes the non-interacting kinetic energy and V_{KS} is an external effective potential in which the particles are moving. If V_{KS} is chosen to be

$$V_{KS} = V + U + (T - T_{KS}) \tag{2.16}$$

then $n_{KS}(\boldsymbol{r}) \equiv n(\boldsymbol{r})$. Thus, one can solve the so-called Kohn-Sham equations of this auxiliary non-interacting system:

$$\left[\frac{-\hbar^2}{2m} \nabla^2 + V_{KS}(\mathbf{r}) \right] \phi_i(\mathbf{r}) = \epsilon_i \phi_i(\mathbf{r}) \tag{2.17}$$

which yields the monoelectronic orbitals, ϕ_i, that reproduce the density, $n(\boldsymbol{r})$, of the original many-body system:

$$n(\mathbf{r}) \equiv n_{KS}(\mathbf{r}) = \sum_{i}^{N} |\phi_i(\mathbf{r})|^2 \tag{2.18}$$

The effective single-particle potential, V_{KS}, includes the external potential, the effects of the Coulomb interactions between the electrons, and the exchange and correlation interactions. V_{KS} can be written in more detail as:

$$V_{KS} = U + \int \frac{e^2 n_{KS}(\mathbf{r}')}{|\mathbf{r} - \mathbf{r}'|} \mathrm{d}^3 r' + V_{\mathrm{XC}}(n_{KS}(\mathbf{r})) \tag{2.19}$$

where U is still the external potential, the second term denotes the so-called Hartree term describing the electron-electron Coulomb repulsion, and the last term, V_{XC}, is known as the exchange correlation potential. Usually, one starts with an initial guess for $n(\boldsymbol{r})$, then calculates the corresponding V_{KS} through Equation 2.19, and solves the Kohn-Sham equations, Equation 2.17 for the ϕ_i. From these, one calculates a new density and starts again. This procedure is then repeated until self-consistency is reached. Therefore, the intractable many-body problem of interacting electrons in a static external potential, V, has been reduced to a tractable problem of non-interacting electrons moving in an effective potential, V_{KS}. It shall be noticed that the KS equations are formally equivalent to the HF ones, only the potential is different.

2.2.3 State-of-the-art exchange-correlation approximations

The exchange energy is the reduction of the energy of the electronic system which results from the anti-symmetry of the wave function under permutation of electrons. The correlation contribution to the energy arises because the motion of an electron depends also on the movements of other electrons. The major problem of DFT is that the exact functionals for exchange and correlation are not known except for the free electron gas. However, approximations exist which permit the calculation of many physical quantities quite accurately. The exchange-correlation functionals hierarchy leads us to an increasing accuracy of the results, and has been schematized by Perdew and Schmidt in the Jacob's ladder of DFT approximations, [28] as can be seen in Figure 2.1.

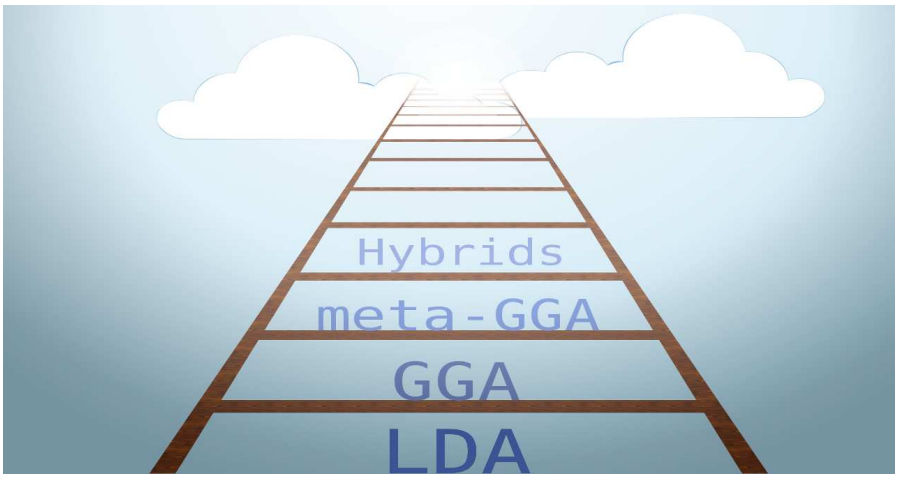

Figure 2.1: Jacob's ladder of density-functional approximations (after Perdew and Schmidt. [28])

The Local Density Approximation, LDA

The lowest rung of the ladder to the exchange-correlation interaction is the local-density approximation, LDA, [26] in which the functional depends only on the density, $n(\boldsymbol{r})$, at the position where the functional is evaluated. In order to find the exchange-correlation energy, E_{XC}, for an inhomogeneous electron gas, it is assumed that the contribution from each point in the electron gas is the same as in a homogeneous electron gas with the same density $n(\boldsymbol{r})$:

$$E_{XC}^{LDA} = \int n(\mathbf{r})\varepsilon_{XC}^{hom}(n)\mathrm{d}\mathbf{r} \tag{2.20}$$

The spin-polarised version of LDA is termed as Local-Spin Density Approximation, LSDA, and allows difference between the spatial parts of $n_\uparrow$ and $n_\downarrow$. It is needed for atoms and molecules with unpaired electrons and for magnetic condensed materials:

$$E_{XC}^{LSDA}(n_\uparrow, n_\downarrow) = \int \varepsilon_{XC}(n_\uparrow, n_\downarrow)n(\mathbf{r})\mathrm{d}^3\mathbf{r} \tag{2.21}$$

LDA can manage to solve many bulk [29] and surface problems. However, it tends to over-bind when treating chemical reactions occurring at surfaces. [30] Moreover, the potential-energy profiles for dissociations of diatomic molecules on metallic surfaces are badly described by LDA. For these reasons, climbing the next rung of the ladder becomes mandatory. [31, 32]

The Generalised Gradient Approximation, GGA

Generalised Gradient Approximations, GGA, are still local but also take into account the gradient of the charge density at the same coordinate:

$$E_{XC}^{GGA}(n(\mathbf{r})) = \int n(\mathbf{r})\varepsilon_{XC}(n(\mathbf{r}), \nabla n(\mathbf{r}))\mathrm{d}\mathbf{r} \tag{2.22}$$

GGA can also be extended to spin-polarised systems:

$$E_{XC}(n_\uparrow, n_\downarrow) = \int \varepsilon_{XC}(n_\uparrow, n_\downarrow, \nabla n_\uparrow, \nabla n_\downarrow)n(\mathbf{r})\mathrm{d}^3\mathbf{r} \tag{2.23}$$

The second rung of the Perdew's ladder corrects the over-binding tendency of the LDA. Furthermore, for many chemical reactions, the GGA achieves sufficient accuracy and, for most of the reactions on metals, it constitutes the proper description level. [32, 33] Unfortunately, GGA's have two disadvantages that may be dangerous depending on the object under study. The first one is that they do not account for van der Waals interactions resulting from dynamical correlations between fluctuating charge distributions. [34] The second disadvantage is the so-called self-interaction error, SIE, that arises from the exchange-correlation approximation term and is the cause of failures like too small band gaps, [35, 36] and wrong dissociation energies for molecules. [37] The SIE is basically the non-zero

interaction of a single electron with its own density. [32, 38]

Several groups have constructed GGA functionals, of which the most commonly used in molecular chemistry are BP86, [39] BLYP, [40] and in solid state problems PW91, [41] PBE, [42] and RPBE [43] are by far the most commonly used functionals. Geometries are good with LDA while thermochemistry demands at least GGA. One approach to reduce SIE and treat complex structures with strongly correlated d and f electrons need *on-site* Coulomb interactions: L(S)DA+U methods. The Hubbard parameter, U, can be fitted to reproduce experimental band-gaps, geometries or other properties. In the present Chapter a GGA functional, RPBE, is used throughout when not taking into account the van der Waals interactions. RPBE is extremely sensitive to density gradients, and provides better thermochemistry data than other GGAs. [43]

The next two rungs on the DFT ladder, just to be mentioned as they will not be used in the present work, are the the meta-GGA [44] and the hybrid functionals. [45, 46] The former includes higher-order terms of the gradient of the local kinetic energy. However, it does not improve GGA results systematically, but for certain specific systems. [44] The latter, as can be guessed from its name, is a mixture or hybrid between HF and exchange functionals. Hybrid orbitals become very useful in molecular chemistry, although the results obtained for solids are unclear. [32, 47, 48]

2.3 How to treat dispersion forces: different approaches

Non-covalent forces, such as hydrogen bonding and van der Waals, vdW, interactions are crucial for the formation, stability, and function of molecules and materials. [49] Although the precise microscopic knowledge of van der Waals interactions is crucial for understanding bonding in weakly bonded compounds, very little quantitative information on the strength of interactions is available, either from experiments or simulations. [50] In terms of theoretical chemistry, this lack of knowledge is due to the intrinsically non-local correlation effect of the vdW interaction *vs.* the local approximations that are conventionally applied in DFT. [51–53] In order to overcome this issue, many methods [49, 54–60] of different complexity have been developed during the past decade. In this work, two popular computational approaches for treating the vdW interaction

will be considered, the Grimme's semi-empirical force-field corrections, DFT-D2, [57] later improved by Tkatchenko and Scheffler, [49] and the non-local van der Waals density functionals, [58–60] vdW-DF. [50]

2.3.1 DFT-D2 method

As said above, popular density functionals are unable to describe correctly van der Waals interactions resulting from dynamical correlations between fluctuaing charge distributions. A pragmatic method to work around this problem has been given by the DFT-D approach, [61] which consists in adding a semi-empirical dispersion potential to the conventional Kohn-Sham DFT energy:

$$E_{DFT-D} = E_{KS-DFT} + E_{disp} \tag{2.24}$$

In the DFT-D2 method of Grimme, [57] the van der Waals interactions are described via a simple pair-wise force field, which is optimized for several popular DFT functionals. The dispersion energy for periodic systems is defined as

$$E_{disp} = -\frac{s_6}{2} \sum_{i=1}^{N_{at}} \sum_{j=1}^{N_{at}} \sum_{\mathbf{L}}{}' \frac{C_6^{ij}}{|\mathbf{r}^{i,0} - \mathbf{r}^{j,\mathbf{L}}|^6} f(|\mathbf{r}^{i,0} - \mathbf{r}^{j,\mathbf{L}}|), \tag{2.25}$$

where the summations are over all atoms, N_{at}, and all translations of the unit cell, $L = (l_1, l_2, l_3)$, the prime indicates that i for $L = 0$, s_6 is a global scaling factor, C_6^{ij} denotes the dispersion coefficient for the atom pair ij, $r^{i,L}$ is a position vector of atom i after performing L translations of the unit cell along lattice vectors. In practice, terms corresponding to interactions over distances longer than a certain suitably chosen cutoff radius contribute only negligibly to E_{disp} and can be ignored. The term $f(r^{ij})$ is a damping function

$$f(r^{ij}) = \frac{1}{1 + e^{-d(r^{ij}/R_0^{ij} - 1)}}, \tag{2.26}$$

whose role is to scale the force field such as to minimize contributions from interactions within typical bonding distances. Combination rules for dispersion coefficients C_6^{ij} and vdW radii R^{ij} are

$$C_6^{ij} = \sqrt{C_6^i C_6^j}, \tag{2.27}$$

and

$$R_0^{ij} = R_0^i + R_0^j, \tag{2.28}$$

respectively. The global scaling parameter, s_6, has been optimized for several different DFT functionals such as PBE ($s_6 = 0.75$), BLYP ($s_6 = 1.20$), and B3LYP ($s_6 = 1.05$). The default values for C_6^{ij} and R^{ij} of the first five rows of the periodic table are compiled and can be found in reference. [57]

So far, several methods exist to determine the C_6 coefficients. [56, 62, 63, 63–65] Unfortunately, the errors are quite large, sometimes up to 60%, due to the overestimation of the polarizability associated to the use of the local-density or gradient corrected exchange-correlation functionals of density-functional theory.

2.3.2 vdW-DF method

The non-local van der Waals density functionals, vdW-DF, proposed by Dion *et al.* [60] are also non-local correlation functionals that approximately account for dispersion interactions. In VASP, the method is implemented using the algorithm of Roman-Perez and Soler, [66] which transforms the double real space integral to reciprocal space and reduces the computational effort. Several proposed versions of the method can be used: the original vdW-DF, [60] vdW-DF with exchange functionales optimized for the correlation part, [67] and the vdW-DF2 of Langreth and Lundqvist groups. [59] In the present Chapter, the version developed by Michaelides *et al.* will be performed, with its corresponding LDA correlation and optB86b exchange functionals. [67]

2.4 Implementation

2.4.1 Plane waves

For a numerical description of the Kohn-Sham wavefunctions, a basis set has to be chosen. In DFT calculations for solid surfaces, a plane wave basis set is often chosen due to the periodicity of the systems. The expansion of the wavefunctions is based on Bloch's theorem. [68, 69] A *Bloch state* is the wavefunction of a particle, usually an electron, placed in a periodic potential. Then the *Bloch state* can be expressed as the product of a plane wave envelope function, $e^{i\boldsymbol{kr}}$, and a periodic function, $U_n(\boldsymbol{r})$, which has the same periodicity as the potential.

$$\psi_n(\mathbf{r}) = e^{i\boldsymbol{k}\mathbf{r}} U_n(\mathbf{r}) \tag{2.29}$$

The periodic part of the wavefunction can be expanded using a basis set consisting of a discrete set of plane waves whose wave vectors are reciprocal lattice vectors of the crystal:

$$U_n(\mathbf{r}) = \sum_{\mathbf{G}} c_{n,}\boldsymbol{G} e^{i\boldsymbol{G}\mathbf{r}} \tag{2.30}$$

where the reciprocal lattice vectors $\boldsymbol{G}$ are defined by $\boldsymbol{Gl} = 2\pi m$ for all $\boldsymbol{l}$. $\boldsymbol{l}$ is a lattice vector of the crystal and m is an integer. Therefore, each electronic wavefunction can be written as sum of plane waves,

$$\psi_n(\mathbf{r}) = \sum_{G} c_{n,\boldsymbol{k}+\boldsymbol{G}} e^{i(\boldsymbol{k}+\boldsymbol{G})\mathbf{r}} \tag{2.31}$$

where k is the wave vector limited to the first Brillouin zone (multiplied by the reduced Planck's constant, this is the particle's crystal momentum) and $\boldsymbol{G}$ is a reciprocal lattice vector. The corresponding energy eigenvalue is periodic, $E_{n\boldsymbol{k}} = E_{n(\boldsymbol{k}+\boldsymbol{G})}$, with periodicity of a reciprocal lattice vector, $\boldsymbol{G}$. All distinct values of E_n occur for $\boldsymbol{k}$ values within the first Brillouin zone of the reciprocal lattice. The plane wave wavevector, or Bloch wavevector, $\boldsymbol{k}$, is unique only up to a reciprocal lattice vector, so one only needs to consider the wavevectors inside the first Brillouin zone. Therefore, using plane waves with periodic boundary conditions, we get rid of the infinite number of atoms and electron wavefunctions but end up having an infinite number of $\boldsymbol{G}$-vectors. However, the coefficients $c_{n,\boldsymbol{k}+\boldsymbol{G}}$ for the plane waves with small kinetic energy $(\frac{\hbar^2}{2m})|\boldsymbol{k}+\boldsymbol{G}|^2$ are typically more important that those with large kinetic energy. Thus the number of plane waves can be safely truncated by introducing the cutoff energy, E_{cut}, [70] which is given as a kinetic energy of the largest $\boldsymbol{G}$-vector. For a given wavevector and potential, there are a number of solutions, indexed by n, to Schrödinger's equation for a Bloch electron. These solutions, called bands, are separated in energy by a finite spacing at each $\boldsymbol{k}$; if there is a separation that extends over all wavevectors, it is called a band gap. In short, the band structure is the collection of energy eigenstates within the first Brillouin zone. All the properties of electrons in a periodic potential can be calculated from this band structure and the associated wave functions, at least within the independent electron approximation.

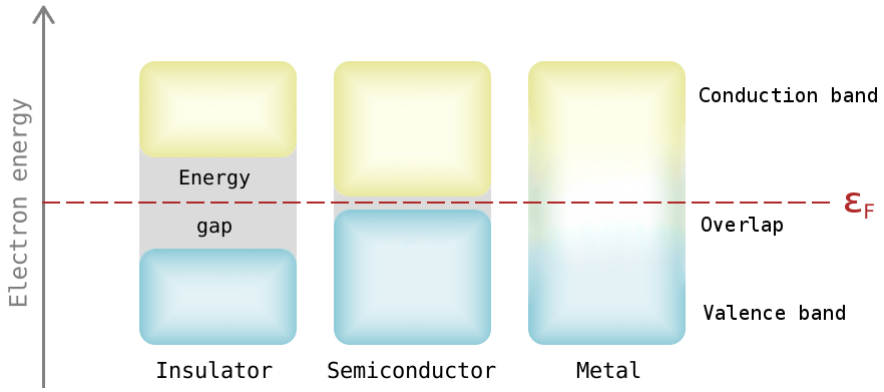

Figure 2.2: Comparison of the electronic band structures of metals, semiconductors and insulators.

2.4.2 k-point sampling

Although Bloch's theorem gives the electronic states for a set of k-points, the size of the set is infinite. However, the wavefunctions at k-points close to each other are very similar, therefore when performing integrations, only a discrete set of k-points is needed to represent the k-space. The electronic structure calculations of metals are more demanding than those of semiconductors and insulators, since more k-points are needed to describe reliably the Fermi surface. Unlike metals, insulators and semiconductors have a gap between occupied and unoccupied states, and the shape of the Fermi surface is simple, see Figure 2.2. For metals, the k-space integrals converge slowly with increasing number of k-points.

To decrease the number of k-points further, special k-points are often used where the symmetry of the system is exploited. The Monkhorst-Pack grid, is usually used. [71] In Figure 2.3 the first Brillouin zone for a face centred cubic, *fcc*, structure is represented.

2.4.3 Pseudopotentials

Although Bloch's theorem states that the electronic wavefunctions can be expanded using a discrete set of plane waves, PW, a plane wave is usually very poorly suited to describe electronic wavefunctions. This is because a very large number of PW are needed to expand the tightly bound core orbitals and to follow the rapid oscillations of the wavefunctions of the valence electrons in the core

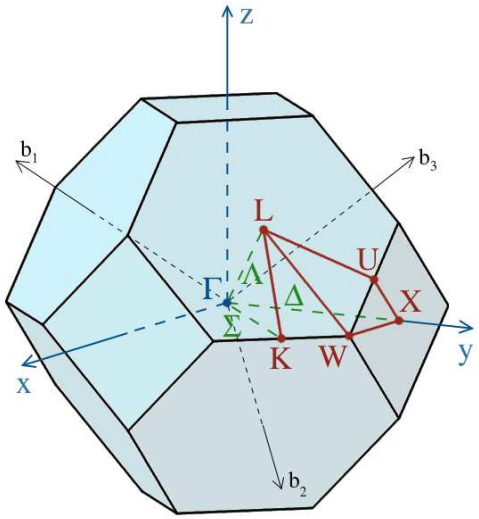

Figure 2.3: Most relevant symmetry points on the Brillouin zone of a *fcc* crystal. b_1, b_2 and b_3 are the primitive recoprocal lattice vectors. Γ , X, L, W, U and K represent the symmetry points. Δ, Λ, and Σ symbolize the symmetry lines. [68, 72]

region. An extremely large plane wave basis set would be required to perform all electron calculations, and a vast amount of computational time would be required to calculate the electronic wavefunctions. However, only the outermost electrons in an atom normally influence the chemical properties of matter, while electrons in the inner shells are almost inert. Therefore, the distribution of the core electrons basically does not change when the atoms are placed in a different chemical environments. It is thus justified to assume the core electrons to be *frozen*, [73] and to keep the core electron distribution of the isolated atom in the crystal environment.

The pseudopotential approximation exploits this by removing the core electrons, and by replacing them and the strong ionic potential by a weaker pseudopotential that acts on a set of pseudo wavefunctions rather than the true valence wavefunctions. An ionic potential, a valence wavefunction and the corresponding pseudopotential and pseudo wavefunction are illustrated schematically in Figure 2.4. The pseudopotential approximation [74] the electronic wavefunctions to be expanded using a much smaller number of plane wave basis states.

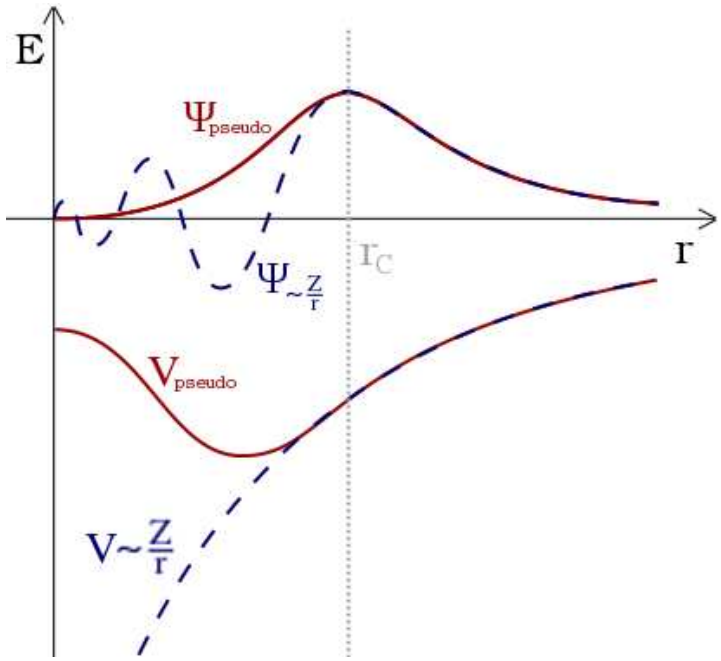

Figure 2.4: Schematic illustration of all electron (blue lines) and pseudoelectron (red lines) potentials and their corresponding wavefunctions. The radius at which all electron and pseudoelectron values match is known as cutoff radius, r_c. [70]

The valence wavefunctions oscillate rapidly in the region occupied by the core electrons due to the strong ionic potential in this region. These oscillations maintain the orthogonality between the core wavefunctions and the valence wavefunctions, which is required by the exclusion principle. The pseudopotential is constructed so that its scattering properties or phase shifts for the pseudo wavefunctions are identical to the scattering properties of the ion and the core electrons for the valence wave functions, but in such a way that the pseudo wavefunctions have no radial nodes in the core region. Outside the core region, the two potentials are identical and the scattering from the two potentials is indistinguishable.

The pseudopotentials must be as transferable as possible, because although they are always constructed for a single atom, they are applied in various chemical environments. Furthermore, the pseudopotential should be as *soft* as possible. It means that the number of plane waves required to expand the pseudo wavefunc-

tions should be as small as possible. Both properties, transferability and softness, are closely related to the cutoff radius, r_c, and compete with each other. Low cutoffs give pseudopotentials with a very good transferability. However, increasing r_c makes the pseudopotentials softer. Usually one has to find a compromise between the two requirements. In this work the Projector Augmented Wave, PAW, pseudopotentials have been used [75, 76] in order to represent the inner electrons.

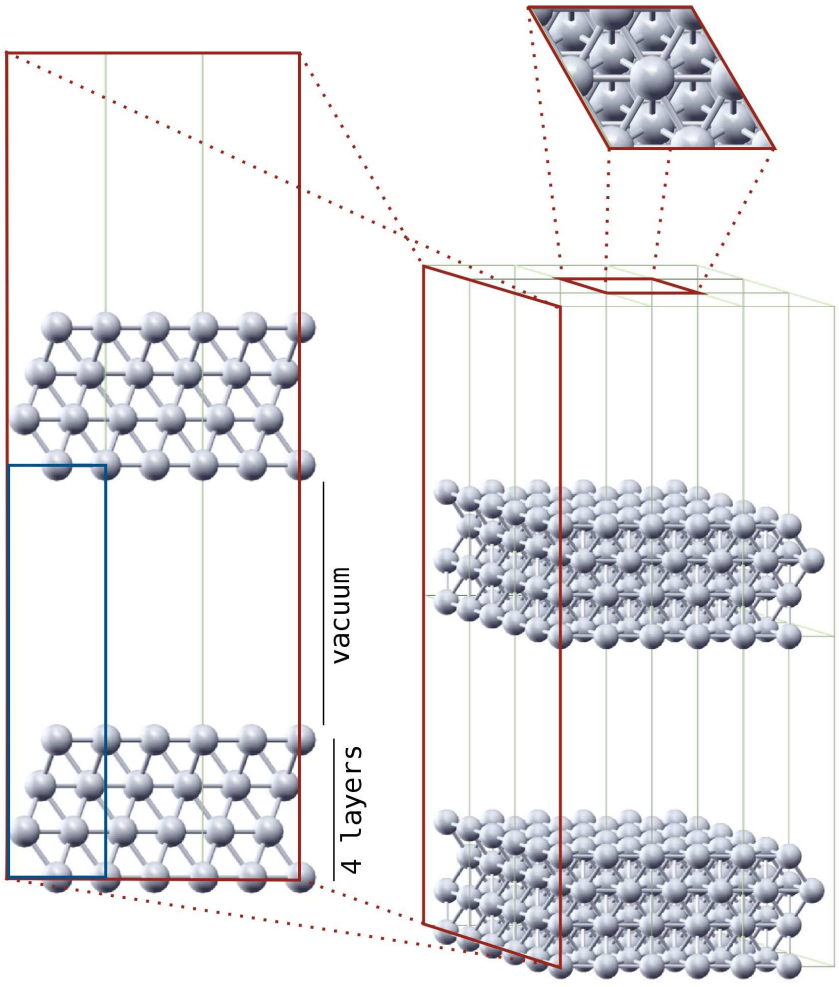

Figure 2.5: Schematic illustration of a four atomic layer-thick metallic slab (right) of a *fcc* (111) surface, its top view (top-right) and its side view (left) where a supercell enclosed by blue lines can be distinguished.

2.4.4 Supercells

When using plane waves as basis functions, the system has to be periodic in all directions in space because Bloch's theorem only applies for such systems. Atoms and molecules in vacuum, as well as clusters and surfaces, are not periodical as such, therefore in calculations these systems have to be surrounded by enough empty space to prevent artificial or cell-to-cell interactions, which are due to periodic boundary conditions. The supercell for a surface calculation is illustrated schematically in Figure 2.5.

A surface may have periodicity in the plane, but it cannot have periodicity perpendicular to the surface. This leads to the creation of the slab, a geometry where the surface is modelled with few atomic layers and a vacuum region, which separates the slabs in the z-direction, see again Figure 2.5. To ensure that the results of the calculation accurately represent an isolated surface, the vacuum region must be wide enough, each slab has to be several atomic layers thick so that faces of adjacent crystal slabs do not interact across the vacuum region, and the crystal slab must be thick enough so that the two surfaces of each slab do not interact through the bulk crystal.

2.4.5 Chemical bonding

The essence of catalytic action is that it assists in breaking strong intramolecular bonds at lower temperatures than those needed in the direct gas-phase reaction. Chemisorbed adsorbate binds to a surface through a chemical bond. This bond is formed due to the coupling of the adsorbate molecular orbitals to the metal electron bands. Simple models can be used to analyze the coupling. A model has been proposed by Hammer and Nørskov [77] where the interaction of the adsorbate orbitals with the metal bands is divided into two parts, one describing the coupling with the s and p valence electrons and another the coupling with the d valence bands. To describe the chemisorption bond it is necessary to review briefly solid state theory that is relevant to understand the adsorption on surfaces.

The solid surface

All metals have extended outer s or p-orbitals, which ensure large overlap. The orbitals are very close in a metal and form

an almost continuous band of levels. [77] The d-orbitals have pronounced shapes and orientations that are largely retained in the metal. Hence, the overlap between the individual d-orbitals of the atoms is much smaller than that of the outer s and p electrons. The latter are strongly delocalised and they form an almost free electron gas that spreads out over the entire metal. Then, the atomic sp electron wave functions overlap to a great extent, and consequently the band they form is much broader, see Figure 2.6.

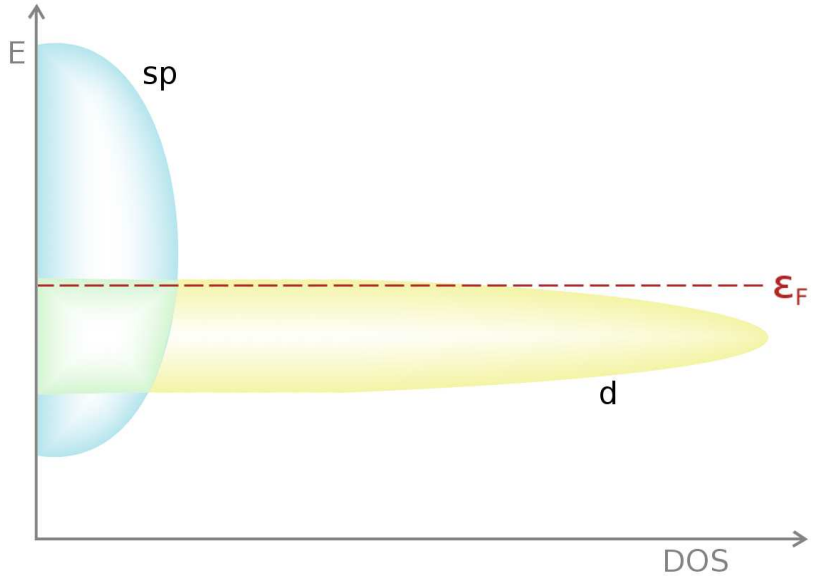

Figure 2.6: Schematic representation of the broad sp-band and the narrow d-band. ε_F is the Fermi level and DOS stands for density of states.

A knowledge of the behaviour of d-orbitals is essential to understand the differences and trends in reactivity of the transition metals. [77] The width of the d-band decreases as the band is filled when going to the right in the periodic system since the molecular orbitals become ever more localised and the overlap decreases. Thus, a band is simply a collection of many molecular orbitals. The lower levels in the band are bonding, the upper ones antibonding and the ones in the middle non-bonding. Each energy level in the band is called a state and an important quantity to look at is the density of states, DOS, at a given energy. The density of states curves of transition metals show complicated structures, due to crystal structure and symmetry.The bands are filled with valence electrons of the atoms up to the Fermi level, ϵ_F. In a molecule this is known as highest occupied molecular orbital or HOMO.

Chapter 3

Objectives

The main goal of the present Doctoral Thesis is to provide an atomistic viewpoint to old widely discussed topics in the literature. To this aim I provide new data to the large database of the adsorption properties of gases to metal surfaces.

In particular, the next objectives are aimed to be reached:

- Database building of molecular adsorption containing the main functional groups on a series of characteristic crystallographic facets of transition metals.
- Carrying out representative studies of one of these transition metals in order to compare its data with those of experiments extracted from the literature. Extending this comparison to the theoretical data performed by adding the most modern approaches to van der Waals dispersion contributions.
- Identifying descriptors for molecular adsorption so as to simplify theoretical research and ease the experimental works.
- Understanding, up to molecular level, all components of Pd-based catalysts in the selective hydrogenation of olefins mixtures. From the co-catalyst metals forming the surface alloys to other possible promoters, like quinoline in the case of the Lindlar catalyst. The modification of the conversion and selectivity at will could then be done.

UNIVERSITAT ROVIRA I VIRGILI
THEORETICAL STUDIES ON MOLECULAR ADSORPTION AND SELECTIVE HYDROGENATION CATALYSTS
Crisa Vargas Fuentes

Part II

Results

UNIVERSITAT ROVIRA I VIRGILI
THEORETICAL STUDIES ON MOLECULAR ADSORPTION AND SELECTIVE HYDROGENATION CATALYSTS
Crisa Vargas Fuentes

Chapter 4

Molecular adsorption on transition metals facets: building a database

Contents

In the present Chapter, we present a thorough analysis of the behaviour of a number of small organic molecules (acetylene, ethylene, formaldehyde, hydrogen cyanide, methanol, and formic acid) and fragments (methoxy and formate) adsorbed on four different facets of the stable *fcc* crystallographic structure of eight monometallic systems (Pd, Pt, Rh, Ir, Cu, Ni, Ag, and Au), moreover testing various sites on each surface. This work has been performed by means of Density Functional theory within the well-known Revised Perdew-Burke-Ernzerhof exchange model, as well as with the addition of the still-under-study approximations to van der Waals interactions. A database for all energies has been built and the parameters controlling adsorption have been identified.

4.1 Previous works

The adsorption of organic molecules on solid surfaces and their chemical reactions catalyzed by the contact with these surfaces are of growing interest because of the fundamental importance of an improved understanding of the interaction and bonding mechanism between organic films and metallic or insulating substrates in many different fields in the industry. [34] For this reason, theoretical approaches of heterogeneous catalysis aim at determining the adsorption energies, structures and geometries of a molecule on a catalytic substrate. [78] Although an extensive source of data obtained from DFT calculations can already be found in the literature of the last four decades, it is necessary to create a large database encompassing both the existing and the missing data, as well as dispersion forces, all of them calculated with the same most suitable up-to-date approximations in order to be able to compare data. Having a look to the metals under study, in general, the ones with larger lack of references in the literature are rhodium, iridium, silver and gold, especially in the case of the insaturated hydrocarbons, formic acid and methoxy fragment. Regarding to the molecules, formic acid is the real missing one within the framework of the current studies, probably due to the endothermic character of its adsorption to any reactive surface. The errors associated with adsorption energies derived from DFT calculations are typically on the order of 0.3 eV. [79] In the present Section, some of the most relevant molecular adsorption studies theoretically performed and mentioned in the literature will be described per metals.

Palladium surface has been studied numerous times because of its large use nowadays in catalytic converters, among other applications. On the other hand, the adsorption of unsaturated hydrocarbons on metallic surfaces is of fundamental and applied interest and also a vast number of experimental and theoretical studies have dealt with these systems, in view of its implications as a model system for catalysis in the refining industry. [80–94] In particular, the relation between the type of hydrocarbon and its adsorption strength on metallic surfaces remains an open question. Binding energies for acetylene and ethylene on Pd(111) were found to be -1.78 and -0.85 eV, respectively, by Smith *et al.* In both cases, the molecule adsorbs with the double bond parallel to the surface. [80, 95] This couple of data is consistent with other publications, *i.e.* -2.03 [80] and -1.78 eV [89] for acetylene; -0.87 [80] and -0.85 eV [89] for ethylene. Aldehyde adsorption on group VIII metal sur-

faces has been extensively examined by Barteau *et al.* [96–100] The binding energy of formaldehyde on the (111) facet of Pd is calculated as -0.46 eV [101] and on Pd(100) -0.79 eV. [102] In the case of methanol, it is one of the most important synthetic chemicals because of its importance in direct methanol fuel cells, as well as in petroleum industry, among others. In the literature, the values for methanol binding energy range from -0.39 [101] on the (111) facet of palladium to -0.44 eV [103] on the (211) one. Quite weak bond as expected. All these calculated energies are in good agreement with the experimental value, -0.47 eV. [104] The methoxy species is formed by the O-H bond scission of CH_3OH. The adsorption energy of -2.30 eV on Pd(211) indicates stronger chemisorption than on the no stepped facets. [103] The binding is much tighter than that on Pd(111), which has an adsorption energy of -1.73 eV. [101]

Platinum and its alloys are the catalysts of choice in many industrial processes, including the hydrogenation of olefins, the dehydrogenation and cracking of paraffins, and the synthesis of nitric acid and hydrogen cyanide. [105] Because of the versatility of Pt catalysts, many adsorbates and reactions have been studied on platinum surfaces using a wide variety of techniques. [1, 106] The reported adsorption energy for ethylene on Pt(111) is -1.10 eV and for acetylene -2.26 eV. [80] In the case of methanol, formaldehyde and formic acid, the binding energies on the (111) facet are found in the literature to be -0.32, -0.58 and -0.42 eV, respectively. [107] Regarding to the CHN molecule, its binding energy to the Pt(111) surface is described by Mavrikakis *et al.* as -0.64 eV. [105] For the fragment methoxy, it is reported as -1.49 eV. [108] The value for the binding energy of the formate fragment on the (110) facet is found to be -1.42 eV. [109]

Rhodium and iridium are extremely valuable and versatile transition metals for applications in heterogeneous catalysis. Natural reserves of rhodium are currently in rapid decline, and as a result Rh is by far the most expensive precious metal today. Hence, it is of great importance to find new catalysts with high activity and selectivity to replace the current generation of rhodium catalysts. Understanding the surface chemistry of rhodium might suggest efficient ways of proceeding with this catalyst design process. In particular, comprehending critical elementary reaction steps such as adsorption and bond breaking/making over rhodium surfaces can provide substantial insights into why rhodium is so essential in catalysis and as to how it can best be replaced. [110] On one hand, several theoretical studies have been performed to study chemisorption

and reactivity on rhodium surfaces. Periodic DFT calculations have been used to investigate adsorbates like atomic oxygen binding on Rh(111), [111–113] and the adsorption of other atomic species such as nitrogen, [112] sulfur, [114] and hydrogen [113] has also been considered on this surface. Zhang *et al.* carried out periodic DFT studies to determine interactions between chemisorbed CO and S on Rh(111). [114] Loffreda *et al.* performed periodic DFT calculations on rhodium (100) and (111) surfaces for molecular and dissociative chemisorption of nitric oxide. [112] Water formation on Rh(111) surfaces has also been explored using DFT, providing thermodynamic and kinetic parameters. [113] However, there is a lack of references in the literature dealing with the systems under study in the present Chapter, except for the work of Nakamura *et al.*, where the chemisorption of formate on some metal surfaces including Rh(110) are described. They point out the value of -1.73 eV as the binding energy of formate fragment to the (110) facet of the *fcc* rhodium structure. [109] On the other hand, iridium is a potential catalyst for the CO_x-free production of hydrogen from ammonia, [115] Ir and Ir-alloy catalysts are used in reactions that require the activation of C-H bonds, [116] and it is being considered for the improvement of the automobile catalytic converter because of its ability to decompose NO [117] and to reduce NO_x with hydrocarbons. [118] The desire to gain an understanding of the above processes has motivated much fundamental research on single-crystal iridium. Its interactions with atomic species have been the subject of several research studies. [119] Lim *et al.* studies on the field give the values for the binding energies of CH_2O and CH_2O_2 on Ir (100) of -1.39 and -0.63, respectively. [120]

Copper has a widespread use in a range of applications. It has been shown that copper catalyst, mostly used as a pure metal, is highly selective in the hydrogenation of edible oils and fats. [121] Hydrogenations with copper catalysts are milder than with their nickel or platinum counterparts, and they have selectivities that are exploited commercially. [122] The Cu/ZnO system has been extensively studied because it comprises the key components for the preponderate catalyst for the technologically important methanol synthesis from $CO/CO_2/H_2$ reactants and hydrogen production from methanol by the reverse water gas-shift reaction. [123–125] According to the results obtained by Gomes *et al.* using the cluster model approach for ethylene on the (110) surface of copper the atop adsorption site (the molecule adsorbed directly on top of a copper atom) is energetically more favoured than the shortbridge adsorp-

tion site (-0.60 vs -0.49 eV). [126, 127] In the case of formaldehyde, similar to previous finding, [128–131] Lim *et al.* calculations suggest that CH_2O binds very weakly to the Cu substrate with binding energies of about -0.25 eV [131] for all the Cu(100) surfaces studied. This is in good agreement with previously reported value of -0.11 eV for the CH_2O/Cu(111) system using PW91 GGA, [129] -0.46 eV for PBE GGA CH_2O/Cu(110) [132] system and $\sim$-0.2 eV for Cu_{22} B3LYP/6-31G** cluster model CH_2O/Cu(111) system. [130] The slightly higher binding energies obtained here compared to the Cu(111) surface [129, 130] are due to the more open and less coordinated surface Cu atoms in agreement when the current result is compared to the more open Cu(110) surface. [130–132] On Cu(110) formaldehyde is adsorbed in two different forms [133]: (i) Molecularly, with the C-O axis tilted away from the normal to the surface. This leads to overlap not only with the oxygen lone pair orbital but also with the C-O *p*-bonding orbital. (ii) In a polymeric form (paraformaldehyde), where there are only C-O single bonds, -(CH_2O)n-. This polymeric form was also found for CH_2O adsorption on Ag(110) and Ag(111). [130, 134, 135] Formaldehyde is also weakly adsorbed on the Cu(111) surface and the adsorption energy is close to -0.21 eV (-0.10 for Mavrikakis *et al.* [136] and -0.11 eV for Lim's team [137]). The almost unchanged internal structure of adsorbed formaldehyde when compared with this molecule in the gas phase results in the calculated low interaction energy for formaldehyde on the Cu(111) surface. [130] Finally, the adsorption energy for the most stable site of CH_2O on the (211) stepped facet is -0.46 eV as reported in the literature. [120, 129]

Although the most important industrial use of nickel is that of an alloying element in ferrous alloys to subsequently catalyse different reactions, it is also used by itself finely divided to catalyse the hydrogenation of olefins. The binding energy of acetylene on Ni(111) is reported to be -2.52 eV, [138] while for ethylene the value is -1.76 eV on the (100) facet. [139] Regarding to formaldehyde, it binds quite weakly on Ni(111); its binding energy is only -0.14 eV. In the lowest energy geometry, formaldehyde binds along a bridge Ni(111) site, with C and O bonded to one Ni surface atom each. Methanol has no unsaturated bonds, and as it is the lowest molecular weight alcohol it is not expected to bind strongly to a metal surface. Indeed, the strongest binding energy Nørskov *et al.* calculated for methanol on Ni(111) was only -0.02 eV, whereas its radical methoxy binds through oxygen on top of a Ni atom, with binding energy of -1.86 eV compared to the free radical. [140] Formate rad-

ical adsorbs on the (110) surface of nickel giving a value for the binding energy of -1.71 eV. [109] Finally, hydrogen cyanide, CHN, adsorption on Ni(111) is likely to adsorb either perpendicularly to the surface through the lone-pair of the nitrogen atom or flat with the C-N bond parallel or tilted with respect to the metal surface. The parallel adsorption modes are energetically favoured over the perpendicular ones. The most stable adsorption state for CHN involves two adjacent *hcp* and *fcc* 3-fold hollow sites and shows a binding energy of -1.50 eV. [141, 142]

To come to an end with the analysis of previous works, it is worth mentioning that metallic silver and gold applications as catalysts are increasingly focused on their size-dependent properties. By way of illustration, Dong Chan Lim carries out some studies about oxidation patterns of Ag and Au nanoparticles and shows that uptakes of oxygen of smaller nanoparticles are significantly higher than those of larger particles and bulk-like metal, [143] what means that the reactivity decreases with the growth of the particle. Therefore, in the framework of the present work, articles in the literature referring to bulk-like surfaces of silver and gold are scant. On one hand, Gomes *et al.* disclose a value of -0.35 eV for the binding energy of C_2H_2 on Ag(110), [126] whereas for the formate radical also on Ag(110) it is found to be -0.62 eV. [109] In the other hand, gold surface adsorption properties are described by Lu *et al.*, giving binding energies on Au(111) of -0.25, -1.00, and -0.57 eV for CH_3OH, CH_3O, and CH_2O eV, respectively. [144] This property for C_2H_4 on Au(110) has a value of -0.44 eV, [78] for CH_2O_2 on the (100) facet is -0.19 eV, [145] and for its radical, CHO_2, on Au(110) the binding energy is -0.15 eV. [109]

4.2 Computational details

Density Functional Theory, DFT, has been used to determine the binding energies of the following organic molecules and fragments: acetylene (C_2H_2), ethylene (C_2H_4), formaldehyde (CH_2O), hydrogen cyanide (CHN), methanol (CH_4O), formic acid (CH_2O_2), as well as methoxy (CH_3O) and formate radicals (CHO_2), each of them adsorbed on the (100), (110), (111), and (211) facets of the stable *fcc* crystallographic structure of eight monometallic systems of transition metals: Pd, Pt, Rh, Ir, Cu, Ni, Ag, and Au, moreover testing various sites on each surface.

DFT calculations were performed with the Vienna Ab-initio Simulation Package, VASP. [146] The Revised Perdew-Burke-Ernzerhof, RPBE, has been employed as exchange-correlation functional to obtain the energies with no van der Waals interactions taken under consideration. [43] Monoelectronic states corresponding to the valence electrons were expanded in plane waves with a kinetic cutoff energy of 400 eV, while the core electrons were represented by Projector Augmented Wave, PAW, pseudopotentials. [75] A finite temperature of $k_BT = 0.2$ eV is used in order to avoid the discontinuous jump in the occupancy of states at the Fermi level at 0 K. Spin polarization is needed for the Ni calculations. When the dispersion forces are taken into account, two kinds of approximations have been used, *i.e.* the DFT-D2 and the vdW-DF methods, [147, 148] both of them already described in detail in Chapter 2.

4.3 Monometallic systems

As said above, calculations have been performed for a series of transition metals, *i.e.* Pd, Pt, Rh, Ir, Cu, Ni, Ag, and Au, in a faced-centred cubic structure, *fcc*, which is the most stable for all of them. Metal bulk properties have been calculated performing a Brillouin zone integration with 5x5x1 k-point grids, generated with the Monkhorst-Pack method. [71]

Table 4.1: Calculated (*calc*) cell parameters, a (in Å), versus the experimental (*exp*) ones. $Error(\%) = \frac{a_{calc} - a_{exp}}{a_{exp}} 100$

	Rh	Ir	Ni	Pd	Pt	Cu	Ag	Au
a_{calc}	3.856	3.879	3.551	3.987	3.990	3.676	4.227	4.208
a_{exp}	3.803	3.839	3.524	3.891	3.924	3.615	4.085	4.078
Error(%)	1.37	1.03	0.76	2.41	1.65	1.60	3.36	3.09

4.3.1 Bulk parameters

The cell paremeter, a, optimization has been performed by calculating the energies for a set of a in a region close to the experimental value. A solid has a certain equilibrium volume, V_0, and the energy increases quadratically as volume is increased or decreased a

small amount from that value. The simplest dependence of energy on volume would be a harmonic solid, with:

$$E = E_0 + \frac{1}{2k_T}\frac{(V - V_0)^2}{V_0} \tag{4.1}$$

where k_T, the isothermal compressibility, is a measure of the relative volume change of a solid as a response to a pressure change at constant temperature.

$$k_T = -\frac{1}{V}\left(\frac{\partial V}{\partial P}\right)_T \tag{4.2}$$

The theoretical and experimental cell parameters are compiled in Table 4.1, showing that the former are larger than the latter ones. This agrees with previous benchmarks with the RPBE functional. The agreement between the two sets of data is quite good, as can be seen in the *Error (%)* column, being all of them below 3.5%.

Table 4.2: Cohesive energies, E_{coh}, in eV/atom and differences between the experimental and calculated values, ΔE, same units.

	Rh	Ir	Ni	Pd	Pt	Cu	Ag	Au
E_{coh} Calculated	-4.87	-6.22	-4.04	-3.04	-4.63	-2.75	-1.69	-2.21
E_{coh} Experimental	-5.29	-6.94	-4.44	-3.89	-5.84	-3.49	-2.95	-3.81
Error (ΔE)	0.42	0.72	0.40	0.85	1.21	0.74	1.26	1.60

4.3.2 Cohesive energy

The cohesive energy, E_{coh}, of a solid is the energy required to break the atoms of the solid into isolated species, that is:

$$E_{coh} = E_{bulk} - \sum_A E_A^{isolated} \tag{4.3}$$

where E_{bulk} is the solid energy and the label A represents the different atoms that constitute it. The results for the eight metals are compiled in Table 4.2. The correlations with experimental values are not as good as desirable because the value E_{coh} is severely affected by the estimation of the atomic energy. Since pseudopotentials are fitted to describe metals, they might not be 100% transferable to represent the isolated atoms in their gas-phase ground state.

Indeed, for palladium the gas-phase configuration is not the experimentally observed. With the present approach the isolated atomic metal atoms are sometimes not properly described.

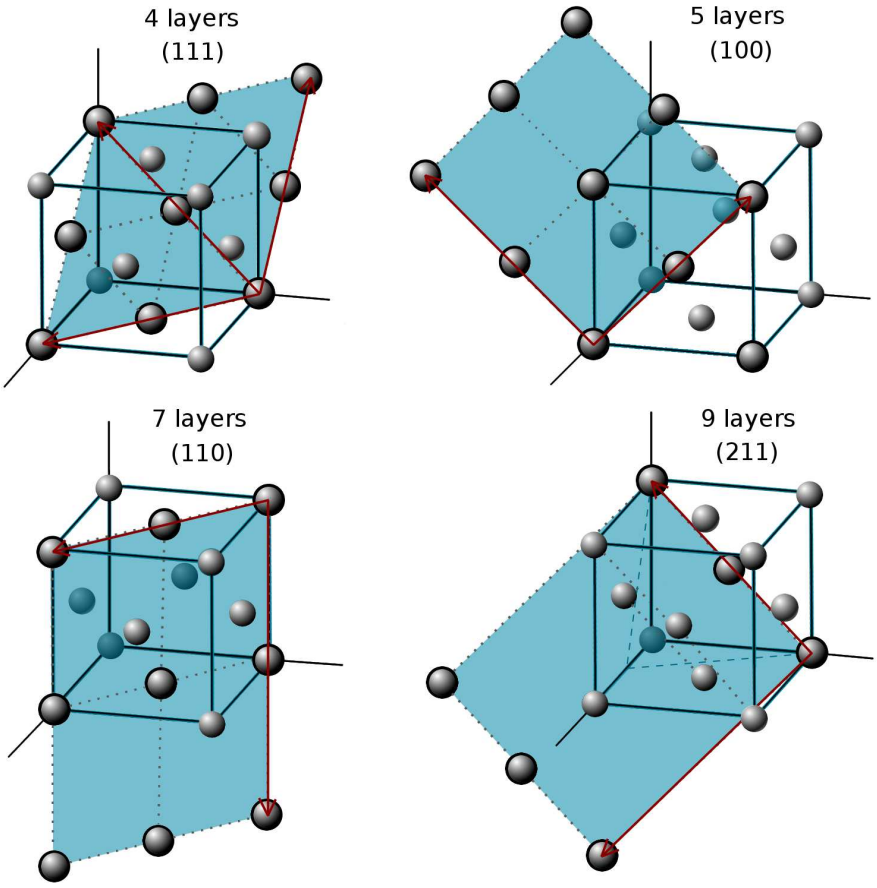

Figure 4.1: (111), (100), (110), and (211) surfaces in a faced-centered structure.

4.3.3 Crystallographic facets

The surrounding surface of any piece of crystalline material is made up of various facets with different atomic arrangements, and therefore unlike properties, as has been seen in Section 1.2.2. In order to analyze the reactivity of a specific material a set of its faces should be considered. In the present Chapter, the (111), (110), and (100) as stable surfaces, and (211) as model with defect, of *fcc* crystals have been considered. See Figures 4.1 and 4.2. We have seen

in Section 1.2.1 that the (111) surface of an *fcc* crystal consists on a triangular ensembles, the (110) and (100) surfaces show rectangular and square shapes, respectively, and the (211) one, non-planar rectangular contour.

In all cases in the present Chapter, surfaces have been modelled with a $p(2x2)$ supercell. The (111) surfaces have been performed by 4-layer slabs, the (100) and (110) ones by 5 and the (211) surfaces contain 9-layer slabs, since the more compact the crystal is, the less its atoms can move. The three kinds of supercell are separated by a vacuum layer larger than 12 Å. The top two metal layers were allowed to relax in the (111) and (110) surfaces, and the third and fourth layers were fixed to the bulk values in order to represent the bulk of the material. In the case of the (100) and (211) surfaces, the top three metal layers were allowed to relax, and the rest were fixed.

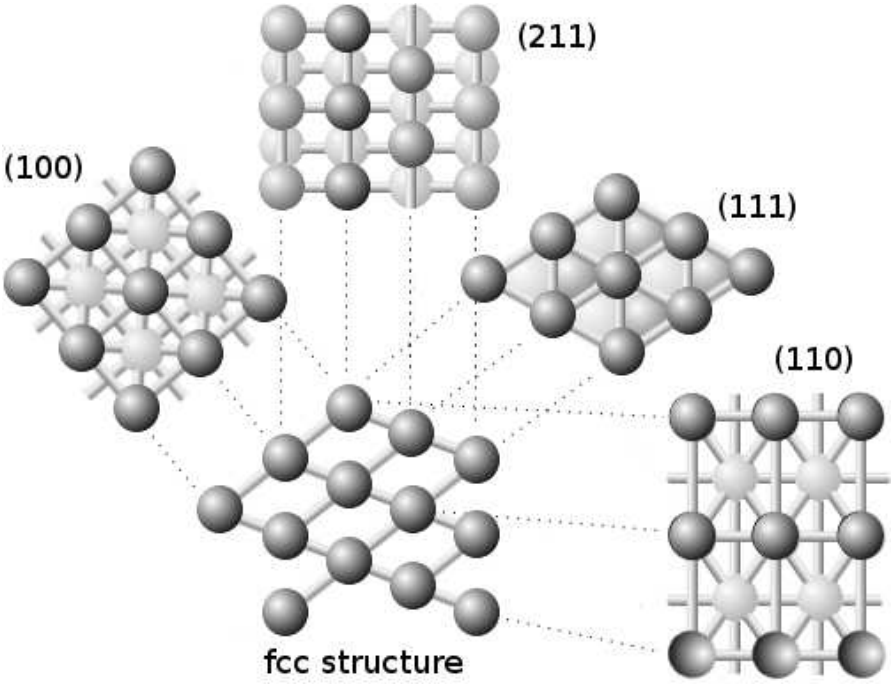

Figure 4.2: (111), (100) and (211) surfaces in a faced-centered structure.

Table 4.3: Surface energies, γ, in J/m^2; and *% relax* of (111), (100) and (211) surfaces of Rh, Ir, Ni, Pd, Pt, Cu, Ag and Au metals, in the case of (211) surface.

	γ			*% relax*		
Metal	(111)	(100)	(211)	(111)	(100)	(211)
Rh	1.76	2.07	2.49	-0.155	-0.114	-1.033
Ir	1.87	2.54	3.00	-0.138	-0.152	-1.110
Ni	1.69	1.96	2.23	-0.035	-0.083	-0.703
Pd	1.01	1.19	1.58	-0.001	-0.003	-0.906
Pt	1.29	1.63	1.81	-0.016	-0.057	-0.323
Cu	1.17	1.93	1.46	-0.003	-0.066	0.041
Ag	0.59	0.63	0.75	-0.001	-0.003	-0.004
Au	0.63	0.76	0.79	0.025	0.707	-0.003

4.3.4 Surface energy and relaxation

In a bulk material, all the bonding requirements of its constituent atoms are filled by other atoms. However, atoms on the surface of the adsorbent are not wholly surrounded by other adsorbent atoms and therefore can attract adsorbates. As a consequence, the formation of surfaces is energetically costly. Surface energy, γ, quantifies the disruption of chemical bonds, that occurs when a surface is created, giving an estimation of the stability of the surface and can be obtained in a slab calculation as follows:

$$\gamma = \gamma^{unrel} + E^{rel} \tag{4.4}$$

where E^{rel} is the energy change after relaxation, and γ^{unrel} is:

$$\gamma^{unrel} = \frac{1}{2}\left(E_{surf} - N_{atoms}E_{bulk}\right) \tag{4.5}$$

E_{surf} is the total energy of the unrelaxed surface, N_{atoms} is the total number of atoms in the slab and E_{bulk} is the energy of a bulk atom. Relaxation is a small rearrangement of the surface layers. It involves adjustments in the layer spacings perpendicular to the surface, there is no change either in the periodicity parallel to the surface or to the symmetry of the surface. The surface relaxation has been calculated as:

$$\%\, relax = \frac{Z_{s-relax} - Z_{s-unrelax}}{d_{(hkl)interplanar}} * 100 \tag{4.6}$$

where $d_{(hkl)interplanar}$ is the (hkl) interplanar distance, $a/\sqrt{3}$ for the (111) surface and $a/2$ for the (100), and the difference $Z_{s-relax} - Z_{s-unrelax}$ is the change of the surface position after relaxation. Table 4.3 shows that most values of relaxation are negative, what means that the surface layer of atoms is pulled in towards the second layer. These results are in line with those previously reported by experimental and theoretical investigations. [149, 150]

4.4 Molecular adsorption

4.4.1 Adsorption sites

The number of adsorption sites on a surface per unit area follows straightforwardly from the geometry. In Figure 4.3, definition of the most common adsorption sites on facets under study are shown. They are named on-top site, bridge sites (long or short bridge), and hollow sites, which may be three-fold or four-fold in character. In case of three-fold adsorption on the *fcc*(111) surface it is also necessary to distinguish between *hcp* and *fcc* sites, having an atom just below the site or not, respectively. Consider, for example, adsorption on a four-fold hollow site on the (100) surface. The number of available sites is simply the number of unit cells with area $\left(a/\sqrt{2}\right)^2$ per m^2, where a is the cell parameter of the *fcc* lattice.

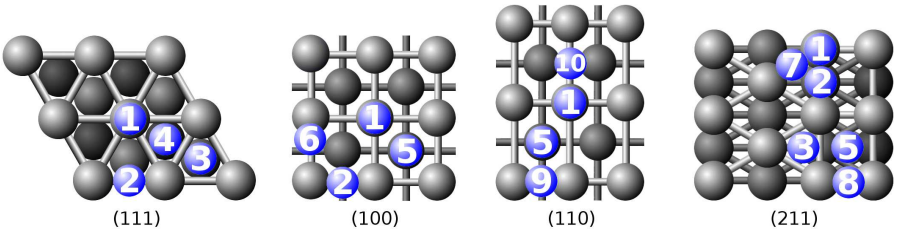

Figure 4.3: Adsorption sites on the four types of surfaces used in the present studies of adsorption. Number 1 corresponds to the adsorption on top of a metal atom (called t or t_e for (211) from now on, where the subscript e stands for edge), 2 is the adsorption on a bridge position (b or b_e for (211)), 3 on a three fold hollow (*fcc*/f of h_{111} for (211)), 4 on a three fold hollow (*hcp*), 5 on a four fold hollow (h), 6 top-bridge (tb), 7 bridge (b_{100}), 8 bridge (b_{111}), 9 short bridge on (110) (sb), and 10 long bridge also on (110) (lb).

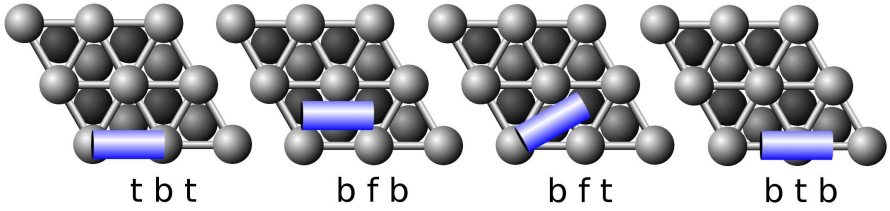

Figure 4.4: Adsorption sites on the (111) surface. See also Figure 4.3.

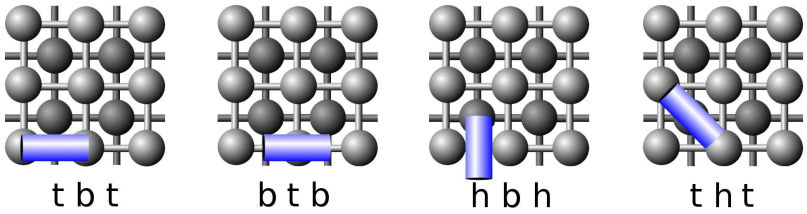

Figure 4.5: Adsorption sites on the (100) surface. See also Figure 4.3.

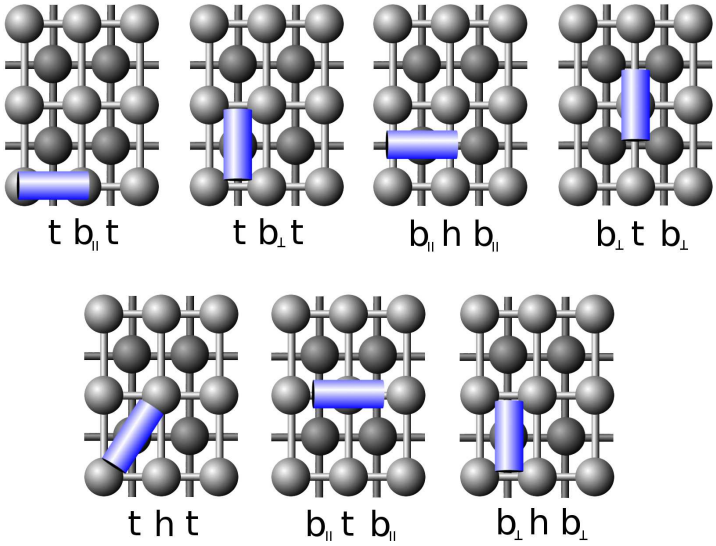

Figure 4.6: Adsorption sites on the (110) surface. See also Figure 4.3.

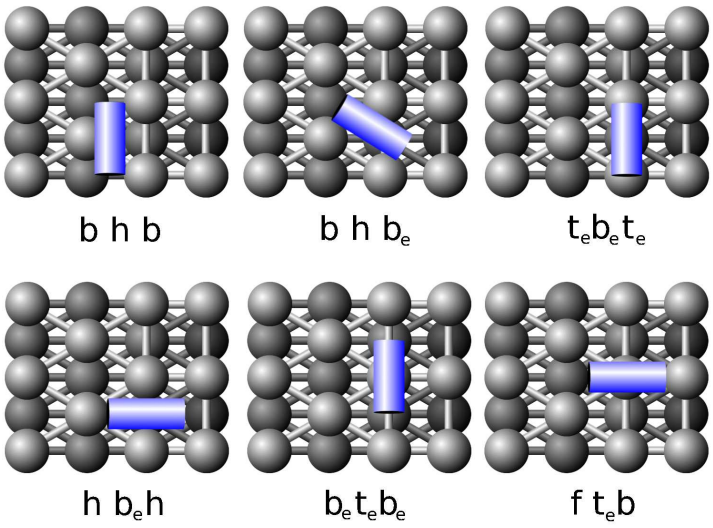

Figure 4.7: Adsorption sites on the (211) surface. See also Figure 4.3.

4.4.2 Adsorption energies

In this section, the adsorption of all molecules and fragments mentioned in Section 4.3, in addition to C, O, N, and H atoms on the four crystallographic facets (already seen in the previous Section) of the eight considered transition metals are described. Binding energies and geometric structures were calculated with the adsorbates occupying different adsorption sites, described in Figures 4.4 to 4.7, in order to find out the most stable one for each of them.

Tables 5.6 to 5.15, shown in the Appendix for clarity, let us see all data obtained from all positions. They have been divided into crystallographic faces: Tables 5.10 (molecules and fragments) and 5.6 (atoms), correspond to the adsorption on the (111) facet. Tables 5.13 and 5.8, to the adsorption on the (100) facet. Then, Tables 5.11, 5.12 and 5.7, to the adsorption on the (110) facet. Finally, Tables 5.14, 5.15 and 5.9, on the (211) facet. The adsorption sites are described in Figures 4.4 to 4.7.

In general, the order in the energies, from strongest to weakest bond, is $E_C > E_N > E_O > E_H$. On the other hand, regarding to the metals, their activity can be divided into their groups in the periodic system, that is, 9-group (Rh, Ir), 10-group (Ni, Pd, Pt), and 11-group (Cu, Ag, Au). The order in the activity so observed

is 9-group > 10-group > 11-group. That is consistent with proximity of the Fermi level to the top of the *d*-band, in other words, the larger amount of empty levels there are, the more active the metal is. These characteristics explained above are general for all the facets, (111), (100), (110), and (211), as it only depends on the adsorbates and the metals.

Table 5.6, where the adsorption energies of C, O, N, and H on the (111) facet are shown, we can see that the energy of the atoms of each occupied site depends on their valence, as previously supposed by Abild-Pedersen. [22] In the case of carbon atom, for instance, the adsorption on any of the two hollows is more exothermic than on top of a metal atom. It makes sense, since the valence for this atom is four. Along the series, this feature decreases, as the valence also does it. So, for hydrogen, all the energies are similar, as there are not preference sites. Thus, the potential energy surface corrugation is the smallest and the diffusion of H is faster than that of C, N, and O.

Table 5.10 compiles the results for the adsorption of molecules (C_2H_2, C_2H_4, CH_2O, CHN, CH_4O, CH_2O_2), and fragments (CH_3O, CHO_2) on the (111) surface and shows that gold is not a good metal for adsorption when performing surfaces from bulks, and silver and copper reach endothermic adsorption in most cases (see Figure 1.7), as the binding energies are positive. The rest of the metals adsorb exothermically. In general, each molecule (and fragment) seems to have a preferential adsorption site regardless of the metal. On the other hand, C_2H_2, C_2H_4, CH_2O, and CHN molecules are good adsorbates, except on the 11-group metals. The case of CH_4O and CH_2O_2 is different, as they do not usually adsorb, probably due to steric effects and to the lack of π-orbitals, since none of they two achieves a bond order of two. The way to adsorb them would be as fragments, that is, CH_4O as CH_3O + H and CH_2O_2 as CHO_2 + H, since all of them can easily be adsorbed on any surface.

For the (100) surfaces, the adsorption energies are shown in Tables 5.8 and 5.13. The former reports atoms and the latter the molecules and fragments. Basically, the same features than in the case of (111) surfaces can be observed, but considering a few exceptions. First of all, the adsorption sites are not equivalent (see Figures 4.3, 4.5, and 4.4). As the (100) surface is less dense than the (111) one, it is also more reactive, so the adsorption energies are, in general, more negative (stronger bond). For instance, it renders Cu much more active since many adsorption energies for the investi-

gated fragments are exothermic in this case, unlike the (111) surface.

To come to an end regarding to the adsorption energies, Tables 5.9, 5.14, and 5.15 compile atoms and molecules adsorption energies, respectively, on (211) surfaces. See Figures 4.3 and 4.4 for the adsorption sites. The step is the most reactive part of the surface since the coordination number of its atoms is larger. Another feature to emphasize here is that the step presents higher activity binding highly unsaturated molecules: the C_2H_2 and CHN molecules have stronger adsorption energy on the defect than that of the rest of the studied molecules, as they have a bond order of three.

The next six tables (Tables 4.6-4.11) show the most stable adsorption sites for each adsorbate and facet; (111) for Tables 4.4 and 4.5, (100) for 4.6 and 4.7, (110) for 4.8 and 4.9, and (211) for 4.10 and 4.11, being on each surface the former for the adsorption of atoms and the latter for the molecules.

Table 4.4: Most stable atomic adsorption energies with respect to the gas phase species, in eV, on (111) metal surfaces. In Table 5.6 of the Appendix all the sites tested and their energies are shown.

(111)	Adsorbates			
Metal	C	O	N	H
Rh	-6.87	-4.97	-4.94	-2.67
Ir	-6.64	-4.60	-4.63	-2.57
Ni	-6.51	-5.37	-4.93	-2.68
Pd	-6.46	-4.19	-4.22	-2.68
Pt	-6.67	-4.02	-4.35	-2.58
Cu	-4.61	-4.68	-3.41	-2.31
Ag	-3.24	-3.52	-1.87	-1.99
Au	-4.03	-2.95	-2.19	-2.11

Table 4.5: Most stable molecular adsorption energies with respect to the gas phase species, in eV, on (111) metal surfaces. See Table 5.10.

(111)	Adsorbates							
Metal	C_2H_2	C_2H_4	CH_2O	CHN	CH_4O	CH_2O_2	CH_3O	CHO_2
Rh	-2.07	-0.48	-0.39	-0.82	0.00	0.48	-1.61	-1.69
Ir	-2.01	-0.39	-0.13	-0.46	0.02	-0.10	-1.42	-1.15
Ni	-1.67	-0.13	-0.33	-0.72	0.04	0.42	-1.76	-1.82
Pd	-1.38	-0.37	-0.21	-0.45	0.44	0.28	-1.26	-1.25
Pt	-1.63	-0.62	-0.01	-0.49	0.04	0.15	-1.19	-0.71
Cu	-0.42	0.22	0.26	0.27	0.03	0.13	-1.67	-1.85
Ag	0.27	0.24	0.11	0.07	0.06	0.26	-1.32	-1.83
Au	0.28	0.07	0.02	0.05	0.04	0.04	-0.69	-0.85

Table 4.6: Most stable atomic adsorption energies with respect to the gas phase species, in eV, on (100) metal surfaces. See Table 5.8.

(100)	Adsorbates			
Metal	C	O	N	H
Rh	-7.61	-4.92	-5.11	-2.61
Ir	-7.62	-4.84	-4.82	-2.81
Ni	-7.69	-5.54	-5.62	-2.61
Pd	-7.53	-5.33	-4.32	-2.56
Pt	-7.33	-4.11	-4.04	-2.78
Cu	-6.86	-6.04	-5.26	-3.27
Ag	-4.03	-3.82	-2.39	-1.84
Au	-4.52	-2.91	-2.09	-2.12

Table 4.7: Most stable molecular adsorption energies with respect to the gas phase species, in eV, on (100) metal surfaces. See Table 5.13.

(100)	Adsorbates							
Metal	C_2H_2	C_2H_4	CH_2O	CHN	CH_4O	CH_2O_2	CH_3O	CHO_2
Rh	-2.41	-0.54	-0.20	-1.30	0.01	0.08	-2.04	-1.72
Ir	-2.87	-0.61	-0.10	-1.42	0.05	0.13	-2.01	-1.79
Ni	-2.06	-0.33	-0.22	-1.25	0.05	0.26	-2.24	-1.85
Pd	-2.01	-0.45	-0.04	-0.96	-0.02	0.10	-1.54	-1.35
Pt	-2.72	-0.70	0.05	-1.15	0.06	0.07	-1.58	-1.06
Cu	-1.84	-1.01	-0.97	-0.92	-1.03	-1.12	-3.09	-3.17
Ag	0.31	0.28	0.04	0.17	0.02	0.15	-1.48	-2.05
Au	-0.18	0.08	0.07	0.09	0.05	0.15	-1.06	-1.27

Table 4.8: Most stable atomic adsorption energies with respect to the gas phase species, in eV, on (110) metal surfaces. See Table 5.7.

(110)	Adsorbates			
Metal	C	O	N	H
Rh	-7.15	-5.05	-4.83	-2.53
Ir	-6.94	-5.33	-5.28	-2.65
Ni	-7.08	-5.07	-5.01	-2.52
Pd	-7.23	-3.98	-4.39	-2.54
Pt	-6.96	-4.24	-4.32	-2.64
Cu	-5.06	-4.35	-3.46	-2.22
Ag	-3.40	-3.40	-1.86	-1.90
Au	-3.84	-2.92	-1.69	-2.05

Table 4.9: Most stable molecular adsorption energies with respect to the gas phase species, in eV, on (110) metal surfaces. See Tables 5.11 and 5.12.

(110)	Adsorbates							
Metal	C_2H_2	C_2H_4	CH_2O	CHN	CH_4O	CH_2O_2	CH_3O	CHO_2
Rh	-1.88	-0.77	-0.43	-1.58	0.01	0.11	-1.87	-2.80
Ir	-2.19	-1.05	-0.66	-1.67	-0.05	0.27	-2.11	-3.03
Ni	-1.84	-0.65	-0.67	-2.02	-0.07	0.19	-2.24	-2.90
Pd	-1.66	-0.06	-0.22	-1.46	-0.13	0.17	-1.51	-2.01
Pt	-1.70	-0.96	-0.29	-1.74	-0.05	0.15	-1.70	-2.37
Cu	-0.59	-0.14	-0.05	-0.63	-0.03	0.13	-1.93	-2.61
Ag	0.08	0.04	0.01	-0.53	-0.01	0.10	-1.36	-2.28
Au	0.13	-0.01	0.05	-0.46	0.02	0.23	-0.91	-1.70

Table 4.10: Most stable atomic adsorption energies with respect to the gas phase species, in eV, on (211) metal surfaces. See Table 5.9.

(211)	Adsorbates			
Metal	C	O	N	H
Rh	-7.12	-5.17	-5.17	-2.70
Ir	-7.12	-5.51	-5.30	-2.90
Ni	-6.56	-5.45	-5.01	-2.67
Pd	-6.81	-4.22	-4.42	-2.66
Pt	-6.92	-4.62	-4.53	-2.85
Cu	-4.61	-4.75	-3.41	-2.38
Ag	-3.11	-3.44	-1.70	-1.99
Au	-3.99	-3.00	-1.94	-2.14

Table 4.11: Most stable molecular adsorption energies with respect to the gas phase species, in eV, on (211) metal surfaces. See Tables 5.14 and 5.15.

(211)	Adsorbates							
Metal	C_2H_2	C_2H_4	CH_2O	CHN	CH_4O	CH_2O_2	CH_3O	CHO_2
Rh	-2.25	-0.97	-0.71	-1.22	-0.08	0.04	-2.16	-2.74
Ir	-2.67	-1.25	-0.80	-1.33	-0.48	-0.13	-2.29	-2.28
Ni	-1.85	-0.57	-0.68	-1.14	-0.41	0.01	-2.22	-2.59
Pd	-1.88	-0.71	-0.43	-0.78	-0.06	0.09	-1.62	-1.86
Pt	-2.33	-0.97	-0.59	-0.83	-0.09	0.36	-1.75	-1.71
Cu	-0.60	-0.06	-0.02	0.02	-0.02	0.10	-2.27	-2.43
Ag	0.17	0.02	0.16	0.06	0.01	0.18	-1.52	-2.3
Au	0.06	-0.02	0.08	0.11	0.09	0.13	-0.97	-1.46

In addition, a few correlations with the data presented above have been plotted (Graphs 4.8 to 4.11). Graphs 4.8 and 4.9 show the C_2H_2 and C_2H_4 binding energies *vs.* C atom binding energy, BE_C; the former on the (111) and the latter on the (211) metal surfaces. In Graph 4.10, CHN binding energy *vs.* E_x on (211) can be seen. E_x is described as follows:

$$E_x = \frac{\chi_C}{\chi_C + \chi_N} BE_C + \frac{\chi_N}{\chi_C + \chi_N} BE_N \tag{4.7}$$

where χ is Pauling electronegativity and BE the carbon and nitrogen binding energies. In this way, the heteronuclear nature of CHN is taken into account. The last graph, 4.11, accounts for the CH_3O adsorption energy versus BE_O on (111) surfaces due to the monohapticity of the CH_3O radical.

As can be seen, adsorption energies of different molecules can be scaled with those of their constituent atoms, when these are directly bound to the surface. This correlations throw light on the quest of a good set of descriptors that simplify and reduce cost of calculations, one of our aims in the present Chapter. Descriptors can be employed to guide the calculations of new complex compounds such as those derived from biomass.

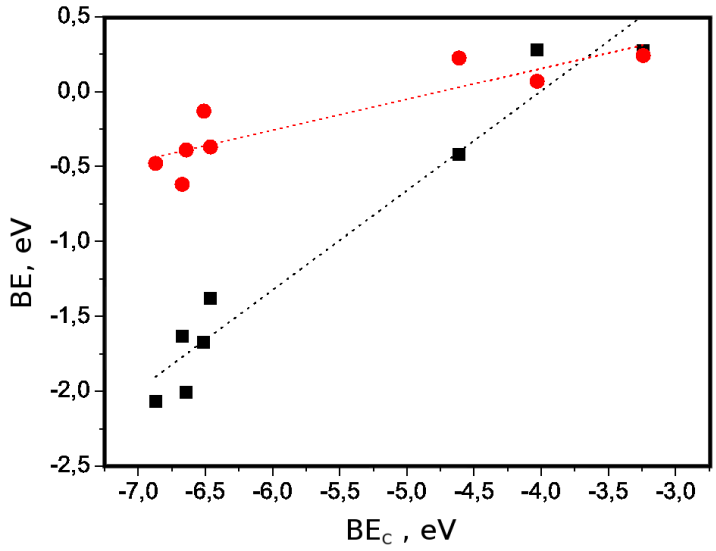

Figure 4.8: C_2H_2 (black) and C_2H_4 (red) binding energies, BE, *vs.* carbon atom binding energy, BE_C, on (111) metal surfaces. All energies in eV.

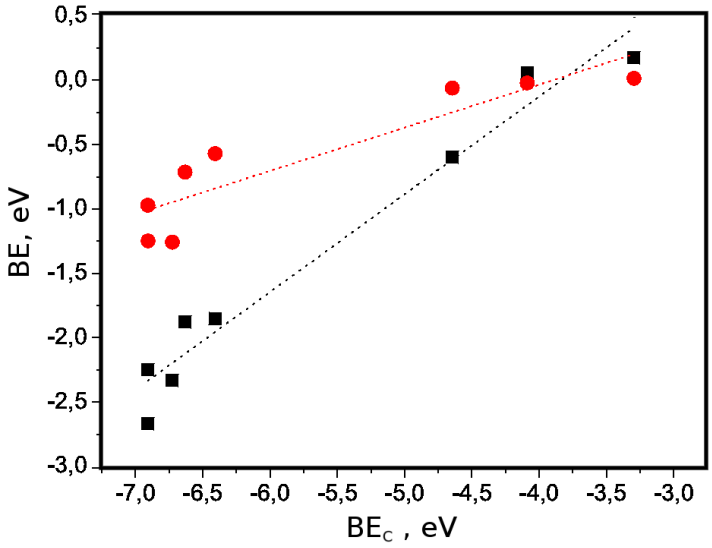

Figure 4.9: C_2H_2 (black) and C_2H_4 (red) binding energies, BE, *vs.* carbon atom binding energy, BE_C, on (211) metal surfaces. All energies in eV.

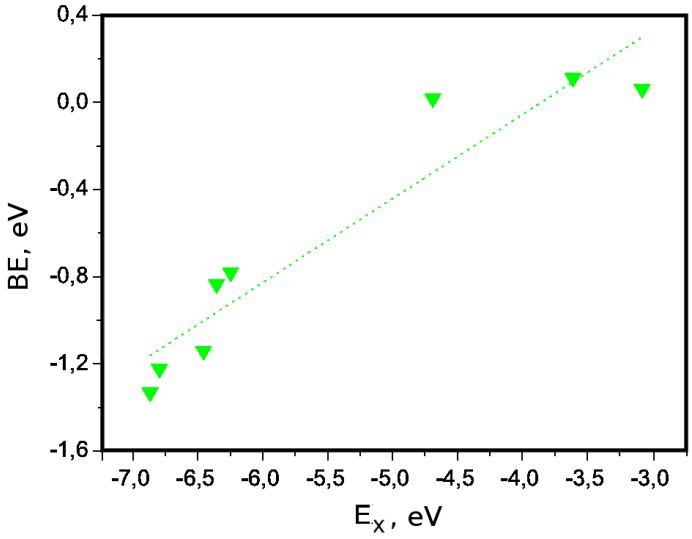

Figure 4.10: CHN binding energies, BE, *vs.* E_x, on (211) metal surfaces. All energies in eV.

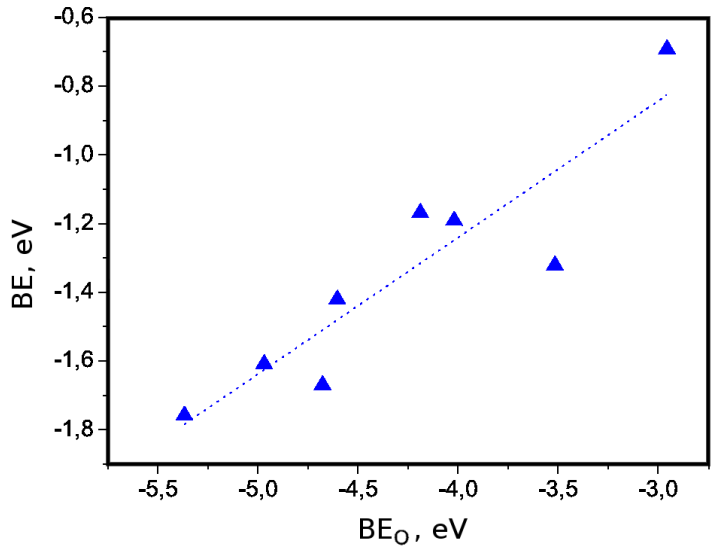

Figure 4.11: CH_3O binding energies, BE, *vs.* BE_O, on (111) metal surfaces. All energies in eV.

Revised Perdew-Burke-Ernzerhof exchange model

Traditional Density Functional Theory (DFT) calculations do account for the chemical regime in which bonds are strong. However they do not consider other kinds of weaker bonds, like the ones based on dispersion. This problem was not estimated acute enough when describing reactions at surfaces as in general strong binding of reactants is a requirement and even GGA can provide results comparable to experiments. [11, 33] Nevertheless, van der Waals interactions can be essential in many studies, such as systems controlled by thermodynamic factors [151] with large molecules considered, [152, 153] or when multiple minima with different degrees of dispersion contributions (*i.e.*, solvent effects [154]) are present. The achievement of these objectives depends on the ability of the theoretical methods to describe the interaction between a molecule or a molecular layer and a substrate of choice properly. [155]

van der Waals interactions

Generalized Gradient Approximations have a serious shortcoming despite the success of traditional DFT, *i.e.* they do not account for dispersion or van der Waals (vdW) interactions that result from dynamical correlations between fluctuating charge distributions. Different approximations have been proposed during the last years to account for dispersion interactions. By way of illustration, some of the most popular ones will be enumerated. Lundqvist *et al.* [32, 59, 60, 156–158] proposed a non-local correlation functional that accounts for dispersion interactions approximately. The drawbacks of this approach lay both in its computational cost and its extreme sensitivity to the judicious combination of the local and non-local contributions to the functional. [32, 159] Another example of approximation that accounts for dispersion interactions is the Random Phase Approximation (RPA), combined with the Adiabatic Connection and Fluctuation Dissipation Theorem (ACFDT) as proposed by Kresse and Harl [160] calculates the vdW energy accurately but at the expense of a huge computacional cost. Therefore, this method can be employed as a criterion in small calculations to evaluate the reliability of less sophisticated approaches.

A pragmatic semiempirical approach was provided by Grimme *et al.* [12, 57] This method consists in adding a semi-empirical dispersion potential to the conventional Kohn-Sham DFT energy, where the van der Waals interactions are described via a simple pair-wise

force field from the London formula, [51] which is optimized for several popular DFT functionals, leading to the C_6R^{-6} term. More recently, Bučko *et al.* [161] applied Grimme's DFT-D2 method [57] to a large number of solids showing a wide range of chemical bonds: molecular, ionic and covalent. The authors indicate that PBE-D2 performs very well also for systems in which the van der Waals interactions are not supposed to play an important role, which indicates that this approach can be used for arbitrary systems regardless of the nature of dominant interactions. [161] Moreover, a careful choice of the substrate interaction coefficient C_6 [162, 163] provides a good starting point to study the adsorption of molecules and films on conducting metal surfaces [11] and, potentially, on ionic or semiconducting solids. [163] Thus the Grimme or similar approaches constitute the minimum meaningful theory level when van der Waals interactions are important, *i.e.* in layered compounds (as PtO_2), or in physisorption. [32]

Even if the DFT-D2 method has been proposed as suitable to describe the adsorption of molecules on conducting metal surfaces, [162, 164, 165] there has been a heated debate on the way to obtain the metal interaction coefficient, C_6. It is now well established that the use of this parameter from the corresponding atomic properties can lead to an overbinding. A recent improvement by Tonigold and Groß[164] derived the parameters of the C_6R^{-6}-type correction employing a hybrid QM:QM approach, where the dispersion energy is approximated as the difference between the adsorption energies of the MP2 calculations and the adsorption energy of the DFT-PBE ones fitting the energy difference to obtain the C_6 terms. [164] Another approach to determine the metal interaction coefficient has been proposed by Tkatchenko *et al.* [162] who employed the Lifshitz-Zaremba-Kohn (LZK) [166, 167] theory for the vdW interaction between an atom and a solid surface, which includes the many-body collective response of the substrate electrons in the determination of the C_6 parameter and leads to a reduction of C_6 by up to a factor of 4 for coinage metals. [11, 159]

4.5 A particular case: adsorption on Pt(111)

In order to evaluate the reliability of calculations performed with the different methods used in the present Chapter, *i.e.* PBE, RPBE, PBE-D2, and RPBE-D2, a paradigm of metallic surface as

Table 4.12: Binding energies, in eV, on the (111) facet of Pt. Some of the data obtained with different methods in the current Chapter can be compared with reported theoretical and experimental values. Micro. means microcalorimetry, FD: stands for Flash Desorption, TPD: Temperature Programmed Desorption, t: top, b: bridge, and f: *fcc* hole.

Pt(111)		C_2H_2	C_2H_4	CH_2O	CH_4O	CH_3O
	Site	bfb	tbt	tbt	bfb	btb
Reported data	Theoretical BE	-2.17 [168]	-1.05 [169]	-0.54 [11]	-0.51 [11]	-1.67 [170]
	Method	PW91	PW91	PBE-D2	PBE-D2	PW91
	Experimental BE	-2.07 [171]	-1.24 [171]	-0.57 [172]	-0.49 [133]	-
	Method	Micro.	Micro.	FD	TPD	-
Our data	PBE	-2.18	-1.05	-0.46	-0.12	-1.54
	PBE-D2	-2.52	-1.48	-0.75	-0.29	-2.22
	$\triangle$E	0.33	0.44	0.29	0.16	0.68
	RPBE	-1.64	-0.62	-0.05	0.05	-1.18
	RPBE-D2	-2.04	-1.06	-0.35	-0.10	-1.90
	$\triangle$E	0.39	0.44	0.30	0.15	0.72

widely used industrial catalyst has been chosen to compare its theoretical binding energies with the reported experimental and theoretical ones. See Table 4.12 and Figure 4.12.

As can be seen in both Table 4.12 and Figure 4.12, in general, different functionals involve unlike results in Computational Chemistry. In this case, four functionals have been used, two of them with the vdW dispersion included and the other two without it. Although PBE results get quite close to the the experimental values taken from the literature, [133, 171, 172] probably due to error compensation, the best results are in all cases the ones that count for the dispersion, in particular, the RPBE-D2. We can see that RPBE throws binding energies too weak comparing with the experimental data, while PBE-D2 overshoots dramatically.

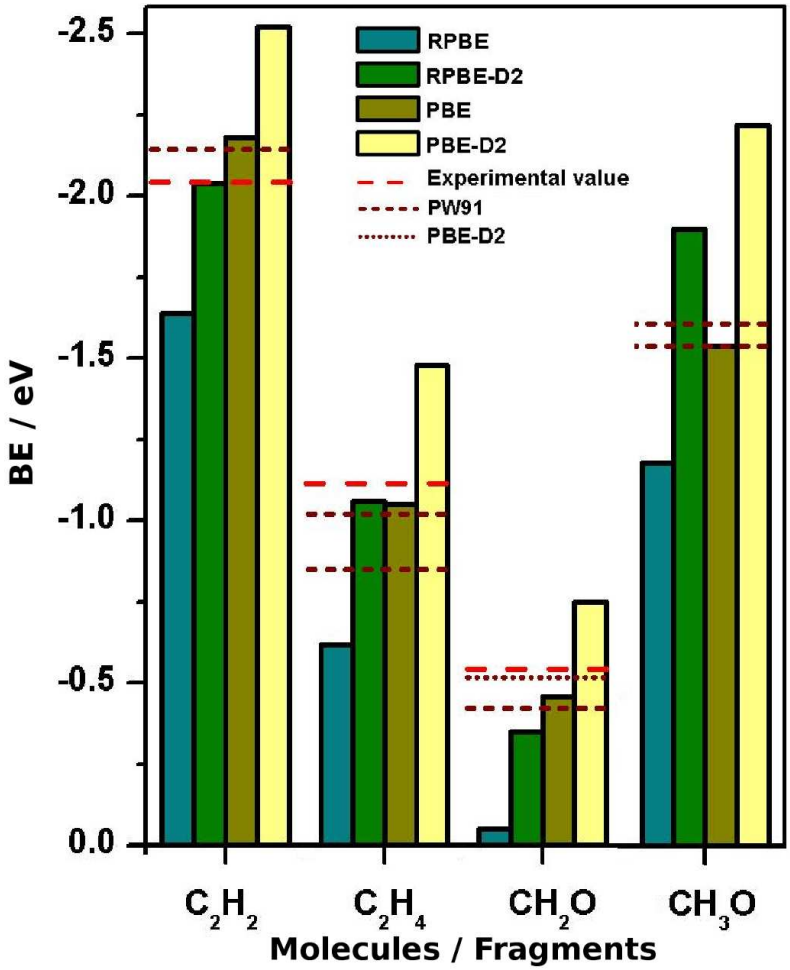

Figure 4.12: Binding energies, in eV, of three molecules and the radical formate.

4.6 Conclusions and outlook

In the present Chapter, an analysis of the behaviour of a number of organic molecules (C_2H_2, C_2H_4, CH_2O, CHN, CH_4O, and CO_2H_2) and fragments (CH_3O, and CO_2H) adsorbed on four different facets, (100), (110), (111), and (211), of the stable *fcc* crystallographic structure of eight monometallic systems (Pd, Pt, Rh, Ir, Cu, Ni, Ag, and Au), moreover testing various sites on each surface. The conclusions of this first work are in agreement with previous works and are enumerated below.

- With respect to the isolated molecules and fragments: The calculated bond length are in good agreement with the experimental values.

- With respect to the metal bulk parameters: The theoretical cell parameters are larger than the experimental ones. This agrees with previous benchmarks with the RPBE functional. The agreement with the experimental data is good, being the errors in the cell parameters with respect to the experimental values below 3.5%.

- With respect to the cohesive energies of the solid metals of the solid metals: The correlations with the experimental values are not so good because the value E_{coh} is severely affected by the estimation of the atomic energy. With the present approach the isolated atomic metal atoms are sometimes not properly described.

- With respect to the surface energy and relaxation: The surface energy of each metal increases along the series: $\gamma_{(111)} < \gamma_{(111)} < \gamma_{(110)} < \gamma_{(211)}$. This correlates with the coordination number of the atoms in the surface. The values obtained are in agreement with previous theoretical estimates.

- With respect to the atomic and molecular adsorption:

  - Atoms: In general, the order in the absolute values of the adsorption energies, from strongest to weakest bond, is E_C

$> E_N > E_O > E_H$. Usually highly coordinated positions (hollow sites) are preferred for all these atoms, in agreement with previous theoretical descriptions.

- Molecules: As a general feature, the larger the π-system of the molecule is, the stronger it binds to the surface.

- Metal activity: Metal activity in this case can be divided into their groups of the periodic system, that is, 9-group (Rh, Ir), 10-group (Ni, Pd, Pt), and 11-group (Cu, Ag, Au). The order in the activity so observed is 9-group>10-group>11-group. This is consistent with proximity of the Fermi level to the top of the *d*-band, in other words, the more amount of empty levels there are, the more active the metal is.

- Facet activity: As the the (100) and (110) surfaces are less dense than the (111) one, they are also more reactive, so the adsorption energies are, in general, lower (stronger bond). For instance, it renders Cu much more active since many adsorption energies for the investigated fragments are exothermic in these cases, unlike the (111) surface. On the other hand, (211) surface has a defect, so at the step all species have higher reactivity than on the rest of the surface.

- Preferential sites: This aspect depends on the species. For atoms, the valence plays an important role. In the case of carbon atom, for instance, the adsorption on any of the two hollows is more exothermic than on top of a metal atom, according to its valence. Along the series, this feature decreases, as the valence decreases. So, for hydrogen, all the energies are similar, as there are almost not preferential sites. Thus, the potential energy surface corrugation is the smallest and the diffusion of H is faster than that of C, N, and O. In the case of molecules, it depends on their size, their π-system and the activity of the metal. In general, if the molecule is small and contains at least a π-bond, it will bind preferentially hollow sites.

- Descriptors: Adsorption energies of different molecules can be scaled with those of their constituent atoms, when these

are directly bound to the surface. The huge interest of these feature is essential for the development of computational chemistry in general, and heterogeneous catalysis in particular.

UNIVERSITAT ROVIRA I VIRGILI
THEORETICAL STUDIES ON MOLECULAR ADSORPTION AND SELECTIVE HYDROGENATION CATALYSTS
Crisa Vargas Fuentes

Chapter 5

Promoters in the selective hydrogenation of alkynes in mixtures: insights from DFT

Contents

Selective hydrogenation of alkyne-alkene mixtures of small sized hydrocarbons has been traditionally performed with Pd-based catalysts modified by a second metal. [14–16] The main aim in the present Chapter is to give a rational understanding of the role of the different modifiers, *i.e.* quinoline and Pb, in Lindlar-type catalysts [173, 174] by comparison with pure palladium as well as with systems containing other kind of co-catalysts besides lead.

5.1 Previous works

5.1.1 The Lindlar Catalyst: PdPb systems

The development of selective processes is key in the research aimed to help the chemical industry in the twenty-first century. [14] Hydrogenation reactions can involve a single unsaturated reactant, multifunctionalized molecules, and/or complex mixtures presenting more than a single active species, where only one of the reactants or functional groups should be partially hydrogenated selectively. For partial alkyne hydrogenations, the three kinds of selectivity described in Chapter 1.4.2 are required: namely stopping the hydrogenation process at the thermodynamically metastable alkene (product selectivity), eliminating the competition of different substrates for the catalyst (reactant selectivity), and blocking oligomerization reactions (reaction selectivity). The adsorption and selective hydrogenation of alkynes versus that of alkenes have been considered as a model reaction and have been subject to several theoretical studies. [17] In fine chemistry, the Lindlar catalyst is stereotypic for hydrogenation of acetylenic compounds in the liquid phase, [173, 174] see Table 5.1. This well-established catalyst contains up to 5 wt.% Pd supported on either $CaCO_3$ or $BaSO_4$. In the preparation, a solution of $Ba(OAc)_2$ is added to the initial catalyst to deactivate it. Then, the system is heated at low temperature (95 °C), and usually the organic moiety is eliminated and some form of metallic lead deposit appears. [175, 176]

The PdPb system forms solid solutions with different compositions and structure. [177–182] Studies on the interaction of Pb films with Pd(111) surfaces demonstrate that formation of alloys is favoured; in particular, at low Pb concentration, a solid solution where Pb substitutes Pd has been described. [183] It has been suggested that a surface alloy with composition Pd_3Pb is formed as the active species of the Lindlar catalyst, [173, 174, 182] although the real surface stoichiometry of the material is not clear. In addition, penetration of Pb toward the bulk has been also put forward. [175, 184, 185] Rearrangement of Pd particles when Pb is incorporated in the catalyst has also been suggested in the literature. [186] Studies on the liquid phase hydrogenation of 1,3-butadiene indicated that the amount of molecules transformed *via* the competing mechanisms depends on the hydrogen coverage and the geometric and electronic effects of the materials. [187, 188] In these studies two different options are considered: either Pb deactivates Pd

by rearranging its surface structure, [186] or a strong interaction between Pd and Pb giving rise to electronic modification of the valence band of Pd. [188] Then, a second kind of modifier, a molecule with a strong interaction to the surface, is added to the catalyst. Usually, these molecules are organic compounds possessing oxygen, sulfur, phosphorous, or nitrogen heteroatoms. The ratio of an efficient modifier to the substrate is in the range 0.01-1 mol%. [189] In the Lindlar catalyst, usually quinoline is employed ($C_{11}H_{11}N$, denoted as Q), although piperidine and 2,2´(ethylenedithio)diethanol have been used too. [174] Quinoline has been proposed to:

(1) Compete with alkynes for the adsorption to the surface.

(2) To inhibit alkene surface interactions. [190]

(3) To reduce isomerization processes.

Moreover, quinoline is thought to act as an electron donor to the surface and modify the polarization of the Pd-H bond. [191, 192]

Table 5.1: Comparison between the hydrogenation catalyst in hydrorefining and the Lindlar catalyst. [17]

	Hydrorefining catalyst	Lindlar catalyst
Substrate	Ethyne, propyne	Long chain alkynes
Medium	Gas phase or liquid phase	Liquid phase
Pd content (wt.%)	0.01-0.05	1-5
Second metal	Ag, Au, etc.	Pb, Bi, Cu
Selectivity modifier	CO	Quinoline
Support	Al_2O_3	$CaCO_3$, $BaSO_4$
Temperature	RT-350 K	RT
Solvent	None	Benzene, toluene, methanol
Regioselectivity	-	*cis*
p_{H_2}	Up to 20 bar	1-10 bar
Operation	Continuous	Batch

In order to understand how the Lindlar catalyst works and why it is so selective, a detailed analysis of reports about hydrogenation catalysts can provide useful insight. In the current Chapter, besides a thorough study of the Lindlar catalyst, different aspects regarding

the gas-phase hydrogenation of alkynes in the presence of alkenes have been explored for different metals including Au, [151] Ni and Cu, [127] ternary Cu-Ni-Fe, [193] and the interplay between different phases and the selectivity on Pd. The three main controllers of the alkene selectivity are: [192]

1. *Thermodynamic selectivity*: it is the ability to adsorb preferentially only the alkyne moieties in the presence of any other functional group. This is the only controlling factor in Au nanoparticle-based catalysts. [194]

2. *Inability to form a hydride phase.* Hydrides overhydrogenate adsorbed moieties due to the presence of high potential subsurface H species. Those present smaller kinetic demand than the surface counterpart and thus invalidate the thermodynamic control. The catalyst of choice, Pd, has a large versatility in the formation of hydrides [195] and thus, at high hydrogen-to-alkyne ratios, the performance of the Pd catalyst alone is extremely poor.

3. *Definition of small ensembles.* Two of the competing routes in the process involve the activation of H atoms toward the reactive moiety or, alternatively, the formation of C-C bonds. The ensembles required for the second reaction are larger than those for the hydrogenation and thus are detrimental for selectivity. Moreover, oligomers can block the active sites. Therefore, reducing oligomerization is to ensemble control.

In order to shed light into the properties observed in the Pd metal by the presence of a second metal or promoter, a series of calculations aimed at illustrating all the possible behaviour induced by the presence of promoters have been performed and will be described during the present Chapter. Surface structures can be modified by diluting the active element with a second, less active one, or by changing the particle distribution. [196, 197] There are several problems due to mixing:

(i) The element with lower surface energy is usually segregated towards the surface.

(ii) The distribution may be random, or islanding, or preferentially decorated. [198]

(iii) These effects can be reversed by the atmosphere. Recent examples of the complex interplay between the atmosphere and the properties of bimetallic surfaces have been reported in the literature. [199–205]

The calculations contain the following promoters, M: the noble metal triad: Cu, Ag, Au; and *sp* metals: Zn, Ga, Sn, Pb (forming part of the so-called Lindlar Catalyst), and Bi. The visual summary of the concepts behind these parameters is shown in Fig. 5.1. The investigated properties are:

- **Intrinsic stability properties** given by the solubility, E_{sol}; segregation, E_{seg}; near-surface alloy formation, E_{NSA}; islanding, E_{isl}; step substitution, E_{ss}; and step decoration, E_{sd}; intrinsic electronic structure modification measured by the Pd *d*-band shift, ε_{Pd}. See Figures 5.1 and 5.9.
- **Adsorption properties:** measured as the binding energy for the C_2 prototypes: ethylene and acetylene, E_{HC} and average binding energy of the dense CO layer, E_{CO}.
- **Ability to form carbide or hydride phases:** measured through the average adsorption energies of H and C, both on the surface and the bulk: $E_{H,s}$, $E_{H,b}$ and $E_{s,C}$, in near and far configurations (*n,f*) and in the subsurface $E_{ss,C}$ only in the long distance configuration. See Figures 5.1 and 5.9.
- **Atmosphere-dependent properties** given by the hydrogen induced segregation, $E_{seg}(H)$, and CO induced segregation, $E_{seg}(CO)$. This second part of the stability analysis concerns the dynamic properties of the catalyst under realistic working conditions.

5.1.2 Other possible co-catalyst

Alternative metals to Pb were already suggested in the first report by Lindlar in 1952. [173]

PdAg

The current generation of a selective promoted catalyst for acetylene, PdAg composition, was first reported by Dow in 1957. [206] Later developments include the Süd Chemie family of PdAg for all front-end services and tail-end acetylene hydrogenation [207–209] and BASF's for tail-end acetylene hydrogenation. Chevron Phillips [210–212] at the "1993 Ethylene Producers Conference" listed a series of properties for these catalysts:

(i) Pd shall be in microns of the surface.

(ii) Addition of silver implies a small loss in activity and a large increase in selectivity.

(iii) There is an optimum in the Ag composition, as too high levels render inactive catalysis.

Experimentally, the formation of a PdAg alloy was observed and charge transfer from Ag to Pd X-ray adsorption sprectroscopy suggested, [213] the catalyst seemed to be surface Pd rich, [214] even if Ag has a lower surface energy than Pd. [215] Yield increases of about four-fold times were reported for the liquid-phase hydrogenation of 2-methyl-1,3-butadiene. [216] Moreover, the synthetic methods employed by Kahn and co-workers determined that no significant changes in size distribution occurred. [217] These authors proposed that the PdAg should have a Pd-rich surface able to dissociate hydrogen and hydrogenate the alkyne while the Ag-rich core would prevent the formation of the hydride phase. [217] Other lab test studies indicate a better initial performance of low Ag content (mol fraction 0.4) alloys due to increased stability. [218] In Surface Science studies, CO adsorption is demoted by the presence of Ag. [109] Reduction of these catalysts at higher temperatures improves Ag mobility and leads to more homogeneous distributions of Ag. [219]

Complementarily, several theoretical studies have been devoted to the study of the PdAg in acetylene hydrogenation. Following their deep analysis on the Pd system, Neurock and co-workers investigated the Ag containing model catalysts by Kinetic Monte Carlo applied to Density Functional Theory based parameters. These authors described the best performance of the silver containing 50% of each compound, [79, 89, 95] and explained both ensemble and electronic effects reducing the binding energies of acetylene and hydrogen to the surface as main features of this material. A model for this alloy was also employed by Nørskov and co-workers [21] to illustrate their study in overhydrogenation. The main property of the catalyst was defined as that weakening the bond of alkenes to the surface while keeping that of alkynes. More recently, an analysis of the formation of subsurface species was performed for this alloy. Their results indicated that when Ag is present, both the formation of H and C subsurface species are more difficult than for the monometallic system. [220]

PdCu

Cu was already proposed as alternative co-catalyst by Lindlar in his first report. [173] The structure of PdCu alloys has been

studied by DFT analyzing segregation and CO adsorption properties. [132, 221] The CO uptake was reduced by the presence of Cu in a liquid phase reactor. [222] Scanning Tunneling Microscope experiments, STM showed that isolated Pd atoms are able to split hydrogen. [223] The high selectivity observed in the hydrogenation process for acetylene was found to be lost when high temperatures were employed. It was suggested that this was due to an increase in the amount of Pd centers on the surface. [224] This points out to a quite dynamic behaviour under these conditions.

PdAu

The structure of these materials has been the subject of deep study over the last few years due to high selectivity in oxidation reactions and important ensemble effects both in gas- and liquid-phase processes. [225–235] In addition, they were tested in selective hydrogenation of butadiene and alkynes[236–239] for both low and high Au contents. [240] According to these studies, Pd is the main active component and they confirmed the formation of an alloy. STM experiments indicated a strong restructuring of the PdAu system upon hydrogen exposure, reversing the Pd tendency to segregate towards the surface. [223] $Pd_{76}Au_{24}$ exposed to H_2 at 1 bar[241] pointed out Ostwald ripening of the catalyst that changes both the distribution and composition of the nanoclusters and suggest that large clusters are Pd-enriched and small are Au-rich. In the experiments on liquid-phase hydrogenation, the TOF raised by 10 when increasing Au content to $Pd_{40}Au_{60}$, [216] where Pd enrichment was documented. Finally, Au has been proven to smooth out the formation of benzene from acetylene. [242]

PdZn

Initial studies indicated charge transfer and rehybridization in the formation of such alloys. [243] These alloys were tested for the hydrogenation of 1-pentyne and 1,3-butadiene, improving in both cases the selectivity when compared to Pd. [244, 245] PdZn is found to be reasonably stable under these reaction conditions. The presence of the alloy was confirmed, and the performance was reported to be similar to that of copper. Other results have suggested the limited adsorption of hydrogen and the isolation of active sites as main driving forces for selectivity. [246] Compared to Pd, the Zn-containing compound does not generate over-hydrogenated hydrocarbons but it is selective to oligomers. Unfortunately, the conversion to the

oligomer was significant (up to 20% at 100 °C). [244, 245]

PdGa

Ordered PdGa alloys with compositions Pd_2Ga, PdGa and Pd_3Ga_7 have been proposed as active, selective, and stable catalysts over the last few years both in gas- and liquid-phase hydrogenation processes. [247–251] High selectivities of C_2 alkynes to alkenes with little oligomerization (5-10%) are the fingerprint of these catalysts that upon nanostructures have an activity similar to Pd and a selectivity to ethylene higher than 70% (compared to 50% $Pd_{20}Ag_{80}$ with a much lower activity) in mixtures with the H_2:C_2H_2 ratio of 10:1 and 200°C. These ordered alloys present an increase in the coordination up to 13 [252, 253] in most of the cases, with a mixed coordination sphere in rather asymmetric environments, and a pronounced covalent interaction. The selectivity has been attributed to the reduction of the ensembles and the changes in the electronic structure, in particular the depletion of states at the Fermi level [249] that might reduce hydrogen coverage on the surface.

PdSn

The preparation of this material demonstrated the presence of bimetallic particles. [252, 253] PdSn was employed to analyze the selectivity of 1,3-butadiene by reducing the formation of the β-PdH phase and a reduction of the size of the ensembles. [254] Conversion of 1,3-butadiene was up to 80% with a similar Turnover Frequency, ToF, for Pd and PdSn. CO adsorption therein confirmed the change in the surface adsorption properties by changing the nature of the sites and electronic properties. On one of the supports, mixed phase alumina, the Sn-containing material, was found to be more active than the Pd counterpart. No overhydrogenated products were observed for Pd-Sn. The overall activity towards 1,3-butadiene was lowered when increasing the Sn concentration. [255, 256] When compared to Pd, Pd_3Sn showed a good selectivity towards hydrogenation without coking while Pd_2Sn had the most inert surface. [257] Liquid phase tests confirmed that activity decreases while selectivity boosts also because isomerization is reduced. These effects were explained by dilution and it was shown that Pd_3Sn was better than Pd_2Sn. [258] Weak adsorption was also identified in another set of experiments and shift of 4d states to higher binding energies when increasing Sn was reported. [259, 260]

PdBi

Bismuth, together with copper, was already proposed as alternative co-catalyst by Lindlar in his first report in 1952. [173] Bi has been proposed to be present on Pd [261, 262] as a way to eliminate the presence of soluble Pb compounds that present less environment impact, but other authors propose that the role of Bi is to maintain Pd dispersion and control its charge. [263]. It has been suggested that Bi preferentially decorates low-coordinated Pd atoms in open surfaces. [264] Experiments on hexyne hydrogenation (liquid phase) by Anderson and co-workers [265] indicate that Bi stops the reactions of 1-hexyne once formed, and that it blocks the active CO adsorption positions. As drawbacks Bi is a poor modifier for the 2-hexyne reaction when compared to Pb due to different behaviour in the isomerization. FTIR experiments were able to determine that Bi preferentially blocks steps and edge sites. In a different study by Karski, [266] X-ray Diffraction, XRD, and Time-of-Flight Secondary Ion Mass Spectrometry, ToF-SIMS, prove a strong interaction between Pd and Bi and the formation of BiPd and Bi_2Pd alloys at about 5-8% Bi content, while for low Bi fractions the intermetallic was found.

5.2 Computational details

Density functional theory applied to slabs with the 4.6 version of the Vienna Ab-initio Simulation Package code, VASP, has been employed in the present Chapter. [146] The energies have been obtained through the PW91 version of the exchange and correlation functional. [41] The inner electrons have been represented through Projector Augmented Wave pseudopotentials, PAW, [75] while the valence electrons have been expanded in plane waves with a cut off energy of 400 eV. The (111) surface has been employed for the reactivity studies, since this is the one showing the lowest energy for *fcc* metals. The slabs contain four layers in a p(2x2) reconstruction for molecular adsorption (except for quinoline) and hydride formation, and has been extended to six layers for the solubility studies. In that case, a single Pd atom was substituted by the co-catalyst. These systems are denoted as M@Pd, where M represents the second metal or co-catalyst. Islanding was computed in a p(3x3) configuration with two M atoms in the surface. For the segregation studies, six layers were used to assess properly the difference between the layers.

For the adsorption of quinoline on both clean Pd and Pb@Pd sys-

Table 5.2: Models employed in this Section calculations. Q is referred to quinoline. The number of co-catalyst atoms, M, is per unit cell.

Surface	(111)			(211)
Test	M Solubility	M Islanding	Molecular adsorption	M Decoration
Reconstruction	*p(2x2)*	*p(3x3)*	*p(4x4)*	*p(3x1)*
Pd	4 layers	4 layers	4 layers	9 layers
M@Pd	6 layers	6 layers	6 layers	9 layers
	1 M atom	2 M atoms	1 and 4 M atoms	1 M atom

tems, a larger supercell with a p(4x4) reconstruction was employed, denoted as Pd-Q_{Pd} and Pb@Pd-Q_{Pd}, respectively. In the second case, the amount of Pb was taken as either 0.25 or 0.0625 ML. As a representative model for the alkyne-alkene pair, the smallest possible hydrocarbons have been employed in these studies: ethyne and ethene. As seen in previous works, thermodynamic and kinetic properties of the hydrogenation reaction are similar for C_2 and C_3, although other properties, *i.e.*, carbide formation, are a strong function of the number of carbon atoms in the aliphatic molecule. [192, 251]

In any case, the vacuum space interleaving the different slabs was set to be larger than 10 Å. The k-point sampling was performed with the Monkhorst-Pack[71] scheme with 5x5x1 points for the small cells, and 3x3x1 for the larger ones; in other words, the k-point density is always as dense as 0.83 $Å^{-1}$. To illustrate the decoration at steps, we have employed a Pd(211) cut with a (3x1) reconstruction and nine layers, the k-points sampling being 3x3x1. Adsorption was performed on one side of the unit cell and the adsorbate was allowed to relax as well as the two outermost layers of the slab in all calculations. All the energies reported here do not contain the entropic effects given by the configuration problems. [267] Entropic contributions would destabilize configurations with smaller degrees of freedom, as a single layer or the edge positions when compared to the bulk or to terrace positions. In Table 5.2, a summary with all the models employed is shown.

Please note that our results concentrate on the equilibrium properties, *i.e.*, those showing the lowest energy on the potential energy surfaces. Under experimental conditions in some cases kinetic con-

trol and metastable structures can be obtained and employed for sufficiently long lab-scales. Therefore, some discrepancies might arise between some of the prepared catalysts and the results presented here.

5.3 The Lindlar Catalyst

As thoroughly described in Section 5.1.1, the Lindar catalyst is widely used for the partial hydrogenation of acetylenic compounds in organic synthesis. The additives strategically deactivate palladium sites. Alkyne reduction is stereoselective, occurring via *syn* addition to give the *cis*-alkene. Even if it has been employed for about 60 years, there is a lack of molecular level understanding of the Lindlar catalyst. It is crucial to analyze in minute detail the structure and the nature of the interplay between the multiple chemical modifiers in the Lindlar catalyst.

$$\text{Alkyne} \xrightarrow[\text{Quinoline}]{\text{Pb@Pd}} \textit{cis}\text{-Alkene}$$

5.3.1 The PdPb system. (111) surface

Solubility

We have calculated the solubility for Pb impurities and the corresponding segregation profile for Pb in the Pd lattice. The energy profile is shown in Figure 5.2. The solubility was calculated as:

$$E_{sol}^{(111)} = \overbrace{E_{Pb@Pd}^{(2x2-6layer)}}^{1} + \overbrace{E_{Pd(bulk)}}^{2} - \overbrace{E_{Pd}^{(2x2-6layer)}}^{3} - \overbrace{E_{Pb(bulk)}}^{4} \quad (5.1)$$

where the first term is the energy of the Pd slab with a substituted Pb atom, the second and the forth ones are the corresponding bulk energies per atom for both metals, and the third term is the energy of the Pd slab. From Equation 5.1, the substitution of Pb in the Pd lattice at the bulk position (L-3) is exothermic by 1.12 eV. Therefore, the formation of the Pb-Pd bond is more favourable than the Pd-Pd one and the solubility of Pb atoms is very likely considering also the contribution from configurational entropy. [267]

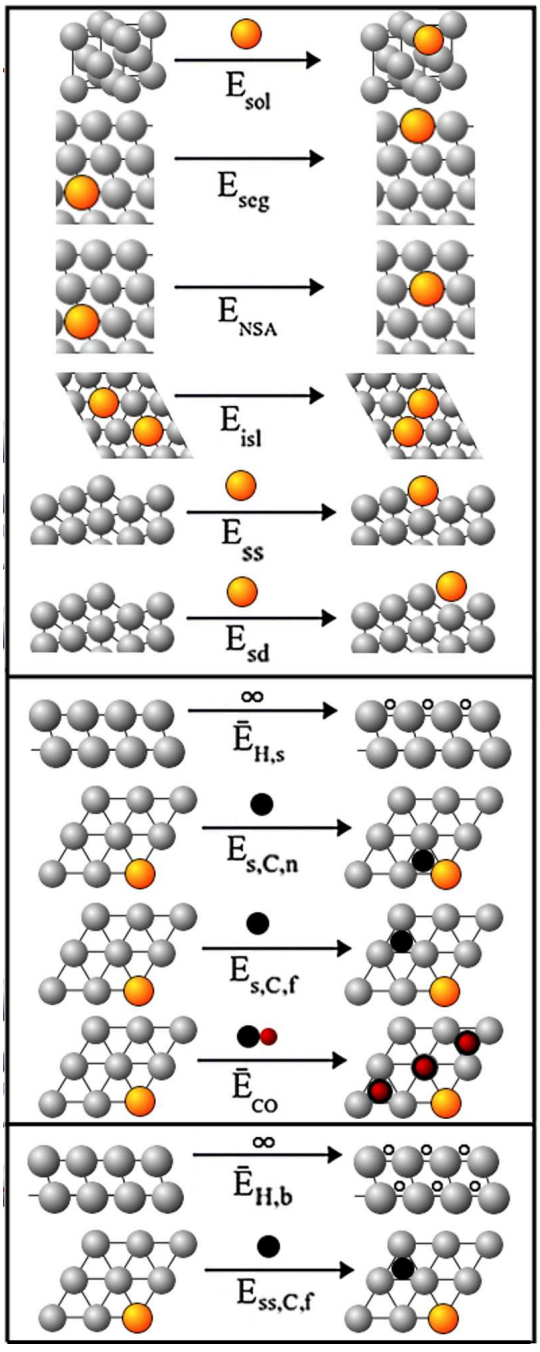

Figure 5.1: Schematic representation of the alloy calculated properties. Grey spheres represent Pd, orange the promoter, small white H, black C and red O. Front or side views are employed when convenient.

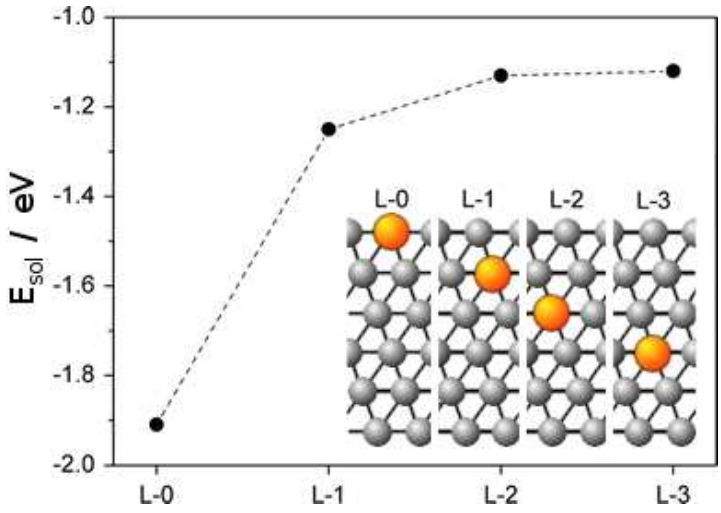

Figure 5.2: Solubility energy of a Pb impurity in Pd(111). The inset indicates the positions of the lead atom in the palladium slab. Same colour code as in Fig. 5.1

Segregation energy

We have also calculated the segregation energy to asses whether surface or bulk positions are more likely for the Pb impurities. Segregation is defined as the difference between the energy of Pb incorporated in the surface and the energy of Pb included in the bulk. The segregation energy has been calculated as follows:

$$E_{seg} = \overbrace{E^{(2x2-6layer)}_{(L-X)@Pd}}^{1} - \overbrace{E^{(2x2-6layer)}_{Pb(L-3)@Pd}}^{2} \tag{5.2}$$

where the first term is the energy for the impurity in the position L-X and L-3 represents the impurity sitting at the bulk. Calculations indicate the likely segregation of Pb toward the surface, see Figure 5.2. The energy gain is 0.79 eV with respect to Pb in the bulk position. Surface Pb atoms are relaxed toward the vacuum by 0.227 Å. In addition, the Lindlar preparation method described in Section 5.1.1 will also promote Pb impurities to stay on the surface [268] and thus surface impurity models and near-surface ones will be employed as the most likely structures under reaction conditions.

Pb islands

The results found in the previous sections confirm that the inclusion of Pb atoms into the Pd surface is very favourable in the

positions closest to the surface. We now extend our simulations to model the formation of Pb islands with two Pb atoms together in the surfaces of Pd. The energy of island formation has been calculated as follows:

$$E_{isl} = \overbrace{E^{(3x3-4layer)}_{Pb2@Pd}}^{1} - \overbrace{E^{(3x3-4layer)}_{Pb+Pb@Pd}}^{2} \tag{5.3}$$

where the first term is the energy of a Pb dimer on the Pd surface and the second one is the energy of separated atoms in the same supercell. Pb islanding is endothermic by 0.6 eV and, as the formation of the Pb-Pd bond is more favourable than the Pb-Pb one, then isolated Pb atoms are more likely on the surface.

5.3.2 The PdPb system. (211) surface

Solubility at step

A final aspect regarding the formation of the alloy is the preferential adsorption of Pb substituting Pd at step sites. Indeed, competing reactions such as *cis-trans* isomerization and bond shift isomerization are more likely to occur on rough surfaces, *i.e.*, rich in steps and kinks, [269] and there have been some claims that the selective poisoning by Pb of these sites can be at least partially responsible for the enhanced selectivity. [269, 270] We have investigated this aspect by calculating the solubility at the steps.

$$E^{(211)}_{sol} = \overbrace{E^{(3x1-9layer)}_{Pb-step@Pd}}^{1} + \overbrace{E_{Pd(bulk)}}^{2} - \overbrace{E^{(3x1-9layer)}_{Pb-step}}^{3} - \overbrace{E_{Pb(bulk)}}^{4} \tag{5.4}$$

where the first term is the energy of the Pb impurity at the step site, the third one the energy of the clean Pd step, and the second and forth terms are the bulk energies per atom of Pd and Pb, respectively. Then, compared to an impurity in the terrace, Pb atoms at the step are more stable by 0.37 eV. Regarding the possibility of step decoration, there would be a chance as it is apparently more stable than the substitution, if it weren't for strong thermal treatment performed on the catalyst. [271]

The electronic structure of Pd surfaces and Pb@Pd alloys is described in Figure 5.3 through the Projected Density Of States, PDOS. The top figure illustrates the reference system, Pd slab. The bands for bulk and surface Pd atoms are clearly shown and the corresponding *d*-band structures indicate the presence of lower states

for the fully coordinated Pd bulk atoms. The d-band center [77] for the bulk parameter for Pd atoms on the pure surface is closer to the Fermi level, 1.41 eV. As shown in Figure 5.3, the Pd surface layer and, in particular, the d-band is modified by the presence of Pb in the alloys. Upon the formation of the Pb@Pd alloy, the d-bands of the Pd atoms are shifted downwards by 0.16 eV. In turn, the Pb levels (only s and p states are plotted in Figure 5.3) show a deep band at about -10 eV and a broad band crossing the Fermi level. Thus, the electronic structure analysis indicates that Pd atoms at the Pb@Pd structures are less reactive than the clean surface. This means that the surface is less prone to adsorb incoming alkyne or alkene molecules.

Projected Density Of States

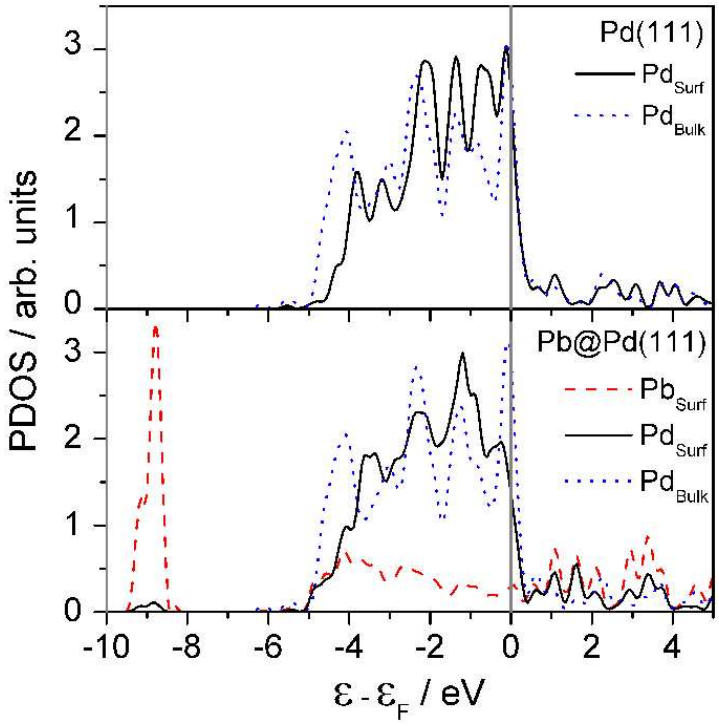

Figure 5.3: Projected Density of States for Pd (*top*) and Pb@Pd (*bottom*) alloys. The *black line* represents the states for a surface Pd atom, *blue dotted* those of the bulk and *red dashed* the Pb states

5.3.3 Hydride and carbide formation in Pd and Pb@Pd

Palladium is known to form different phases depending on the environment. Hydrides [272] are formed at room temperature at pressures as low as 0.024 atm. [273] Carbides come from the decomposition of organic molecules as indicated by Honkala *et al.* [274–277] and sit at octahedric sites in the subsurface region. In particular, this phenomenon is important since both carbides and hydrides are the key to control the selectivity of the catalyst. [13, 278]

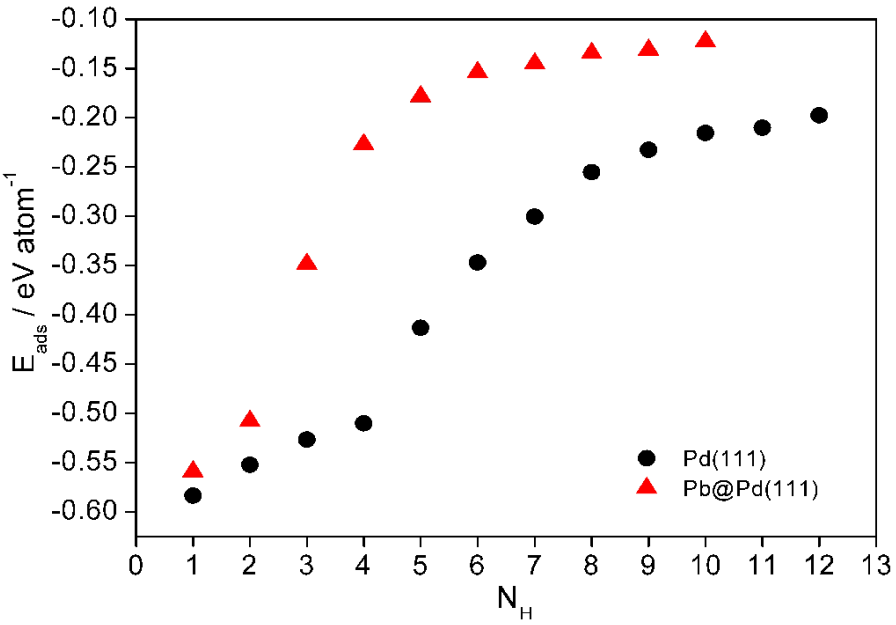

Figure 5.4: Average adsorption energy, E_{ads} in eV/atom, for the adsorption of N_H hydrogen atoms (from 1 to 12) in a $p(2x2)$ supercell. *Black circles* represent Pd(111) and *red triangles* Pb@Pd(111). Notice that four H atoms are required to fill a monolayer in the Pd(111) case while for the Pb@Pd surface the two *fcc* positions in contact with the Pb site do not adsorb H.

H_2 dissociation is known to happen even at high coverage with small energy requirements. [195, 279] The simplest way to illustrate the formation of hydrogen in the sub-surface can be addressed by the sequential H insertion. [205] We have investigated the occupation of H in the surface *fcc* sites and then on the sub-surface and positions closer to he bulk. In all cases, the H atoms sit at the octahedric sites. The average energy gained when adsorbing a monolayer of H atoms on the Pd surface is 0.54 eV/H atom. In the bulk, the average energy is lower, but still favourable as can be seen in Figure 5.4. For

the Pb@Pd system when the Pb atoms are on the surface, we have explored the adsorption in both the *fcc* involving Pd-Pb centers and those only formed by Pd. The *fcc* sites containing one Pb and two Pd do not efficiently adsorb hydrogen. The average adsorption energies for Pb@Pd are the following: the surface value corresponds to -0.53 eV/H atom and in the bulk -0.23 eV/H atom. These results agree very well with the observations performed by Ultra-High Vacuum experiments, UHV, indicating that the shape and maxima for the hydrogen evolution in a temperature-programmed desorption experiment is not significantly modified by the presence of Pb but instead it decreases the total amount of hydrogen adsorbed. [280]

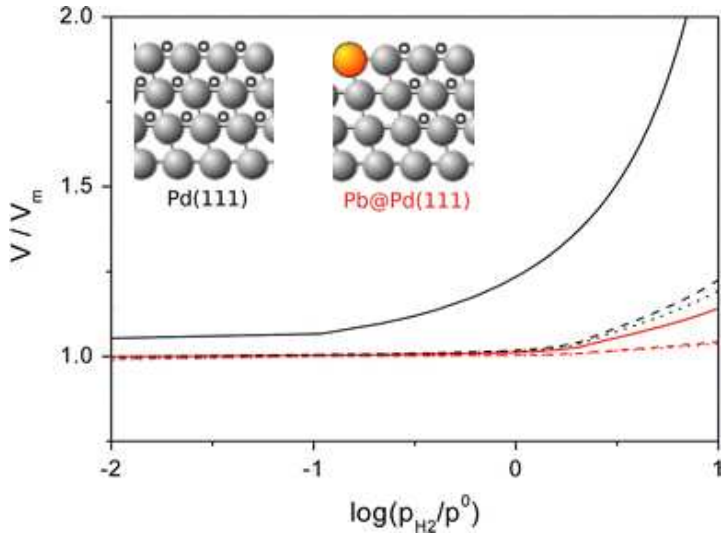

Figure 5.5: Hydrogen volume uptake, V/Vm, as a function of the hydrogen pressure at 300 K considering different solvents. The *black lines* represent Pd and *red* Pb@Pd(111). *Solid lines* represent gas-phase models, *dashed lines* methanol and *dotted lines* toluene.

In order to address the effect of the solvent on the hydrogen uptake, we employed the model for multilayer adsorption described in our previous work, [192] see Figure 5.5. The model states that the amount of hydrogen in the surface and bulk of Pd can be obtained as a particular case of multilayer adsorption. [281] For the clean Pd system, this means that at atmospheric pressures, $\log(p_{H_2}/p^0)$, the amount of hydrogen is larger than a single monolayer accupying the whole surface, $V/V_{\mathrm{m}} > 1$, and then the hydride is formed. When the solvent is present, it modifies the effective pressure of hydrogen in contact with the catalyst due to solubility effects. In Fig. 5.5,

it is shown how organic solvents (toluene and methanol) do reduce the total hydrogen uptake when compared to gas-phase systems. In the case of the Pb@Pd alloy the resistance to form the hydride is increased even for the pure gas-phase system. Again, the effect of the solvent is to reduce hydride formation.

The formation of the carbide phase is controlled kinetically and competes with the formation of the hydride phase. [192] Carbide formation in sub-surface positions of Pd is -0.56 eV with respect to gas-phase ethyne and H_2, and +0.58 eV with respect to gas-phase ethene and H_2. As for the Pb@Pd alloy, the formation of the carbide is -0.25 eV for ethyne, and 0.89 eV for ethene. Thus, Pb@Pd(111) is less prone to form the carbide phase than pure Pd.

5.3.4 Quinoline adsorption on Pd and Pb@Pd

Quinoline is a base with a naphtalene structure where one of the CH groups has been substituted by nitrogen, see Figure 5.6. The rings are planar and the N atom exhibits a lone pair sticking out from the carbon ring. In previous theoretical works, [282] adsorption of quinoline has been studied by employing cluster models and different metals including Pd. These authors performed an extensive survey of different adsorption sites and indicated that the most likely positions for adsorption correspond to planar structures where quinoline rings are over bridge positions, di-bridge configuration. In this configuration, the carbon and nitrogen are bonded in total to seven Pd atoms, noted as di-bridge, $N_{Pd=7}$ in Ref. [282], as can be seen in Figure 5.6. Obviously, given the confined characteristics of the cluster and the poor definition of the *s*-bands in these models, the energies reported seem to be much smaller than those determined experimentally. [283] Another difficulty in the evaluation of quinoline adsorption comprises the large contributions that can be anticipated from its close nature and extended π-system. We have attempted to evaluate the contributions from dispersion through Grimme-like corrections [57] and re-optimize the structure. Those contributions have been reported to strongly modify the adsorption energies of large molecules. [153] In the case of quinoline on Pd, an extra exothermic contribution of 0.12 eV was obtained.

The perpendicular N-down structure was found unstable. The largest adsorption energies for quinoline on Pd correspond to the di-bridge site, -1.79 eV, see Table 5.3 and Figure 5.6. The average distance from the carbon atoms in the rings to the neighboring

metal atoms is 2.233 Å, while the distance from the N atom to a Pd on the surface is at 2.187 Å from the surface. The average C-C distances are enlarged to 1.447 Å with respect to the gas-phase values, 1.421 Å. This enlargement is due to the formation of the bond at the interface.

Table 5.3: Adsorption site, adsorption energy, E_{ads} in eV, and most relevant geometric parameters: distance from the surface to the N atom in the quinoline, $d_{N\text{-}M}$; and from the metal ring to the neighbouring metal atoms $d_{C\text{-}M}$; and average C-C distance, $d_{C\text{-}C}$; and α the angle for the distortion with respect to planarity. All distances in Å and α in degrees.

	Pb/ML	Site	E_{ads}	d_{N-M}	d_{C-C}	d_{C-M}	α
Pd	0	Di-bridge	-1.79	2.187	1.447	2.233	20.8
Pb@Pd	0.25	Di-bridge	0.41	2.541	1.421	2.640	5.7
Pb@Pd	0.0625	Di-bridge	-1.57	2.203	1.446	2.248	22.3

Regarding the adsorption on the Pb@Pd model system, the number of adsorption possibilities increases due to the birth of different sites. We have calculated two different Pb concentrations on the surface. While at high Pb concentration, 0.25 ML, adsorption is endothermic by 0.41 eV, an exothermic value is obtained for lower Pb coverages, 0.0625 ML. In this case, the most stable adsorption site corresponds to position where quinoline is far away from the Pb atoms, di-bridge, $N_{Pd} = 7$. At Pb positions or close to these centers, adsorption energy is endothermic. Thus, the Pb centers are not decorated by the quinoline molecules. Instead, the clean Pd areas of the Pb@Pd alloys do adsorb quinoline in similar configurations as those found for the clean surface, thereby covering different areas of the catalyst where Pb is not present. The adsorption energies Pb@Pd are reduced to -1.57 eV. The projected density of states in Figure 7 shows the important overlap between the states of the molecules and those of the surface, responsible for the strong interaction found. Moreover, the Pd atoms on the surface not close to the quinoline molecule are not significantly perturbed.

The role of the quinoline appears to be, at least partially, equivalent to that of CO on Pd in the gas-phase alkyne hydrogenation. Both quinoline and CO have binding energies to the Pd or Pb@Pd surfaces that are larger than that of the triple C-C bond. This means that they are not displaced by the reactants but instead, they block

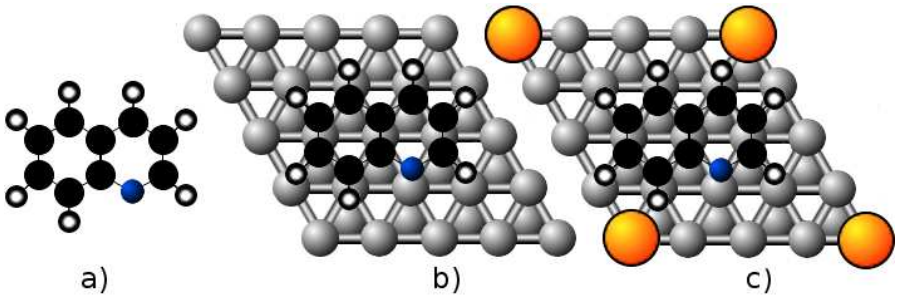

Figure 5.6: Structures of **a)** gas-phase quinoline and quinoline adsorbed on the surfaces: **b)** di-bridge position on Pd and **c)** di-bridge configuration at the Pb@Pd(111) surface. Colour code: N (*dark blue*), C (*small black*), H (*white*), Pd (*grey*), and Pb (*large orange*)

some of the sites. This size reduction implies that the reaction ensembles, *i.e.*, the group of atoms involved in an elementary step, are effectively reduced. Ensembles are known to rule activity and selectivity [284, 285] and their size reduction is particularly effective when the competing reactions require different ensembles, as for the hydrogenation and oligomerization processes, and the desired reaction needs the smallest one. In the case of quinoline, the large size of this molecule favours the isolation of small ensembles. Isolation also contributes to the reduction of oligomerization reactions as diffusion of alkynes on the surface is required and it is hindered when other adsorbates are present.

In order to check the role of other potential compounds on this reaction, we have analyzed the binding energy of pyridine and naphtalene to Pd. While the first contains a part of the active molecule, the second, $C_{10}H_{10}$ is isostructural with quinoline and with a CH group substituting N. The corresponding adsorption energies to the clean surface are found to be -1.14 eV for pyridine, and -1.84 eV for naphtalene. Thus, pyridine is much less adsorbed than both naphtalene and quinoline and it would not be strong enough to compete with the alkynes for the adsorption sites.

5.3.5 Thermodynamic factors of ethyne and ethene on Pd and Pb@Pd

One of the major components controlling the selective hydrogenation is the thermodynamic factor. This represents the ability of the catalysts to adsorb the alkyne while the alkene is not bonded.

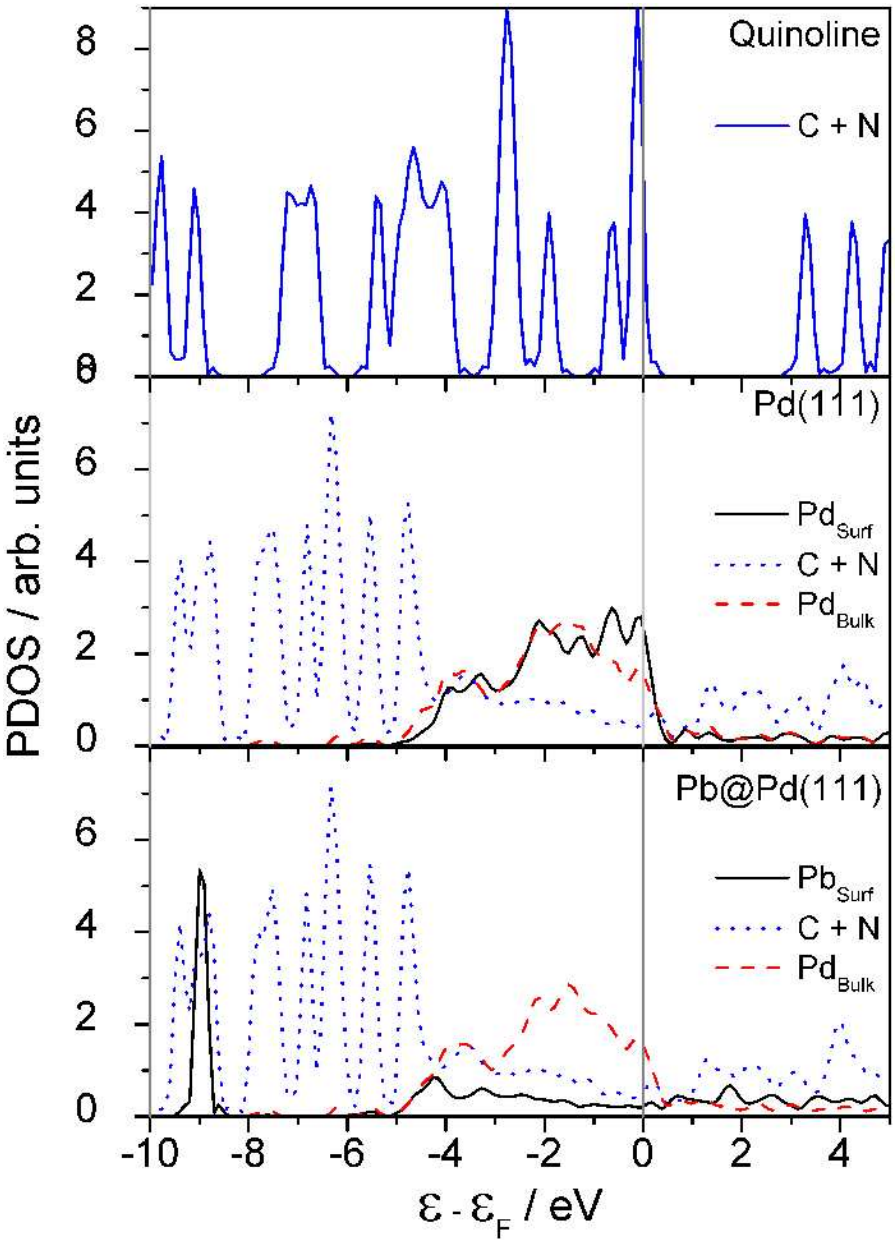

Figure 5.7: Projected Density Of States, PDOS, for the most stable adsorption sites of quinoline on the Pd and Pb@Pd surfaces.

Table 5.4: Reaction energies, ΔE, and activation barrier, E_a, both in eV, for the first and the second hydrogenation steps of ethyne. For the Pb@Pd alloy (0.0625 ML Pb), two different structures: close (c) and far (f) from Pb have been studied.

System	Pd		Pd-Q		Pb@Pd(c)		Pb@Pd(f)		Pb@Pd-Q_{Pd}	
Reaction	ΔE	E_a	ΔE	E_a	ΔE	E_a	ΔE	E_a	ΔE	E_a
$C_2H_2 + H \rightarrow C_2H_3$	-0.17	0.66	0.14	1.28	0.13	1.24	0.11	1.17	0.12	1.20
$C_2H_3 + H \rightarrow C_2H_4$	-0.42	0.81	-0.38	0.76	-0.28	0.90	-0.25	0.87	-0.45	0.72

[286] However, the adsorption of the alkyne-alkene pair depends on the binding energy of carbon due to the bond-order conservation rules. [22, 287] The slope of the linear dependence found for the binding energies of alkyne and alkenes with that of carbon, points out where selective regions exist. However, this parameter is only valid provided that the same active species is responsible for the hydrogenation.

On the clean surface, the adsorption energies of ethyne and ethene are -1.78 and -0.82 eV, respectively. Thus, once formed the alkene stays adsorbed on the system that can be over-hydrogenated leading to the corresponding alkanes. For the clean surface, earlier experiments and calculations at stoichiometric conditions, H_2/alkyne= 1/1, lead to less than 50% selectivity for the partial hydrogenation. On the Pd-Pb sites, adsorption is controlled by the relative position with respect to the Pb center. Adsorption at the Pd *fcc* sites on the Pb@Pd surface is less exothermic than on the pure Pd surface, the adsorption energy is -1.11 and -0.30 eV for ethyne and ethene, respectively. This was calculated in a $p(2x2)$ reconstruction with a Pb coverage of 0.25 ML. Thus, the effect of alloying is to reduce the adsorption of energies of both moieties by about 0.5-0.7 eV. At the *fcc* or bridge structures containing a Pb atom, the binding energies are even lower, thus the positions around Pb atoms can be considered as inactive. These results confirm the suggestion by Palczewska *et al.* [280] that with a very low Pb coverage, adsorbed ethene was not detectable in the Temperature Programmed Desorption, TPD, spectra and disappeared completely at higher coverages. The change of the metal-molecule bond strength was more decisive than site blocking. [288] When Pd is partially covered by quinoline, the binding energies are also smaller than those corresponding

to the clean Pd surface. The E_{ads} is then -1.46 and -0.65 eV for ethyne and ethene, respectively. Thus, quinoline also reduces the adsorption of the double and triple bonds to the surface, but the effect is smaller than that of the Pb. In the large cell, we have also placed simultaneously quinoline and Pb, Pd@Pd-Q_{Pd}. On this system, the alkyne-alkene adsorption energies are reduced further, -1.35 and -0.61 eV, respectively, but still the synergetic contribution of quinoline and Pb is rather small.

5.3.6 Discussion: differences between palladium and the Lindlar Catalyst

In the literature, selectivity modifiers have been classified in terms of reversible and irreversible adsorbates. Irreversible modifiers perturb the ensembles restricting their shape and size, while reversible adsorbates are usually seen as stoppers of consecutive over-hydrogenation or oligomerization reactions, in particular when the binding energy of the modifier is larger than that of the intermediate (thermodynamic selectivity). [289] In the present Section, we describe the effect of the irreversible (Pb) and reversible (quinoline) modifiers.

On regular Pd catalyst, H_2 is easily dissociated with the subsequent formation of hydrides. When hydrides are formed, ethyne (more generally, alkynes), over-hydrogenate due to the high chemical potential of H atoms stored in Pd bulk. In the Lindlar catalysts, hydrides are scarcer. Still, H_2 splitting is easy due to the similar activity of Pd, but the presence of Pb inhibits the adsorption of H in the neighbouring region. This exclusion area also implies that hydride formation is less exothermic and less likely. Moreover, the solvent modulates the amount of hydrogen in contact with the surface due to the solubility of H_2 in different liquids reducing the equivalent pressure. Thus, for the Lindlar catalyst over-hydrogenation problem is much less an issue. The role of the irreversible modifier is to reduce the sites available for hydrogen adsorption, isolate and shape the ensembles, and enhance the intrinsic selectivity of the catalyst by improving the thermodynamic factor. Finally, due to the Pb decoration at steps, carbon deposits are less likely.

Quinoline adsorption on Pd also reduces the amount of possible adsorption sites for H. This is due to the effective blocking of these molecules that adsorb so strongly that can compete with the alkyne for the sites. The presence of quinoline slightly reduces the average

Table 5.5: Adsorption energies of ethyne and ethene on both Pd(111) and Pb@Pd(111) surface with and without quinoline. Energies are expressed in eV and distances in Å. The elongation, $\Delta d_{C\text{-}C}$ is the difference between the C-C distance as calculated on the surface and in the gas phase.

	System	Pb(ML)	Quinoline	Site	E_{ads}	$d_{C\text{-}M}$	$\Delta d_{C\text{-}C}$
C_2H_2	Pd	-	No	*fcc*	-1.78	2.001	0.153
C_2H_4	Pd	-	No	Bridge	-0.82	2.131	0.117
C_2H_2	Pb@Pd	0.25	No	*fcc*	-1.11	2.055	0.135
C_2H_4	Pb@Pd	0.25	No	Bridge	-0.30	2.164	0.110
C_2H_2	Pd	-	Yes	Bridge	-1.46	2.255	0.041
C_2H_4	Pd	-	Yes	Bridge	-0.65	2.241	0.041
C_2H_2	Pb@Pd	0.0625	Yes	*fcc*	-1.35	2.255	0.039
C_2H_4	Pb@Pd	0.0625	Yes	Bridge	-0.61	2.253	0.040

H binding energy. Furthermore, isolation of the sites is a clear effect of quinoline, its large size and quite good fitting with the symmetry of the surface allows the reduction of side reactions. However, quinoline is not as effective as Pb in improving the thermodynamic factor. For the complete Pb@Pd-Q_{Pd} system, the thermodynamic factor is similar to that observed for the quinoline alone.

Therefore, a hierarchical ordering on the effect of modifiers [265] can be obtained from the calculations above. A two-dimentional tesselation problem with two kinds of building blocks is described in Figure 5.8. The Pb exclusion area forms the main modifier to the catalyst. Still, Pb is an additive that modifies very strongly the properties of adsorb alkynes and alkenes and indeed it can completely block the surface, provided that an extensive quantity is employed. Moreover, Pb in the Pd alloys is preferentially found isolated. The reversible adsorbate quinoline is indirectly ordered by the presence of Pb and isolates very small sites of about four palladium atoms that allow hydrogenation but block oligomarization. Thus, at complete quinoline coverage the Pb@Pd-Q_{Pd} leaves active less than 10% of the surface palladium sites for the hydrogenation reaction. This fact, together with the smaller intrinsic activity (larger activation barriers for hydrogenation are found) explains why two orders of magnitude more Pd weight percentage is required in the formulations of the Lindlar catalyst when compared to the gas-phase

hydrogenation, Table 5.1. Finally, the outstanding selectivity of the Lindlar catalyst would be difficult to be obtained by a single chemical modifier. The effect of Pb poisoning is so important (as shown in Table 5.5) that can eliminate all the active sites on the surface even at modetare coverages. Similarly, quinoline on Pd alone could also form very dense packing motives reducing the number of sites. By employing a hierarchically ordered set of modifiers (lead and quinoline) these problems are avoided as the two building blocks are different but complementary enough to limit the drawbacks of each other.

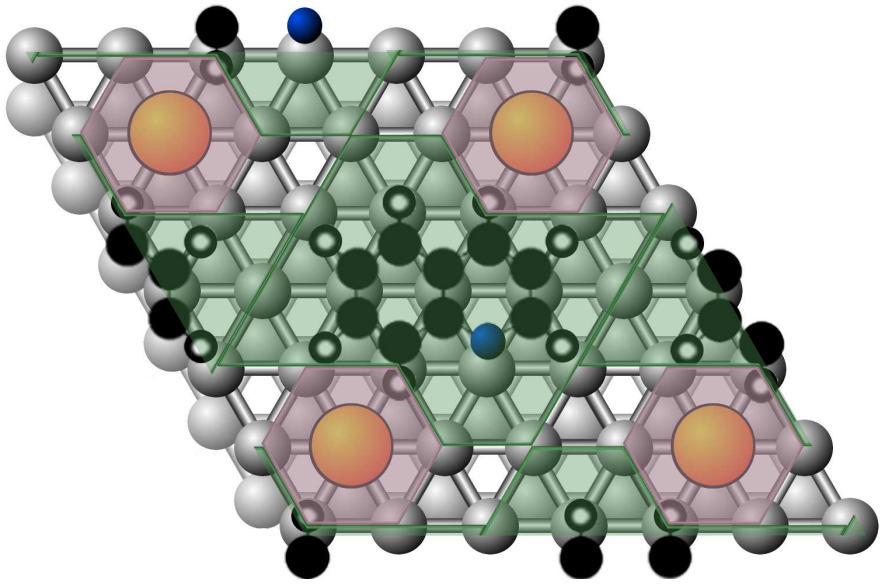

Figure 5.8: Schematic representation of the mosaic generated by the superposition of the Pb exclusion areas (*pink*) and the quinoline ones (*green*). The only active sites, without tiling, able to adsorb the alkyne are marked by white regions. The tessellation with two different kinds of structures provides a subtle way to control the ensemble size and shape.

A second question is why different reversible modifiers are employed in gas-phase (CO) and three-phase (quinoline) hydrogenation. CO is widely employed in hydrogenations and indeed the catalyst is not selective without it in gas-phase reactions. [290] In the Lindlar catalyst, quinoline is regarded as one of the most effective modifiers. Both CO and quinoline show larger binding energies to the surface than ethyne, and therefore they both fulfill the requirement of improving the thermodynamic factor and not been replaced

by the reactant. However, the coverage of both species is necessarily different; while a very dense CO layer is observed for CO, a sparse structure is obtained for quinoline. Therefore, both to modify the ensembles but through different mechanisms: highly occupation by small molecule (CO) or large blocking by size (quinoline). However, CO might show solubility problems in the liquids, and it is dangerous to handle in an open environment, moreover the shape of the active sites is difficult to control. Therefore, it is not recommended in standard fine chemistry procedures. Similarly, N-containing compounds shall be removed from the streams in gas-phase hydrogenation due to incompatibilities with other parts of the process. Finally, we have tried different alternative molecules to investigate this effect. Naphtalene is one of them and its adsorption properties are similar to those obtained with quinoline. In contrast, pyridine is not an option as its low binding energy to Pd and Pb@Pd would not be strong enough to block the surfaces (*i.e.*, it would be displaced by the alkyne).

5.4 Other possible co-catalysts

In this Section, the main parameters that control the stability of the hydrogenation catalyst are summarized. All the results are shown in Figure 5.9 for the static properties. The colours in the heat map indicate the relative position of each metal promoter in the spectra spanned by all M@Pd (M = Pd, Cu, Ag, Au, Zn, Ga, Sn, Pb -Lindlar-, and Bi) for each particular property.

5.4.1 Intrinsic stability properties

Solubility

Solubility is mandatory in order to form a stable material. This parameter has been calculated in a four layer slab where the M impurity has been placed in a bulk structure with 32 atoms in Pd. The overall M content is thus 3%. The energy is obtained as:

$$E_{sol} = \overbrace{E_{M@Pd}^{(2x2-4layer)}}^{1} - \overbrace{E_{Pd(bulk)}}^{2} - \overbrace{E_{M(bulk)}}^{3} \qquad (5.5)$$

where **1** is the energy of the structure with the promoter in a substitutional position (*i.e.*, replacing a Pd atom); **2** and **3** the corresponding energies for the bulk structures. Negatives E_{sol} values indicate exothermic processes. In the optimization, all the atoms surrounding the impurity have been allowed to relax. The largest

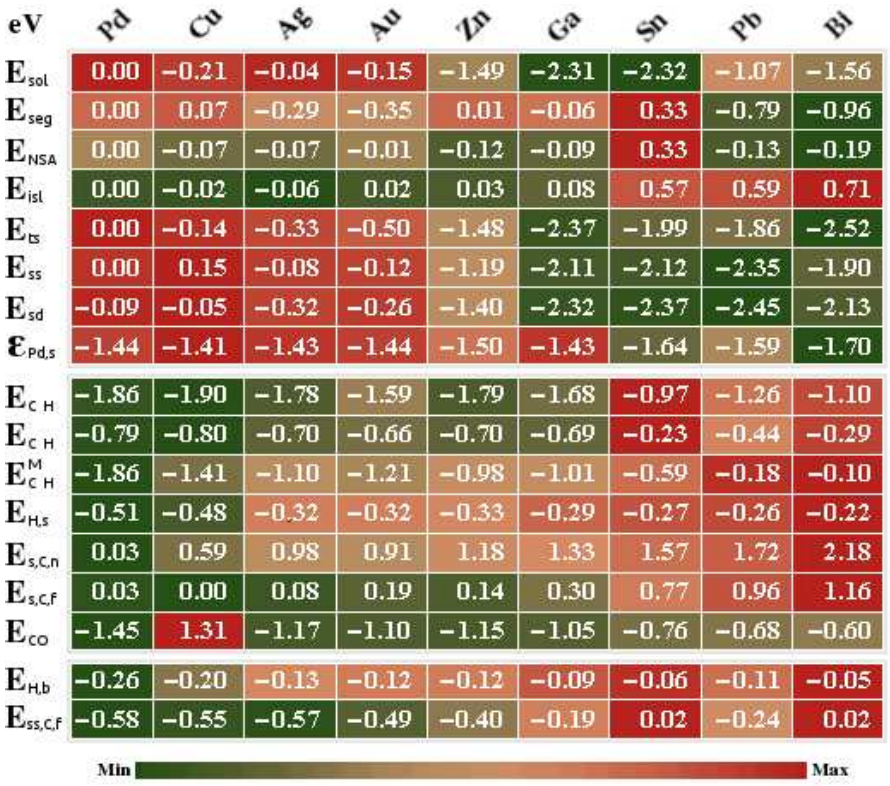

Figure 5.9: Heat map for the static properties of M@Pd alloys, where M represents the co-catalyst: Pd, cu, Ag, Au, Zn, Ga, Sn, Pb, and Bi. All the energies are shown in eV. The definitions correspond to those in Figure 5.1: solubility, E_{sol}; segregation E_{seg} and NSA formation, E_{NSA}; islanding E_{isl}; terrace substitution: E_{ts}; step substitution: E_{ss}; step decoration: E_{sd}; *d*-band center, $\varepsilon_{Pd,s}$. Adsorption energies for C_2H_2, C_2H_4, at Pd-only sites: $E_{C_2H_2}$ and $E_{C_2H_4}$; $E^{M}_{C_2H_2}$ at mixed *fcc* sites. Hydrogen surface and subsurface energies: $E_{H,s}$ $E_{H,b}$ and average E_{CO} energy for the *p(2x2)*-3CO configuration. Carbide formation with respect to the C_2H_2 molecule and hydrogen: different configurations are investigated $E_{s,C,n}$ surface in a near configuration; or far (Pd-only) $E_{s,C,f}$ or subsurface Pd-only configuration $E_{ss,C,f}$. The colour code spans the maximum and the minimum value per row.

solubility, about 2 eV, is observed for Ga and Sn. Indeed different ordered and substitutional alloys with all the promoters discussed here have been reported in the literature. Still large values are obtained for the other *sp* metals: Zn, Bi, and Pb, between 1.5 and 1 eV. Lower solubility values are obtained for the noble metal triad, in the order of tenths of eV.

Segregation energy and NSA formation

Segregation and near-surface alloy formation have been investigated in thick slab containing 6 layers and a $p(2x2)$ reconstruction and calculated as follows:

$$E_{seg} = \overbrace{E^{(2x2-6layer)}_{M@Pd(s)}}^{1} - \overbrace{E^{(2x2-6layer)}_{M@Pd(bulk)}}^{2} \tag{5.6}$$

where the impurity has been placed in the central part of the slab, second term of the equation, or in upper position, the first one. Negative values for E_{seg} or E_{NSA} indicate exothermic processes. The secondary metals studied here segregate towards the surface to a very large extent. This is the case for Bi, same as for Pb, with segregation energies larger than 0.7 eV. A second group with E_{seg} of about 1/3 eV is formed by Ag and Au while almost no preference for the surface or subsurface state is found for Ga and Zn. For the Ga alloys it is well-known that segregation does not influence much the composition profiles with depth. [247–250] A rather different case is presented by Sn where a rather strong anti-segregation is found, 1/3 eV. Our results for the noble metals are similar to those reported earlier by Ruban and co-workers, [215] although in their database only transition metals were reported. However, even in the cases when the segregation is favoured energetically, due to the temperature ranges employed it might be that the equilibrium configuration is not reached. Still, experiments have shown the formation of a surface alloy for Sn by the combination of Low-Energy Electron Diffraction, LEED, and Auger Electron Spectroscopy, AES. [256] Similarly the formation of a surface PdZn alloy was found by Xanes, [244, 245] and intermetallic compounds with Bi have also been reported. [266]

Near-surface alloys, NSA, are those compounds where the secondary metal is not placed in the surface position but rather underneath the surface. [291] These materials have been shown to

have very interesting properties and therefore this possibility has also been considered in the calculations. Compared to the numbers for the segregation, it is important to notice that while Cu is segregated towards the surface the subsurface position is even more stable. This is the case for Zn and to a minor extent for Ga.

M islands

A further consideration on the stability of these materials is given by the formation of islands on the surface. Islanding has been studied in a larger reconstruction $p(3x3)$ and four layers that allow the islands to be completely surrounded by Pd. The energy is given by:

$$E_{isl} = \overbrace{E^{(3x3-4layer)}_{M_2@Pd}}^{1} - \overbrace{E^{(3x3-4layer)}_{M@Pd_2}}^{2} \tag{5.7}$$

where the first term is the promoter dimer, and **2** the corresponding to the separated configuration. Pb, Bi, and Sn show a strong lateral repulsion and thus isolated atoms are expected. For Pb this agrees with the formation of ordered PdPb phases where the Pb atoms are completely surrounded by Pd, [182] as has already seen in the previous Section. For the remaining atoms, Au, Zn, and Ga, island formation is weakly repulsive or slightly bonding for Cu and Ag. Of course, entropic configurations would change the final values by favouring non-ordered configurations and thus a very limited number of dimers shall be expected at low promoter concentrations. Dispersed tin in PdSn alloys was identified by Xanes [255] while the low energy found for Ag segregation is in agreement with the results in Ref. [214].

Steps: solubility *vs.* decoration

The analysis of the steps was done in a $p(2x1)$ reconstruction of the (211) surface with a slab containing 9 layers. The energy parameter was defined as:

$$E_{step} = \overbrace{E^{(2x1-9layer)}_{M-step@Pd}}^{1} - \overbrace{E^{(2x1-9layer)}_{Pd-step}}^{2} - \overbrace{E_{M(bulk)}}^{3} \tag{5.8}$$

where the first term is the energy of the Pd step. Step substitution is favoured for the large atoms like Sn, Pb, and Bi but also

for Ga (2 eV) which makes these sites, particularly active in C-C bond breaking, less common. The ordering in the substitution of the noble metal triad parallels the size of the metals. Therefore, a lower coordinated position is less crowded and can accommodate large atoms such as Au better.

We have also inspected the possibility of step decoration. In that case, the secondary metal is not placed as a part of the lattice but close to the edge in the form of a growing terrace. Then, decoration is calculated as:

$$E_{sd} = \overbrace{E^{(2x1-9layer)}_{M-step@Pd}}^{1} - \overbrace{E^{(2x1-9layer)}_{Pd-step}}^{2} - \overbrace{E_{M(bulk)}}^{3} \tag{5.9}$$

where the first term is the energy with the M atom decorating the Pd step. This is actually the preferred situation for Sn and Pb by about 0.2 eV. Step decoration would then be preferred if no strong thermal treatment is performed on the catalyst.

Combining the energies above it is possible to illustrate if terrace or step positions are favoured. The energy of terrace positions obtained as $E_{\mathrm{ts}} = E_{\mathrm{sol}} + E_{\mathrm{seg}}$, is favoured for Cu, Ag, Au, Zn, and Ga by 0.2-0.5 eV. With respect to the decoration, this is favoured when compared to the edge substitution for Pb, and Sn. Decoration is less stable than the terrace positions for Au, Pb, and Bi. However, Bi has been experimentally proposed to preferentially decorate the areas in the surrounding of the edges. [264, 265] According to our calculations this could correspond to a metastable state as the step substitution is energetically hindered $\Delta E = E_{\mathrm{ss}} + E_{\mathrm{sd}} = 0.23$ eV. This view would agree with the high dispersion found for Bi by Kereszegi *et al.* [261, 262]

Projected Density Of States

The chemical consequences of all the above can be summarized by the change in the electronic structure of Pd represented in Figure 5.10 and visualized by the shift in the d-band, ε_{Pd}. On one hand, Cu, Ag, Au, and Ga almost do not perturb the electronic structure of the surface Pd metal. Zn modifies little the structure while Pb, Sn, and Bi strongly shift down the bands for Pd rendering these surfaces less available to adsorption. In addition, for PdGa ordered alloys it has been reported that the number or states at the Fermi level is lowered with respect to pure Pd. [247–250]

In Figure 5.10, this is clearly represented, similarly the other alloys present this feature. The downward shift of has been reported experimentally for Sn. [254]

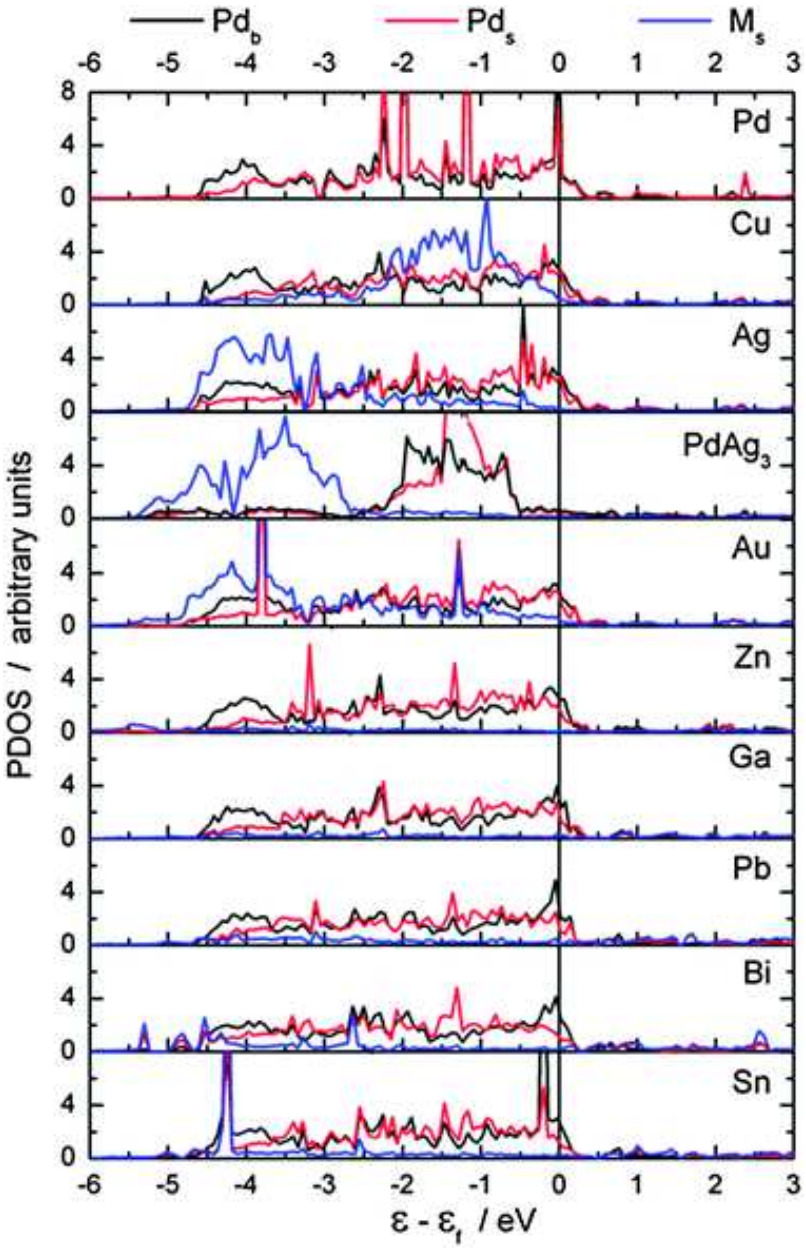

Figure 5.10: Projected density of states for all the calculated alloys, a Pd atom from the bulk, Pd_b; one of the surface, Pd_s; and the promoter, M_s; are presented.

5.4.2 Adsorption properties

All the adsorption parameters were explored in the *p(2x2)* supercell with four layers.

Acetylene and ethylene adsorption

The energy has been computed as:

$$E_{HC} = E_{HC-M@Pd} - E_{M@Pd} - E_{HC(gas)} \tag{5.10}$$

The adsorption energy of the hydrocarbon, E_{HC}, is calculated as the difference between the energy of the adsorbed system, $E_{HC\text{-}M@Pd}$, the surface, $E_{M@Pd}$, and the energy of the hydrocarbon in the gas phase, $E_{HC(gas)}$, either acetylene or ethylene. Therefore, exothermic processes show negative E_{HC} values. In the models employed, the Pd-only sites are more active towards adsorption than the mixed sites and acetylene is always adsorbed more strongly than ethylene. Acetylene is adsorbed in *fcc* positions while ethylene is adsorbed in a bridge position with carbons directly bonded to the Pd atoms. As seen before, the large *d*-band shift induced by Pb and Bi produces an important reduction of the adsorption energy of the double bond. The adsorption of the molecules with triple bonds while desorbing those with double bonds, known as the thermodynamic selectivity, is the first requirement when searching for a selective hydrogenation catalyst. [192] Therefore, both Pb and Bi are good enough to improve selectivity. Instead, the presence of Cu on the surface of the alloy is detrimental as both the double and the triple bond are stabilized with respect to Pd. Moreover, the Au-containing alloy is less available for alkyne adsorption while keeping a large binding energy for the alkene adsorption thus being also problematic for selectivity. For the NSA Cu alloy, the adsorption therein. C_2H_2 is bonded to the surface by 1.72 and C_2H_4 by 0.73 eV. Both are then lower than the surface model by a rigid shift of 0.2 eV. When comparing to the experiments for the Sn-containing materials the adsorption energy and activation of the double bond was found to be reduced when raising the Sn content thus in agreement with our computational results. [256]

CO adsorption

As for CO adsorption, the control parameter is the average adsorption energy for the structures corresponding to the experi-

mentally determined $p(2x2)$-3CO that is very well-established for Pd. [292–294] The energy is then calculated as follows:

$$E_{CO} = (E_{(3CO-M@Pd)} - E_{M@Pd} - 3E_{HCO})/3 \tag{5.11}$$

where $E_{3CO\text{-}M@Pd}$ is the energy corresponding to the configuration with three CO molecules in the $p(2x2)$ supercell, and E_{CO} the energy of CO. This energy density is very high for Pd surface and is still quite similar for Cu, Ag, Zn, Au, and Ga. For the other atoms the $p(2x2)$ structure does not adsorb exothermically three molecules, and therefore the average CO adsorption density plummets to less than 0.75 eV. On the Cu-NSA the alloy is less prone to hydrocarbon adsorption but more likely to adsorb CO than the clean Pd surface.

It is important to indicate that while the adsorption of the first CO molecule is more favoured than that of C_2H_2 on Pd, Pb, and Bi, this is not the case for the coinage metals, Zn, and Ga. Therefore, a much stronger competition for the potential sites is envisaged in the latter cases, thus making CO a less powerful molecular modifier at low CO concentrations.

5.4.3 Phase formation

Hydride formation can be assessed by the adsorption energies for H atoms in subsequent layers either at the surface or in the interior of the material. At high pressure, H_2 readily dissociates on the Pd surface and forms two kinds of hydrides: the first one, α-phase, contains very little amount of H and does not imply a change in the structure of the material. For the denser β-phase, the H content in the bulk represents about a 70% of the amount of Pd. H atoms sit at octahedral sites in the subsurface positions and the Pd lattice is slightly enlarged (about 10%) to accommodate the hydrogens. [272] In our case we have estimated two key parameters to unveil the formation of hydride phases. [205]

The first one is the surface adsorption energies, which would control the formation of an α-like phase and the real amount of H on the surface. This has been calculated in the $p(2x2)$ model with four layers by occupying all the possible positions on the surface, the energy was obtained as follows:

$$E_{H(s)} = \frac{E_{(NH-M@Pd)} - E_{M@Pd} - NE_{H_2}/2}{N} \tag{5.12}$$

where N is the number of occupied positions, $E_{NH\text{-}M@Pd}$, the alloy with N H atoms on the surface, and E_{H_2} the energy of a hydrogen molecule. The second corresponds to the adsorption energy of internal positions once the surface ones are filled. The energy in this case has been calculated as:

$$E_{H(bulk)} = \frac{E_{(NH-M@Pd)} - E_{M@Pd} - NE_{H_2}/2}{N} \tag{5.13}$$

where now both surface and subsurface positions were occupied. As can be seen in Figure 5.9, the energy for surface positions is quite similar to that of the regular surface for the coinage metals. This is not the case for *sp* metals, where only two positions out of the four available on the surface can be occupied. This is because the promoters create an exclusion area for adsorption. Therefore, hydrogen surface coverage is forbidden in these areas and the total amount of available hydrogen is smaller than for the other M@Pd. As for the subsurface positions, in all cases the energy gain is much smaller for the M@Pd alloys than for the pure system. The average energy (including also surface atoms) almost vanishes for Bi, Sn, and Ga, thus indicating that those materials are not likely to form hydrides. In the X-ray Absorption Fine Structure experiments, XAFS, for Sn@Pd, the suppression of the β-PdH phase was reported in Ref. [255], while for the Ag containing catalyst the presence of an external Pd-rich surface with a Ag core where no hydride can be formed is usually regarded as positive effect in the kinetic experiments. [217]

Regarding the carbide formation we have explored a number of possibilities. Surface C atoms, $E_{s,C}$, in both near and far configuration, were investigated as they illustrate the corrugation of the potential energy surface. The energy was calculated as follows on a $p(2x2)$ model:

$$E_{C(s)} = E_{(C-M@Pd)} - E_{M@Pd} - \frac{1}{2}E_{C_2H_2} + \frac{1}{2}E_{H_2} \tag{5.14}$$

with C near the *fcc* position with the M atom ($E_{C(s,n)}$) or far away ($E_{C(s,f)}$). Negative values indicate exothermic processes. C atoms can only be formed on the surface far away from the impurities. For Sn, Pb, and Bi any position on the surface is strongly poisoned enough so that the formation energies of carbon are larger than 0.75 eV. Therefore, carburization of the surface is unlikely. In a similar manner, the formation of subsurface carbide was analyzed. The energy parameter employed was:

$$E_{C(ss)} = E_{(C-M@Pd)} - E_{M@Pd} - \frac{1}{2}E_{C_2H_2} + \frac{1}{2}E_{H_2} \qquad (5.15)$$

but only in the far configuration. C can occupy *fcc* sites below the surface and this is exothermic when the reference is acetylene by close to -0.6 eV in Pd. This energy is severely reduced for the *sp* metals and in particular Sn, and Bi complete remove the possibility of carbide formation for the surface alloys.

5.4.4 Side reactions: overhydrogenation, coking and oligomerization

Two different types of side reactions compromise the yield of hydrogenation catalysts. On one hand, secondary hydrogenation paths can take place. These include ethylene hydrogenation or overhydrogenation of ethyne. The control of the first problem is usually achieved by improving what is known as thermodynamic selectivity, *i.e.*, keeping ethyne adsorbed while desorbing ethene from the surface. If this were the only control parameter then Au nanoparticles would outperform any of the possible catalytic materials described so far. [127, 151, 194] Shown by Nørskov and co-workers, [21] this requirement poses a further problem as the adsorption of ethyne and ethylene is controlled by a single parameter, the adsorption of C, and thus the opportunity window is a compromise between activity and selectivity towards over-hydrogenation. Then, a part of the selectivity can be traced back to the adsorption properties of the C_2 moieties and the ability to adsorb H in subsurface layers. As we have seen in Figure 5.9, Pb and Bi are very effective in reducing the binding energies of the double bonds while still keeping a strong binding energy for ethyne. Thus, of all the model system studies only these two are effective enough for suppressing C=C adsorption. This can be correlated to the downshift of the Pd *d*-band center.

Still this is just one part of the problem. As we have seen before, under typical reaction conditions the interplay with the hydride phases might be very strong and thus more constraints need to be added to suppress overhydrogenation of the alkynes. Recently we have seen how a model β-PdH phase shows an alternative route, already proposed by Ceyer and co-workers, [295] where subsurface hydrogen generates ethylidene directly from vinyl due to the high chemical potential of the subsurface hydrogen. [192]

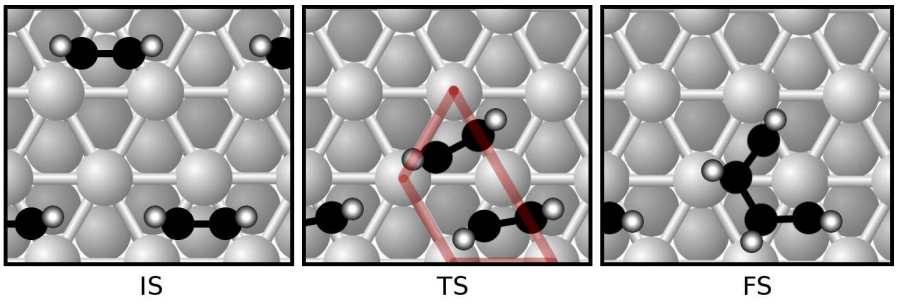

Figure 5.11: Schematic representation of the oligomerization of two acetylene molecules on the Pd(111) surface: IS, TS, and FS are the initial, transition ans final states. Grey spheres are Pd atoms, black C and white H. The minimum ensemble for the reaction is shown in red. Figure based on Ref. [192]

The selectivity towards overhydrogenation can be analyzed by the suppression of H subsurface formation; in Figure 5.9, taken from Ref. [192], it can be seen that all the M considered so far reduce the adsorption energy of bulk H. However, the degree of suppression of the β-PdH structure is larger for Bi and Sn and slightly smaller for Pb and Ga. Suppression of the hydride has been reported experimentally for Sn. [255] There are differences, for some of the co-catalysts as the sites in the surroundings are completely blocked and thus present exclusion areas on the surface. All the studied promoters reduce the availability for the β-PdH phase and thus shall be less prone to overhydrogenate vinyl to ethylidene thus blocking overhydrogenation.

The second source of selectivity loss is related to the formation of carbon-derived fragments. On one side, dissociation of hydrocarbons on low-coordinated sites on the surface might occur and so carbon deposits are usually formed close to edges. [192] The so formed C atoms can then penetrate towards the bulk of the material through rather small energy barriers. This fact has been clearly identified in Prompt Gamma Activation Analysis, PGAA. [13, 13, 21, 296] Carbide formation is known to improve selectivity, [13, 21, 296] but the control and homogeneity of the layer are virtually impossible. [192] In any case, C deposits block either active sites for dissociation (when C is sitting at the step) or reduce the binding energy of alkenes. This results in an enhanced selectivity for the partial hydrogenation of the alkynes. Preferential decoration of step positions reported in Figure 5.9 for Pb and Sn reduces the binding energies of C atoms to step positions. This results in a lower probability for the

dissociation of hydrocarbons due to the kinetic limitations. In addition, Figure 5.9 shows that the ability of the promoters, specially when *sp* metals are considered, results in a lower energy for the formation of the carbide phase thus making thermodynamic factors also less favourable. The effect is not seen for Group 11 metals. The final effect on the selectivity of the competition between secondary metals and carbon-related species is difficult to assess as one limits the effect of the other.

The most important cause for the loss of selectivity under several conditions has been overlooked in many theoretical studies. Oligomerization of the alkyne or partially hydrogenated intermediates to C_{4+} and larger compounds has been described for all the Pd catalysts. In many cases, while controlling overhydrogenation is easy; the control of oligomerization turns out to be extremely difficult. The reaction paths leading to C_{4+} can be formed by the coupling of two acetylene molecules on the surface as shown in Figure 5.11. However, some authors indicate that the presence of a certain amount of hydrogen coverage is needed. [297] The barriers for C-C bond formation are 1.38 eV for two acetylene molecules, but decrease to 1.19 eV for the vinyl-acetylene one. [192]

Two different ways can be envisaged to reduce the amount of oligomers produced on the catalyst surface:

(i) By reducing the overall adsorption energy and thus the coverage on the surface at given acetylene pressure.

(ii) By reducing the size of the available ensembles as the site needed for C-C. bounding implies the use of two neighbouring *fcc*, see Figure 5.11.

This can be seen also as a hindered diffusion of alkynes or partially hydrogenated alkynes on the surface.

In the calculations, we have checked this aspect by analyzing the binding energy of acetylene to *fcc* positions where one of the atoms is replaced by the impurity, $E^{M}_{C_2H_2}$, Figure 5.9. Two types of behaviours are obtained. On one side, Sn, Pb, and Bi behave as true spacers as their adsorption on sites that contain these metals is nearly 1 eV less strong than on the Pd sites, thus inhibiting oligomerization at the surface. On the other hand, C_2H_2 diffusion paths on PdCu, and PdAu are very flat and thus this couple of metals would behave closer to pure Pd surfaces with respect to oligomerization.

Ag, Zn, and Ga show adsorption energies in mixed sites of about 0.60-0.75 eV. For these particular cases, then adsorption on a mixed site would promote the oligomerization as the initial state would be activated and the final state could be stabilized by no direct interaction with the impurity. Indeed the catalysts with Ag, Zn, and Ga are found to produce oligomers. This is a reason to increase the amount of Ag under operation, specially in the tail-end, as more silver is needed to achieve site isolation. For Zn, [244, 245] a 5-20% of oligomers has been reported in 1-pentyne hydrogenation, the higher values corresponding to high temperature (100 °C) operation. For the intermetallic ordered PdGa compounds the oligomerization corresponds to a 5-10%, [247–250] (200 °C for C_2) thus somehow lower than the previous values. This value is smaller than the corresponding value for Zn. There are two potential reasons for this behaviour:

(i) The lower diffusion barrier and the weaker adsorption energy resulting in a smaller coverage.

(ii) The higher temperature and high H_2 pressure that implies lower hydrocarbon coverage on the surface employed in the PdGa experiments.

Our results agree with different experiments, for instance Verdier and co-workers [257] identified lower mobility for the adsorbed species hydrocarbons and hydrogen in PdSn catalysts.

The PdAu case is quite significant. It is well-established that important ensemble effects exist for these alloys in H adsorption in electrochemical environments and in oxidation reactions to form vinylacetate from acetate and ethylene. [225–235, 285] From the results above, the ensemble effects in hydrogenations are less pronounced than for other metals in particular when the mobility of ethyne is considered. Therefore, ensemble effects depend on the reaction. The reduction of the binding energy and a more slightly hindered mobility explain the reduction of benzene formation for these alloys reported in Ref. [242].

5.4.5 Dynamic properties

As the catalysts are exposed to harsh environment, we discuss the stability of the alloys as a function of the external hydrogen and CO pressures. The schematic representations of the processes investigated and the values are presented in Figure 5.12 and 5.13. Experimentally, induced segregation by hydrogen or CO has been reported on PdAu alloys. [223, 240]

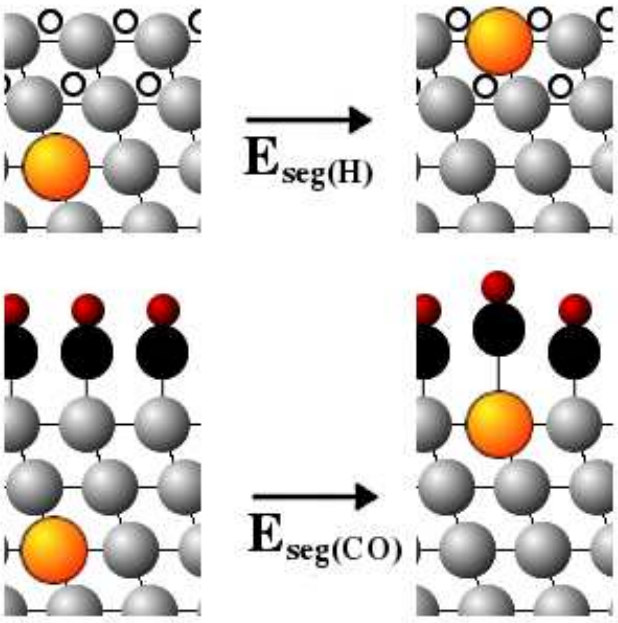

Figure 5.12: Schematic representation of the induced segregation properties. Grey spheres represent Pd, orange the promoter, small white H, black C and red O.

Starting with hydrogen, the surface structures can displace the co-catalyst from the surface. This is clearly seen for Sn, antisegregation is favoured by nearly 1 eV. Still the effect is common to all the systems investigated in Figure 5.13. The heat map shows large antisegregation for Ga, Zn, (0.75 eV), mild for Ag, Au (0.5 eV) and small but still relevant for Cu, Pb, and Bi, around 1/4 eV.

Therefore, none of the investigated alloys show enough resistance towards induced segregation under the high H contents present for instance in the front-end (large H_2:alkyne ratio). This is one of the reasons why the PdGa alloys employed as ordered compounds are

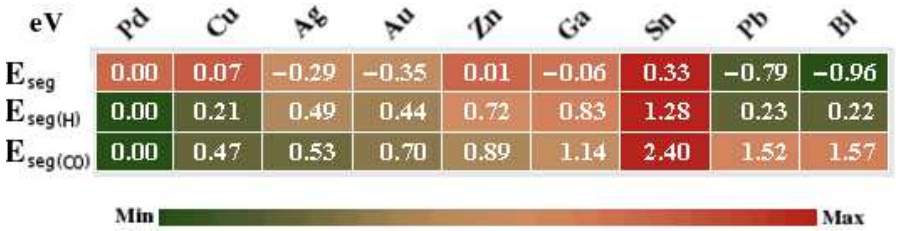

Figure 5.13: Heat map for the dynamic properties of M@Pd alloys. All the energies are shown in eV. The definitions correspond to those in Figure 5.1: segregation, E_{seg}; hydrogen induced segregation $E_{seg(H)}$; and CO induced segregation $E_{seg(CO)}$. The colour code spans the maximum and the minimum value per row.

more resistant. [247–251] Indeed these materials are less prone to induced segregations as the repulsive nature of the Ga-Ga helps in modulating the amount of hydrogen both by reducing the average hydrogen energy and simultaneously improving the repulsion of the secondary metals in the lattice.

For CO the situation is quite similar. CO induces strong antisegregation for Sn but also more than 1.5 eV for Pb and Bi. Therefore, none of these compounds would be suitable for front-end formulations where CO is added to the feed. Medium segregation is found for Au, Zn, and Ga, from 0.7-1.14 eV. The effect is smaller for Cu and Ag, but still moderate, therefore not fully adapted to CO-rich operation.

5.4.6 Ag-rich effects

The patent for the PdAg catalyst in hydrogenation indicates a very wide composition range. In fact, Ag contents can be as large as a 75-80% of the material in many cases, specially in tail-end operation. [206] We have thus investigated the adsorption properties of a material with a nominal composition of $PdAg_3$ with the aim of investigating the differences with the low Ag content alloy. We shall bear in mind that the formation of Ag islands is not strongly hindered as for other promoters, which might lead to small aggregates on the surface but also if the hydrogen pressures are large the stability of Ag on the surface is compromised. Pd site isolation was then obtained by employing larger Ag contents in the alloys. When considering adsorption in the $PdAg_3$ structure, the C_2H_2 is very weakly bound, by -0.4 eV, as instead of the *fcc* site adsorption with π-type

characteristics an on-top σ-bonded structure is retrieved. The C_2H_4 molecules is only physisorbed to this surface, by -0.1 eV which is a positive feature in terms of the thermodynamic selectivity. In this system, subsurface Pd atoms can be segregated towards the surface through an energy penalty of 0.29 eV. This value is almost independent of the amount of Pd on the surface as the maximum energy per atom for the extraction for the model employed is 0.33 eV/Pd atom. Therefore, segregation can be reversed by C_2H_2 adsorption, and then surface Pd dimer is favoured by -0.06 eV, dragging Pd towards the surface. This is induced by the change of the C_2H_2 adsorption from a monomer Pd site to a Pd_2 site on the surface. A complex interplay between the reaction atmosphere and the outermost layer compositions is therefore likely. Thus, for $PdAg_3$ the active hydrogenation ensembles are formed as they are promoted by the reactant. As H is very weakly adsorbed, -0.11 eV/H on the sites containing Pd the reaction could proceed as follows: C_2H_2 is adsorbed, extracts some more Pd from the subsurface where an H atom can also be adsorbed and then first and second hydrogenation takes place. Of course, the dynamic behaviour of the active site being either a monomer or a dimer blocks the possibility for oligomerization that requires around five atoms, see Figure 5.11 (more than 1.2 eV). This picture agrees very well with the suggestions from the experiments reported in Ref. [217].

Finally, CO cannot be added to this catalyst formulation. The reason being that CO adsorbs on top the isolated palladium atoms by a much larger amount, 1.35 eV, than the alkyne. Thus, all the positions would be completely blocked if CO were present.

5.4.7 Compatibility between the promoter, the molecular modifier and the reaction conditions

In the description of Figure 1.10 we have indicated that the complete catalysts are formed by the active material, the promoter or co-catalyst and the molecular modifier. Obviously the structure of the active/selective materials shall be preserved under reaction conditions and thus a significant effect of both temperature and pressure needs to be taken into account. As shown in Figure 5.9, all the metals employed as co-catalysts are compatible with the main material, as all of them form solid solutions. Then the question comes from the stability under reaction conditions.

For instance, surface alloys will suffer of induced hydrogen segregation in almost all cases. Therefore, these structures would be

dynamic under high H_2 conditions. Indeed the fact that the *sp* metals show very weak interaction energy with H turns to be a problem because antisegregation is favoured at high H_2 pressures. The situation is much less effective for Zn, and Ga. For the coinage metals, Cu is already in the form of a NSA alloy and thus it is more stable than if placed on the surface.

Still Pb and Bi are used in Lindlar type catalysts, the reason is related to the modulating effect of the solvent in controlling the total pressure of H_2 in contact with the catalyst. Solubility then needs to be taken into account to understand why these materials are stable under reaction conditions. Moreover, the Lindlar catalyst is employed usually at room or near room temperatures, thus making the diffusion of the metal towards the bulk of the material a less likely process and the issue of stability less crucial. In addition, batch reactors and no continuous operation are more suited to less compatible modifiers.

A second aspect consists in the evaluation of the cross effects between the typical gas-phase modifier and the co-catalyst. Pb and Bi could not be used with CO in any case, because of the large reduction of the binding energies of CO in dense phases when compared to the plane Pd catalysts. This is yet another reason why the Lindlar catalyst avoids CO in its formulation. This is also why a controlled modulation in the relative amounts of CO pressures on the Ag containing catalysts employed in the industry (specially in tail-end operation) is needed to optimize the performance of these materials. The higher the Ag content in the alloy, the lower the amount of CO that can be tolerated.

5.5 Conclusions and outlook

In the current Chapter, the concluding remarks have been drawn from the investigation of the roles of the different components in the Lindlar catalyst in the first place, and then palladium with other possible co-catalysts besides lead, making a comparison between them and also with the clean palladium catalyst. Indeed three characteristics are required to obtain selectivity in the hydrogenation of alkyne-alkene mixtures:

- Thermodynamic separation of reactants (*i.e.*, high alkyne adsorption and low alkene binding energies)

- Avoidance of hydride phases (as hydrides over-hydrogenate)
- Elimination of oligomerization paths

In general, palladium is active in both H_2 splitting and hydrogenation. However, both over-hydrogenation and oligomerization limit the selectivity of the catalyst. In the Lindlar catalyst, DFT shows that the three characteristics shown above are achieved as follows:

1. The solvent helps in reducing the effective H_2 pressure on the surface as it is modulated by the gas solubility in the liquid phase.
2. The exceedingly large ability of Pd to form palladium hydrides is partially modulated by the presence of lead that reduces the overall amount of H in the catalyst.
3. Pb improves the thermodynamic factor as alkene adsorption is strongly reduced when significant amounts of Pb are present.
4. Quinoline basically acts by blocking possible H and alkyne adsorption sites. The isolation of the active centers is beneficial as it impedes the formation of C-C bonds. (*i.e.*, oligomerization)

In summary, regarding to the former part of this Chapter, we have analyzed by means of first principle studies the fundamental role of all the components in the Lindlar catalyst. This is the first time that an extensive computational approach is devoted to understand at the molecular level this famous catalyst that has been successfully employed in industry for nearly six decades. However, the field is far from complete and many remaining challenges await for more accurate descriptions, in particular when related to the role of the second metal and that of molecular modifiers, which are still in the grey zone. The studies on hydrogenation and the comparison to the organic synthesis pave the way towards the systematization of theoretical studies on the reactivity of more complex molecules, with more than one functional group, specially these transformations for which no active catalysts have been proposed that could open new platforms to convert new raw materials (as those derived from biomass) into useful building blocks for the chemical industry. Concerning the latter part of the present Chapter, the main conclusions of the study of potential secondary metals are presented below:

1. - A database containing all static and dynamic properties of M@Pd have been built.

- The importance of the dynamic effects (besides the static ones) in stability have been proved.
- The 8 secondary metals under study can be divided into 3 groups according to their ability to modify palladium reactivity. On one hand, Cu, Ag, and Au atoms located within the Pd surface do not perturb significantly the behaviour of the catalyst. On the other hand, Zn and Ga do modify slightly the reactivity of palladium. Finally, the group formed by Pb, Sn, and Bi can strongly perturb the activity of the catalyst.

2. PdAg are stable only at low H_2 pressures, otherwise dynamic effects come into play. $PdAg_3$ species favours the thermodynamic selectivity towards the hydrogenation of triple bonds, which agrees very well with the suggestions from the experiments reported in Ref. [217].

3. Under external H_2 and CO pressures, all the alloys studied show antisegregation to some extend. Therefore, none of these compounds would be suitable for front-end formulations (large H_2:alkyne ratio) where CO is added to the feed.

4. Bi behaviour is the most similar to Pb and, indeed, it has been proposed as replacement for it. But some of the key parameters for site blocking are worse than those of Pb. There would be interesting to continue some studies in this direction, maybe testing different promoters to improve the key parameters.

5. As Zn and Ga alloys could seem positive in improving selectivity as they reduce the binding energy of the alkenes. However, dynamic effects and oligomerization paths have not been avoided on these catalysts so far.

Part III

Concluding remarks

UNIVERSITAT ROVIRA I VIRGILI
THEORETICAL STUDIES ON MOLECULAR ADSORPTION AND SELECTIVE HYDROGENATION CATALYSTS
Crisa Vargas Fuentes

The current Dissertation is basically divided in two main blocks performed by means of Density Functional Theory, i.e. Molecular Adsorption and Promoters in the Selective Hydrogenation of Alkynes in Mixtures. The former describes an analysis of the behaviour of a number of organic molecules (C_2H_2, C_2H_4, CH_2O, CHN, CH_4O, and CO_2H_2) and fragments (CH_3O, and CO_2H) adsorbed on four different facets, (100), (110), (111), and (211), of the stable *fcc* crystallographic structure of eight monometallic systems (Pd, Pt, Rh, Ir, Cu, Ni, Ag, and Au), moreover testing various sites on each surface. The conclusions of this first work are in agreement with previous works and are enumerated below.

- With respect to the isolated molecules and fragments: The calculated bond length are in good agreement with the experimental values.

- With respect to the metal bulk parameters: The theoretical cell parameters are larger than the experimental ones. This agrees with previous benchmarks with the RPBE functional. The agreement with the experimental data is good, being the errors in the cell parameters with respect to the experimental values below 3.5%.

- With respect to the cohesive energies of the solid metals of the solid metals: The correlations with the experimental values are not so good because the value E_{coh} is severely affected by the estimation of the atomic energy. With the present approach the isolated atomic metal atoms are sometimes not properly described.

- With respect to the surface energy and relaxation: The surface energy of each metal increases along the series: $\gamma_{(111)} < \gamma_{(111)} < \gamma_{(110)} < \gamma_{(211)}$. This correlates with the coordination number of the atoms in the surface. The values obtained are in agreement with previous theoretical estimates.

- With respect to the atomic and molecular adsorption:

  - Atoms: In general, the order in the absolute values of the adsorption energies, from strongest to weakest bond, is E_C

$> E_N > E_O > E_H$. Usually highly coordinated positions (hollow sites) are preferred for all these atoms, in agreement with previous theoretical descriptions.

- Molecules: As a general feature, the larger the π-system of the molecule is, the stronger it binds to the surface.

- Metal activity: Metal activity in this case can be divided into their groups of the periodic system, that is, 9-group (Rh, Ir), 10-group (Ni, Pd, Pt), and 11-group (Cu, Ag, Au). The order in the activity so observed is 9-group>10-group>11-group. This is consistent with proximity of the Fermi level to the top of the *d*-band, in other words, the more amount of empty levels there are, the more active the metal is.

- Facet activity: As the the (100) and (110) surfaces are less dense than the (111) one, they are also more reactive, so the adsorption energies are, in general, lower (stronger bond). For instance, it renders Cu much more active since many adsorption energies for the investigated fragments are exothermic in these cases, unlike the (111) surface. On the other hand, (211) surface has a defect, so at the step all species have higher reactivity than on the rest of the surface.

- Preferential sites: This aspect depends on the species. For atoms, the valence plays an important role. In the case of carbon atom, for instance, the adsorption on any of the two hollows is more exothermic than on top of a metal atom, according to its valence. Along the series, this feature decreases, as the valence decreases. So, for hydrogen, all the energies are similar, as there are almost not preferential sites. Thus, the potential energy surface corrugation is the smallest and the diffusion of H is faster than that of C, N, and O. In the case of molecules, it depends on their size, their π-system and the activity of the metal. In general, if the molecule is small and contains at least a π-bond, it will bind preferentially hollow sites.

- Descriptors: Adsorption energies of different molecules can be scaled with those of their constituent atoms, when these

are directly bound to the surface. The huge interest of these feature is essential for the development of computational chemistry in general, and heterogeneous catalysis in particular.

Regarding to the second block of this dissertation presented in Chapter 5, *i.e.* Molecular Adsorption and Promoters in the Selective Hydrogenation of Alkynes in Mixtures, the concluding remarks have been drawn from the investigation of the roles of the different components in the Lindlar catalyst in the first place, and then palladium with other possible co-catalysts besides lead, making a comparison between them and also with the clean palladium catalyst. Indeed three characteristics are required to obtain selectivity in the hydrogenation of alkyne-alkene mixtures:

- Thermodynamic separation of reactants (*i.e.*, high alkyne adsorption and low alkene binding energies)
- Avoidance of hydride phases (as hydrides over-hydrogenate)
- Elimination of oligomerization paths

In general, palladium is active in both H_2 splitting and hydrogenation. However, both over-hydrogenation and oligomerization limit the selectivity of the catalyst. In the Lindlar catalyst, DFT shows that the three characteristics shown above are achieved as follows:

1. The solvent helps in reducing the effective H_2 pressure on the surface as it is modulated by the gas solubility in the liquid phase.
2. The exceedingly large ability of Pd to form palladium hydrides is partially modulated by the presence of lead that reduces the overall amount of H in the catalyst.
3. Pb improves the thermodynamic factor as alkene adsorption is strongly reduced when significant amounts of Pb are present.
4. Quinoline basically acts by blocking possible H and alkyne adsorption sites. The isolation of the active centers is beneficial as it impedes the formation of C-C bonds. (*i.e.*, oligomerization)

In summary, regarding to the former part of Chapter 5, we have analyzed by means of first principle studies the fundamental role of all the components in the Lindlar catalyst. This is the first time that an extensive computational approach is devoted to understand

at the molecular level this famous catalyst that has been successfully employed in industry for nearly six decades. However, the field is far from complete and many remaining challenges await for more accurate descriptions, in particular when related to the role of the second metal and that of molecular modifiers, which are still in the grey zone. The studies on hydrogenation and the comparison to the organic synthesis pave the way towards the systematization of theoretical studies on the reactivity of more complex molecules, with more than one functional group, specially these transformations for which no active catalysts have been proposed that could open new platforms to convert new raw materials (as those derived from biomass) into useful building blocks for the chemical industry.

To come to an end with the concluding remarks of the present dissertation and concerning the latter part of Chapter 5, the main conclusions of the study of potential secondary metals are presented below:

1.
   - A database containing all static and dynamic properties of M@Pd have been built.
   - The importance of the dynamic effects (besides the static ones) in stability have been proved.
   - The 8 secondary metals under study can be divided into 3 groups according to their ability to modify palladium reactivity. On one hand, Cu, Ag, and Au atoms located within the Pd surface do not perturb significantly the behaviour of the catalyst. On the other hand, Zn and Ga do modify slightly the reactivity of palladium. Finally, the group formed by Pb, Sn, and Bi can strongly perturb the activity of the catalyst.

2. PdAg are stable only at low H_2 pressures, otherwise dynamic effects come into play. $PdAg_3$ species favours the thermodynamic selectivity towards the hydrogenation of triple bonds, which agrees very well with the suggestions from the experiments reported in Ref. [217].

3. Under external H_2 and CO pressures, all the alloys studied show antisegregation to some extend. Therefore, none of these compounds would be suitable for front-end formulations (large H_2:alkyne ratio) where CO is added to the feed.

4. Bi behaviour is the most similar to Pb and, indeed, it has been proposed as replacement for it. But some of the key parameters

for site blocking are worse than those of Pb. There would be interesting to continue some studies in this direction, maybe testing different promoters to improve the key parameters.

5. As Zn and Ga alloys could seem positive in improving selectivity as they reduce the binding energy of the alkenes. However, dynamic effects and oligomerization paths have not been avoided on these catalysts so far.

As seen in the Objectives Chapter, the main goal of the present Doctoral Thesis has been to provide an atomistic viewpoint to old widely discussed topics in the literature. To this aim we have provided new data to the large database of the adsorption properties of gases to metal surfaces and an understanding at molecular level of the behaviour of the different components in Pd-based catalysts for selective hydrogenation, like the Lindlar catalyst.

UNIVERSITAT ROVIRA I VIRGILI
THEORETICAL STUDIES ON MOLECULAR ADSORPTION AND SELECTIVE HYDROGENATION CATALYSTS
Crisa Vargas Fuentes

Part IV

Appendix

UNIVERSITAT ROVIRA I VIRGILI
THEORETICAL STUDIES ON MOLECULAR ADSORPTION AND SELECTIVE HYDROGENATION CATALYSTS
Crisa Vargas Fuentes

Table 5.6: Adsorption energies with respect to the gas phase species, E_{ads} (in eV), of atoms on the (111) facet. See Figure 4.3 and 4.4 for the positions.

		(111)							
Adsorbate	Position	Pd	Pt	Rh	Ir	Cu	Ag	Ni	Au
C	t	-4.04	-4.58	-5.13	-5.35	-2.76	-1.75	-4.25	-2.34
	hcp	-6.43	-6.67	-6.66	-6.42	-4.61	-3.24	-6.44	-4.03
	fcc	-6.46	-6.55	-6.87	-6.64	-4.56	-3.16	-6.51	-3.79
	b	-5.70	-5.88	-5.87	-4.66	-1.92	-1.72	-0.28	-2.56
O	t	-2.60	-2.69	-3.61	-3.60	-2.94	-2.11	-3.55	-1.82
	hcp	-4.19	-4.02	-4.97	-4.60	-4.68	-3.52	-5.37	-2.95
	fcc	-3.97	-3.62	-4.86	-4.38	-4.56	-3.42	-5.28	-2.66
	b	-3.65	-3.47	-3.86	-2.56	-2.08	-2.11	0.75	-0.94
N	t	-1.72	-1.99	-3.11	-3.41	-1.34	-0.23	-2.57	-0.35
	hcp	-4.22	-4.35	-4.80	-4.56	-3.41	-1.87	-4.90	-2.19
	fcc	-4.08	-4.09	-4.94	-4.63	-3.29	-1.75	-4.93	-1.96
	b	-3.43	-3.46	-3.94	-2.56	-0.65	-0.44	1.33	-1.23
H	t	-2.15	-2.58	-2.33	-2.57	-1.77	-1.51	-2.10	-1.86
	hcp	-2.68	-2.55	-2.67	-2.43	-2.31	-1.99	-2.68	-2.11
	fcc	-2.63	-2.51	-2.64	-2.42	-2.31	-1.98	-2.67	-2.07
	b	-2.53	-2.55	-1.64	-0.84	0.04	-0.60	3.33	-1.23

Table 5.7: Adsorption energies with respect to the gas phase species, E_{ads} (in eV), of atoms on the (110) facet. See Figure 4.3 and 4.6 for the positions.

		(110)							
Adsorbate	Position	Pd	Pt	Rh	Ir	Cu	Ag	Ni	Au
C	t	-4.20	-5.22	-5.33	-5.86	-2.58	-1.58	-4.19	-2.38
	h	-5.84	-6.51	-6.48	-6.89	-3.78	-2.53	-5.69	-3.62
	sb	-7.23	-6.96	-7.15	-6.94	-5.06	-3.40	-7.08	-3.84
	lb	-5.66	-5.37	-6.05	-5.95	-4.71	-2.96	-6.25	-3.04
O	t	-3.02	-3.50	-4.05	-4.58	-3.03	-2.07	-3.96	-2.03
	h	-3.98	-4.24	-5.05	-5.33	-4.31	-3.08	-5.07	-2.92
	sb	-3.65	-3.12	-4.20	-4.01	-4.35	-3.40	-4.75	-2.45
	lb	-3.65	-3.08	-4.29	-3.96	-4.35	-3.37	-4.72	-2.42
N	t	-2.02	-2.96	-3.53	-4.29	-1.24	-0.12	-2.69	-0.50
	h	-3.63	-4.32	-4.83	-5.28	-2.65	-1.19	-4.23	-1.69
	sb	-4.39	-3.72	-4.62	-4.10	-3.46	-1.86	-5.01	-1.42
	lb	-3.28	-2.96	-3.96	-3.80	-3.21	-1.61	-4.28	-1.18
H	t	-2.14	-2.63	-2.20	-2.56	-1.67	-1.42	-2.07	-1.84
	h	-2.54	-2.64	-2.53	-2.65	-2.22	-1.90	-2.52	-2.05
	sb	-3.79	-3.48	-3.68	-3.48	-3.43	-3.05	-3.76	-2.86
	lb	-3.58	-3.42	-3.59	-3.39	-3.24	-2.83	-3.62	-2.72

Table 5.8: Adsorption energies with respect to the gas phase species, in eV, of atoms on the (100) facet. See Figure 4.3 and 4.5 for the positions.

		(100)							
Adsorbate	Position	Pd	Pt	Rh	Ir	Cu	Ag	Ni	Au
C	t	-4.13	-4.92	-5.24	-5.53	-3.83	-1.72	-4.27	-2.33
	b	-5.68	-6.24	-6.29	-6.46	-4.90	-2.61	-5.68	-3.52
	h	-7.53	-7.33	-7.61	-7.62	-6.86	-4.03	-7.69	-4.52
	tb	-5.67	-6.24	-6.29	-6.47	-4.89	-2.61	-5.68	-3.50
O	t	-2.84	-3.15	-3.91	0.83	-4.06	-2.02	-3.78	-1.86
	b	-3.87	-4.11	-4.79	-4.84	-5.20	-3.01	-4.88	-2.76
	h	-4.12	-3.72	-4.92	-4.55	-6.04	-3.82	-5.54	-2.91
	tb	-5.33	-4.11	-4.79	-6.25	-5.19	-3.01	-4.87	-2.73
N	t	-1.89	2.78	-3.36	-3.88	-2.39	-0.17	-2.68	-0.38
	b	-3.47	-4.03	-4.57	-4.69	-3.72	-1.21	-4.16	-1.54
	h	-4.32	-4.04	-5.11	-4.82	-5.26	-2.39	-5.62	-2.09
	tb	-3.46	-4.02	-4.56	-3.29	-3.73	-1.20	-4.15	-1.55
H	t	-2.12	-2.64	-2.32	-2.73	-2.77	-1.40	-2.09	-1.84
	b	-2.56	-2.78	-2.61	-2.81	-3.22	-1.84	-2.52	-2.10
	h	-2.55	-2.40	-2.56	-2.44	-3.27	-1.80	-2.61	-1.79
	tb	-2.56	-2.78	-2.61	-2.80	-3.22	-1.84	-2.51	-2.12

Table 5.9: Adsorption energies with respect to the gas phase species, in eV, of atoms on the (211) facet. See Figure and for the positions.

		(211)							
Adsorbate	Position	Pd	Pt	Rh	Ir	Cu	Ag	Ni	Au
C	b_{111}	-6.81	-6.92	-7.12	-7.12	-4.61	-3.11	-6.56	-3.99
	t_eb_e	-4.31	-5.10	-5.32	-5.50	-2.56	-1.64	-4.27	-2.37
	b_e	-5.97	-6.62	-6.53	-6.90	-3.79	-2.48	-5.80	-3.68
	bt_e	-6.06	-6.62	-7.12	-7.12	-4.15	-2.77	-5.85	-3.41
	t	-5.93	-5.22	-5.43	-5.88	-2.51	-1.50	-4.27	-2.37
	b_{100}	-4.30	-5.87	-5.96	-5.69	-4.04	-2.75	-5.54	-3.36
O	b_{111}	-4.21	-4.09	-5.05	-4.95	-4.75	-3.44	-5.44	-2.90
	t_eb_e	-3.04	-3.47	-4.22	-4.75	-3.06	-2.04	-4.02	-2.06
	b_e	-4.22	-4.62	-5.17	-5.51	-4.40	-3.05	-5.28	-3.00
	bt_e	-3.85	-3.62	-5.04	-4.93	-4.24	-3.08	-5.45	-2.54
	t	-3.08	-3.50	-4.39	-4.88	-3.03	-1.97	-4.06	-1.98
	b_{100}	-3.73	-3.57	-4.37	-4.26	-3.92	-2.91	-4.51	-2.49
N	b_{111}	-4.42	-4.47	-5.17	-5.05	-3.41	-1.70	-5.01	-1.94
	t_eb_e	-2.10	-2.83	-3.59	-4.35	-1.23	-0.12	-2.75	-0.48
	b_e	-3.80	-4.53	-4.89	-5.30	-2.67	-1.11	-4.38	-1.75
	bt_e	-3.62	-3.63	-5.16	-5.06	-3.40	-1.33	-4.22	-1.39
	t	-2.13	-3.02	-3.77	-4.49	-1.18	-0.01	-2.77	-0.46
	b_{100}	-3.41	-3.50	-3.96	-3.96	-2.56	-1.18	-3.85	-1.26
H	b_{111}	-2.66	-2.49	-2.60	-2.47	-2.38	-1.99	-2.67	-1.88
	t_eb_e	-2.22	-2.65	-2.45	-2.67	-1.93	-1.68	-2.16	-1.91
	b_e	-2.64	-2.85	-2.70	-2.90	-2.35	-1.99	-2.62	-2.14
	bt_e	-2.57	-2.51	-2.53	-2.46	-2.26	-1.84	-2.57	-1.85
	t	-2.19	-2.72	-2.39	-2.77	-1.84	-1.53	-2.11	-1.95
	b_{100}	-2.53	-2.60	-2.54	-2.60	-1.94	-1.61	-2.39	-1.86

Table 5.10: Adsorption energies with respect to the gas phase species, in eV, of molecules and fragments on the (111) facet. See Figure 4.4 for the positions.

		(111)							
Adsorbate	Position	Pd	Pt	Rh	Ir	Cu	Ag	Ni	Au
C_2H_2	tbt	-0.97	-1.33	-1.36	-1.40	-0.02	0.57	-0.98	0.28
	bfb	-1.38	-1.63	-2.07	-2.01	-0.42	0.51	-1.67	0.44
	bft	-1.24	-1.61	-2.06	-2.01	-0.42	0.50	-1.67	0.45
	btb	-0.21	-0.19	-0.57	-0.33	0.31	0.27	-0.46	0.30
C_2H_4	tbt	-0.37	-0.62	-0.40	-0.39	0.44	0.24	-0.09	0.68
	bfb	0.04	0.20	-0.17	0.09	0.22	0.33	0.04	0.11
	bft	-0.01	0.04	-0.22	0.03	0.65	0.32	0.04	0.07
	btb	-0.22	-0.22	-0.48	-0.33	0.29	0.24	-0.13	0.29
CH_2O	tbt	-0.08	-0.01	-0.26	-0.12	0.26	0.24	-0.20	0.02
	bfb	-0.21	0.20	-0.37	-0.12	0.27	0.11	-0.32	0.12
	bft	0.00	0.23	-0.39	-0.13	0.29	0.28	-0.33	0.19
	btb	0.11	0.31	-0.13	0.18	0.27	0.24	-0.03	0.16
CHN	tbt	-0.45	-0.49	-0.59	-0.41	0.27	0.07	-0.47	0.66
	bfb	-0.34	-0.29	-0.82	-0.46	0.34	0.63	-0.72	0.12
	bft	-0.28	-0.01	-0.69	-0.32	0.39	0.68	-0.68	0.61
	btb	0.07	0.24	-0.17	0.14	0.32	0.18	-0.04	0.05
CH_4O	tbt	0.44	0.15	0.00	0.13	0.03	0.23	0.13	0.04
	bfb	0.45	0.04	0.01	0.02	0.08	0.12	0.04	0.13
	bft	0.68	0.07	0.15	0.13	0.08	0.06	0.17	0.17
	btb	0.98	0.20	0.16	0.23	0.14	0.30	0.09	0.18
CH_2O_2	tbt	0.42	0.70	0.52	0.78	0.26	0.33	0.56	0.13
	bfb	0.63	0.99	0.48	-0.10	0.18	0.41	0.41	0.12
	bft	0.67	0.99	0.48	0.82	0.41	0.26	0.56	0.04
	btb	0.28	0.15	0.48	0.91	0.13	0.30	0.42	0.13
CH_3O	tbt	-0.93	-0.99	-1.44	-1.35	-1.23	-0.95	-1.40	-0.52
	bfb	-1.07	-0.83	-1.61	-1.26	-1.67	-1.32	-1.76	-0.59
	bft	-1.00	-1.02	-1.44	-1.42	-1.59	-1.27	-1.70	-0.54
	btb	-1.17	-1.19	-0.20	0.14	-1.42	-1.04	-0.37	-0.69
CHO_2	tbt	-1.58	-0.71	-1.69	-1.33	-1.66	-1.69	-1.68	-0.65
	bfb	-1.98	-0.54	-1.62	-1.03	-1.83	-1.77	-1.73	-0.90
	bft	-1.05	-0.76	-1.61	-1.04	-1.85	-1.79	-1.76	-0.85
	btb	-1.07	-0.73	-1.70	-1.15	-1.90	-1.83	-1.82	-0.72

Table 5.11: Adsorption energies with respect to the gas phase species, in eV, of C_2H_2, C_2H_4, CH_2O, and CHN on the (110) facet. See Figure 4.6 for the positions.

		(110)							
Adsorbate	Position	Pd	Pt	Rh	Ir	Cu	Ag	Ni	Au
	$tb_{\parallel}t$	-1.20	-0.31	-1.48	-2.19	0.33	0.34	0.52	0.63
	$tb_{\perp}t$	-1.15	-1.69	-1.45	-1.99	0.76	0.27	-1.13	0.64
	$b_{\parallel}hb_{\parallel}$	-1.07	-0.76	-1.29	-1.36	-0.16	1.06	-1.37	1.37
C_2H_2	$b_{\perp}tb_{\perp}$	-1.66	-1.70	-1.88	-2.18	-0.59	0.64	-1.84	0.68
	tht	-1.64	-1.59	-1.88	-1.62	-0.53	0.74	-1.76	0.70
	$b_{\parallel}tb_{\parallel}$	-0.53	-0.76	-0.86	-1.09	-0.02	0.24	-0.80	0.23
	$b_{\perp}hb_{\perp}$	-0.57	-0.92	-0.85	-1.13	-0.04	0.08	-0.63	0.13
	$tb_{\parallel}t$	-0.60	-0.83	-0.71	-0.92	-0.14	0.04	-0.65	0.05
	$tb_{\perp}t$	-0.27	-0.56	-0.29	-0.65	0.41	0.14	-0.10	0.12
	$b_{\parallel}hb_{\parallel}$	0.28	1.69	0.76	0.94	1.52	0.19	0.66	0.23
C_2H_4	$b_{\perp}tb_{\perp}$	-0.62	-0.96	-0.68	-1.05	-0.07	0.05	-0.46	-0.01
	tht	0.44	0.61	0.39	0.48	0.98	0.04	0.17	0.10
	$b_{\parallel}tb_{\parallel}$	-0.54	-0.87	-0.77	-0.92	-0.13	0.09	-0.64	0.03
	$b_{\perp}hb_{\perp}$	0.25	0.60	-0.05	0.10	0.63	1.86	-0.29	2.30
	$tb_{\parallel}t$	-0.15	-0.19	-0.43	-0.50	-0.05	0.01	-0.48	0.17
	$tb_{\perp}t$	-0.22	-0.23	-0.43	-0.66	0.15	0.03	-0.39	0.16
	$b_{\parallel}hb_{\parallel}$	0.64	0.47	0.26	0.47	0.43	0.18	0.03	0.07
CH_2O	$b_{\perp}tb_{\perp}$	-0.18	-0.29	-0.41	-0.60	0.11	0.24	-0.28	0.14
	tht	0.23	0.12	0.29	0.13	0.26	0.19	0.05	0.05
	$b_{\parallel}tb_{\parallel}$	-0.18	-0.08	-0.42	-0.39	-0.01	0.22	-0.14	0.26
	$b_{\perp}hb_{\perp}$	0.07	0.58	-0.27	0.00	0.06	0.08	-0.67	0.12
	$tb_{\parallel}t$	-1.42	-1.74	-1.56	-1.20	-0.63	-0.45	-1.36	-0.32
	$tb_{\perp}t$	-1.38	-1.61	-1.58	-1.28	-0.57	-0.40	-1.13	-0.46
	$b_{\parallel}hb_{\parallel}$	-0.64	0.03	-0.77	0.17	0.06	-0.48	-1.16	-0.46
CHN	$b_{\perp}tb_{\perp}$	-1.46	-1.40	-1.18	-1.33	-0.36	0.21	-1.22	0.21
	tht	-1.00	-1.41	-1.48	-1.67	-0.36	0.14	-2.02	-0.18
	$b_{\parallel}tb_{\parallel}$	-0.80	-0.90	-1.08	-1.11	-0.60	-0.53	-1.12	-0.45
	$b_{\perp}hb_{\perp}$	0.04	-0.14	-0.11	-0.22	0.15	0.15	0.00	0.08

Table 5.12: Adsorption energies with respect to the gas phase species, in eV, of CH_4O, CH_2O_2, CH_3O, and CHO_2 on the (110) facet. See Figure 4.6 for the positions.

		(110)							
Adsorbate	Position	Pd	Pt	Rh	Ir	Cu	Ag	Ni	Au
	$tb_{\parallel}t$	0.14	-0.05	0.06	-0.05	0.00	0.09	-0.04	0.02
	$tb_{\perp}t$	0.14	0.03	0.07	0.14	0.04	0.02	0.36	0.12
	$b_{\parallel}hb_{\parallel}$	-0.12	0.17	0.20	0.08	0.10	0.32	0.13	0.35
CH_4O	$b_{\perp}tb_{\perp}$	-0.03	0.08	0.13	0.00	-0.03	-0.01	-0.07	0.02
	tht	0.14	0.10	0.01	0.02	0.11	0.19	1.22	0.16
	$b_{\parallel}tb_{\parallel}$	0.27	0.05	0.09	0.08	0.06	0.05	0.13	0.12
	$b_{\perp}hb_{\perp}$	-0.13	0.06	0.19	0.15	0.05	0.07	0.11	0.30
	$tb_{\parallel}t$	0.33	0.27	0.23	0.28	0.27	0.19	0.91	0.23
	$tb_{\perp}t$	0.17	0.22	0.11	0.11	2.07	0.22	1.46	0.41
	$b_{\parallel}hb_{\parallel}$	0.98	1.02	0.86	0.83	0.91	1.30	1.00	0.37
CH_2O_2	$b_{\perp}tb_{\perp}$	0.21	0.23	0.17	0.40	0.15	0.25	0.19	0.33
	tht	0.20	0.15	0.16	0.30	0.13	0.10	0.15	0.26
	$b_{\parallel}tb_{\parallel}$	0.85	0.78	0.17	0.46	1.23	1.25	0.96	1.29
	$b_{\perp}hb_{\perp}$	0.26	0.22	0.23	0.33	0.16	0.22	0.28	0.32
	$tb_{\parallel}t$	-1.48	-1.69	-1.87	-2.11	-1.57	-0.95	-1.84	-0.88
	$tb_{\perp}t$	-1.19	-1.44	-1.72	-1.80	-1.47	-1.11	-1.71	-0.68
	$b_{\parallel}hb_{\parallel}$	-0.93	-0.76	-1.30	-1.20	-1.48	-1.15	-1.49	-0.40
CH_3O	$b_{\perp}tb_{\perp}$	-1.51	-1.70	-1.83	-2.00	-1.67	-1.10	-1.98	-0.91
	tht	-0.60	0.06	-0.86	-0.37	-1.13	-1.06	-1.13	-0.33
	$b_{\parallel}tb_{\parallel}$	-1.28	-1.48	-1.76	-1.43	-1.52	-1.02	-1.86	-0.66
	$b_{\perp}hb_{\perp}$	-1.43	-1.38	-1.83	-1.79	-1.93	-1.36	-2.24	-0.89
	$tb_{\parallel}t$	-1.33	-0.88	-1.92	-1.73	-1.88	-1.90	-1.70	-1.28
	$tb_{\perp}t$	-1.33	-0.83	-1.42	-0.96	-2.09	-1.98	-1.70	-1.27
	$b_{\parallel}hb_{\parallel}$	-1.92	-1.56	-2.33	-1.90	-2.61	-2.28	-2.84	-1.35
CHO_2	$b_{\perp}tb_{\perp}$	-1.26	-1.40	-1.54	-1.26	-1.96	-1.89	-2.04	-0.71
	tht	-1.90	-1.73	-2.32	-2.14	-2.61	-2.25	-2.78	-1.43
	$b_{\parallel}tb_{\parallel}$	-1.30	-0.91	-1.61	-1.36	-1.90	-1.92	-1.74	-1.09
	$b_{\perp}hb_{\perp}$	-2.01	-2.37	-2.80	-3.03	-2.48	-2.28	-2.90	-1.70

Table 5.13: Adsorption energies with respect to the gas phase species, in eV, of molecules and fragments on the (100) facet. See Figure 4.5 for the positions.

		(100)							
Adsorbate	Position	Pd	Pt	Rh	Ir	Cu	Ag	Ni	Au
C_2H_2	btb	-0.32	-0.57	-0.70	-0.71	-0.82	0.35	-0.61	0.33
	hbh	-0.79	-1.05	-1.52	-1.53	-1.15	0.88	-1.40	1.15
	tht	-2.01	-2.72	-2.41	-2.87	-1.84	0.31	-2.06	-0.18
C_2H_4	tbt	-0.45	-0.67	-0.54	-0.59	-0.96	0.34	-0.33	0.08
	btb	-0.32	-0.70	-0.54	-0.61	-0.97	0.33	-0.33	0.24
	hbh	0.17	0.20	0.31	0.52	-1.01	0.37	0.39	0.14
	tht	0.15	0.18	0.29	0.43	-0.90	0.28	0.37	0.08
CH_2O	tbt	-0.04	0.06	-0.20	-0.09	-0.95	0.21	-0.22	0.09
	btb	-0.02	0.05	-0.20	-0.10	-0.96	0.25	-0.21	0.09
	hbh	0.31	0.33	0.13	0.35	-0.97	0.04	1.34	0.07
	tht	0.26	0.10	0.39	0.19	-0.96	0.20	0.21	0.28
CHN	tbt	-0.58	-0.85	-0.73	-0.83	-0.88	0.23	-0.64	0.41
	btb	-0.02	0.00	-0.21	-0.13	-0.87	0.17	-0.18	0.13
	hbh	0.02	0.22	-0.46	-0.22	-0.57	0.21	-0.51	0.09
	tht	-0.96	-1.15	-1.30	-1.42	-0.92	0.87	-1.25	0.97
CH_4O	tbt	-0.02	0.08	0.04	0.05	-1.03	0.17	0.65	0.32
	btb	0.01	0.07	0.04	0.05	-1.03	0.09	0.05	0.28
	hbh	0.10	0.06	0.01	0.17	-0.99	0.30	0.83	0.05
	tht	0.00	0.12	0.03	0.11	-0.99	0.02	0.08	0.13
CH_2O_2	tbt	0.10	0.07	0.08	0.13	-1.00	0.20	0.29	0.21
	btb	0.24	0.16	0.25	0.16	-0.99	0.15	0.26	0.15
	hbh	0.11	0.14	0.16	0.29	-0.90	0.21	0.67	0.31
	tht	0.16	0.16	0.19	0.22	-1.12	0.24	0.83	0.19
CH_3O	tbt	-1.14	-1.32	-1.67	-1.72	-2.51	-1.06	-1.59	-0.82
	btb	-1.16	-1.39	-1.61	-1.76	-2.51	-1.05	-1.65	-0.80
	hbh	-1.50	-1.58	-2.02	-1.96	-3.07	-1.48	-2.20	-1.06
	tht	-1.54	-1.58	-2.04	-2.01	-3.09	-1.45	-2.24	-1.06
CHO_2	tbt	-1.07	-0.41	-1.55	-1.51	-2.88	-1.59	-1.57	-0.89
	btb	-1.12	-1.15	-1.52	-1.79	-2.82	-1.69	-1.52	-0.94
	hbh	-1.24	-1.06	-1.23	-1.45	-3.07	-1.90	-1.51	-1.51
	tht	-1.35	-1.03	-1.72	-1.36	-3.17	-2.05	-1.85	-1.27

Table 5.14: Adsorption energies with respect to the gas phase species, in eV, of C_2H_2, C_2H_4, CH_2O, and CHN on the (211) facet. See Figure 4.7 for the positions.

		(211)							
Adsorbate	Position	Pd	Pt	Rh	Ir	Cu	Ag	Ni	Au
C_2H_2	bhb	-1.54	-1.82	-1.94	-2.16	-0.60	0.43	-1.65	0.06
	bhb_e	-1.77	-2.33	-2.25	-2.67	-0.60	0.47	-1.85	0.13
	$t_eb_et_e$	-1.88	-2.03	-2.13	-2.28	-0.21	0.75	-1.69	0.48
	hb_eh	-1.26	-1.72	-1.94	-2.35	-0.28	0.17	-1.61	0.51
	$b_et_eb_e$	-0.54	-0.30	-1.00	-0.74	0.50	1.65	-0.71	0.43
	ft_eb	0.16	0.08	-0.04	-0.19	1.02	0.64	0.72	0.56
C_2H_4	bhb	-0.03	-1.26	-0.15	0.12	0.52	0.23	-0.04	0.25
	bhb_e	-0.25	-0.52	-0.60	-1.07	0.20	0.13	-0.40	0.27
	$t_eb_et_e$	0.61	0.99	0.55	0.68	1.62	0.99	0.62	2.81
	hb_eh	-0.19	0.99	-0.38	-0.22	0.27	0.15	-0.20	0.06
	$b_et_eb_e$	0.13	1.07	0.80	2.54	0.12	0.17	1.07	0.16
	ft_eb	-0.71	-0.97	-0.97	-1.25	-0.06	0.02	-0.57	-0.02
CH_2O	bhb	0.13	0.28	-0.57	0.34	0.22	0.16	-0.44	0.15
	bhb_e	-0.23	0.25	-0.67	-0.80	0.02	0.20	-0.68	0.10
	$t_eb_et_e$	-0.43	-0.59	-0.71	0.41	-0.02	0.33	0.01	0.08
	hb_eh	0.09	0.37	-0.21	0.07	0.27	0.17	-0.25	0.22
	$b_et_eb_e$	0.38	-0.57	0.30	0.82	0.23	0.30	0.55	0.16
	ft_eb	-0.25	-0.23	-0.63	-0.74	0.05	0.20	-0.44	0.11
CHN	bhb	-0.59	-0.35	-0.82	-0.68	0.09	0.06	-0.77	0.67
	bhb_e	-0.78	-0.83	-1.22	-1.33	0.02	0.17	-1.14	0.70
	$t_eb_et_e$	-0.63	-0.31	-0.84	-0.64	0.65	1.08	-0.71	1.49
	hb_eh	-0.41	-0.40	-0.94	-1.08	3.40	0.12	1.30	0.20
	$b_et_eb_e$	-0.26	-0.28	-0.59	-0.71	0.15	0.15	4.37	0.11
	ft_eb	-0.30	-0.30	-0.64	-0.75	0.12	0.08	-0.41	0.12

Table 5.15: Adsorption energies with respect to the gas phase species, in eV, of CH_4O, CH_2O_2, CH_3O, and CHO_2 on the (211) facet. See Figure 4.7 for the positions.

		(211)							
Adsorbate	Position	Pd	Pt	Rh	Ir	Cu	Ag	Ni	Au
CH_4O	bhb	0.05	2.95	0.09	2.25	0.18	0.09	0.06	0.14
	$t_eb_et_e$	-0.06	-0.02	0.12	-0.09	-0.02	0.01	-0.15	0.09
	hb_eh	0.86	0.62	0.20	-0.10	0.58	1.43	0.16	1.94
	$b_et_eb_e$	0.04	-0.09	-0.08	-0.10	0.06	0.10	0.00	0.11
	ft_eb	2.12	2.34	2.06	-0.07	0.04	2.55	1.88	3.08
CH_2O_2	bhb	0.33	0.93	0.91	-0.13	1.43	1.95	2.79	2.54
	bhb_e	0.35	0.77	0.31	0.14	1.15	0.33	0.51	0.24
	$t_eb_et_e$	1.04	1.61	1.06	-0.18	1.53	1.18	1.57	1.65
	hb_eh	3.31	3.35	3.32	2.09	0.19	2.41	3.44	2.32
	$b_et_eb_e$	0.09	3.78	0.04	3.55	0.10	0.21	0.01	0.13
	ft_eb	0.29	0.36	0.16	0.27	0.28	0.18	0.17	0.36
CH_3O	bhb	-1.14	-0.61	-1.67	-1.22	-1.64	-1.17	-1.82	-0.53
	bhb_e	-1.25	-1.71	-1.15	0.05	-1.59	-1.12	-0.60	-0.79
	$t_eb_et_e$	-1.17	-1.55	-1.40	-2.24	-1.45	-0.94	-1.85	-0.45
	hb_eh	0.31	-0.20	-1.55	-1.38	-2.27	-1.52	-1.65	1.60
	$b_et_eb_e$	-1.62	-1.66	-2.10	-2.29	-1.88	-1.19	-2.22	-0.97
	ft_eb	-1.56	-1.75	-2.16	-0.14	-1.69	-1.15	-2.08	-0.92
CHO_2	bhb	-1.19	-0.47	-1.60	-1.33	-1.67	-1.60	-0.65	-0.60
	bhb_e	-1.81	-1.52	-2.43	-2.28	-2.41	-2.08	-2.59	-1.46
	$t_eb_et_e$	-1.50	-1.23	-1.96	-2.22	-2.06	-1.73	-1.91	-0.94
	hb_eh	-1.55	-1.71	-1.95	-2.27	-2.36	-1.90	-2.04	-1.28
	$b_et_eb_e$	-1.86	-1.47	-2.74	-2.24	-2.43	-2.30	-2.55	-1.72
	ft_eb	-1.74	-1.64	-2.19	-2.19	-2.10	-1.92	-2.25	-1.34

Part V

List of publications

UNIVERSITAT ROVIRA I VIRGILI
THEORETICAL STUDIES ON MOLECULAR ADSORPTION AND SELECTIVE HYDROGENATION CATALYSTS
Crisa Vargas Fuentes

1. **A density functional theory study of the 'mythic' Lindlar hydrogenation catalyst** García-Mota, M.; Gómez-Díaz, J.; Novell-Leruth, G.; Vargas-Fuentes, C.; Bellarosa, L.; Bridier, B.; Pérez-Ramírez, J.; López, N. *Theor. Chem. Acc.* **2011**, 128:663-673

2. **Promoters in the hydrogenation of alkynes in mixtures: insights from density functional theory** López, N.; Vargas-Fuentes, C. *Chem. Commun.* **2012**, 48, 1379-1391

The author has performed the majority of the numerical work in the publication 2, and part of the calculations in the publication 1 by using the Density Functional Theory code VASP. She has participated actively in the writing of all the publications and has also contributed to the next paper:

- **C-N coupling on transition metal surfaces: A density functional theory study** Gómez-Díaz, J.; Vargas-Fuentes, C.; López, N.; *J. Chem. Phys.* **2011**, 135, 124707

which is excluded from the thesis.

UNIVERSITAT ROVIRA I VIRGILI
THEORETICAL STUDIES ON MOLECULAR ADSORPTION AND SELECTIVE HYDROGENATION CATALYSTS
Crisa Vargas Fuentes

Theor Chem Acc (2011) 128:663–673
DOI 10.1007/s00214-010-0800-0

REGULAR ARTICLE

A density functional theory study of the 'mythic' Lindlar hydrogenation catalyst

M. García-Mota · J. Gómez-Díaz · G. Novell-Leruth · C. Vargas-Fuentes · L. Bellarosa · B. Bridier · J. Pérez-Ramírez · N. López

Received: 6 July 2010 / Accepted: 16 August 2010 / Published online: 7 September 2010

Abstract A Lindlar catalyst is a popular heterogeneous catalyst that consists of 5 wt.% palladium supported on porous calcium carbonate and treated with various forms of lead and quinoline. The additives strategically deactivate palladium sites. The catalyst is widely used for the partial hydrogenation of acetylenic compounds in organic syntheses. Alkyne reduction is stereoselective, occurring via *syn* addition to give the *cis*-alkene. Even if it has been employed for about 60 years, there is a lack of molecular level understanding of the Lindlar catalyst. We have applied density functional theory simulations to understand the structure and the nature of the interplay between the multiple chemical modifiers in the Lindlar catalyst. Indeed, the poisons influence different parameters controlling selectivity to the alkene: Pb modifies the thermodynamic factor and hinders the formation of hydrides, while quinoline isolates Pd sites thus minimizing oligomerization.

Keywords Hydrogenation · Acetylenic compounds · Lindlar catalyst · Selectivity · DFT

Published as part of the special issue celebrating theoretical and computational chemistry in Spain.

M. García-Mota · J. Gómez-Díaz · G. Novell-Leruth · C. Vargas-Fuentes · L. Bellarosa · N. López (✉)
Institute of Chemical Research of Catalonia (ICIQ), Avgda. Països Catalans 16, 43007 Tarragona, Spain
e-mail: nlopez@iciq.es

B. Bridier · J. Pérez-Ramírez
Institute for Chemical and Bioengineering, Department of Chemistry and Applied Biosciences, ETH Zürich, HCI E 125, Wolfgang-Pauli-Strasse 10, CH-8093 Zürich, Switzerland

1 Introduction

Heterogeneous catalysis has been the main contributor to the development of chemical industry development over the last century. Those catalysts are complex systems that contain a multiple set of ingredients; most commonly, they are presented in the form of solids and are ubiquitous in chemical and petrochemical transformation processes. Unlike the study of homogeneous catalysts and enzymes, the structure and composition of heterogeneous catalyst is very difficult to characterize. Therefore, the complementary use of computational tools based on density functional theory (DFT) and experiments has shown to improve our knowledge of the catalytic phenomena. The type of simulations required for these studies (based on DFT and periodic boundary conditions) is computationally highly demanding and, only in the last two decades, reliable computational tools and enough computer power to perform these simulations has been achieved. Indeed, the theoretical study of heterogeneous catalysis has provided guidelines to improve activity; however, this might not be enough when more industrially relevant problems are addressed.

The development of selective processes is the key for the research in the chemical industry in the twenty-first century [1]. Sharp reactions are a must to achieve eco-efficient alternatives to existing processes. A large fraction of reactions, in the production of bulk chemicals, fine chemicals, and pharmaceuticals, corresponds to selective hydrogenations [2, 3]. Hydrogenation reactions can involve a single unsaturated reactant that is then partially hydrogenated, multifunctionalized molecules, and/or complex mixtures presenting more than a single active species where only one of the reactants or functional groups should be partially hydrogenated. Selectivity can be classified in three different terms: selectivity to a reaction, to a reactant,

and to a product [4]. For partial alkyne hydrogenations, all these selectivities are required: namely stopping the hydrogenation process at the thermodynamically metastable alkene (product selectivity), eliminating the competition of different substrates for the catalyst (reactant selectivity), and blocking oligomerization reactions (reaction selectivity). Recently, our research efforts aimed at establishing links between material and pressure gaps for the gas-phase hydrogenation of alkyne + alkene mixtures and also the differences between homogeneous and heterogeneous catalysis for this particular type of reactions [5, 6]. The catalysts in both hydrorefining (i.e., gas-phase alkyne hydrogenation in alkene cuts of steam crackers) and the hydrogenation of acetylenic compounds in fine chemistry are based on palladium. However, the preparation of both catalysts and the conditions at which they run differ substantially.

The adsorption and selective hydrogenation of alkynes versus that of alkenes have been considered as a model reaction and have been subject to several theoretical studies mostly concentrated on the properties of clean palladium surfaces [7] and alloys [8]. Recently, the role of the formation of different phases, their correlation with the activity and selectivity and the effect of selectivity moderators have been investigated [9]. Attempts to identify more selective catalysts by means of theoretical calculations have also been performed [10]. In particular, for NiZn alloys a complete quenching of the over-hydrogenation route was proposed [10].

Alkyne hydrogenation in C2 and C3 cuts is widely implemented downstream of the steam crackers [3]. The main aim is to selectively reduce the amount of ethyne–propyne in the presence of ethene and propene-rich streams. This is done to increase the purity of these feeds to meet the strict demands (few ppm of the alkyne) of the polymerization units. The particular specifications of the catalyst of choice depend on the position in the plant, which determines the composition of the mixture (namely the hydrogen-to-alkyne ratio). A general catalyst contains very small amounts of Pd (<0.05 wt.%), supported on low-surface area alumina and with metal promoters (Ag, Au) and selectivity modifiers, mainly CO, see Table 1.

In fine chemistry, the Lindlar catalyst is stereotypic for hydrogenation of acetylenic compounds in the liquid phase [11, 12], see Table 1. This well-established catalyst contains up to 5 wt.% Pd supported on either $CaCO_3$ or $BaSO_4$. In the preparation, a solution of 5 wt.% of $Pb(OAc)_2$ is added to the initial catalyst to deactivate it. Then, the system is heated at low temperature (95 °C), and it is likely that the organic moiety is eliminated and some form of metallic lead deposit appears [13, 14]. It is well known that Pb and Pd do form solid solutions [15, 16], and studies on the interaction of Pb films with Pd(111) surfaces

Table 1 Comparison between the hydrogenation catalyst in hydrorefining units and the Lindlar catalyst

	Hydrorefining catalyst	Lindlar catalyst
Substrate	Ethyne, propyne	Long chain alkynes
Medium	Gas phase or liquid phase	Liquid phase
Pd content (%)	0.01–0.05	1–5
Second metal	Ag, Au, etc.	Pb, Bi, Cu
Selectivity modifier	CO	Quinoline
Support	Al_2O_3	$CaCO_3$, $BaSO_4$
Temperature	RT-350 K	RT
Solvent	None	Benzene, toluene, methanol
Regioselectivity	–	*cis*
p_{H2}	Up to 20 bar	1–10 bar
Operation	Continuous	Batch

demonstrate that formation of alloys is favored [17]. It has been suggested that a surface alloy with composition Pd_3Pb is formed, as the active species of the Lindlar catalyst [18], although the real surface stoichiometry of the material is not clear. In addition, penetration of Pb toward the bulk has been also put forward [13, 19, 20]. The rearrangement of Pd particles, when Pb is incorporated in the catalyst has also been suggested in the literature [21]. Alternative metals to Pb suggested in the first report by Lindlar were Bi and Cu [11]. Then, a second kind of modifier, a molecule with a strong interaction to the surface is added to the catalyst. Usually, these molecules are organic compounds possessing oxygen, sulfur, phosphorous, or nitrogen heteroatoms. The ratio of an efficient modifier to the substrate is in the range 0.01–1 mol% [22]. In the Lindlar catalyst, usually quinoline ($C_{11}H_{11}N$), is employed, although piperidine and 2,2′-(ethylenedithio)diethanol have been suggested too [12]. Quinoline has been proposed to: (1) compete with alkynes for the adsorption to the surface, (2) to inhibit alkene surface interactions [23], and (3) to reduce isomerization processes. Moreover, quinoline is thought to act as an electron donor to the surface and then modifies the polarization of the Pd–H bond [24].

In summary, in the Lindlar catalyst the Pd particles are likely to contain Pb as a dopant and to be poisoned by the N-containing organic rings. The Lindlar catalyst works at room to medium temperature and deactivates at higher temperatures. It is usually employed with organic solvents, (i.e., benzene and toluene), and when reactants are not soluble in this media, methanol can be employed. Selectivity results from the Lindlar catalyst are exceptional in the competition of alkyne and alkene groups and more than 85% is routinely obtained [11]. In addition, for complex substrates mainly *cis* insertion is observed. Thus, the Lindlar catalyst provides also some degree of regio-

selectivity. However, usually these processes are carried out in batch reactors and the selectivity is found to depend on the reaction time. At very long residence times, the preference to the *cis* is smoothed out and some degree of alkene hydrogenation can also be observed.

In order to understand how the Lindlar catalyst works and why it is so selective the comparison to what is known about hydrogenation catalysts can provide a lot of insight. Previous investigations on the hydrogenation of C2 and C3 cuts and the careful comparison of experimental and theoretical work have clarified the issue. We have explored different aspects regarding the gas-phase hydrogenation of alkynes in the presence of alkenes for different metals including Au [25], Ni and Cu [26], ternary Cu–Ni–Fe [27], and the interplay between different phases and the selectivity on Pd [9]. The three main controllers of the alkene selectivity are as follows:

1. *Thermodynamic selectivity*, this is the ability to adsorb preferentially only the alkyne moieties in the presence of any other functional group. This is the only controlling factor in Au nanoparticle-based catalysts.
2. *Inability to form a hydride phase*, hydrides overhydrogenate adsorbed moieties due to the presence of high potential sub-surface H species. Those present a smaller kinetic demand than the surface counterpart and thus invalidate the thermodynamic control. The catalyst of choice, Pd, has a large versatility in the formation of hydrides and thus, at high hydrogen-to-alkyne ratios, the performance of the Pd catalyst alone is extremely poor.
3. *Definition of small ensembles.* Two of the competing routes in the process involve the activation of H atoms toward the reactive moiety or, alternatively, the formation of C–C bonds. The ensembles required for the second reaction are larger than those of hydrogenation and thus are detrimental for selectivity. Moreover, oligomers can block the active sites. Therefore, reducing oligomerization is linked with the control of the ensemble size.

Our aim in the present work is to understand how the Lindlar catalyst deals with the points described above: thermodynamic factors, hydride formation and active ensembles. The 'mythic' Lindlar catalyst has been industrially applied for around 60 years; it is still used in natural product syntheses (like A vitamin) and remains the most popular catalyst for the partial hydrogenation of acetylinic compounds [12, 28]. Surprisingly, the reasons for the outstanding selectivity are still not well grounded. For instance, the study of the co-metal effect has been the subject of some investigations but a complete picture has not yet emerged [29]. There is a lack of studies that can unravel at the molecular level the role of the various ingredients in the Lindlar catalyst. This is precisely the aim of the present work, to give a rational understanding of the modifiers in Lindlar-type catalysts by comparison with pure palladium. In order to do this, the stability, activity, and selectivity properties of both Pd and a series of systems of increasing complexity (Pd–Pb alloys, Pd–quinoline and Pd–Pb–quinoline systems) that represent the Lindlar catalyst have been studied. To analyze the thermodynamic and kinetic factors of the hydrogenation process we have employed the simplest alkyne–alkene pair. This is supported by our previous calculations that indicate the similarities for C2 and C3 compounds for the Pd case.

2 Computational details

We have employed density functional theory applied to slabs with the VASP code [30]. The energies have been obtained through the PW91 version of the exchange and correlation functional [31]. The inner electrons have been represented through PAW pseudopotentials [32], while the valence electrons have been expanded in plane waves with a cut off energy of 400 eV. With this set up, the cell parameter for Pd was found to be 3.966 and 5.023 Å was obtained for Pb. The (111) surface has been employed for the reactivity studies, since this is the one showing the lowest energy for fcc metals. The slabs contain four layers in a $p(2 \times 2)$ reconstruction for the hydrogen formation and have been extended to six layers for the Pb solubility studies. In that case, a single Pd atom was substituted by Pb. These systems are denoted as Pb@Pd. Islanding was computed in a $p(3 \times 3)$ configuration with two Pb atoms on the surface. For the adsorption of quinoline on both Pd clean and Pb@Pd systems, a larger supercell with a $p(4 \times 4)$ reconstruction was employed, denoted Pd–Q_{Pd} and Pb@Pd–Q_{Pd}. In the second case, the amount of Pb was taken as either 0.25 or 0.0625 ML. The vacuum space interleaving the different slabs was set to >10 Å. The *k*-point sampling was performed with the Monkhorst–Pack [33] scheme with $5 \times 5 \times 1$ points for the small cell, and $3 \times 3 \times 1$ for the larger ones. To illustrate the decoration at steps, we have employed a Pd(211) cut with a (3×1) reconstruction and nine layers, the *k*-point sampling being $3 \times 3 \times 1$. These computational settings have been demonstrated to produce energies that are converged by 0.02 eV. In Fig. 1, a summary with all the models employed in the present calculations is shown.

As a representative model for the alkyne–alkene pair, we employed the smallest possible hydrocarbons: ethyne and ethene. In previous studies, we have seen how thermodynamic and kinetic properties of the hydrogenation reaction are similar for C2 and C3, although other properties, i.e., carbide formation, are a strong function of the

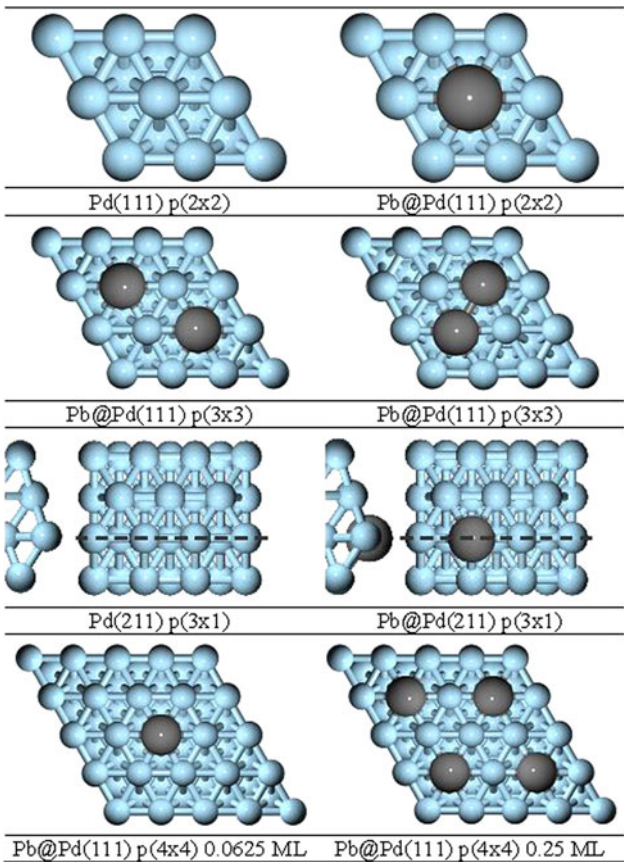

Fig. 1 Models for the different surfaces employed in the calculations. *Blue spheres* represent Pd and *gray* Pb. The *lines* indicate the edge for the step models

number of carbon atoms [9]. Adsorption was performed on one side of the unit cell and both the adsorbate and two upper layers were allowed to relax (z-direction). To determine the transition states CI-NEB calculations [34] were performed.

3 Results

3.1 The Pd–Pb system

The Pd–Pb system forms solid solutions with different compositions and structure [15]. In particular, at low Pb concentration, a solid solution where Pb substitutes Pd has been described. We have calculated the solubility for Pb impurities and the corresponding segregation profile for Pb in the Pd lattice. The energy profile is shown in Fig. 2. The solubility was calculated as:

$$E_{\mathrm{sol}} = E_{\mathrm{Pb@Pd}}^{(2\times2-6\mathrm{layer})} + E_{\mathrm{Pd(bulk)}} - E_{\mathrm{Pd}}^{(2\times2-6\mathrm{layer})} - E_{\mathrm{Pb(bulk)}} \quad (1)$$

where $E_{\mathrm{Pb@Pd}}^{(2\times2-6\mathrm{layer})}$ is the energy of the Pd slab with a substituted Pb atom, $E_{\mathrm{Pd(bulk)}}$ and $E_{\mathrm{Pb(bulk)}}$ are the corresponding bulk energies per atom for both metals, and $E_{\mathrm{Pb}}^{(2\times2-6\mathrm{layer})}$ the energy of the Pd slab. From Eq. 1, the substitution of Pb in the Pd lattice at the bulk position (L-3) is exothermic by 1.12 eV. Therefore, the formation of the Pb–Pd bond is more favorable than the Pb–Pb one and the solubility of Pb atoms is very likely considering also the contribution from configurational entropy [35]. We have also calculated the segregation energy to assess whether surface or bulk positions are more likely for the Pb impurities. The segregation energy has been calculated as follows:

$$E_{\mathrm{seg}} = E_{\mathrm{Pb(L-X)@Pd}}^{(2\times2-6\mathrm{layer})} - E_{\mathrm{Pb(L-3)@Pd}}^{(2\times2-6\mathrm{layer})} \quad (2)$$

where $E_{\mathrm{Pb(L-X)@Pd}}^{(2\times2-6\mathrm{layer})}$ is the energy for the impurity in the position L-X and L-3 represents the impurity sitting at the bulk. Calculations indicate the likely segregation of Pb toward the surface, see Fig. 2. The energy gain is 0.79 eV with respect to Pb in the bulk position. Surface Pb atoms are relaxed toward the vacuum by 0.227 Å. In addition, the Lindlar preparation method described in the Introduction will also promote Pb impurities to stay on the surface and thus surface impurity models and near-surface ones will be employed as the most likely structures under reaction conditions. A third aspect concerns the formation of Pb islands when considering impurities in the alloy. Island formation has been calculated as follows:

$$E_{\mathrm{isl}} = E_{\mathrm{Pb2@Pd}}^{(3\times3-4\mathrm{layer})} - E_{\mathrm{Pb+Pb@Pd}}^{(3\times3-4\mathrm{layer})} \quad (3)$$

where $E_{\mathrm{Pb2@Pd}}^{(3\times3-4\mathrm{layer})}$ is the energy of a Pb dimer on the Pd surface and $E_{\mathrm{Pb+Pb@Pd}}^{(3\times3-4\mathrm{layer})}$ is the energy of separated atoms in

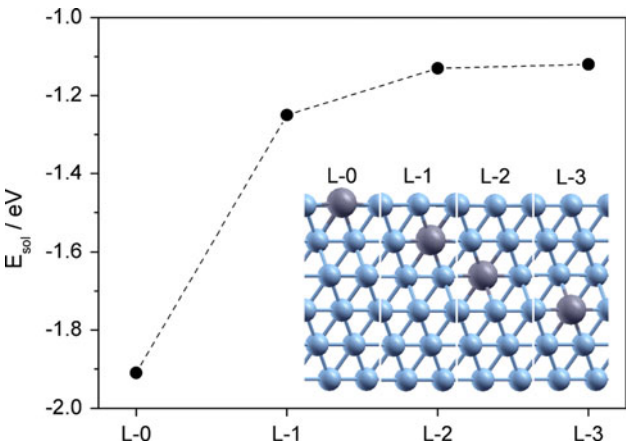

Fig. 2 Solubility energy of a Pb impurity in Pd(111). The inset indicates the positions of the lead atom in the palladium slab. Same color code as in Fig. 1

the same supercell. Pb islanding is endothermic by 0.6 eV and thus isolated Pb atoms are more likely on the surface.

A final aspect regarding the formation of the alloy is the preferential adsorption of Pb at step Pd sites. Indeed, competing reactions such as *cis–trans* isomerization and bond shift isomerization are more likely to occur on rough surfaces, i.e., rich in steps and kinks [36], and there have been some claims that the selective poisoning by Pb of these sites can be at least partially responsible for the enhanced selectivity [37, 38]. We have investigated this aspect by calculating the solubility at the steps.

$$E_{\text{step}} = E^{(3\times1-9\text{layer})}_{\text{Pb-step@Pd}} + E_{\text{Pd(bulk)}} - E^{(3\times1-9\text{layer})}_{\text{Pd-step}} - E_{\text{Pb(bulk)}} \quad (4)$$

where $E^{(3\times1-9\text{layer})}_{\text{Pb-step@Pd}}$ is the energy of the Pb impurity at the step site, $E^{(3\times1-9\text{layer})}_{\text{Pd-step}}$ the energy of the clean Pd step, and $E_{\text{Pd(bulk)}}$ and $E_{\text{Pb(bulk)}}$ the bulk energies per atom of Pd and Pb, respectively. Then, compared to an impurity in the terrace, Pb atoms at the step are more stable by 0.37 eV.

The electronic structure of Pd surfaces and Pb@Pd alloys is described in Fig. 3 through the Projected Density Of States, PDOS. The top figure illustrates the reference system, Pd slab. The bands for bulk and surface Pd atoms are clearly shown and the corresponding *d*-band structures indicate the presence of lower states for the fully coordinated Pd bulk atoms. The *d*-band center [39] for the bulk Pd is placed at 1.76 eV below the Fermi level while the corresponding parameter for Pd atoms on the pure surface is closer to the Fermi level, 1.41 eV. As shown in Fig. 3, the Pd surface layer and in particular the *d*-band is modified by the presence of Pb in the alloys. Upon the formation of the Pb@Pd alloy, the *d*-bands of the Pd atoms are shifted downwards by 0.16 eV. In turn, the Pb levels (only *s* and *p* states are plotted in Fig. 3) show a deep band at about −10 eV and a broad band crossing the Fermi level. Thus, the electronic structure analysis indicates that Pd atoms at the Pb@Pd structures are less reactive than the clean surface. This means that the surface is less prone to adsorb incoming alkyne or alkene molecules.

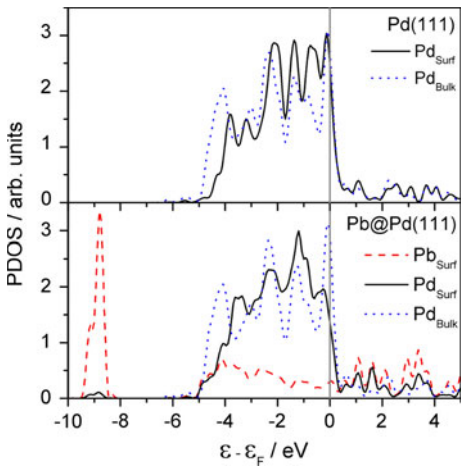

Fig. 3 Projected Density of States for Pd (*top*) and Pb@Pd (*bottom*) alloys. The *black line* represents the states for a surface Pd atom, *blue dotted* those of the bulk and *red dashed* the Pb states

3.2 Hydride and carbide formation in Pd and Pb@Pd

Pd is known to form different phases depending on the environment. Hydrides [40] are formed at room temperature at pressures as low as 0.024 atm [41]. Carbides come from the decomposition of organic molecules as indicated by Honkala et al. [42–45] and sit at octahedric sites in the subsurface region. In particular, this phenomenon is important since both carbides and hydrides are the key to control the selectivity of the catalyst [46, 47].

H_2 dissociation is known to happen even at high coverage with small energy requirements [48, 49]. The simplest way to illustrate the formation of hydrogen in the sub-surface can be addressed by the sequential H insertion [50]. We have investigated the occupation of H in the surface fcc sites and then on the sub-surface and positions closer to the bulk. In both cases, the H atoms sit at the octahedric sites. The average energy gained when adsorbing a monolayer of H atoms on the Pd surface is 0.54 eV/H atom. In the bulk, the average energy is lower, but still favorable as can be seen in Fig. 4. For the Pb@Pd system when the Pb atoms are on the surface, we have explored the adsorption in both the fcc involving Pd–Pb centers and those only formed by Pd. The fcc sites containing one Pb and two Pd do not efficiently adsorb hydrogen. The average adsorption energies for Pb@Pd are the following: the surface value corresponds to −0.53 eV/H atom and in the bulk −0.23 eV/H atom. These results agree very well with the observations performed by UHV experiments that indicated that the shape and maxima for the hydrogen evolution in a temperature-programmed desorption experiment is not significantly modified by the presence of Pb but instead it decreases the total amount of hydrogen adsorbed [51].

In order to address the effect of the solvent on the hydrogen uptake, we have employed the model for multilayer adsorption described in our previous work [9], see Fig. 5. The model states that the amount of hydrogen in the surface and bulk of Pd can be obtained as a particular case of multilayer adsorption [52]. For the clean Pd system, this means that at atmospheric pressures ($\log(p_{H2}/p^0) = 0$) the amount of hydrogen is larger than a single monolayer occupying the whole surface, $V/V_m > 1$, and then the hydride is formed. When the solvent is present, it modifies the effective pressure of hydrogen in contact with the catalyst due to solubility effects. In Fig. 5, it is shown how organic solvents (toluene and methanol) do reduce the total

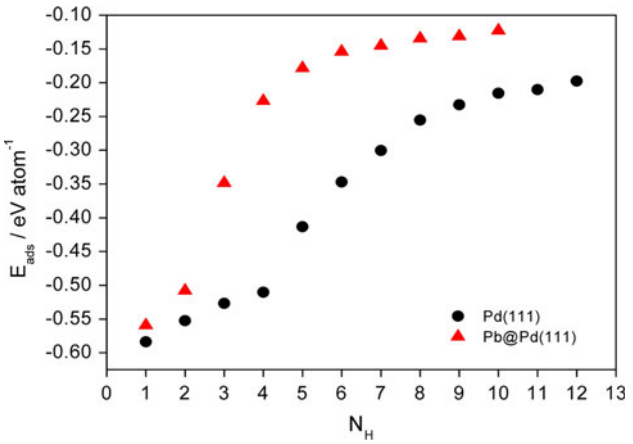

Fig. 4 Average adsorption energy, E_{ads} in eV/atom, for the adsorption of N_H hydrogen atoms in a $p(2 \times 2)$ supercell. *Black circles* represent Pd(111) and *red triangles* Pb@Pd(111). Notice that four H atoms are required to fill a monolayer in the Pd(111) case while for the Pb@Pd surface the two fcc positions in contact with the Pb site do not adsorb H

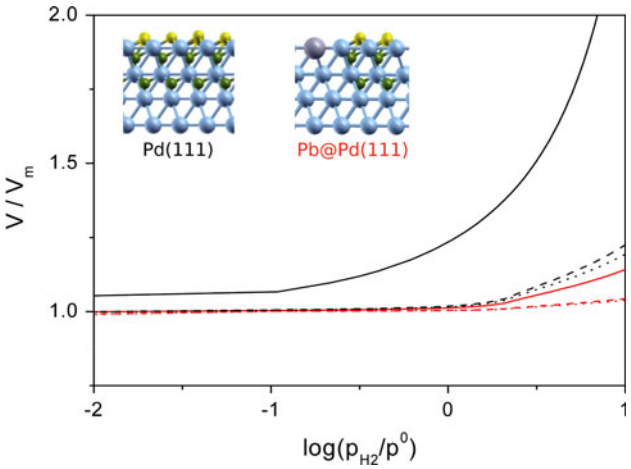

Fig. 5 Hydrogen volume uptake, V/V_m, as a function of the hydrogen pressure at 300 K considering different solvents. The *black lines* represent Pd and *red* Pb@Pd(111). *Solid lines* represent gas-phase models, *dashed lines* methanol and *dotted lines* toluene

hydrogen uptake when compared to gas-phase systems. In the case of the Pb@Pd alloy the resistance to form the hydride is increased even for the pure gas-phase system. Again, the effect of the solvent is to reducing hydride formation.

The formation of the carbide phase is controlled kinetically and competes with the formation of the hydride phase [9]. Carbide formation in sub-surface positions of Pd is −0.56 eV (with respect to gas-phase ethyne and H_2) and +0.58 eV (with respect to gas-phase ethene and H_2). As for the Pb@Pd alloy, the formation of the carbide is −0.25 eV (ethyne), 0.89 eV (ethene). Thus, Pb@Pd(111) is less prone to form the carbide phase than pure Pd.

3.3 Quinoline adsorption on Pd and Pb@Pd

Quinoline is a base with a naphtalene structure where one of the CH group has been substituted by nitrogen, see Fig. 6. The rings are planar and the N atom exhibits a lone pair sticking out from the carbon ring. In previous theoretical works [53], adsorption of quinoline has been studied by employing cluster models and different metals including Pd. These authors performed an extensive survey of different adsorption sites and indicated that the most likely positions for adsorption correspond to planar structures where the quinoline rings are over bridge positions (di-bridge configuration). In this configuration, the carbon and nitrogen are bonded in total to seven Pd atoms (this site was noted as di-bridge ($N_{Pd} = 7$) in Ref. [53]). Obviously, given the confined characteristics of the cluster and the poor definition of the *s*-bands in these models, the energies reported seem to be much smaller than those determined experimentally [54]. Another difficulty in the evaluation of quinoline adsorption comprises the large contributions that can be anticipated from its close nature and extended π-system. We have attempted to evaluate the contributions from dispersion through Grimme-like corrections [55] and reoptimized the structure. Those contributions have been reported to strongly modify the adsorption energies of large molecules [56]. In the case of quinoline on Pd, an extra exothermic contribution of 0.12 eV was obtained.

The perpendicular N-down structure was found unstable. The largest adsorption energies for quinoline on Pd correspond to the di-bridge site, −1.79 eV, see Table 2 and Fig. 6. The average distance from the carbon atoms in the rings to the neighboring metal atoms is 2.233 Å, while the distance from the N atom to a Pd on the surface is at 2.187 Å from the surface. The average C–C distances are enlarged to 1.447 Å with respect to the gas-phase values (1.421 Å). This enlargement is due to the formation of the bond at the interface.

Regarding the adsorption on the Pb@Pd model system, the number of adsorption possibilities increases due to the presence of different sites. We have calculated two different Pb concentrations on the surface. While at high Pb

Table 2 Adsorption site, adsorption energy, E_{ads} in eV, and most relevant geometric parameters, distance from the surface to the N atom in the quinoline, $d_{N–M}$; and from the metal ring to the neighboring metal atoms $d_{C–M}$; and average C–C distance, $d_{C–C}$; and α the angle for the distortion with respect to planarity. All distances in Å and α in °

	Pb/ML	Site	E_{ads}	$d_{N–M}$	$d_{C–C}$	$d_{C–M}$	α
Pd	0	Di-bridge	−1.79	2.187	1.447	2.233	20.8
Pb@Pd	0.25	Di-bridge	0.41	2.541	1.421	2.640	5.7
Pb@Pd	0.0625	Di-bridge	−1.57	2.203	1.446	2.248	22.3

concentration (0.25 ML) adsorption is endothermic by 0.41 eV, an exothermic value is obtained for lower Pb coverages, 0.0625 ML. In this case, the most stable adsorption site corresponds to position where quinoline is far away from the Pb atoms [di-bridge ($N_{Pd} = 7$)]. At Pb positions or close to these centers, adsorption energy is endothermic. Thus, the Pb centers are not decorated by the quinoline molecules. Instead, the clean Pd areas of the Pb@Pd alloys do adsorb quinoline in similar configurations as those found for the clean surface, thereby covering different areas of the catalyst where Pb is not present. The adsorption energies Pb@Pd are reduced to −1.57 eV. The projected density of states in Fig. 7 shows the important overlap between the states of the molecule and those of the surface, responsible for the strong interaction found. Moreover, the Pd atoms on the surface not close to the quinoline molecule are not significantly perturbed.

The role of quinoline appears to be, at least partially, equivalent to that of CO on Pd in the gas-phase alkyne hydrogenation. Both quinoline and CO have binding energies to the Pd or Pb@Pd surfaces that are larger than that of the triple C–C bond. This means that they are not displaced by the reactants but instead, they block some of the sites. This size reduction implies that the reaction ensembles (i.e., the group of atoms involved in an elementary step) are effectively reduced. Ensembles are known to rule activity and selectivity [57, 58] and their size reduction is particularly effective when the competing reactions require different ensembles, as for the hydrogenation and oligomerization processes, and the desired reaction needs the smallest one. In the case of quinoline, the large size of this molecule favors the isolation of small ensembles. Isolation also contributes to the reduction of oligomerization reactions as diffusion of alkynes on the surface is required and it is hindered when other adsorbates are present.

In order to check the role of other potential compounds on this reaction, we have analyzed the binding energy of pyridine and naphtalene to Pd. While the first contains a part of the active molecule, the second, $C_{10}H_{10}$ is isostructural with quinoline and with a CH group substituting N. The corresponding adsorption energies to the clean surface are found to be −1.14 eV (pyridine) and −1.84 eV (naphtalene). Thus, pyridine is much less adsorbed than both naphtalene and quinoline.

3.4 Thermodynamic factors of ethyne and ethene on Pd and Pb@Pd

One of the major components controlling the selective hydrogenation is known as the thermodynamic factor. This represents the ability of the catalysts to adsorb the alkyne while the alkene is not bonded [59]. However, the adsorption of the alkyne–alkene pair depends on the binding energy of carbon due to the bond-order conservation rules [60, 61]. The slope of the linear dependence found for the binding energies of alkyne and alkenes with that of carbon, points out where selective regions exist. However, this parameter is only valid provided that the same active species is responsible for the hydrogenation.

On the clean surface, the adsorption energies of ethyne and ethene are −1.78 and −0.82 eV, respectively. Thus, once formed the alkene stays adsorbed on the system that can be over-hydrogenated leading to the corresponding alkanes. For the clean surface, earlier experiments and calculations at stoichiometric conditions (H_2/alkyne = 1) lead to less than 50% selectivity for the partial hydrogenation. On the Pd–Pb sites, adsorption is controlled by the relative position with respect to the Pb center. Adsorption at the Pd fcc sites on the surface is less exothermic than on the pure Pd surface, the adsorption energy is −1.11 and −0.30 eV for ethyne and ethene, respectively. This was calculated in a $p(2 \times 2)$ reconstruction with a Pb coverage of 0.25 ML. Thus, the effect of alloying is to reduce the adsorption energies of both moieties by about 0.5–0.7 eV. At the fcc or bridge structures containing a Pb atom, the binding energies are even lower, thus the positions around Pb atoms can be considered as inactive. These results confirm the suggestion by Palczewska et al. [51] that with a very low Pb coverage, adsorbed ethene was not detectable in the TPD spectra and disappeared completely at higher coverages. The change of the metal–molecule bond strength was more decisive than site blocking [62]. When Pd is partially covered by quinoline, the binding energies are also smaller than those corresponding to the clean Pd surface. The E_{ads} is then −1.46 and −0.65 eV for ethyne

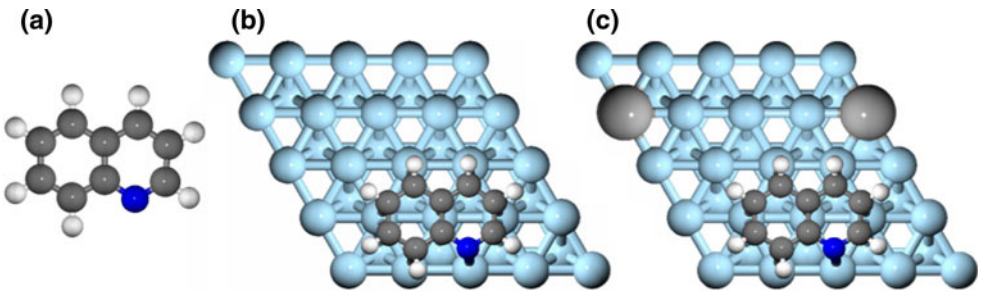

Fig. 6 Structures of **a** gas-phase quinoline and quinoline adsorbed on the surfaces: **b** di-bridge position on Pd and **c** di-bridge configuration at the Pb@Pd(111) surface. Color code: N (*dark blue*), C (*small gray*), H (*white*), Pd (*light blue*), and Pb (*large gray*)

Table 3 Reaction energies, ΔE, and activation barrier, E_a, both in eV, for the first and the second hydrogenation steps of ethyne

System	Pd		Pd–Q		Pb@Pd (c)		Pb@Pd (f)		Pb@Pd–Q_{Pd}	
Reaction	ΔE	E_a	ΔE	E_a	ΔE	E_a	ΔE	E_a	ΔE	E_a
$C_2H_2 + H \rightarrow C_2H_3$	−0.17	0.66	0.14	1.28	0.13	1.24	0.11	1.17	0.12	1.20
$C_2H_3 + H \rightarrow C_2H_4$	−0.42	0.81	−0.38	0.76	−0.28	0.90	−0.25	0.87	−0.45	0.72

For the Pb@Pd alloy (0.0625 ML Pb), two different structures: close (c) and far (f) from Pb have been studied

and ethene, respectively. Thus, quinoline also reduces the adsorption of the double and triple bonds to the surface, but the effect is smaller than that of Pb. In the large cell, we have also placed simultaneously quinoline and Pb, Pd@Pd–Q_{Pd}. On this system, the alkyne–alkene adsorption energies are reduced further (−1.35 and −0.61 eV, respectively) but still the synergetic contribution of quinoline and Pb is rather small.

3.5 Kinetics of ethyne and ethene hydrogenation on the Lindlar catalyst

Hydrogenation of unsaturated organic moieties takes place through the sequential addition of H atoms. This scheme is known as the Horiuti–Polanyi mechanism [63] and has been confirmed through computational DFT-based studies by Neurock et al. [7]. The reaction network for the hydrogenation of ethyne is known to show a branching point when vinyl can convert to ethene or to ethylidene. We have addressed this point previously [9], and found that conversion to ethylidene is particularly important for hydride phases. Given the results in the previous section with respect to the formation of hydrides, we have focused on the calculation of the reaction energies and kinetic parameters for the first and second hydrogenation steps leading to C_2H_3 and C_2H_4. The systems chosen are a Pd clean surface, and the Pb@Pd alloy with and without quinoline. The two calculated reactions were:

$$HC \equiv CH + H \rightarrow HC = CH_2 \quad (5)$$

$$HC = CH_2 + H \rightarrow H_2C = CH_2 \quad (6)$$

For the palladium surface, the first hydrogenation is exothermic by 0.2 eV, and the barrier is about 0.7 eV. Formation of ethene has an activation energy of 0.8 eV, see Table 3 and Fig. 8. When Pb is present, we have calculated two different configurations, either close (c) or far (f) from the Pb atom. The activation energy for the first step is then higher than for the clean Pd surface, about 1.2 eV, while the second hydrogenation requires less energy, about 0.9 eV. Therefore, although the barriers do increase from the Pd case, the energies are low enough for the first hydrogenation to take place at room or slightly higher temperatures. For the system containing quinoline Pd–Q, the first hydrogenation barrier is similar to that found for Pb@Pd, i.e., close to 1.3 eV, but the second hydrogenation is less energy demanding, 0.76 eV. Finally, for the whole system, Pb@Pd–Q_{Pd} with the quinoline adsorbed on the Pd region, the barriers are very similar to those of the quinoline alone: 1.2 and 0.7 eV for the first and second hydrogenations, respectively (see Fig. 8). If alkenes are adsorbed on the Pb@Pd–Q_{Pd} system, the hydrogenation barrier would be similar to those of previous steps ($E_a > 0.7$ eV) thus, the hydrogenation process would not compete with the fast desorption, $E_{des} = 0.6$ eV.

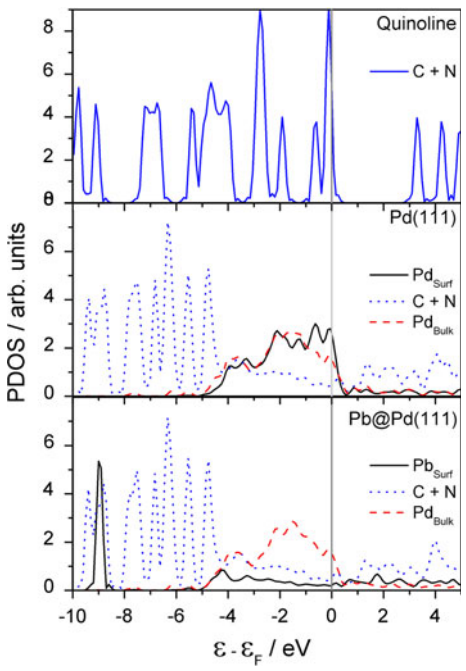

Fig. 7 Projected density of states for the most stable adsorption sites of quinoline on the Pd and Pb@Pd surfaces

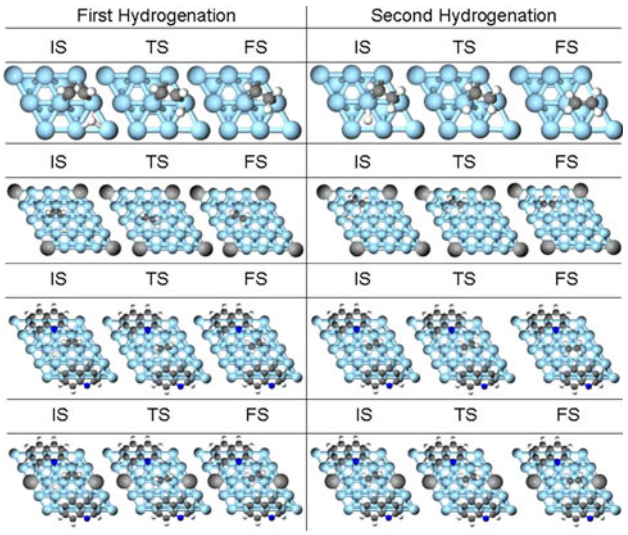

Fig. 8 Hydrogenation process on the clean Pd(111) surface; Pb@Pd alloy; quinoline adsorbed on Pd: Pd–Q; and Pb@Pd–Q_{Pd} Lindlar catalyst. The images show the initial, transition and final steps for each of the elementary steps. *Small white spheres* represent H, *small gray* C, *dark blue* N, *blue* Pd, and *large gray* Pb

4 Discussion: differences between palladium and the Lindlar catalyst

In the literature, selectivity modifiers have been classified in terms of reversible and irreversible adsorbates. Irreversible modifiers perturb the ensembles restricting their shape and size, while reversible adsorbates are usually seen as stoppers of consecutive over-hydrogenation or oligomerization reactions, in particular when the binding energy of the modifier is larger than that of the intermediate (thermodynamic selectivity) [64]. In the present section, we describe the effect of the irreversible (Pb) and reversible (quinoline) modifiers.

On regular Pd catalyst, H_2 is easily dissociated with the subsequent formation of hydrides. When hydrides are formed, ethyne (more generally, alkynes), over-hydrogenate due to the high chemical potential of H atoms stored in the Pd bulk. In the Lindlar catalysts, hydrides are scarcer. Still, H_2 splitting is easy due to the similar activity of Pd, but the presence of Pb inhibits the adsorption of H in the neighboring region. This exclusion area also implies that hydride formation is less exothermic and less likely. Moreover, the solvent modulates the amount of hydrogen in contact with the surface due to the solubility of H_2 in different liquids reducing the equivalent pressure. Thus, for the Lindlar catalyst over-hydrogenation problem is much less an issue. The role of the irreversible modifier is to reduce the sites available for hydrogen adsorption, isolate and shape the ensembles, and enhance the intrinsic selectivity of the catalyst by improving the thermodynamic factor. Finally, due to the Pb decoration at steps, carbon deposits are less likely.

Quinoline adsorption on Pd also reduces the amount of possible adsorption sites for H. This is due to the effective blocking of these molecules that adsorb so strongly that can compete with the alkyne for the sites. The presence of quinoline slightly reduces the average H binding energy. Furthermore, isolation of the sites is a clear effect of quinoline, its large size and quite good fitting with the symmetry of the surface allows the reduction of side reactions. However, quinoline is not as effective as Pb in improving the thermodynamic factor. For the complete Pb@Pd–Q_{Pd} system, the thermodynamic factor is similar to that observed for the quinoline alone.

Therefore, a hierarchical ordering on the effect of modifiers [65] can be obtained from the calculations above. A two-dimensional tessellation problem with two kinds of building blocks is described in Fig. 9. The Pb exclusion area forms the main modifier to the catalyst. Still, Pb is an additive that modifies very strongly the properties of adsorbed alkynes and alkenes and indeed it can completely block the surface, provided that an excessive quantity is employed. Moreover, Pb in the Pd alloys is preferentially found isolated. The reversible adsorbate quinoline is indirectly ordered by the presence of Pb and isolates very small sites of about four Pd atoms that allow hydrogenation but block oligomerization. Thus, at complete quinoline coverage the Pb@Pd–Q_{Pd} leaves active less than 10% of the surface palladium sites for the hydrogenation reaction. This fact, together with the smaller intrinsic activity (larger activation barriers for hydrogenation are found) explains why two orders of magnitude more Pd weight percentage is required in the formulations of the Lindlar catalyst when

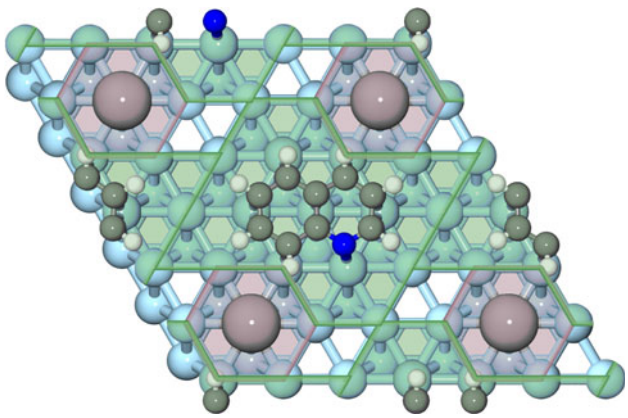

Fig. 9 Schematic representation of the mosaic generated by the superposition of the Pb exclusion areas (*pink*) and the quinoline ones (*gray*). The only active sites, without tiling, able to adsorb the alkyne are marked by white regions. The tessellation with two different kinds of structures provides a subtle way to control the ensemble size and shape

Table 4 Adsorption energies of ethyne and ethene on both Pd(111) and Pb@Pd(111) surface with and without quinoline

	System	Pb(ML)	Quinoline	Site	E_{ads}	d_{C-M}	$e_{\alpha-\beta}$
C_2H_2	Pd	–	No	Fcc	−1.78	2.001	0.153
C_2H_4	Pd	–	No	Bridge	−0.82	2.131	0.117
C_2H_2	Pb@Pd	0.25	No	Fcc	−1.11	2.055	0.135
C_2H_4	Pb@Pd	0.25	No	Bridge	−0.30	2.164	0.110
C_2H_2	Pd	–	Yes	Bridge	−1.46	2.255	0.041
C_2H_4	Pd	–	Yes	Bridge	−0.65	2.241	0.041
C_2H_2	Pb@Pd	0.0625	Yes	Fcc	−1.35	2.255	0.039
C_2H_4	Pb@Pd	0.0625	Yes	Bridge	−0.61	2.253	0.040

Energies are expressed in eV and distances in Å. The elongation, $e_{\alpha-\beta}$ in Å, is the difference between the C–C distance as calculated on the surface and in the gas phase

compared to the gas-phase hydrogenation, Table 1. Finally, the outstanding selectivity of the Lindlar catalyst would be difficult to be obtained by a single chemical modifier. The effect of Pb poisoning is too important (as shown in Table 4) that can eliminate all the active sites on the surface even at moderate coverages. Similarly, quinoline on Pd alone could also form very dense packing motives reducing the number of sites. By employing a hierarchically ordered set of modifiers (lead and quinoline) these problems are avoided as the two building blocks are different but complementary enough to limit the drawbacks of each other.

A second question is why different reversible modifiers are employed in gas-phase (CO) and three-phase (quinoline) hydrogenation. CO is widely employed in hydrogenations and indeed the catalyst is not selective without it in gas-phase reactions. In the Lindlar catalyst, quinoline is regarded as one of the most effective modifier. Both CO and quinoline show larger binding energies to the surface than ethyne, and therefore they both fulfill the requirement of improving the thermodynamic factor and not been replaced by the reactant. However, the coverage of both species is necessarily different; while a very dense CO layer is observed for CO a sparse structure is obtained with quinoline. Therefore, both do modify the ensembles but through different mechanisms: highly occupation by small molecule (CO) or large blocking by size (quinoline). However, CO might show solubility problems in the liquids, and it is dangerous to handle in an open environment, and the shape of the active sites is difficult to control. Therefore, it is not recommended in standard fine chemistry procedures. Similarly, N-containing compounds shall be removed from the streams in gas-phase hydrogenation due to incompatibilities with other parts of the process. Finally, we have tried different alternative molecules to investigate this effect. Naphtalene is one of them and its adsorption properties are similar to those obtained with quinoline. In contrast, pyridine is not an option as its low binding energy to Pd and Pb@Pd would not be enough to block the surfaces (i.e., it would be displaced by the alkyne).

5 Conclusions

We have employed DFT to investigate the roles of the different components in the Lindlar catalyst and compare them to palladium catalyst. Selective catalyst need to show three positive contributions: high thermodynamic factor (i.e., high alkyne adsorption and low alkene binding energies), they should not generate hydrides (as hydrides over-hydrogenate) and should not promote the formation for oligomers through C–C coupling. In the Lindlar catalyst, DFT shows that this is achieved as follows:

1. Pd is active in both H_2 splitting and hydrogenation. However, both over-hydrogenation and oligomerization limit the selectivity of the catalyst.
2. The exceedingly large ability of Pd to form palladium hydrides is partially modulated by the presence of Pb that reduces the overall amount of H in the catalyst.
3. The solvent also helps in reducing the effective H_2 pressure on the surface as it is modulated by the gas solubility in the liquid phase.
4. Pb improves the thermodynamic factor as alkene adsorption is strongly reduced when significant amounts of Pb are present.
5. Quinoline basically acts by blocking possible H and alkyne adsorption sites. The isolation of the active centers is beneficial as it impedes the formation of C–C bonds (i.e., oligomerization).

In summary, we have analyzed by means of first principle studies the fundamental role of all the components in the Lindlar catalyst. This is the first time that an extensive computational approach is devoted to understand at the molecular level this famous catalyst that has been successfully employed in industry for nearly 6 decades.

Acknowledgments We thank MICINN for Grants CTQ2009-07753/BQU and CSD2006-0003 and BSC-RES for providing generous computational resources.

References

1. Somorjai GA, Borodko YG (2001) Catal Lett 76:1
2. Corma A, Serna P (2006) Science 313:33
3. Molnar A, Sarkany A, Varga M (2001) J Mol Catal A 173:185
4. Chorkendorff I, Niemantsverdriet HW (2003) Concepts of modern catalysis and kinetics. Wiley-VCH Verlag GMBH KGaA, Weinheim

5. García-Mota M, Cabello N, Maseras F, Echavarren AM, Pérez-Ramírez J, López N (2008) Chem Phys Chem 9:1624
6. Plata JJ, García-Mota M, Braga AAC, Maseras F, López N (2009) J Phys Chem A 113:11758
7. Mei DH, Sheth PA, Neurock M, Smith CM (2006) J Catal 242:1
8. Mei DH, Neurock M, Smith CM (2009) J Catal 268:181
9. García-Mota M, Bridier B, Pérez-Ramírez J, López N (2010) J Catal 273:92
10. Studt F, Abild-Pedersen F, Bligaard T, Sorensen RZ, Christensen CH, Nørskov JK (2008) Science 320:1320
11. Lindlar H (1952) Helv Chim Acta 35:446
12. Lindlar H, Dubuis R (1973) Org Synth 5:880
13. Mallat T, Baiker A (1991) Appl Catal 79:59
14. Stachurski J, Thomas JM (1988) Catal Lett 1:67
15. Massalski TB, Okamoto H, Subramanian PR, Kacprzak L (1990) Binary alloy phase diagrams. ASM International, Materials Park
16. Chadwick D, Karolewski MA (1983) Surf Sci 126:41
17. Liu G, Davis KA, Meier DC, Bagus PS, Goodman DW (2003) Phys Rev B 68:035406
18. Palczewska W, Szymerska I, Ratajczykowa I, Lipski M (1980) In: Proc ECOSS-3 and ICCS-4 Cannes
19. Szabo S (1991) Int Rev Phys Chem 10:207
20. Mallat T, Baiker A (1995) Top Catal 8:115
21. McEwen AB, Guttieri MJ, Maier WF, Laine RE, Shvo Y (1983) J Org Chem 48:4436
22. Mallat T, Baiker A (2000) App Catal A 200:3
23. Maier WF, Chettle SB, Rai RS, Thomas G (1986) J Am Chem Soc 108:2608
24. Yu J, Spencer JB (1998) Chem Commun 1103
25. Segura Y, López N, Pérez-Ramírez J (2007) J Catal 247:383
26. Bridier B, López N, Pérez-Ramírez J (2010) J Catal 269:80
27. Bridier B, Pérez-Ramírez J (2010) J Am Chem Soc 132:4321
28. Oroshnik W (1977) Synthesis of Vitamin A, intermediates and conversion thereof to Vitamin A "4058569"
29. Coq B, Figueras F (2001) J Mol Catal A 173:117
30. Kresse G, Joubert D (1999) Phys Rev B 59:1758
31. Perdew JP, Chevary A, Vosko SH, Jackson KA, Pederson MR, Singh DJ (1992) Phys Rev B 46:6671
32. Blochl PE (1994) Phys Rev B 50:17953
33. Monkhorst HJ, Pack JD (1976) Phys Rev B 12:5188
34. Henkelman G, Uberuaga BP, Jonsson H (2000) J Chem Phys 113:990
35. Soto-Verdugo V, Metiu H (2007) Surf Sci 601:5332
36. Ulan JG, Maier WF, Smith DA (1987) J Org Chem 52:3132
37. Ulan JG, Kuo E, Maier WF, Rai RS, Thomas G (1987) J Org Chem 52:3126
38. Schlogl R, Noack K, Zbinden H, Reller A (1987) Helv Chim Acta 70:627
39. Hammer B, Morikawa Y, Nørskov JK (1996) Phys Rev Lett 76:2141
40. Greenwood NN, Earnshaw A (2008) In: Chemistry of the elements, 2nd edn. Elsevier, p 1150
41. Knapton AG (1977) Plat Met Rev 21:44
42. Andersin J, López N, Honkala K (2009) J Phys Chem C 113:8278
43. Andersin J, Honkala K (2010) Surf Sci 604:762
44. Nykanen L, Andersin J, Honkala K (2010) Phys Rev B 81:075417
45. Seriani N, Mittendorfer F, Kresse G (2010) J Chem Phys 132:024711
46. Bond GC (2005) Springer, New York, p 395
47. Teschner D, Borsodi J, Wootsch A, Revay Z, Havecker M, Knop-Gericke A, Jackson SD, Schlogl R (2008) Science 320:86
48. Mitsui T, Rose MK, Fomin E, Ogletree DF, Salmeron M (2003) Nature 422:705
49. López N, Łodziana Z, Illas F, Salmeron M (2004) Phys Rev Lett 14:146103
50. Greeley J, Krekelberg WR, Mavrikakis M (2004) Angew Chem Int Ed 43:4296
51. Palczewska W, Ratajczykowa I, Szymerska I, Krawczyk M (1984). In: Proceedings of the 8th international congress on catalysis, Berlin, vol IV, p 713
52. Brunauer S, Emmett PH, Teller E (1938) J Am Chem Soc 60:309
53. Santarossa G, Iannuzzi M, Vargas A, Baiker A (2008) ChemPhysChem 9:401
54. Ulan GJ, Kuo E, Maier WF, Rai RS, Thomas G (1986) J Org Chem 52:3126
55. Grimme S (2006) J Comput Chem 27:1787
56. Mercurio G, McNellis ER, Martin I, Hagen S, Leyssner F, Soubatch S, Meyer J, Wolf M, Tegeder P, Tautz FS, Reuter K (2010) Phys Rev Lett 104:036102
57. Chen MS, Kumar D, Yi CW, Goodman DW (2005) Science 310:291
58. García-Mota M, López N (2008) J Am Chem Soc 130:14406
59. Jia JF, Haraki K, Kondo JN, Domen K, Tamaru K (2000) J Phys Chem B 104:11153
60. Studt F, Abild-Pedersen F, Bligaard T, Sørensen RZ, Christensen CH, Nørskov JK (2008) Angew Chem Int Ed 47:9299
61. Abild-Pedersen F, Greeley J, Studt F, Rossmeisl J, Munter TR, Moses PG, Skulason E, Bligaard T, Nørskov JK (2007) Phys Rev Lett 99:16105
62. Cerveny L, Paseka I, Surma K, Thanh NT, Ruzicka V (1985) Collect Czech Chem Commun 50:61
63. Horiuti J, Polanyi M (1934) Trans Faraday Soc 30:1164
64. Siegel S, Hawkins JA (1986) J Org Chem 51:1638
65. Anderson JA, Mellor J, Wells RPK (2009) J Catal 261:208

ChemComm

Cite this: *Chem. Commun.*, 2012, **48**, 1379–1391

www.rsc.org/chemcomm

FEATURE ARTICLE

Promoters in the hydrogenation of alkynes in mixtures: insights from density functional theory†

Núria López* and Crisa Vargas-Fuentes

Received 9th August 2011, Accepted 7th November 2011
DOI: 10.1039/c1cc14922a

Hydrogenation of alkyne–alkene mixtures of small sized hydrocarbons has been traditionally performed with Pd-based catalysts modified by a second metal. Over the last few years, this hydrogenation process has become a thriving field to understand selective processes that might be applicable to more complex molecules, for instance those derived from biomass. We summarize here the large body of experimental and open industrial documents to show the properties of different catalytic formulations, we concentrated on the role of the secondary metals employed. We compare these results to theoretical work performed over the last few years and to our new results based on Density Functional Theory. With this insight, we illustrate how secondary compounds behave under typical reaction conditions and how the reaction conditions might affect the stability of the catalyst.

Introduction

Selectivity is the main challenge in the development of new catalysts with lower energy requirements and environmental impact.[1] Selectivity can be defined in terms of three different situations: to a reactant (in a mixture), to a product (if more than one are possible), and to a reaction.[2] Among all the reactions conducted *via* heterogeneous catalysis, hydrogen addition to unsaturated bonds constitutes one of the most prominent families of reactions. Hydrogenations are ubiquitous in a myriad of applications and were initially investigated by Sabatier.[3] In later years, the partial hydrogenation of triple carbon–carbon bonds in the presence of double bonds has been taken as a paradigm in the study of selectivity, both experimentally and theoretically.[4] The reasons behind this interest lay on the industrial relevance of the reaction, but also on the, in principle, simple reaction scheme. However, such a simple reaction masks a very dynamic behaviour of the catalysts where several potential phases can appear depending on the reaction conditions. The perspective opened by the reaction is thus much more complex than originally considered.

Institute of Chemical Research of Catalonia, ICIQ, Av. Països Catalans 16, 43007 Tarragona, Spain. E-mail: nlopez@iciq.es
† This article is part of the *ChemComm* 'Emerging Investigators 2012' themed issue.

Núria López

Núria López (Barcelona 1972) obtained her PhD at the University of Barcelona, Spain in 1999. Her post-doctoral studies were carried out in the group of Prof. Nørskov at the Technical University in Denmark. In 2005 she joined ICIQ as a group leader. Her field of expertise is the use of computational simulations to materials in particular those employed as a heterogeneous catalyst. She obtained an ERC-Starting grant in 2010. She is the co-author of about 80 publications and has received about 3000 citations for her work.

Crisa Vargas-Fuentes

Crisa Vargas-Fuentes was graduated in Chemistry at the University of Sevilla, Spain (2009). During her degree she enjoyed a one-year 'Erasmus' scholarship at the University of York. She then moved to Tarragona where she got the masters in 'Computational and Theoretical Chemistry' from the Universitat Rovira i Virgili. Crisa is currently working with Prof. López' Group on selective processes on heterogeneous catalysis for her PhD at the Institut Català d'Investigació Química (ICIQ, Spain).

The selective hydrogenation reaction can take place either in gas-phase or in liquid-phase mixtures and for multifunctionalized molecules in organic synthesis.[5] Most of the problems encountered with the selectivity in partial hydrogenations are common to other reactions, like oxidation, where the interplay between phase formation, impurities, doping and selectivity is mandatory in order to rationally tailor new active and selective catalysts.

Industrially, the selective hydrogenation of C≡C triple bonds in the presence of double C=C bonds in alkene streams is employed to upgrade the C_2 and C_3 fractions from the steam crackers. Usually, these low weight fractions contain acetylenic and diene impurities. Typical compositions are for C_2: 90% ethene and 0.5–3% acetylene; and C_3: 90% propene and 2–8% propyne and propadiene. As alkynes are detrimental to the subsequent polymerization units selective hydrogenation of triple C bonds in the presence of double bonds is usually carried out to achieve a concentration of acetylenic compounds in the order of a few ppms. The catalyst of choice is formulated by a very low Pd content loaded (0.01–0.05% range) onto Al_2O_3 with a medium to small surface area.[6] This means that even if the amount of metal loaded is relatively small, the size of the particles can be as large as 10 nm in diameter.[7,8] In the hydrogenation reaction, selectivity is a must, as either the alkyne compounds or the large alkene fraction can be over-hydrogenated to the alkanes, or large, partially unsaturated, species might appear as a consequence of oligomerization problems. The hydrogenation units are placed in different positions in the plant with different hydrogen to hydrocarbon ratios that can be very large ($\gg$10) front-end units or less than 2.5 in tail-end units.[6] The reaction is usually performed at 333–343 K. The particular specifications for each of these catalysts depend on their particular position in the plant.

In addition to alkyne–alkene pairs in C_{3+} fractions the elimination of diene molecules is required. Indeed, many works discussed in the present manuscript deal with the selective hydrogenation of 1,3-butadiene to butene. Note that depending on the amount of carbon atoms in the alkyne–alkene pairs either gas-phase or liquid-phase hydrogenation operation might be considered. For instance, C_2 fractions are usually carried out under gas conditions but from C_{3+} liquid performance is also possible. Along the description we will specifically indicate the experiments carried out in the liquid phase.

Commonly Pd is not employed alone. Instead it is promoted by a second metal,[9] termed also as a co-catalyst, or just a promoter, which slightly modifies the activity, selectivity and stability of the catalysts. These promoters that can be integrated in the Pd lattice are of three types: (i) metals of group 11: Cu, Ag, Au; (ii) sp metals and semi-metals Pb, Sn, Bi, Ga among others; and (iii) group 1 metal ions: Na and K.

In addition, a selectivity or process modifier is usually added. CO is generally employed for this purpose. Other types of compounds, such as amines, alkali and sulfur compounds, have also been reported as molecular modifiers.[9] The strategy of building a hierarchy of textures for the heterogeneous catalysts is schematically indicated in Fig. 1. This conceptual framework is highly versatile due to the modular structure but imposes several restrictions to achieve the compatibility between the different building blocks.

The most typical representation of catalytic texturing and tessellation in hydrogenation is given by the Lindlar catalyst.[10,11]

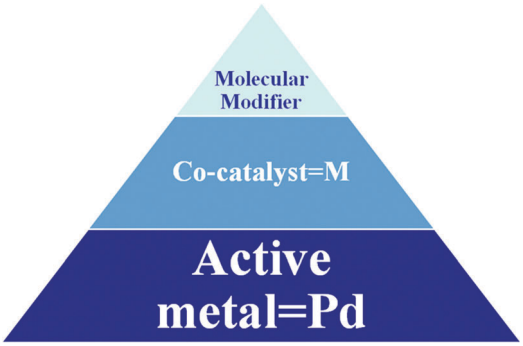

Fig. 1 Schematic representation of the design strategy used in hydrogenation catalysts both for industrial and laboratory purposes.

The Lindlar catalyst has been employed in organic chemistry as a routine material to hydrogenate alkynes to alkenes selectively in molecules containing both functionalities with the use of a solvent.[10] The catalyst is prepared as 1–5% weight of Pd is supported on $CaCO_3$ or $BaSO_4$, then Pb acetate is added and the mixture is heated only to 95 °C. After cleaning a molecular modifier, quinoline, is added. Pb is known to be inserted in the lattice, see below, while quinoline covers part of the rest of the surface leaving only small active sites on the Pd surface.[11]

Although extensive experimental works on the subject of hydrogenation of alkyne–alkene mixtures on Pd have been carried out and reviewed extensively by Borodzinski and Bond,[6,9] these authors still found a list of contradictory results and presented several suggestions for further work. Many of those remaining questions were related to the fact that Palladium is known to be very adaptable to the environment and, therefore, under different atmospheres hydrides and carbides can be formed. The properties of Pd thus depend on the reaction environment as schematically shown in Fig. 2. In 2006, the role of these phases was listed as one of the open questions.[6] Other remaining challenges were regarding the composition and structure of the carbonaceous layer, the description of harmful and harmless coke and the role of support sites. For instance, carbonaceous deposits were claimed to diminish the Pd surface available for the adsorption of acetylene.[12] Over the last few years many experiments and theoretical simulations have shed light into the problem.

In fact, under the harsh reaction conditions encountered in the industrial process, Pd catalysts might undergo a large series

Fig. 2 Schematic representation of the interlocked nature of the catalyst state dominated by the reaction conditions that ultimately control the activity and the selectivity of the catalysts.

of modifications. Pd is well-known to produce hydrides[13] at reasonable hydrogen pressures and temperatures. For Pd only hydrogen is known to dissociate readily on Pd.[14] Then, hydrogenation takes place as a sequential H transfer[15] from the surface to an adsorbed C_2H_2 at the fcc site. All the transition states for hydrogenation show activation of H on top of a Pd atom and the average C–H distance at the transition state ranges from 1.5 to 2.0 Å with activation energies in the range of 0.4–1.2 eV. Ethylene is less adsorbed than acetylene but the binding energy is large enough to maintain this molecule on the surface once formed.[16] This is why it could also be hydrogenated reducing the overall selectivity of the process. When the hydride is formed subsurface H attack to convert vinyl in ethylidene is the most likely reaction path[17] in agreement with experiments.[18] Moreover, when exposed to alkynes and alkenes, dissociation of the hydrocarbon with formation of C deposits (coke) and carbides (subsurface species) are likely events depending on the external conditions.[4,17,19–22] The selectivity of the catalysts is a strong function of the phases in the catalyst as has been both experimentally found[4,21] and theoretically explained.[17] In summary, the hydrides lead to alkanes only while thick carbides are selective to the alkenes. Experiments on Pd particles indicated that the hydrogenation reaction suffers from structure sensitivity due to the formation of partial carbide layers. Borodzinski and Bond reported an increase in the turnover frequency, TOF, with the size up to 26 nm,[6] although this was reduced to 11 nm to obtain a specific activity not size-dependent by Ruta and co-workers on monodispersed Pd.[7] These experiments suggested that deactivation by oligomers was more effective on small particles. Therefore, the activity and selectivity of Pd catalysts are strongly linked to the ability of maintaining an active and selective Pd phase.

If CO is added it forms a compact and dense layer on the Pd surface.[23] The reasons behind the use of CO are twofold: (i) CO streams are readily available in industrial plants; (ii) CO provides a sharp control on the stability, activity and selectivity of Pd containing materials as it provides a robust way to stabilize the structure at the catalyst.[17,24] The drawbacks are that it is a poison to the surface and therefore the number of active sites on the surface is reduced, and that CO is very temperature and pressure dependant.[24] CO blocks the formation of hydride, prevents ethylene adsorption,[25] but shows a high oligomerization rate with CO inclusion.[17] In summary, the theoretical works directly confronted to experiments singled out three requirements to obtain selective Pd catalysts:[17]

- thermodynamic selectivity: only adsorption of C≡C bonds,
- inhibition of the formation of the hydride,
- only small ensembles shall be accessible in order to avoid oligomerization.

High selectivity to alkenes is not limited to palladium, nickel and copper can also perform relatively well. Gold and copper nanoparticles[26–28] and NiCuFe alloys[29] have demonstrated their potentialities for the reaction but at least for the single component materials the temperature window is not well-suited to a dip-in solution due to the low activity of the catalysts. The remaining industrial challenges for the future generation catalysts include the following requirements:[24] operation with a net gain of C=C fraction, low investment (including plant project and execution and energy consumption), long catalyst life and low cost.

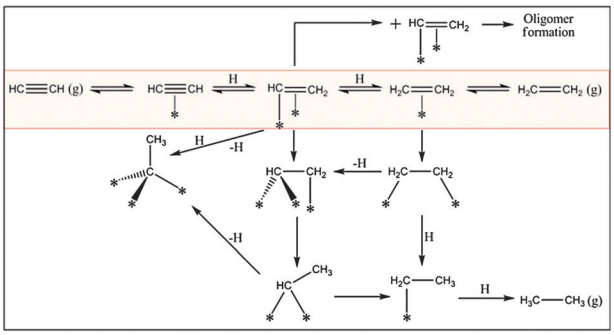

Fig. 3 Schematic representation of the catalytic cycle for hydrogenation on a palladium-based catalyst as suggested by ref. 15. The path on the pink background is the only one that a good co-catalyst or promoter should perform. The asterisks represent the surface.

The role of the co-catalyst

Although much has been done to investigate the nature and the properties of the unpromoted Pd catalyst, little is known about the role of the co-catalysts. The reaction scheme that drives the partial hydrogenation of alkynes is described in Fig. 3. The desired path is indicated in pink. On pure Pd, the lateral paths driving to oligomerization or overhydrogenation take place to a relevant extent. The role of the co-catalyst is then to reduce the amount of molecules that follow these lateral paths. The way this can be achieved has been traditionally discussed in two main terms:[30]

- *Electronic or ligand effect*, under these terms both the perturbations induced by the bonding of the promoter to the active metal, to the changes in overhydrogenation and oligomerization routes and/or reduction of the β-PdH phase have been proposed.
- *Geometric effect*, due to the dilution of Pd on the surface, suggestions that it avoids the formation of multi-bonded alkylidine intermediates responsible for the direct hydrogenation of alkynes to alkanes have been proposed and can be seen in Fig. 3. Other effects are related to the inhibition of the formation of carbides and the reduction of the ensembles that generate oligomers.

The main groups of metals that have been proposed for the hydrogenation of small alkynes in tail-end units or butadienes and large alkyne moieties are described in the following.

PdAg

The current generation of a selective promoted catalyst for acetylene, Pd–Ag composition, was first reported by Dow in 1957.[31] Later developments include the Süd Chemie family of Pd/Ag for all front-end services and tail-end acetylene hydrogenation[32,33] and BASF's for tail-end acetylene hydrogenation. Chevron Phillips[34] at the 1993 Ethylene producers Conference listed a series of properties for these catalysts: (i) Pd shall be in microns of the surface, (ii) addition of silver implies a small loss in activity and a large increase in selectivity; (iii) there is an optimum in the Ag composition, as too high levels render inactive catalysts. Other competitors in the field do not provide information on the promoter in the catalyst.[24]

Experimentally, the formation of an alloy was seen and charge transfer from Ag to Pd suggested by X-ray absorption spectroscopy,[35] the catalyst seemed to be surface Pd rich,[36] even

if Ag has a lower surface energy than Pd.[37] Yield increases of about four-fold times were reported for the liquid-phase hydrogenation of 2-methyl-1,3-butadiene.[38] Moreover, the synthetic methods employed by Kahn and co-workers determined that no significant changes in size distribution occurred.[39] These authors proposed that the Pd–Ag should have a Pd-rich surface able to dissociate hydrogen and hydrogenate the alkyne while the Ag-rich core would prevent the formation of the hydride phase.[39] Other lab test studies indicate a better initial performance of low Ag content (mol fraction 0.4) alloys due to increased stability.[40] In Surface Science studies, CO adsorption is demoted by the presence of Ag.[41] Reduction of these catalysts at higher temperatures improves Ag mobility and leads to more even distributions of Ag.[42]

Complementarily, several theoretical studies have been devoted to the study of the PdAg in acetylene hydrogenation. Following their deep analysis on the Pd system, Neurock and co-workers investigated, by Kinetic Monte Carlo applied to Density Functional Theory based parameters, the Ag containing model catalysts. These authors described the best performance of the silver containing 50% of each compound,[16,43] and described both ensemble and electronic effects reducing the binding energies of acetylene and hydrogen to the surface as main features of this material. A model for this alloy was also employed by Nørskov and co-workers[4b] to illustrate their study on overhydrogenation. The main property of the catalyst was defined as that weakening the bond of alkenes to the surface while keeping that of alkynes. More recently, an analysis of the formation of subsurface species was performed for this alloy. Their results indicated that when Ag is present both the formation of H and C subsurface species are more difficult than for the monometallic system.[44]

PdCu

The structure of PdCu alloys has been studied by DFT analyzing segregation and CO adsorption properties.[45,46] The CO uptake was reduced by the presence of Cu in a liquid-phase reactor.[47] STM experiments showed that isolated Pd atoms are able to split hydrogen.[48] The high selectivity observed in the hydrogenation process for acetylene was found to be lost when high temperatures were employed. It was suggested that this was due to an increase in the amount of Pd centers on the surface.[49] This points out to a quite dynamic behaviour under these conditions.

PdAu

The structure of these materials has been the subject of deep study over the last few years due to high selectivity in oxidation reactions and important ensemble effects both in gas- and liquid-phase processes.[50] In addition, they were tested in selective hydrogenation of butadiene and alkynes[51] for both low and high Au contents.[52] According to these studies, Pd is the main active component and they confirmed the formation of an alloy. STM experiments indicated a strong restructuring of the PdAu system upon hydrogen exposure, reversing the Pd tendency to segregate towards the surface.[48] $Pd_{76}Au_{24}$ exposed to H_2 at 1 bar[53] pointed out Ostwald ripening of the catalyst that changes both the distribution and composition of the nanoclusters and suggests that large clusters are Pd-enriched and small are Au-rich. In the experiments on liquid-phase hydrogenation, the TOF raised by 10 when increasing Au content to $Pd_{40}Au_{60}$,[38] where Pd enrichment was documented. Finally, Au has been proven to smooth out the formation of benzene from acetylene.[54]

PdZn

Initial studies indicated charge transfer and rehybridization in the formation of such alloys.[55] These alloys were tested for the hydrogenation of 1-pentyne and 1,3-butadiene improving in both cases the selectivity when compared to Pd.[56] PdZn is found to be reasonably stable under these reaction conditions. The presence of the alloy was confirmed, and the performance was reported to be similar to that of copper. Other results have suggested the limited adsorption of hydrogen and the isolation of active sites as main driving forces for selectivity.[57] Compared to Pd, the Zn-containing compound does not generate over-hydrogenated hydrocarbons but it is selective to oligomers. Unfortunately, the conversion to the oligomer was significant (up to 20% at 100 °C).[56]

PdGa

Ordered PdGa alloys with compositions Pd_2Ga, PdGa and Pd_3Ga_7 have been proposed as active, selective, and stable catalysts over the last few years both in gas- and liquid-phase hydrogenation processes.[58] High selectivities of C2 alkynes to alkenes with little oligomerization (5–10%) are the fingerprint of these catalysts that upon nanostructuring have an activity similar to Pd and a selectivity to ethylene higher than 70% (compared to 50% $Pd_{20}Ag_{80}$ with a much lower activity) in mixtures with the $H_2:C_2H_2$ ratio of 10 and 200 °C. These ordered alloys present an increase in the coordination up to 13[59] in most of the cases with a mixed coordination sphere in rather asymmetric environments and a pronounced covalent interaction. The selectivity has been attributed to the reduction of the ensembles and the changes in the electronic structure, in particular the depletion of states at the Fermi level[58c] that might reduce hydrogen coverage on the surface.

PdSn

The preparation of this material demonstrated the presence of bimetallic particles.[59] PdSn was employed to analyze the selectivity of 1,3-butadiene by reducing the formation of the β-PdH phase and a reduction of the size of the ensembles.[60] Conversion of 1,3-butadiene was up to 80% with a similar TOF for Pd and PdSn. CO adsorption therein confirmed the change in the surface adsorption properties by changing the nature of the sites and electronic properties. On one of the supports, mixed phase alumina, the Sn-containing material, was found to be more active than the Pd counterpart. No overhydrogenated products were observed for Pd–Sn. The overall activity towards 1,3-butadiene was lowered when increasing the Sn concentration.[61] When compared to Pd, Pd_3Sn showed a good selectivity towards hydrogenation without coking while Pd_2Sn had the most inert surface. Further experiments indicated that Pd dilution by Sn is likely to reduce hydrogen and hydrocarbon diffusion on the surface.[62] Liquid phase tests confirmed that activity decreases while selectivity boosts also because isomerization is reduced.

These effects were explained by dilution and it was shown that Pd_3Sn was better than Pd_2Sn.[63] Weak adsorption was also identified in another set of experiments and shift of 4d states to higher binding energies when increasing Sn was reported.[64]

PdPb

These systems have been studied in many cases in connection with the Lindlar catalyst. Pb and Pd form solid solutions.[65] A surface alloy with composition Pd_3Pb was proposed as the active phase in the Lindlar catalyst,[10] although the real surface stoichiometry of the material is not known. The rearrangement of Pd particles, when Pb is incorporated in the lattice, has also been suggested in the literature.[66] Studies on the liquid-phase hydrogenation of 1,3-butadiene indicated that the amount of molecules transformed *via* the competing mechanisms depends on the hydrogen coverage and the geometric and electronic effects of the materials.[67] In these studies two different options are considered: either Pb deactivates Pd by rearranging its surface structure,[66] or a strong interaction between Pd and Pb giving rise to electronic modification of the valence band of Pd.[67b]

PdBi

Bi-containing catalysts were proposed as a way to eliminate the presence of soluble Pb compounds that present less environmental impact. It has been suggested that Bi preferentially decorates low-coordinated Pd atoms in open surfaces.[68] Bi has been proposed to be present on Pd[69] but other authors propose that the role of Bi is to maintain Pd dispersion and control its charge.[70] Experiments on hexyne hydrogenation (liquid phase) by Anderson and co-workers[71] indicate that Bi stops the reactions of 1-hexene once formed, and that it blocks the active CO adsorption positions. As drawbacks Bi is a poor modifier for the 2-hexyne reaction when compared to Pb due to different behaviour in the isomerisation. FTIR experiments were able to determine that Bi preferentially blocks steps and edge sites. In a different study by Karski,[72] XRD and ToF-SIMS prove a strong interaction between Pd and Bi and the formation of BiPd and Bi_2Pd alloys at about 5–8% Bi content, while for low Bi fractions the intermetallic was found.

Computational details

In order to shed light into the properties observed in the Pd metal by the presence of a second metal we have performed a series of Density Functional Theory calculations aimed at illustrating all the possible behaviour induced by the presence of promoters.

Surface structures can be modified by diluting the active element with a second, less active one, or by changing the particle distribution.[73] There are several problems due to the mixing: (i) the element with lower surface energy is usually segregated towards the surface, (ii) the distribution might be random, or islanding or preferential decoration might occur,[74] (iii) these effects can be reversed by the atmosphere.[75] Recent examples of the complex interplay between the atmosphere and the properties of bimetallic surfaces have been reported in the literature.[76]

The calculations contain the following promoters: the noble metal triad: Cu, Ag, Au; and *sp* metals: Zn, Ga, Sn, Pb and Bi. The visual summary of the concepts behind these parameters is shown in Fig. 4 and the results are shown as a heat map in Fig. 5. The investigated properties are:

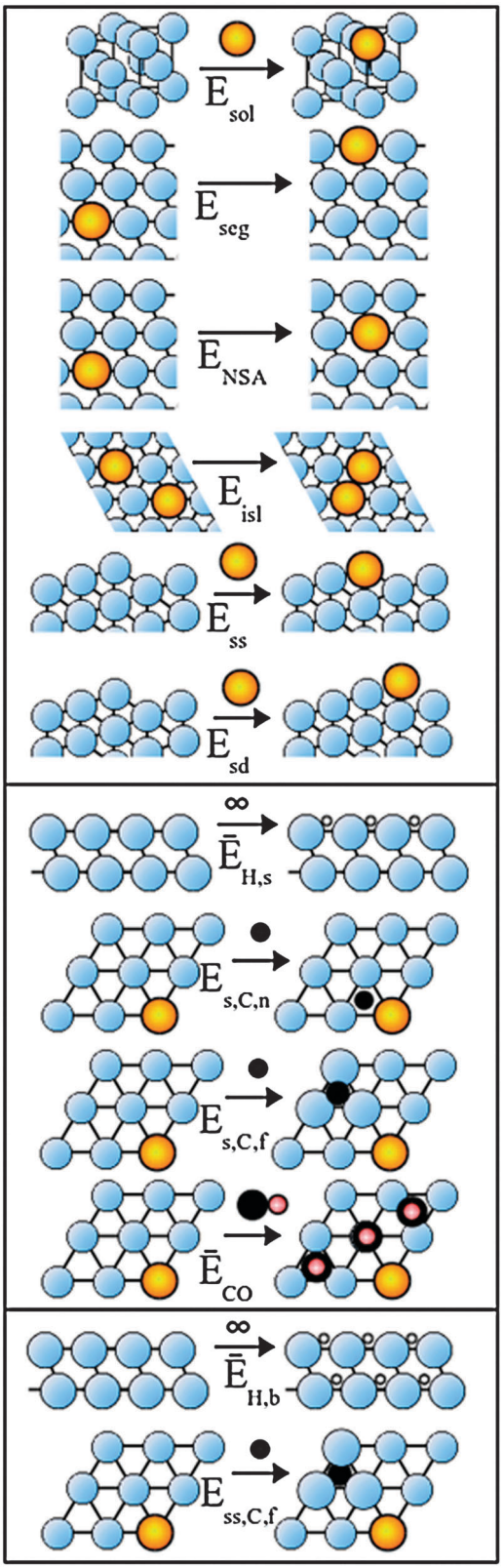

Fig. 4 Schematic representation of the alloy calculated properties. Blue spheres represent Pd, yellow the promoter, small white H, black C and red O. Front or side views are employed when convenient.

• ***Intrinsic stability properties*** given by the solubility, E_{sol}; segregation, E_{seg}; near-surface alloy formation, E_{NSA}; islanding, E_{isl}; step substitution, E_{ss}; and step decoration, E_{sd}; intrinsic electronic structure modification measured by the Pd *d*-band shift, ε_{Pd}.

• ***Adsorption properties***: measured as the binding energy for the C_2 prototypes: ethylene and acetylene, E_{HC} and average binding energy of the dense CO layer, E_{CO}.

• ***Ability to form carbide or hydride phases***: measured through the average adsorption energies of H and C both on the surface and the bulk: $E_{H,s}$, $E_{H,b}$ and $E_{s,C}$, in near and far configurations (*n*,*f*) and in the subsurface $E_{ss,C}$ only in the long distance configuration.

A second part of the stability analysis concerns the dynamic properties of the catalyst under realistic working conditions. The investigated properties correspond to:

• ***Atmosphere-dependent properties*** given by the hydrogen induced segregation E_{seg}(H) and CO induced segregation, $E_{seg,}$(CO).

To this end the VASP code[77] with the PW91 functional[78] has been employed in the calculations. The inner electrons were replaced by PAW pseudopotentials[79] while the valence ones were expanded in a plane wave basis set with a cutoff energy of 400 eV. Different models have been employed to describe the Pd slabs, where one or more atoms were substituted by the co-catalyst. Bulk structures with 2 × 2 × 2 supercells (32 atoms) were used to analyze the solubility, while Pd(111) $p(2\times2)$ reconstructions with four layers were employed for molecular adsorption and hydride formation. A somewhat larger reconstruction $p(3\times3)$ was employed in the formation of small aggregates. For the segregation studies, six layers were used to assess properly the difference between the layers. In any case, the *k*-point density was as dense as 0.83 $Å^{-1}$, following a Monkhorst–Pack scheme.[80] In all the structures the adsorbates and the two outermost layers were allowed to relax. All the energies reported here do not contain the entropic effects given by the configuration problems.[81] Entropic contributions would destabilize configurations with smaller degrees of freedom, as a single layer or the edge positions when compared to the bulk or to terrace positions.

However, care shall be taken as in all the cases considered here, because our results concentrate on the equilibrium properties, *i.e.* those showing the lowest energy on the potential energy surfaces. Under experimental conditions in some cases kinetic control and metastable structures can be obtained and employed for sufficiently long lab-scales. Therefore, some discrepancies might arise between some of the prepared catalysts and the results presented here.

Results

In this section, we summarize the main parameters that control the stability of the hydrogenation catalysts. All the results are summarized in Fig. 5 for the static properties. The colours in the heat map indicate the relative position of each metal promoter in the spectra spanned by all PdM (M = Pd, Cu, Ag, Au, Zn, Ga, Sn, Pb, and Bi) for each particular property.

Intrinsic stability properties

Solubility is mandatory in order to form a stable material. This parameter has been calculated in a four layer slab where the

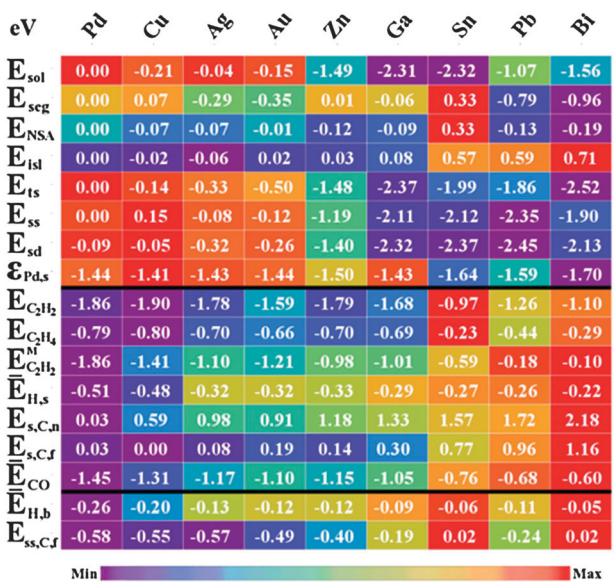

Fig. 5 Heat map for the static properties of PdM alloys. All the energies are shown in eV. The definitions correspond to those in Fig. 4: solubility, E_{sol}; segregation E_{seg} and NSA formation E_{NSA}; islanding E_{isl}; terrace substitution: E_{ts}; step substitution: E_{ss}; step decoration: E_{sd}; *d*-band center, $\varepsilon_{Pd,s}$. Adsorption energies for C_2H_2, C_2H_4, at Pd-only sites: E_{C2H2} and E_{C2H4}; $E_{C2H2}{}^{M}$ at mixed fcc sites. Hydrogen surface and subsurface energies: $E_{H,s}$ $E_{H,b}$ and average E_{CO} energy for the p(2x2)-3CO configuration. Carbide formation with respect to the C_2H_2 molecule and hydrogen: different configurations are investigated $E_{s,C,n}$ surface in a near configuration; or far (Pd-only) $E_{s,C,f}$ or subsurface Pd-only configuration $E_{ss,C,f}$. The colour code spans the maximum and the minimum value per row.

M impurity has been placed in a bulk structure with 32 atoms in Pd. The overall M content is thus 3%. The energy is obtained as $E_{sol} = E_{PdM,bulk} - E_{Pd,bulk} - E_{M,bulk}$ where $E_{PdM,bulk}$ is the energy of the structure with the promoter in a substitutional position (*i.e.* replacing a Pd atom), and $E_{M,bulk}$ the corresponding energies for the bulk structures. Negative E_{sol} values indicate exothermic processes. In the optimization, all the atoms surrounding the impurity have been allowed to relax. The largest solubility, about 2 eV, is observed for Ga and Sn. Indeed different ordered and substitutional alloys with all the promoters discussed here have been reported in the literature. Still large values are obtained for the other *sp* metals: Zn, Bi and Pb, between 1.5 and 1 eV. Lower solubility values are obtained for the noble metal triad, in the order of tenths of eV.

Segregation and near-surface alloy formation have been investigated in thick slab containing 6 layers and a $p(2\times2)$ reconstruction and calculated as follows: $E_{seg} = E_{PdM,s} - E_{PdM,bulk}$, where the impurity has been placed in the central part of the slab, $E_{PdM,bulk}$, or in upper positions, $E_{PdM,s}$. Negative values for E_{seg} or E_{NSA} indicate exothermic processes. The secondary metals studied here segregate towards the surface to a very large extent. This is the case for Pb and Bi with segregation energies larger than 0.7 eV. A second group with E_{seg} of about 1/3 eV is formed by Ag and Au while almost no preference for the surface or subsurface state is found for Ga and Zn. For the Ga alloys it is well-known that segregation does not influence much the composition profiles with depth.[58] A rather different case is presented by Sn where a rather strong anti-segregation is found, 1/3 eV.

Our results for the noble metals are similar to those reported earlier by Ruban and co-workers[37] although in their database only transition metals were reported. However, even in the cases when the segregation is favoured energetically, due to the temperature ranges employed it might be that the equilibrium configuration is not reached. Still, experiments have shown the formation of a surface alloy for Sn by the combination of LEED and AES.[61b] Similarly the formation of a surface PdZn alloy was found by XANES[56] and intermetallic compounds with Bi have also been reported.[72]

Near-surface alloys, NSA, are those compounds where the secondary metal is not placed in the surface position but rather underneath the surface.[82] These materials have been shown to have very interesting properties and therefore this possibility has also been considered in the calculations. Compared to the numbers for the segregation it is important to notice that while Cu is segregated towards the surface the subsurface position is even more stable. This is the case also for Zn and to a minor extent for Ga.

A further consideration on the stability of these materials is given by the formation of islands on the surface. Islanding has been studied in a larger reconstruction $p(3\times3)$ and four layers that allow the islands to be completely surrounded by Pd. The energy is given by $E_{isl} = E_{PdM2} - E_{Pd2M}$, where E_{PdM2} is the promoter dimer and E_{Pd2M} the corresponding to the separated configuration. Pb, Bi, and Sn show a strong lateral repulsion and thus isolated atoms are expected. For Pb this agrees with the formation of ordered PdPb phases where the Pb atoms are completely surrounded by Pd.[65f] For the remaining atoms, Au, Zn, and Ga, island formation is weakly repulsive or slightly bonding for Cu and Ag. Of course entropic configurations would change the final values by favouring non-ordered configurations and thus a very limited number of dimers shall be expected at low promoter concentrations. Dispersed tin in PdSn alloys was identified by XANES[61a] while the low energy found for Ag segregation is in agreement with the results in ref. 36.

The analysis of the steps was done in a $p(2\times1)$ reconstruction of the (211) surface with a slab containing 9 layers. The energy parameter was defined as: $E_{ss} = E_{MstepPd} - E_{Pd,step} - E_{M,bulk}$ where $E_{MstepPd}$ is the energy with the M atom sitting at the step and $E_{Pd,step}$ the energy of the Pd step. Step substitution is favoured for the large atoms like Sn, Pb and Bi but also for Ga (2 eV) which makes these sites, particularly active in C–C bond breaking, less common. The ordering in the substitution of the noble metal triad parallels the size of the metals. Therefore, a lower coordinated position is less crowded and can accommodate large atoms such as Au better.

We have also inspected the possibility of step decoration. In that case, the secondary metal is not placed as a part of the lattice but close to the edge in the form of a growing terrace. Then, decoration is calculated as $E_{sd} = E_{MPdstep} - E_{Pd,step} - E_{M,bulk}$ where $E_{MPdstep}$ is the energy with the M atom decorating the Pd step. This is actually the preferred situation for Sn and Pb by about 0.2 eV. Step decoration would then be preferred if no strong thermal treatment is performed on the catalyst.

Combining the energies above it is possible to illustrate if terrace or step positions are favoured. The energy of terrace positions obtained as $E_{ts} = E_{sol} + E_{seg}$, is favoured for Cu, Ag, Au, Zn, and Ga by 0.2–0.5 eV. With respect to the decoration, this is favoured when compared to the edge substitution for Pb, and Sn. Decoration is less stable than the terrace positions for Au, Pb, and Bi. However, Bi has been experimentally proposed to preferentially decorate the areas in the surrounding of the edges.[68,71] According to our calculations this could correspond to a metastable state as the step substitution is energetically hindered $\Delta E = E_{ss} - E_{sd} = 0.23$ eV. This view would agree with the high dispersion found for Bi by Kereszegi *et al.*[83]

The chemical consequences of all the above can be summarized by the change in the electronic structure of Pd represented in Fig. 6 and visualized by the shift in the *d*-band, ε_{Pd}. On one hand Cu, Ag, Au, and Ga almost do not perturb the electronic structure of the surface Pd metal. Zn modifies little the structure while Pb, Sn, and Bi strongly shift down the bands for Pd rendering these surfaces less available to adsorption. In addition, for PdGa ordered alloys it has been reported that the number of states at the Fermi level is lowered with respect to pure Pd.[58] In Fig. 6, this is clearly represented, similarly the other alloys present this feature. The downward shift of has been reported experimentally for Sn.[60]

Adsorption properties

All the adsorption parameters were explored in the $p(2\times2)$ supercell with four layers. The energy has been computed as $E_{HC} = E_{HCPdM} - E_{PdM} - E_{HC,gas}$. The adsorption energy of the hydrocarbon, E_{HC}, is calculated as the energy for the adsorbed system, $E_{HCPdM,}$ minus the surface, E_{PdM}, and the energy of the hydrocarbon in the gas phase, $E_{HC,gas}$, either acetylene or ethylene. Therefore, exothermic processes show negative E_{HC} values. In the models employed, the Pd-only sites are more active towards adsorption than the mixed sites and acetylene is always adsorbed more strongly than ethylene. Acetylene is adsorbed in fcc positions while ethylene is adsorbed in a bridge position with the carbons directly bonded to the Pd atoms. The large *d*-band shift induced by Pb and Bi induces an important reduction of the adsorption energy of double bond. The adsorption of the molecules with triple bonds while desorbing those with double bonds, known as the thermodynamic selectivity is the first requirement when searching for a selective hydrogenation catalyst.[17] Therefore, both Pb and Bi are good enough to improve selectivity. Instead the presence of Cu on the surface of the alloy is detrimental as both the double and the triple bond are stabilized with respect to Pd. Moreover, the Au-containing alloy is less available for alkyne adsorption while keeping a large binding energy for the alkene thus being also problematic for selectivity. For the NSA Cu alloy the adsorption therein. C_2H_2 is bonded to the surface by 1.72 and C_2H_4 by 0.73 eV. Both are then lower than the surface model by a rigid shift of 0.2 eV. When comparing to the experiments for the Sn-containing materials the adsorption energy and activation of the double bond was found to be reduced when raising the Sn content thus in agreement with our computational results.[61b]

As for CO adsorption, the control parameter is the average adsorption energy for the structures corresponding to the experimentally determined $p(2\times2)$-3CO that is very well-established for Pd.[23] The energy is then calculated as follows:

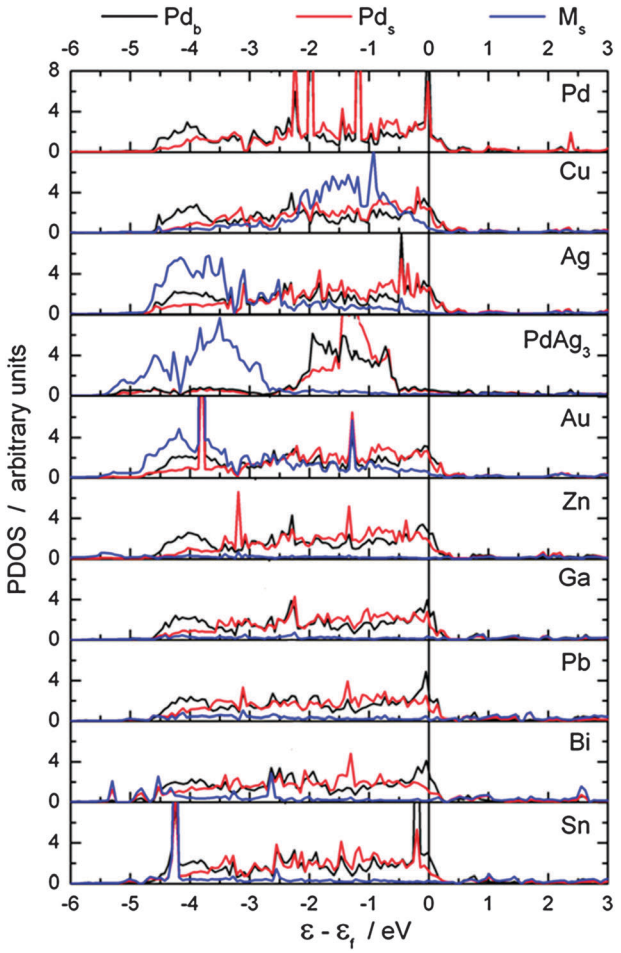

Fig. 6 Projected density of states for all the calculated alloys, a Pd atom from the bulk, Pd_b; one of the surface, Pd_s; and the promoter, M_s; are presented.

$E_{CO} = (E_{3COPdM} - E_{PdM} - 3E_{CO})/3$ where E_{3COPdM} is the energy corresponding to the configuration with three CO molecules in the $p(2\times2)$ supercell, and E_{CO} the energy of CO. This energy density is very high for the Pd surface and is still quite similar for Cu, Ag, Zn, Au, and Ga. For the other atoms the p(2x2) structure does not adsorb exothermically three molecules, and therefore, the average CO adsorption density plummets to less than 0.75 eV. On the Cu-NSA alloy, the average of CO adsorption is 1.38 eV slightly large the surface alloy, 1.31 eV. Therefore, for the Cu-NSA the alloy is less prone to hydrocarbon adsorption but more likely to adsorb CO than the clean Pd surface.

It is important to indicate that while the adsorption of the first CO molecule is more favoured than that of C_2H_2 on Pd, Pb, and Bi, this is not the case for the coinage metals, Zn, and Ga. Therefore, a much stronger competition for the potential sites is envisaged in the latter cases, thus making CO a less powerful molecular modifier at low CO concentrations.

Phase formation

Hydride formation can be assessed by the adsorption energies for H atoms in subsequent layers either at the surface or in the interior of the material. At high pressure H_2 readily dissociates on the Pd surface and forms two kinds of hydrides: the first one α-phase contains very little amount of H and does not imply a change in the structure of the material. For the denser β-phase the H content in the bulk represents about a 70% of the amount of Pd. H atoms sit at octahedral sites in the subsurface positions and the Pd lattice is slightly enlarged (about 10%) to accommodate the hydrogens.[13] In our case we have estimated two key parameters to unveil the formation of hydride phases.[76f]

The first one is the surface adsorption energies, which would control the formation of an α-like phase and the real amount of H on the surface. This has been calculated in the $p(2\times2)$ model with four layers by occupying all the possible positions on the surface, the energy was obtained as follows $E_{H,s} = (E_{NHPdM} - E_{PdM} - N^*E_{H2}/2)/N$, where N is the number of occupied positions, E_{NHPdM} the alloy with N H atoms on the surface and E_{H2} the energy of a hydrogen molecule. The second corresponds to the adsorption energy of internal positions once the surface ones are filled. The energy in this case has been calculated as $E_{H,b} = (E_{NHPdM} - E_{PdM} - N^*E_{H2}/2)/N$ where now both surface and subsurface positions were occupied. As can be seen in Fig. 5 the energy for surface positions is quite similar to that of the regular surface for the coinage metals. This is not the case for *sp* metals, where only two positions out of the four available on the surface can be occupied. This is because the promoters create an exclusion area for adsorption. Therefore, hydrogen surface coverage is forbidden in these areas and the total amount of available hydrogen is smaller than for the other PdM. As for the subsurface positions, in all cases the energy gain is much smaller for the PdM alloys than for the pure system. The average energy (including also surface atoms) almost vanishes for Bi, Sn, and Ga thus indicating that those materials are not likely to form hydrides. In the XAFS experiments for PdSn, the suppression of the β-PdH phase was reported in ref. 61*a* while for the Ag containing catalyst the presence of an external Pd-rich surface with a Ag core where no hydride can be formed is usually regarded as positive effect in the kinetic experiments.[39]

Regarding the carbide formation we have explored a number of possibilities. Surface C atoms, $E_{s,C}$, in both near and far configurations, were investigated as they illustrate the corrugation of the potential energy surface. The energy was calculated as follows on a $p(2\times2)$ model: $E_{s,C} = E_{CPdM} - E_{PdM} - 1/2E_{C2H2} + E_{H2}/2$ with C close to the fcc position with the M atom ($E_{s,C,n}$) or far away ($E_{s,C,f}$). Negative values indicate exothermic processes. C atoms can only be formed on the surface far away from the impurities. For Sn, Pb, and Bi any position on the surface is strongly poisoned enough so that the formation energies of carbon are larger than 0.75 eV. Therefore, carburization of the surface is unlikely. In a similar manner, the formation of subsurface carbide was analyzed. The energy parameter employed was $E_{ss,C} = E_{CPdM} - E_{PdM} - 1/2E_{C2H2} + E_{H2}/2$, but only in the far configuration. C can occupy fcc sites below the surface and this is exothermic when the reference is acetylene by close to -0.6 eV in Pd. This energy is severely reduced for the *sp* metals and in particular Sn, and Bi complete remove the possibility of carbide formation for the surface alloys.

Side reactions I: overhydrogenation

Two different types of side reactions compromise the yield of hydrogenation catalysts. On one hand secondary hydrogenation paths can take place. These include ethylene hydrogenation or overhydrogenation of ethyne. The control of the first problem is usually achieved by improving what is known as thermodynamic selectivity, *i.e.* keeping ethyne adsorbed while desorbing ethene from the surface. If this were the only control parameter then Au nanoparticles would outperform any of the possible catalytic materials described so far.[28] Shown by Nørskov and co-workers,[4b] this requirement poses a further problem as the adsorption of ethyne and ethylene is controlled by a single parameter, the adsorption of C, and thus the opportunity window is a compromise between activity and selectivity towards over-hydrogenation. Then a part of the selectivity can be traced back to the adsorption properties of the C_2 moieties and the ability to absorb H in subsurface layers. As we have seen in Fig. 5, Pb and Bi are very effective in reducing the binding energies of the double bonds while still keeping a strong binding energy for ethyne. Thus, of all the model system studies only these two are effective enough for suppressing C=C adsorption. This can be correlated to the downshift of the center of the *d*-band for Pd.

Still this is just one part of the problem. As we have seen before, under typical reaction conditions the interplay with the hydride phases might be very strong and thus more constraints need to be added to suppress overhydrogenation of the alkynes. Recently we have seen how a model β-PdH phase shows an alternative route, already proposed by Ceyer and co-workers,[84] where subsurface hydrogen generates ethylidene directly from vinyl due to the high chemical potential of the subsurface hydrogen.[17]

The selectivity towards overhydrogenation can be analyzed by the suppression of H subsurface formation; in Fig. 5 it is possible to see that all the M considered so far reduce the adsorption energy of bulk H. However, the degree of suppression of the β-PdH structure is larger for Bi and Sn and slightly smaller for Pb and Ga. Suppression of the hydride has been reported experimentally for Sn.[61a] There are differences, for some of the co-catalysts as the sites in their surroundings are completely blocked and thus present exclusion areas on the surface. All the studied promoters reduce the availability for the β-PdH phase and thus shall be less prone to overhydrogenate vinyl to ethylidene thus blocking overhydrogenation.

Side reactions II: coking and oligomerization

The second source of selectivity loss is related to the formation of carbon-derived fragments. On one side, dissociation of hydrocarbons on low-coordinated sites on the surface might occur and so carbon deposits are usually formed close to edges.[17] The so formed C atoms can then penetrate towards the bulk of the material through rather small energy barriers. This fact has been clearly identified in PGAA experiments.[4,21] Carbide formation is known to improve selectivity[4] but the control and homogeneity of the layer are virtually impossible.[17] In any case, C deposits block either active sites for dissociation (when C is sitting at the step) or reduce the binding energy of alkenes. This results in an enhanced selectivity for the partial hydrogenation of the alkynes. Preferential decoration of step positions reported in Fig. 5 for Pb and Sn reduces the binding energies of C atoms to step positions. This results in a lower probability for the dissociation of hydrocarbons due to kinetic limitations. In addition, Fig. 5 shows that the ability of the promoters, especially when sp metals are considered, results in a lower energy for the formation of the carbide phase thus making thermodynamic factors also less favourable. The effect is not seen for Group 11 metals. The final effect on the selectivity of the competition between secondary metals and carbon-related species is difficult to assess as one limits the effect of the other.

The most important cause for the loss of selectivity under several conditions has been overlooked in many theoretical studies. Oligomerization of the alkyne or partially hydrogenated intermediates to C_{4+} and larger compounds has been described for all the Pd catalysts and, in many cases, while controlling overhydrogenation is easy; the control of oligomerization turns out to be extremely difficult. The reaction paths leading to C_{4+} can be formed by the coupling of two acetylene molecules on the surface as shown in Fig. 7. However, some authors indicate that the presence of a certain amount of hydrogen coverage is needed.[85] The barriers for C–C bond formation are 1.38 eV for two acetylene molecules, but decrease to 1.19 eV for the vinyl-acetylene one.[17]

Two different ways can be envisaged to reduce the amount of oligomers produced on the catalyst surface: (i) by reducing the overall adsorption energy and thus the coverage on the surface at given acetylene pressure, (ii) by reducing the size of the available ensembles as the site needed for C–C bonding implies the use of two neighbouring fcc, see Fig. 7. This can be seen also as a hindered diffusion of alkynes or partially hydrogenated alkynes on the surface.

In the calculations, we have checked this aspect by analyzing the binding energy of acetylene to fcc positions where one of the atoms is replaced by the impurity, $E_{C2H2}{}^{M}$, Fig. 5. Two types of behaviours are obtained. On one side, Sn, Pb and Bi behave as true spacers as their adsorption on sites that contain these metals is nearly 1 eV less strong than on the Pd sites, thus inhibiting oligomerization at the surface. On the other hand, C_2H_2 diffusion paths on PdCu, and PdAu are very flat and thus this couple of metals would behave closer to pure Pd surfaces with respect to oligomerization. Ag, Zn, and Ga show adsorption energies in mixed sites of about 0.6–0.75 eV. For these particular cases, then adsorption on a mixed site would promote the oligomerization as the initial state would be activated and the final state could be stabilized by no direct

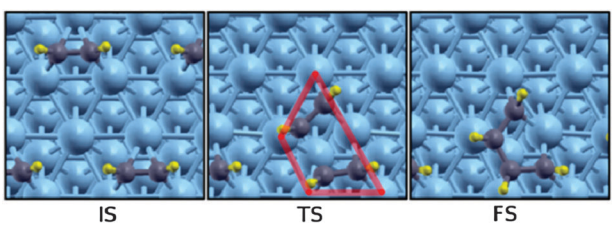

Fig. 7 Schematic representation of the oligomerization of two acetylene molecules on the Pd(111) surface: IS, TS, and FS are the initial, transition and final states. Blue spheres represent Pd atoms, grey C and yellow H. The minimum ensemble for the reaction is shown in red.

interaction with the impurity. Indeed the catalysts with Ag, Zn, and Ga are found to produce oligomers. This is a reason to increase the amount of Ag under operation, especially in the tail-end, as more silver is needed to achieve site isolation. For Zn,[56] a 5–20% of oligomers has been reported in 1-pentyne hydrogenation, the higher values corresponding to high temperature (100 °C) operation. For the intermetallic ordered PdGa compounds the oligomerization corresponds to a 5–10%,[58] (200 °C for C_2) thus somehow lower than the previous values. This value is smaller than the corresponding value for Zn. There are two potential reasons for this behaviour: (i) the lower diffusion barrier and the weaker adsorption energy resulting in a smaller coverage and (ii) the higher temperature and high H_2 pressure that implies lower hydrocarbon coverage on the surface employed in the PdGa experiments. Our results agree with different experiments, for instance Verdier and co-workers[62] identified lower mobility for the adsorbed species hydrocarbons and hydrogen in PdSn catalysts.

The PdAu case is quite significant. It is well-established that important ensemble effects exist for these alloys in H adsorption in electrochemical environments and in oxidation reactions to form vinylacetate from acetate and ethylene.[50,86] From the results above, the ensemble effects in hydrogenations are less pronounced than for other metals in particular when the mobility of ethyne is considered. Therefore, ensemble effects depend on the reaction. The reduction of the binding energy and a more slightly hindered mobility explain the reduction of benzene formation for these alloys reported in ref. 54.

Dynamic properties

As the catalysts are exposed to a harsh environment, we discuss the stability of the alloys as a function of the external hydrogen and CO pressures. The schematic representations of the processes investigated and the values are presented in Fig. 8 and 9. Experimentally induced segregation by hydrogen or CO has been reported on PdAu alloys.[48,52]

Starting with hydrogen, the surface structures can displace the co-catalyst from the surface. This is clearly seen for Sn, antisegregation is favoured by nearly 1 eV. Still the effect is common to all the systems investigated in Fig. 9. The heat map shows large antisegregation for Ga, Zn, (0.75 eV), mild for Ag, Au (0.5 eV) and small but still relevant for Cu, Pb, and Bi, around 1/4 eV. Therefore, none of the investigated alloys show enough resistance towards induced segregation under the high H contents present for instance in the front-end (large H_2 : alkyne ratio). This is one of the reasons why the PdGa alloys employed as ordered compounds are more resistant. Indeed these materials are less prone to induced segregations as the repulsive nature of the Ga–Ga helps in modulating the amount of hydrogen both by reducing the average hydrogen energy and simultaneously improving the repulsion of the secondary metals in the lattice.

For CO the situation is quite similar. CO induces strong antisegregation for Sn but also more than 1.5 eV for Pb and Bi. Therefore none of these compounds would be suitable for front-end formulations where CO is added to the feed. Medium segregation is found for Au, Zn and Ga, from 0.7–1.14 eV.

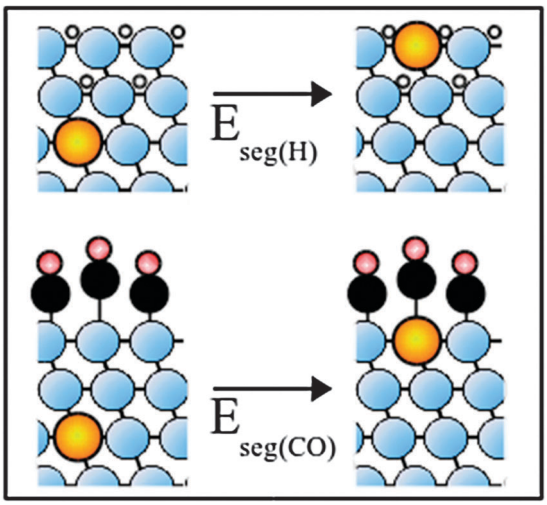

Fig. 8 Schematic representation of the induced segregation properties. Blue spheres represent Pd, yellow the promoter, small white H, black C and red O.

eV	Pd	Cu	Ag	Au	Zn	Ga	Sn	Pb	Bi
E_{seg}	0.00	0.07	-0.29	-0.35	0.01	-0.06	0.33	-0.79	-0.96
$E_{seg(H)}$	0.00	0.21	0.49	0.44	0.72	0.83	1.28	0.23	0.22
$E_{seg(CO)}$	0.00	0.47	0.53	0.70	0.89	1.14	2.40	1.52	1.57

Min — Max

Fig. 9 Heat map for the dynamic properties of PdM alloys. All the energies are shown in eV. The definitions correspond to those in Fig. 8: segregation, E_{seg}; hydrogen induced segregation $E_{seg(H)}$; and CO induced segregation $E_{seg(CO)}$. The colour code spans the maximum and the minimum value per row.

The effect is smaller for Cu and Ag, but still moderate, therefore not fully adapted to CO-rich operation.

Ag-rich effects

The patent for the PdAg catalyst in hydrogenation indicates a very large composition range. In fact, Ag contents can be as large as a 75–80% of the material in many cases, especially in tail-end operation.[31] We have thus investigated the adsorption properties of a material with a nominal composition of $PdAg_3$ with the aim of investigating the differences with the low Ag content alloy. We shall bear in mind that the formation of Ag islands is not strongly hindered as for other promoters, which might lead to small aggregates on the surface but also if the hydrogen pressures are large the stability of Ag on the surface is compromised. Pd site isolation was then obtained by employing larger Ag contents in the alloys. When considering adsorption in the $PdAg_3$ structure, the C_2H_2 is very weakly bound, by −0.4 eV, as instead of the fcc site adsorption with π-type characteristics an on-top σ-bonded structure is retrieved. The C_2H_4 molecule is only physisorbed to this surface, by −0.1 eV which is a positive feature in terms of the thermodynamic selectivity. In this system, subsurface Pd atoms can be segregated towards the surface through an energy penalty of 0.29 eV. This value is almost independent of the amount of Pd on the surface as the maximum energy per atom for the extraction for the model employed is 0.33 eV/Pd atom. Therefore, segregation can

be reversed by C_2H_2 adsorption, and then surface Pd dimer is favoured by −0.06 eV, dragging Pd towards the surface. This is induced by the change of the C_2H_2 adsorption from a monomer Pd site to a Pd_2 site on the surface. A complex interplay between the reaction atmosphere and the outermost layer compositions is therefore likely. Thus, for $PdAg_3$ the active hydrogenation ensembles are formed as they are promoted by the reactant. As H is very weakly adsorbed, −0.11 eV/H on the sites containing Pd the reaction could proceed as follows. C_2H_2 is adsorbed, extracts some more Pd from the subsurface where an H atom can also be adsorbed and then first and second hydrogenation takes place. Of course, the dynamic behaviour of the active site being either a monomer or a dimer blocks the possibility for oligomerization that requires around five atoms, see Fig. 7 (more than 1.2 eV). This picture agrees very well with the suggestions from the experiments reported in ref. 39.

Finally, CO cannot be added to this catalyst formulation. The reason being that CO adsorbs on top the isolated palladium atoms by a much larger amount, 1.35 eV, than the alkyne. Thus, all the positions would be completely blocked if CO were present.

Compatibility between the promoter, the molecular modifier and the reaction conditions

In the description of Fig. 1 we have indicated that the complete catalysts are formed by the active material, the promoter or co-catalyst and the molecular modifier. Obviously the structure of the active/selective materials shall be preserved under reaction conditions and thus a significant effect of both temperature and pressure needs to be taken into account. As shown in Fig. 5, all the metals employed as co-catalysts are compatible with the main material, as all of them form solid solutions. Then the question comes from the stability under reaction conditions.

For instance surface alloys will suffer of induced hydrogen segregation in almost all cases. Therefore, these structures would be dynamic under high H_2 conditions. Indeed the fact that the sp metals show very weak interaction energy with H turns to be a problem because antisegregation is favoured at high H_2 pressures. The situation is much less effective for Zn, and Ga. For the coinage metals, Cu is already in the form of a NSA alloy and thus it is more stable than if placed on the surface.

Still Pb and Bi are used in Lindlar type catalysts, the reason is related to the modulating effect of the solvent in controlling the total pressure of H_2 in contact with the catalyst. Solubility then needs to be taken into account to understand why these materials are stable under reaction conditions. Moreover, the Lindlar catalyst is employed usually at room or near room temperatures, thus making the diffusion of the metal towards the bulk of the material a less likely process and the issue of stability a less crucial one. In addition, batch reactors and no continuous operation are more suited to less compatible modifiers.

A second aspect consists in the evaluation of the cross effects between the typical gas-phase modifier and the co-catalyst. Pb and Bi could not be used with CO in any case, because of the large reduction of the binding energies of CO in dense phases when compared to the plane Pd catalysts. This is yet another reason why the Lindlar catalyst avoids CO in its formulation. This is also why a controlled modulation in the relative amounts of CO pressures on the Ag containing catalysts employed in the industry (specially in tail-end operation) is needed to optimize the performance of these materials. The higher the Ag content in the alloy, the lower the amount of CO that can be tolerated.

Conclusions and outlook

The study of selectivity represents the next frontier in heterogeneous catalysis. New materials with very specific properties are required to improve energy use and atom economy, two crucial elements in enhancing the sustainability of our industries. Selectivity represents a challenge from a theoretical point of view as the main reaction pathway side reactions need to be considered and, in order to be truly representative, high accuracy for a large number of paths needs to be evaluated. Simultaneously, an accurate description of the state of the material in response to the environment is required.

In the last few years, great efforts have been devoted to the study of selectivity in the hydrogenation of triple bonds and dienes in the presence of double bonds either in a single molecule or in a mixture of molecules. Large improvements achieved by the cooperative experimental and theoretical work have been presented recently and the versatility of theoretical studies based on Density Functional Theory has been powerful enough to assess the state of the system, but also its reactivity, and to single out proper descriptors. Indeed three characteristics are required to obtain selectivity in the hydrogenation of alkyne–alkene mixtures: (i) thermodynamic separation of reactants, (ii) avoidance of hydride phases, and (iii) elimination of oligomerization paths. The field is far from complete and many remaining challenges await for more accurate descriptions, in particular when related to the role of the second metal and that of molecular modifiers, which are still in the grey zone. The high dynamic character of the hydrogenation catalysts under relevant reaction conditions poses a further challenge to theoretical simulations. In the present work, we have provided qualitative indications of the interplay between hydride, carbide and CO overlayers with promoters. The results presented here illustrate also how the reaction atmosphere could alter the properties of in principle active PdM alloys but more is needed as kinetic parameters for all the possible reaction mechanisms are strongly related to the presence of active phases, for instance hydrides. Therefore structure–activity/selectivity relationships require an adequate assessment on the structure and more sophisticated Kinetic Monte Carlo studies including the processes that involve subsurface species and the dynamics of the promoters.

The studies on hydrogenation and the comparison to the organic synthesis pave the way towards the systematization of theoretical studies on the reactivity of more complex molecules especially these transformations for which no active catalyst has been proposed that could open new platforms to convert new raw materials (as those derived from biomass) into useful building blocks for the chemical industry.

Acknowledgements

We would like to thank Prof. Pérez-Ramírez (ETH) and Drs B. Bridier (ETH) and M. García-Mota (SLAC) for many

discussions. Financial support from Bio2chem-d ERC-StG'10, Consolider Ingenio 2010 CSD2006-003, CTQ2009-07553/BQU is greatly acknowledged and BSC-RES is thanked for providing generous computational resources.

Notes and references

1 G. A. Somorjai and Y. G. Borodko, *Catal. Lett*., 2001, **76**, 1.
2 I. Chorkendorff and J.-W. Nietmasverdriet, *Introduction to Modern Catalysis Wiley*, 2002.
3 P. Sabatier, *Nobel Lectures, Chemistry 1912*, Elsevier Publishing Company, Amsterdam, 1966.
4 (*a*) D. Teschner, J. Borsodi, A. Wootsch, Z. Révay, M. Hävecker, A. Knop-Gericke, S. D. Jackson and R. Schlögl, *Science*, 2008, **320**, 86; (*b*) F. Studt, F. Abild-Pedersen, T. Bligaard, R. Z. Sorensen, C. H. Christensen and J. K. Nørskov, *Science*, 2008, **320**, 1320; (*c*) B. Bridier, J. Pérez-Ramírez, A. Knop-Gericke, R. Schlögl and D. Teschner, *Chem. Sci*., 2011, **2**, 1379.
5 (*a*) A. Molnár, A. Sárkány and M. Varga, *J. Mol. Catal. A: Chem*., 2001, **173**, 185; (*b*) G. C. Bond, *Metal-Catalysed Reactions of Hydrocarbons*, Springer, New York, 2005.
6 A. Borodzinski and G. C. Bond, *Catal. Rev. Sci. Eng*., 2006, **48**, 91.
7 M. Ruta, N. Semagina and L. Kiwi-Minsker, *J. Phys. Chem. C*, 2008, **112**, 13635.
8 A. Borodzinski, *Catal. Lett*., 2001, **71**, 169.
9 A. Borodzinski and G. C. Bond, *Catal. Rev. Sci. Eng*., 2008, **50**, 379.
10 (*a*) H. Lindlar, *Helv. Chim. Acta*, 1952, **35**, 446; (*b*) H. Lindlar and R. Dubuis, *Org. Synth*., 1973, **5**, 880.
11 (*a*) M. Garcia-Mota, J. Gomez-Diaz, G. Novell-Leruth, C. Vargas-Fuentes, L. Bellarosa, B. Bridier, J. Pérez-Ramírez and N. Lopez, *Theor. Chem. Acc*., 2011, **128**, 663; (*b*) G. Santarossa, M. Iannuzzi, A. Vargas and A. Baiker, *ChemPhysChem*, 2008, **9**, 401.
12 V. Ponec, *Adv. Catal*., 1983, **32**, 149.
13 N. N. Greenwood and A. Earnshaw, *Chemistry of the elements*, Elsevier, 2nd edn, 2008, p. 1150; and references therein.
14 (*a*) T. Mitsui, M. K. Rose, E. Fomin, D. F. Ogletree and M. Salmeron, *Nature*, 2003, **422**, 705; (*b*) N. Lopez, Z. Łodziana, F. Illas and M. Salmeron, *Phys. Rev. Lett*., 2004, **93**, 146103; (*c*) S. Y. Zaginaichenko, Z. A. Matysina, D. V. Schur, L. O. Teslenko and A. Veziroglu, *Int. J. Hydrogen Energy*, 2011, **36**, 1152.
15 J. Horiuti and M. Polanyi, *Trans. Faraday Soc*., 1934, **30**, 1164.
16 (*a*) P. A. Sheth, M. Neurock and C. M. Smith, *J. Phys. Chem. B*, 2003, **107**, 2009; (*b*) D. H. Mei, P. A. Sheth, M. Neurock and C. M. Smith, *J. Catal*., 2006, **242**, 1.
17 M. García-Mota, B. Bridier, J. Pérez-Ramírez and N. López, *J. Catal*., 2010, **273**, 92.
18 A. M. Doyle, S. K. Shaikhutdinov, S. D. Jackson and H.-J. Freund, *Angew. Chem., Int. Ed*., 2003, **42**, 5240.
19 (*a*) M. K. Rose, A. Borg, T. Mitsui, D. F. Ogletree and M. Salmeron, *J. Chem. Phys*., 2001, **115**, 10927; (*b*) L. Gracia, M. Calatayud, J. Andres, C. Minot and M. Salmeron, *Phys. Rev. B: Condens. Matter Mater. Phys*., 2005, **71**, 033407; (*c*) L. Nykanen, J. Andersin and K. Honkala, *Phys. Rev. B: Condens. Matter Mater. Phys*., 2010, **81**, 075417; (*d*) C. Ling and D. S. Sholl, *Phys. Rev. B: Condens. Matter Mater. Phys*., 2009, **80**, 214202.
20 (*a*) J. Andersin, N. Lopez and K. Honkala, *J. Phys. Chem. C*, 2009, **113**, 8278; (*b*) J. Andersin and Honkala, *Surf. Sci*., 2010, **604**, 762.
21 D. Teschner, Z. Revay, J. Borsodi, M. Hävecker, A. Knop-Gericke, R. Schlögl, D. Milroy, S. D. Jackson, D. Torres and P. Sautet, *Angew. Chem., Int. Ed*., 2008, **47**, 9274.
22 P. Sautet and F. Cinquini, *ChemCatChem*, 2010, **2**, 636.
23 (*a*) M. K. Rose, T. Mitsui, J. Dunphy, A. Brog, D. F. Ogletree, M. Salmeron and P. Sautet, *Surf. Sci*., 2002, **512**, 48; (*b*) D. Loffreda, D. Simon and P. Sautet, *Surf. Sci*., 1999, **425**, 68; (*c*) K. Honkala, P. Pirila and K. Laasonen, *Surf. Sci*., 2001, **489**, 72.
24 E. L. Mohundro, Am. Inst. Chem. Enging. 15th Ethylene producers Conference, 2003 Spring National Meeting, New Orleans 2003.
25 N. López, B. Bridier and J. Pérez-Ramírez, *J. Phys. Chem. C*, 2008, **112**, 9346.
26 B. Bridier, N. López and J. Pérez-Ramírez, *Dalton Trans*., 2010, **39**, 8412.
27 J. F. Jia, K. Haraki, J. N. Kondo, K. Domen and K. Tamaru, *J. Phys. Chem. B*, 2000, **104**, 11153.
28 (*a*) Y. Segura, N. López and J. Pérez-Ramírez, *J. Catal*., 2007, **247**, 383; (*b*) M. García-Mota, N. Cabello, F. Maseras, A. M. Echavarren, J. Pérez-Ramírez and N. López, *ChemPhysChem*, 2008, **9**, 1624; (*c*) B. Bridier, N. López and J. Pérez-Ramírez, *J. Catal*., 2010, **269**, 80.
29 B. Bridier and J. Pérez-Ramírez, *J. Am. Chem. Soc*., 2010, **132**, 4321.
30 B. Coq and F. Figueras, *J. Mol. Catal. A: Chem*., 2001, **173**, 117.
31 Dow Chemical Company, US 2,802,889 (1957).
32 R. W. Voight, J. S. Meriam, S. A. Blankenship, AIChE, Session 19, February 1996, New Orleans.
33 (*a*) B. Didillion, P. Sarrazin, J. P. Boitiaux, AIChe, Session 43, March 1995, Houston; (*b*) J. P. Boitiaux, J. Cosyns, M. Derrien, G. Leger, Hydrocarbon Processing, March 1985.
34 (*a*) V. Kaiser, J. P. Laugier, R. DiCinto, M. Picciotti, AIChE, Session 68, March 1999, Houston; (*b*) E. Sughrue, M. Johnson, AIChE, Session 18, April 1993, Houston; (*c*) D. B. Tiedke, T. T. P. Cheung, J. Leger, S. A. Zisman, J. J. Bergmeister, G. A. Delzer, AIChE, Session 80, March 2001, Houston.
35 K. H. Chae, S. M. Jung, Y. S. Lee, C. N. Whang, Y. Jeon, M. Croft, D. Sills, P. H. Ansaci and K. Mack, *Phys. Rev. B: Condens. Matter*, 1996, **53**, 10238.
36 E. Andrade Sales, B. Benhamida, V. Caizergues, J.-P. Lagier, F. Fievet and F. Bozon-Verduraz, *Appl. Catal., A*, 1998, **172**, 273.
37 A. V. Ruban, H. L. Skriver and J. K. Nørskov, *Phys. Rev. B: Condens. Matter*, 1999, **59**, 15990.
38 G. C. Bond and A. F. Rawle, *J. Mol. Catal. A: Chem*., 1996, **109**, 261.
39 N. A. Khan, S. Shaikhutdinov and H. J. Freund, *Catal. Lett*., 2006, **108**, 159.
40 A. Pachulski, R. Schodel and P. Claus, *Appl. Catal., A*, 2011, **400**, 14.
41 Y. Ma, J. Bansmann, T. Diemant and R. J. Behm, *Surf. Sci*., 2009, **603**, 1046.
42 Y. M. Jin, A. K. Datye, E. Rightor, R. Gulotty, W. Waterman, M. Smith, M. Holbrook, J. Maj and J. Blackson, *J. Catal*., 2001, **203**, 292.
43 D. H. Mei, M. Neurock and C. M. Smith, *J. Catal*., 2009, **268**, 181.
44 P. Tiruppathi, J. J. Low, A. S. Y. Chan, S. R. Bare and R. J. Meyer, *Catal. Today*, 2011, **165**, 106.
45 N. Lopez and J. K. Nørskov, *Surf. Sci*., 2001, **477**, 59.
46 S. Sakong, C. Mosch and A. Gross, *Phys. Chem. Chem. Phys*., 2007, **9**, 2216.
47 S. Sitthisa, T. Pham, T. Prasomsri, T. Sooknoi, R. G. Mallinson and D. E. Resasco, *J. Catal*., 2011, **280**, 17.
48 A. E. Baber, H. L. Tierney, T. J. Lawton and E. C. H. Sykes, *ChemCatChem*, 2011, **3**, 607.
49 S. Leviness, V. Naier, A. H. Weiss, Z. Schay and L. Guczi, *J. Mol. Catal*., 1984, **25**, 131.
50 (*a*) F. Maroun, F. Ozanam, O. M. Magnussen and R. J. Behm, *Science*, 2001, **293**, 1811; (*b*) D. Kumar, M. S. Chen and D. W. Goodman, *Catal. Today*, 2007, **123**, 77; (*c*) Z. Li, F. Gao, Y. Wang, F. Calaza, L. Burkholder and W. T. Tysoe, *Surf. Sci*., 2007, **601**, 1898; (*d*) Z. Li, O. Furlong, F. Calaza, L. Burkholder, H. C. Poon, D. Saldin and W. T. Tysoe, *Surf. Sci*., 2008, **602**, 1084; (*e*) K. Luo, T. Wei, C. W. Yi, S. Axnanda and D. W. Goodman, *J. Phys. Chem. B*, 2005, **109**, 23517; (*f*) T. Wei, J. Wang and D. W. Goodman, *J. Phys. Chem. C*, 2007, **111**, 8781; (*g*) P. Han, S. Axnanda, I. Lyubinetsky and D. W. Goodman, *J. Am. Chem. Soc*., 2007, **129**, 14355; (*h*) F. Gao, Y. Wang and D. W. Goodman, *J. Phys. Chem. C*, 2009, **113**, 14993; (*i*) J. A. Boscoboinik, C. Plaisance, M. Neurock and W. T. Tysoe, *Phys. Rev. B: Condens. Matter Mater. Phys*., 2008, **77**, 045422; (*j*) J. A. Boscoboinik, F. C. Calaza, M. T. Garvey and W. T. Tysoe, *J. Phys. Chem. C*, 2010, **114**, 1875; (*k*) M. García-Mota and N. Lopez, *Phys. Rev. B: Condens. Matter Mater. Phys*., 2010, **82**, 075411.
51 (*a*) H. Miura, M. Terasaka, K. Oki and T. Matusda, *Stud. Surf. Sci. Catal*., 1993, **75**, 2379; (*b*) A. Sarkany, A. Horvath and B. Beck, *Appl. Catal., A*, 2002, **229**, 117; (*c*) A. Sarkany, O. Geszti and G. Safran, *Appl. Catal., A*, 2008, **350**, 157; (*d*) T. V. Choudhary, C. Sivadinarayana, A. K. Datye, D. Kumar and D. W. Goodman, *Catal. Lett*., 2003, **86**, 1.
52 A. Hugon, L. Delannoy, J.-M. Krafft and C. Louis, *J. Phys. Chem. C*, 2010, **114**, 10823.

53 M. Di Vece, S. Bals, J. Verbeeck, P. Lievens and G. Van Tendeloo, *Phys. Rev. B: Condens. Matter Mater. Phys.*, 2009, **80**, 125420.
54 E. Gross and M. Asscher, *Langmuir*, 2010, **26**, 16226.
55 J. A. Rodriguez, *J. Phys. Chem.*, 1994, **98**, 5758.
56 (*a*) M. W. Tew, H. Emerich and J. A. van Bokhoven, *J. Phys. Chem. C*, 2011, **115**, 8457; (*b*) A. Sarkany, Z. Zsoldos, B. Furlong, J. W. Hightower and L. Guczi, *J. Catal.*, 1993, **141**, 566.
57 P. S. Wehner and B. L. Gustafson, *J. Catal.*, 1992, **135**, 420.
58 (*a*) M. Armbruster, G. Wowsnick, M. Friedrich, M. Heggen and R. Cardoso-Gil, *J. Am. Chem. Soc.*, 2011, **133**, 9112; (*b*) A. Ota, M. Armbruster, M. Behrens, D. Rosenthal, M. Friedrich, I. Kasatkin, F. Girgsdies, W. Zhang, R. Wagner and R. Schlogl, *J. Phys. Chem. C*, 2011, **115**, 1368; (*c*) M. Armbruster, K. Kovnir, M. Behrens, D. Teschner, Y. Grin and R. Schlogl, *J. Am. Chem. Soc.*, 2010, **132**, 14745; (*d*) J. Osswald, K. Kovnir, M. Armbruster, R. Giedigleit, R. E. Jentoft, U. Wild, Y. Grin and R. Schlogl, *J. Catal.*, 2008, **258**, 219.
59 (*a*) M. Armbruster, H. Bormann, M. Wedel, Y. Prots, R. Geidigkeit and P. Gille, *Z. Kristallogr. - New Cryst. Struct.*, 2010, **225**, 617; (*b*) K. Kovnir, M. Schmidt, C. Waurish, M. Armbruster, Y. Prots and Y. Grin, *Z. Kristallogr. - New Cryst. Struct.*, 2008, **223**, 7.
60 K. Pattamakomsan, E. Ehret, F. Morfin, P. Gelin, Y. Jugnet, S. Prakash, J. C. Bertolini, J. Panpranot and F. J. C. S. Aires, *Catal. Today*, 2011, **164**, 28.
61 (*a*) S. H. Choi and J. S. Lee, *J. Catal.*, 2000, **193**, 176; (*b*) C. Breinlich, J. Haubrich, C. Becker, A. Valcarcel, F. Delbecq and K. Wandelt, *J. Catal.*, 2007, **251**, 123.
62 S. Verdier, B. Didillon, S. Morin and D. Uzio, *J. Catal.*, 2003, **218**, 288.
63 E. A. Sales, M. D. Mendes and F. Bozon-Verduraz, *J. Catal.*, 2000, **195**, 96.
64 (*a*) M. Masai, K. Honda, A. Kubota, S. Onhaka, Y. Nishikawa, K. Nakahara, K. Kishi and S. Ikeda, *J. Catal.*, 1977, **50**, 419; (*b*) G. Hamm, T. Schmidt, J. Breitbach, D. Franke, C. Becker and K. Wandelt, *Z. Phys. Chem.*, 2009, **223**, 209.
65 (*a*) T. B. Massalski, H. Okamoto, P. R. Subramanian and L. Kacprzak, *Binary alloy phase diagrams*, ASM International, Materials Park, OH, 1990; (*b*) D. Chadwick and M. A. Karolewski, *Surf. Sci.*, 1983, **126**, 41; (*c*) H. R. Aduriz, C. E. Gigola, A. M. Sica, M. A. Volpe and R. Touroude, *Catal. Today*, 1992, **15**, 459; (*d*) H. R. Aduriz, P. Bodnariuk, B. Coq and F. Figueras, *J. Catal.*, 1991, **129**, 47; (*e*) M. B. Fernandez, C. M. Piqueras, G. M. Tonetto, G. Crapiste and D. E. Damiani, *J. Mol. Catal. A: Chem.*, 2005, **233**, 133; (*f*) W. Palczewska, I. Szymerska, I. Ratajczykowa, M. Lipski M Proc. ECOSS-3 and ICCS-4 Cannes 1980.
66 A. B. McEwen, M. J. Guttieri, W. F. Maier, R. E. Laine and Y. Shvo, *J. Org. Chem.*, 1983, **48**, 4436.
67 (*a*) J. Goetz, M. A. Volpe, C. E. Gigola and R. Touroude, *J. Catal.*, 2001, **199**, 338; (*b*) J. Goetz, M. A. Volpe, A. M. Sica, C. E. Gigola and R. Rouroude, *J. Catal.*, 1997, **167**, 314.
68 J. Sa, J. Montero, E. Duncan and J. A. Anderson, *Appl. Catal., B*, 2007, **73**, 98.
69 (*a*) C. Keresszegi, J. D. Grunwaldt, T. Mallat and A. Baiker, *Chem. Commun.*, 2003, 2304; (*b*) C. Keresszegi, J. D. Grunwaldt, T. Mallat and A. Baiker, *J. Catal.*, 2004, **222**, 268.
70 H. Kimura, A. Kimura, I. Kokubo, T. Wakisaka and Y. Mitsuda, *Appl. Catal., A*, 1993, **95**, 143.
71 J. A. Anderson, J. Mellor and R. P. K. Wells, *J. Catal.*, 2009, **261**, 208.
72 S. Karski, *J. Mol. Catal. A: Chem.*, 2006, **253**, 147.
73 (*a*) G. C. Bond, *Chem. Soc. Rev.*, 1991, **20**, 441; (*b*) G. C. Bond, *Acc. Chem. Res.*, 1993, **26**, 490.
74 M. W. Small and T. S. King, *J. Catal.*, 1990, **120**, 335.
75 W. M. H. Sachtler, *Catal. Rev. Sci. Eng.*, 1976, **14**, 193.
76 (*a*) F. Tao, M. E. Grass, Y. W. Zhang, D. R. Butcher, F. Aksoy, S. Aloni, V. Altoe, S. Alayoglu, J. R. Renzas, C. K. Tsung, Z. W. Zhu, Z. Liu, M. Salmeron and G. A. Somorjai, *J. Am. Chem. Soc.*, 2010, **132**, 8697; (*b*) E. Christoffersen, P. Stoltze and J. K. Norskov, *Surf. Sci.*, 2002, **505**, 200; (*c*) K. L. Andersson, F. Calle-Vallejo, J. Rossmeisl and I. Chorkendorff, *J. Am. Chem. Soc.*, 2009, **131**, 2404; (*d*) J. Greeley and M. Mavrikakis, *J. Phys. Chem. B*, 2005, **109**, 3460; (*e*) A. U. Nilekar, A. V. Ruban and M. Mavrikakis, *Surf. Sci.*, 2009, **603**, 91; (*f*) J. Greeley, W. P. Krekelberg and M. Mavrikakis, *Angew. Chem., Int. Ed.*, 2004, **43**, 4296.
77 G. Kresse and J. Hafner, *Phys. Rev. B: Condens. Matter*, 1993, **47**, 558.
78 J. P. Perdew, J. A. Chevary, S. H. Vosko, K. A. Jackson, M. R. Pederson, D. J. Singh and C. Fiolhais, *Phys. Rev. B: Condens. Matter*, 1992, **46**, 6671.
79 P. E. Blöchl, *Phys. Rev. B: Condens. Matter*, 1994, **50**, 17953.
80 H. J. Monkhorst and J. D. Pack, *Phys. Rev. B: Solid State*, 1976, **13**, 5188.
81 V. Soto-Verdugo and H. Metiu, *Surf. Sci.*, 2007, **601**, 5332.
82 J. Greeley and M. Mavrikakis, *Nat. Mater.*, 2004, **3**, 810.
83 (*a*) C. Kereszegi, J. D. Grunwaldt, T. Mallat and A. Baiker, *Chem. Commun.*, 2003, 2304; (*b*) C. Kereszegi, J. D. Grunwaldt, T. Mallat and A. Baiker, *J. Catal.*, 2004, **222**, 268.
84 A. D. Johnson, S. P. Daley, A. L. Utz and S. T. Ceyer, *Science*, 1992, **257**, 223.
85 G. C. Battiston, L. Dalloro and G. R. Tauszik, *Appl. Catal.*, 1982, **2**, 1.
86 M. García-Mota and N. López, *J. Am. Chem. Soc.*, 2008, **130**, 14406.

Part VI

Bibliography

UNIVERSITAT ROVIRA I VIRGILI
THEORETICAL STUDIES ON MOLECULAR ADSORPTION AND SELECTIVE HYDROGENATION CATALYSTS
Crisa Vargas Fuentes

Bibliography

[1] Chorkendorff, I.; Niemantsverdriet, J. W. *Concepts of Modern Catalysis And Kinetics*, Wiley-VCH, **2003**.

[2] Dahl, S.; Logadottir, A.; Egeberg, R. C.; Larsen, J. H.; Chorkendorff, I.; Tornqvist, E.; Nørskov, J. K. *Phys. Rev. Lett.* **1999** *83*, 1814.

[3] Gibbs, W. *On the Equilibrium of Heterogeneous Substances*, Transactions of the Connecticut Academy, III, **1878**.

[4] Wulff, G. *Zeitschrift Fur Krystallographie Und Mineralogie* **1901,** *34*, 449.

[5] Roosen, A. R.; McCormack, R. P.; Carter, W. C. *Comput. Mater. Sci.* **1998** *11*, 16.

[6] Dinghas, A. *Z. Kristall.* **1944** *105*, 304.

[7] Herring, C. *Phys. Rev.* **1951** *82*, 87.

[8] López, N.; Nørskov, J. K.; Janssens, T. V. W.; Carlsson, A.; Puig-Molina, A.; Clausen, B. S.; Grunwaldt, J. D. *J. Catal.* **2004** *225*, 86.

[9] Hansen, K. H.; Worren, T.; Stempel, S.; Laegsgaard, E.; Baumer, M.; Freund, H. J.; Besenbacher, F.; Stensgaard, I. *Phys. Rev. Lett.* **1999** *83*, 4120.

[10] Atkins, P.; de Paula, J. *Atkins' Physical Chemistry*, Oxford University Press, New York, **2006**.

[11] Błoński, P.; López, N. *J. Phys. Chem. C* **2012** *116*, 15484.

[12] Grimme, S.; Antony, J.; Ehrlich, S.; Krieg, H. *J. Chem. Phys.* **2010** *132*, 154104.

[13] Teschner, D.; Borsodi, J.; Wootsch, A.; Revay, Z.; Haevecker, M.; Knop-Gericke, A.; Jackson, S. D.; Schlögl, R. *Science* **2008** *320*, 86.

[14] Somorjai, G. A.; Borodko, Y. G. *Catal. Lett.* **2001** *76*, 1.

[15] Corma, A.; Serna, P. *Science* **2006** *313*, 332.

[16] Molnar, A.; Sarkany, A.; Varga, M. *J. Mol. Catal. A: Chem.* **2001** *173*, 185.

[17] García-Mota, M.; Gómez-Díaz, J.; Novell-Leruth, G.; Vargas-Fuentes, C.; Bellarosa, L.; Bridier, B.; Pérez-Ramírez, J.; López, N. *Theor. Chem. Acc.* **2011** *128*, 663.

[18] López, N.; Vargas-Fuentes, C. *Chem. Commun.* **2012** *48*, 1379.

[19] Tounge, B. A.; Pfahler, L. B.; Reynolds, C. H. *J. Chem. Inf. Comput. Sci.* **2002** *42*, 879.

[20] Stephens, I. E. L.; Bondarenko, A. S.; Gronbjerg, U.; Rossmeisl, J.; Chorkendorff, I. *Energy Environ. Sci.* **2012** *5*, 6744.

[21] Studt, F.; Abild-Pedersen, F.; Bligaard, T.; Sorensen, R. Z.; Christensen, C. H.; Nørskov, J. K. *Science* **2008** *320*, 1320.

[22] Abild-Pedersen, F.; Greeley, J.; Studt, F.; Rossmeisl, J.; Munter, T. R.; Moses, P. G.; Skulason, E.; Bligaard, T.; Nørskov, J. K. *Phys. Rev. Lett.* **2007** *99*, 1.

[23] Born, M.; Oppenheimer, R. *Ann. Phys.-Berlin* **1927** *84*, 0457.

[24] Dirac, P. A. M. *Proc. R. soc. Lond. Ser. A-Contain. Pap. Math. Phys. Character* **1928** *117*, 610.

[25] Teller, E. *Rev. Mod. Phys.* **1962** *34*, 627.

[26] Kohn, W.; Sham, L. J. *Phys. Rev.* **1965** *140*, 1133.

[27] Hohenberg, P.; Kohn, W. *Phys. Rev. B* **1964** *136*, B864.

[28] Perdew, J. P.; Schmidt, K. *AIP Conf. Proc.* **2001** *577*, 1.

[29] Haas, P.; Tran, F.; Blaha, P. *Phys. Rev. B* **2009** *79*, 8.

[30] Da Silva, J. L. F.; Stampfl, C.; Scheffler, M. *Phys. Rev. Lett.* **2003** *90*, 6.

[31] Darling, G. R.; Holloway, S. *Rep. Prog. Phys.* **1995** *58*, 1595.

[32] López, N.; Almora-Barrios, N.; Carchini, G.; Błoński, P.; Bellarosa, L.; García-Muelas, R.; Novell-Leruth, G.; García-Mota, M. *Catal. Sci. Technol.* **2012** *2*, 2405.

[33] Honkala, K.; Hellman, A.; Remediakis, I. N.; Logadottir, A.; Carlsson, A.; Dahl, S.; Christensen, C. H.; Nørskov, J. K. *Science* **2005** *307*, 555.

[34] Hafner, J. *J. Comput. Chem.* **2008** *29*, 2044.

[35] Godby, R. W.; Schluter, M.; Sham, L. J. *Phys. Rev. Lett.* **1986** *56*, 2415.

[36] Rinke, P.; Qteish, A.; Neugebauer, J.; Freysoldt, C.; Scheffler, M. *New J. Phys.* **2005** *7*, 126.

[37] Kelkkanen, A. K.; Lundqvist, B. I.; Nørskov, J. K. *J. Chem. Phys.* **2009** *131*, 4.

[38] Da Silva, J. L. F.; Ganduglia-Pirovano, M. V.; Sauer, J.; Bayer, V.; Kresse, G. *Phys. Rev. B* **2007** *75*, 4.

[39] Becke, A. D. *Phys. Rev. A* **1988** *38*, 3098.

[40] Perdew, J. P. *Phys. Rev. B* **1986** *33*, 8822.

[41] Perdew, J. P.; Chevary, J. A.; Vosko, S. H.; Jackson, K. A.; Pederson, M. R.; Singh, D. J.; Fiolhais, C. *Phys. Rev. B* **1992** *46*, 6671.

[42] Perdew, J. P.; Burke, K.; Ernzerhof, M. *Phys. Rev. Lett.* **1996** *77*, 3865.

[43] Hammer, B.; Hansen, L. B.; Nørskov, J. K. *Phys. Rev. B* **1999** *59*, 7413.

[44] Perdew, J. P.; Kurth, S.; Zupan, A.; Blaha, P. *Phys. Rev. Lett.* **1999** *82*, 2544.

[45] Becke, A. D. *J. Chem. Phys.* **1993** *98*, 5648.

[46] Stephens, P. J.; Devlin, F. J.; Chabalowski, C. F.; Frisch, M. J. *J. Phys. Chem.* **1994** *98*, 11623.

[47] Paier, J.; Hirschl, R.; Marsman, M.; Kresse, G. *J. Chem. Phys.* **2005** *122*, 23.

[48] Paier, J.; Marsman, M.; Kresse, G. *J. Chem. Phys.* **2007** *127*, 2.

[49] Tkatchenko, A.; Scheffler, M. *Phys. Rev. Lett.* **2009** *102*, 7.

[50] Bjorkman, T.; Gulans, A.; Krasheninnikov, A. V.; Nieminen, R. M. *J. Phys.: Condens. Matter* **2012** *24*, 424218.

[51] London, F. *Trans. Faraday Soc.* **1937** *33*, 8b.

[52] Dzyaloshinskii, I. E.; Lifshitz, E. M.; Pitaevskii, L. P. *Adv. Phys.* **1961** *10*, 165.

[53] Dobson, J. F.; Gould, T. *J. Phys.: Condens. Matter* **2012** *24*, 073201.

[54] Furche, F. *J. Chem. Phys.* **2008** *129*, 114105.

[55] Marini, A.; García-Gonzalez, P.; Rubio, A. *Phys. Rev. Lett.* **2006** *96*, 136404.

[56] Becke, A. D.; Johnson, E. R. *J. Chem. Phys.* **2005** *123*, 154101.

[57] Grimme, S. *J. Comput. Chem.* **2006** *27*, 1787.

[58] Vydrov, O. A.; Van Voorhis, T. *J. Chem. Phys.* **2010** *133*, 244103.

[59] Lee, K.; Murray, E. D.; Kong, L.; Lundqvist, B. I.; Langreth, D. C. *Phys. Rev. B* **2010** *82*, 081101.

[60] Dion, M.; Rydberg, H.; Schroder, E.; Langreth, D. C.; Lundqvist, B. I. *Phys. Rev. Lett.* **2004** *92*, 246401.

[61] Wu, X.; Vargas, M. C.; Nayak, S.; Lotrich, V.; Scoles, G. *J. Chem. Phys.* **2001** *115*, 8748.

[62] Silvestrelli, P. L. *Phys. Rev. Lett.* **2008** *100*, 5.

[63] Andersson, Y.; Rydberg, H. *Phys. Scr.* **1999** *60*, 211.

[64] Chu, X.; Dalgarno, A. *J. Chem. Phys.* **2004** *121*, 4083.

[65] Botti, S.; Castro, A.; Andrade, X.; Rubio, A.; Marques, M. A. L. *Phys. Rev. B* **2008** *78*, 3.

[66] Roman-Perez, G.; Soler, J. M. *Phys. Rev. Lett.* **2009** *103*, 096102.

[67] Klimeš, J.; Bowler, D. R.; Michaelides, A. *J. Phys.: Condens. Matter.* **2010** *22*, 074203.

[68] Ashcroft, N. W.; Mermin, N. D. *Solid State Physics* Science: Physics, Saunders College: **1976**.

[69] Mermin, N. D.; Ashcroft, N. W. *Int. J. Mod. Phys. B* **2006** *20*, 2227.

[70] Payne, M. C.; Teter, M. P.; Allan, D. C.; Arias, T. A.; Joannopoulos, J. D. *Rev. Mod. Phys.* **1992** *64*, 1045.

[71] Monkhorst, H. J.; Pack, J. D. *Phys. Rev. B* **1976** *13*, 5188.

[72] Setyawan, W.; Curtarolo, S. *Comput. Mater. Sci.* **2010** *49*, 299.

[73] Vonbarth, U.; Gelatt, C. D. *Phys. Rev. B* **1980** *21*, 2222.

[74] Phillips, J. C. *Phys. Rev.* **1968** *166*, 832.

[75] Blochl, P. E. *Phys. Rev. B* **1994** *50*, 17953.

[76] Kresse, G.; Joubert, D. *Phys. Rev. B* **1999** *59*, 1758.

[77] Hammer, B.; Morikawa, Y.; Nørskov, J. K. *Phys. Rev. Lett.* **1996** *76*, 2141.

[78] Loffreda, D. *Surf. Scien.* **2006** *600*, 2103.

[79] Mei, D.; Sheth, P. A.; Neurock, M.; Smith, C. M. *J. Catal.* **2006** *242*, 1.

[80] Mittendorfer, F.; Thomazeau, C.; Raybaud, P.; Toulhoat, H. *J. Phys. Chem. B* **2003** *107*, 12287.

[81] Sheppard, N.; Cruz, C. D. L. **1996** *41*, 1.

[82] Yeo, Y.; Stuck, A.; Wartnaby, C.; King, D. *Chem. Phys. Lett.* **1996** *259*, 28.

[83] Ge, Q.; King, D. A. *J. Chem. Phys.* **1999** *110*, 4699.

[84] Sautet, P.; Paul, J.-F. *Catal. Lett.* **1991** *9*, 245.

[85] Abon, M.; Billy, J.; Bertolini, J. *Surf. Sci.* **1986** *171*, L387.

[86] Tysoe, W.; Nyberg, G.; Lambert, R. *Surf. Sci.* **1983** *135*, 128.

[87] Steininger, H.; Ibach, H.; Lehwald, S. *Surf. Sci.* **1982** *117*, 685.

[88] Morgan, A. E.; Somorjai, G. A. *J. Chem. Phys.* **1969** *51*, 3309.

[89] Sheth, P. A.; Neurock, M.; Smith, C. M. *J. Phys. Chem. B* **2003** *107*, 2009.

[90] Sandell, A.; Beutler, A.; Jaworowski, A.; Wiklund, M.; Heister, K.; Nyholm, R.; Andersen, J. *Surf. Sci.* **1998** *415*, 411.

[91] Janssens, T. V. W.; Vlkening, S.; Zambelli, T.; Wintterlin, J. *J. Phys. Chem. B* **1998** *102*, 6521.

[92] Sheppard, N.; Cruz, C. D. L. **1998** *42*, 181.

[93] Dunphy, J. C.; Rose, M.; Behler, S.; Ogletree, D.; Salmeron, M.; Sautet, P. *Phys. Rev. B* **1998** *57*, 12705.

[94] Sellers, H. *J. Phys. Chem.* **1990** *94*, 8329.

[95] Mei, D.; Neurock, M.; Smith, C. M. *J. Catal.* **2009** *268*, 181.

[96] Davis, J. L.; Barteau, M. A. *J. Am. Chem. Soc.* **1989** *111*, 1782.

[97] Henderson, M. A.; Zhou, Y.; White, J. M. *J. Am. Chem. Soc.* **1989** *111*, 1185.

[98] Houtman, C.; Barteau, M. *J. Catal.* **1991** *130*, 528.

[99] Shekhar, R.; Barteau, M. A.; Plank, R. V.; Vohs, J. M. *J. Phys. Chem. B* **1997** *101*, 7939.

[100] Delbecq, F.; Sautet, P. *J. Catal.* **2002** *211*, 398.

[101] Jiang, R.; Guo, W.; Li, M.; Fu, D.; Shan, H. *J. Phys. Chem. C* **2009** *113*, 4188.

[102] Jiang, R.; Guo, W.; Li, M.; Lu, X.; Yuan, J.; Shan, H. *Phys. Chem. Chem. Phys.* **2010** *12*, 7794.

[103] Lin, S.; Ma, J.; Zhou, L.; Huang, C.; Xie, D.; Guo, H. *J. Phys. Chem. C* **2013** *117*, 451.

[104] Christmann, K.; Demuth, J. E. *J. Chem. Phys.* **1982** *76*, 6308.

[105] Ford, D. C.; Xu, Y.; Mavrikakis, M. *Surf. Sci.* **2005** *587*, 159.

[106] Somorjai, G. *Surf. Sci.* **1994** *299300*, 849.

[107] Bak, I.; Plinks, G. *Surf. Sci.* **2006** *600*, 3809.

[108] Karp, E. M.; Silbaugh, T. L.; Crowe, M. C.; Campbell, C. T. *J. Am. Chem. Soc.* **2012** *134*, 20388.

[109] Ma, Y.; Bansmann, J.; Diemant, T.; Behm, R. J. *Surf. Sci.* **2009** *603*, 1046.

[110] Mavrikakis, M.; Rempel, J.; Greeley, J.; Hansen, L. B.; Norskov, J. K. *J. Chem. Phys.* **2002** *117*, 6737.

[111] Ganduglia-Pirovano, M. V.; Scheffler, M. *Phys. Rev. B* **1999** *59*, 15533.

[112] Loffreda, D.; Simon, D.; Sautet, P. *J. Chem. Phys.* **1998** *108*, 6447.

[113] Wilke, S.; Natoli, V.; Cohen, M. H. *J. Chem. Phys.* **2000** *112*, 9986.

[114] Zhang, C.; Hu, P.; Lee, M.-H. *Surf. Sci.* **1999** *432*, 305.

[115] Choudhary, T.; Sivadinarayana, C.; Goodman, D. *Chem. Eng. J.* **2003** *93*, 69.

[116] Johnson, D. F.; Weinberg, W. H. *Science* **1993** *261*, 76.

[117] Cornish, J. C.; Avery, N. R. *Surf. Sci.* **1990** *235*, 209.

[118] Wgerbauer, C.; Maciejewski, M.; Baiker, A. *Appl. Catal. B-Environ.* **2001** *34*, 11.

[119] Krekelberg, W. P.; Greeley, J.; Mavrikakis, M. *J. Phys. Chem. B* **2004** *108*, 987.

[120] Li, X.; Lim, K. H. *ChemCatChem* **2012** *4*, 1311.

[121] Osinga, T.; Linsen, B.; van Beek, W. *J. Catal.* **1967** *7*, 277.

[122] Twigg, M. V.; Spencer, M. S. *Appl. Catal. A-Gen.* **2001** *212*, 161.

[123] Dulub, O.; Batzill, M.; Diebold, U. *Top. Catal.* **2005** *36*, 65.

[124] Geissler, K.; Newson, E.; Vogel, F.; Truong, T.-B.; Hottinger, P.; Wokaun, A. *Phys. Chem. Chem. Phys.* **2001** *3*, 289.

[125] Klier, K. *Academic Press* **1982** *31*, 243.

[126] Bernardo, C.; Gomes, J. *J. Mol. Struct.* **2002** *582*, 159.

[127] Bridier, B.; López, N.; Pérez-Ramírez, J. *J. Catal.* **2010** *269*, 80.

[128] Lim, K. H.; Chen, Z.-X.; Neyman, K. M.; Rsch, N. *J. Phys. Chem. B* **2006** *110*, 14890.

[129] Chen, Z.-X.; Neyman, K. M.; Lim, K. H.; Rsch, N. *Langmuir* **2004** *20*, 8068.

[130] Gomes, J.; Gomes, J.; Illas, F. *J. Mol. Catal. A-Chem.* **2001** *170*, 187.

[131] Foo, A.; Lim, K. *Catal. Lett.* **2009** *127*, 113.

[132] Sakong, S.; Mosch, C.; Gross, A. *Phys. Chem. Chem. Phys.* **2007** *9*, 2216.

[133] Sexton, A. J.; Rochelle, G. T. *Energy Procedia* **2009** *1*, 1179.

[134] Stuve, E.; Madix, R.; Sexton, B. *Surf. Sci.* **1982** *123*, 491.

[135] Fleck, L.; Ying, Z.; Feehery, M.; Dai, H. *Surf. Sci.* **1993** *296*, 400.

[136] Greeley, J.; Mavrikakis, M. *J. Catal.* **2002** *208*, 291.

[137] Bo, J.-Y.; Zhang, S.; Lim, K. *Catal. Lett.* **2009** *129*, 444.

[138] Yang, B.; Burch, R.; Hardacre, C.; Headdock, G.; Hu, P. *ACS Catal.* **2012** *2*, 1027.

[139] Bernardo, C.; Gomes, J. *J. Mol. Struct.* **2001** *542*, 263.

[140] Remediakis, I. N.; Abild-Pedersen, F.; Nrskov, J. K. *J. Phys. Chem. B* **2004** *108*, 14535.

[141] Oliva, C.; van den Berg, C.; Niemantsverdriet, J. H.; Curulla-Ferr, D. *J. Catal.* **2007** *245*, 436.

[142] Oliva, C.; van den Berg, C.; Niemantsverdriet, J. H.; Curulla-Ferr, D. *J. Catal.* **2007** *248*, 38.

[143] Lim, D. C.; Dietsche, R.; Gantefr, G.; Kim, Y. D. *Appl. Surf. Sci.* **2009** *256*, 1148.

[144] Chen, W.-K.; Liu, S.-H.; Cao, M.-J.; Yan, Q.-G.; Lu, C.-H. *J. Mol. Struct.* **2006** *770*, 87.

[145] Yu, Y.; Wang, X.; Lim, K. *Catal. Lett.* **2011** *141*, 1872.

[146] Kresse, G.; Hafner, J. *Phys. Rev. B* **1993** *47*, 558.

[147] Grimme, S. *J. Comput. Chem.* **2006** *27*, 1787.

[148] Klimes, J.; Bowler, D.; Michaelides, A. *Phys. Rev. B* **2011** *83*, 19.

[149] Vitos, L.; Ruban, A. V.; Skriver, H. L.; Kollar, J. *Surf. Sci.* **1998** *411*, 186.

[150] Kwon, S. K.; Nabi, Z.; Kadas, K.; Vitos, L.; Kollar, J.; Johansson, B.; Ahuja, R. *Phys. Rev. B* **2005** *72*, 23.

[151] Segura, Y.; López, N.; Pérez-Ramírez, J. *J. Catal.* **2007** *247*, 383.

[152] Atodiresei, N.; Caciuc, V.; Lazic, P.; Bluegel, S. *Phys. Rev. Lett.* **2009** *102*, 13.

[153] Mercurio, G.; McNellis, E. R.; Martin, I.; Hagen, S.; Leyssner, F.; Soubatch, S.; Meyer, J.; Wolf, M.; Tegeder, P.; Tautz, F. S.; Reuter, K. *Phys. Rev. Lett.* **2010** *104*, 3.

[154] Dzubiella, J.; Swanson, J.; McCammon, J. *Phys. Rev. Lett.* **2006** *96*, 8.

[155] Tkatchenko, A.; Romaner, L.; Hofmann, O. T.; Zojer, E.; Ambrosch-Draxl, C.; Scheffler, M. *MRS Bull.* **2010** *35*, 435.

[156] Dion, M.; Rydberg, H.; Schroder, E.; Langreth, D.; Lundqvist, B. *Phys. Rev. Lett.* **2005** *95*, 10.

[157] Hamada, I.; Lee, K.; Morikawa, Y. *Phys. Rev. B* **2010** *81*, 11.

[158] Poissier, A.; Ganeshan, S.; Fernandez-Serra, M. V. *Phys. Chem. Chem. Phys.* **2011** *13*, 3375.

[159] Hamada, I.; Otani, M. *Phys. Rev. B* **2010** *82*, 15.

[160] Harl, J.; Kresse, G. *Phys. Rev. Lett.* **2009** *103*, 5.

[161] Bucko, T.; Hafner, J.; Lebegue, S.; Angyan, J. G. *J. Phys. Chem. A* **2010** *114*, 11814.

[162] Ruiz, V. G.; Liu, W.; Zojer, E.; Scheffler, M.; Tkatchenko, A. *Phys. Rev. Lett.* **2012** *108*, 14.

[163] Zhang, G.-X.; Tkatchenko, A.; Paier, J.; Appel, H.; Scheffler, M. *Phys. Rev. Lett.* **2011** *107*, 24.

[164] Tonigold, K.; Gross, A. *J. Chem. Phys.* **2010** *132*, 22.

[165] Tonigold, K.; Gross, A. *J. Comput. Chem.* **2012** *33*, 695.

[166] Lifshitz, E. M. *Sov. Phys. JETP* **1956** *2*, 73.

[167] Zaremba, E.; Kohn, W. *Phys. Rev. B* **1976** *13*, 2270.

[168] Basaran, D.; Aleksandrov, H. A.; Chen, Z.-X.; Zhao, Z.-J.; Rsch, N. *J. Mol. Catal. A-Chem.* **2011** *344*, 37.

[169] Hirschl, R.; Eichler, A.; Hafner, J. *J. Catal.* **2004** *226*, 273.

[170] Desai, S. K.; Neurock, M.; Kourtakis, K. *J. Phys. Chem. B* **2002** *106*, 2559.

[171] Spiewak, B.; Cortright, R.; Dumesic, J. *J. Catal.* **1998** *176*, 405.

[172] Abbas, N. M.; Madix, R. J. *Appl. Surf. Sci.* **1981** *7*, 241.

[173] Lindlar, H. *Helv. Chim. Acta* **1952** *35*, 446.

[174] Lindlar, H.; Dubuis, R. *Org. Synth.: Coll.* **1973** *5*, 880.

[175] Mallat, T.; Baiker, A.; Patscheider, J. *Appl. Catal.* **1991** *79*, 59.

[176] Thomas, J. M.; Xian, K.; Stachurski, J. *J. Chem. Soc.-Chem. Commun.* **1988** *3*, 162.

[177] Massalski, T. B.; Okamoto, H. *Binary Alloy Phase Diagrams* Binary Alloy Phase Diagrams, A. S. M. International, Incorporated: **1990**.

[178] Chadwick, D.; Karolewski, M. A. *Surf. Sci.* **1983** *126*, 41.

[179] Aduriz, H. R.; Gigola, C. E.; Sica, A. M.; Volpe, M. A.; Touroude, R. *Catal. Today* **1992** *15*, 459.

[180] Aduriz, H. R.; Bodnariuk, P.; Coq, B.; Figueras, F. *J. Catal.* **1991** *129*, 47.

[181] Fernandez, M. B.; Piqueras, C. M.; Tonetto, G. M.; Crapiste, G.; Damiani, D. E. *J. Mol. Catal. A-Chem.* **2005** *233*, 133.

[182] Palczewska, W.; Szymerska, I.; Ratajczykowa, I.; Lipski, M. *In: Proc ECOSS-3 and ICCS-4*, Cannes, **1980**.

[183] Liu, G.; Davis, K. A.; Meier, D. C.; Bagus, P. S.; Goodman, D. W.; Zajac, G. W. *Phys. Rev. B* **2003** *68*, 3.

[184] Szabo, S. *Int. Rev. Phys. Chem.* **1991** *10*, 207.

[185] Mallat, T.; Baiker, A. *Top. Catal.* **1999** *8*, 115.

[186] Mcewen, A. B.; Guttieri, M. J.; Maier, W. F.; Laine, R. M.; Shvo, Y. *J. Org. Chem.* **1983** *48*, 4436.

[187] Goetz, J.; Volpe, M. A.; Gigola, C. E.; Touroude, R. *J. Catal.* **2001** *199*, 338.

[188] Goetz, J.; Volpe, M. A.; Sica, A. M.; Gigola, C. E.; Touroude, R. *J. Catal.* **1997** *167*, 314.

[189] Mallat, T.; Baiker, A. *Appl. Catal. A-Gen.* **2000** *200*, 3.

[190] Maier, W. F.; Chettle, S. J.; Rai, R. S.; Thomas, G. *J. Am. Chem. Soc.* **1986** *108*, 2608.

[191] Yu, J. Q.; Spencer, J. B. *Chem. Commun.* **1998** *10*, 1103.

[192] García-Mota, M.; Bridier, B.; Pérez-Ramírez, J.; López, N. *J. Catal.* **2010** *273*, 92.

[193] Bridier, B.; Pérez-Ramírez, J. *J. Am. Chem. Soc.* **2010** *132*, 4321.

[194] García-Mota, M.; Cabello, N.; Maseras, F.; Echavarren, A. M.; Pérez-Ramírez, J.; López, N. *ChemPhysChem* **2008** *9*, 1624.

[195] Mitsui, T.; Rose, M. K.; Fomin, E.; Ogletree, D. F.; Salmeron, M. *Nature* **2003** *422*, 705.

[196] Bond, G. C. *Chem. Soc. Rev.* **1991** *20*, 441.

[197] Bond, G. C. *Acc. Chem. Res.* **1993** *26*, 490.

[198] Smale, M. W.; King, T. S. *J. Catal.* **1990** *125*, 335.

[199] Sachtler, W. M. H. *Catal. Rev.-Sci. Eng.* **1976** *14*, 193.

[200] Tao, F.; Grass, M. E.; Zhang, Y.; Butcher, D. R.; Aksoy, F.; Aloni, S.; Altoe, V.; Alayoglu, S.; Renzas, J. R.; Tsung, C.-K.; Zhu, Z.; Liu, Z.; Salmeron, M.; Somorjai, G. A. *J. Am. Chem. Soc.* **2010** *132*, 8697.

[201] Christoffersen, E.; Stoltze, P.; Nørskov, J. K. *Surf. Sci.* **2002** *505*, 200.

[202] Andersson, K. J.; Calle-Vallejo, F.; Rossmeisl, J.; Chorkendorff, L. *J. Am. Chem. Soc.* **2009** *131*, 2404.

[203] Greeley, J.; Mavrikakis, M. *J. Phys. Chem. B* **2005** *109*, 3460.

[204] Nilekar, A. U.; Ruban, A. V.; Mavrikakis, M. *Surf. Sci.* **2009** *603*, 91.

[205] Greeley, J.; Krekelberg, W. R.; Mavrikakis, M. *Angew. Chem.-Int. Edit.* **2004** *43*, 4296.

[206] Frevel, L. K.; Kressley, L. J. *Selective Hydrogenation Of Acetylene In Ethylene And Catalyst Therefor* 2802889 **1957**.

[207] Voight, R. W.; Meriam, J. S.; Blankenship, S. A., AIChE, New Orleans, Session 19, **1996**.

[208] Didillion, B.; Sarrazin, P.; Boitiaux, J. P., AIChE, Houston, Session 43, **1995**.

[209] Boitiaux, J. P.; Cosyns, J.; Derrien, M.; Léger, G. *Hydrocarb. Process.* **1985** *64*, 51.

[210] Kaiser, V.; Laugier, J. P.; DiCinto, R.; Picciotti, M., AIChE, Houston, Session 68, **1999**.

[211] Sughrue, E.; Johnson, M., AIChE, Houston, Session 18, **1993**.

[212] Tiedke, D. B.; Cheung, T. T. P.; J., L.; Zisman, S. A.; Bergmeister, J. J.; A., D. G., AIChE, Houston, Session 80, **2001**.

[213] Chae, K. H.; Jung, S. M.; Lee, Y. S.; Whang, C. N.; Jeon, Y.; Croft, M.; Sills, D.; Ansari, P. H.; Mack, K. *Phys. Rev. B* **1996** *53*, 10328.

[214] Sales, E. A.; Benhamida, B.; Caizergues, V.; Lagier, J. P.; Fievet, F.; Bozon-Verduraz, F. *Appl. Catal. A-Gen.* **1998** *172*, 273.

[215] Ruban, A. V.; Skriver, H. L.; Nørskov, J. K. *Phys. Rev. B* **1999** *59*, 15990.

[216] Bond, G. C.; Rawle, A. F. *J. Mol. Catal. A-Chem.* **1996** *109*, 261.

[217] Khan, N. A.; Shaikhutdinov, S.; Freund, H. J. *Catal. Lett.* **2006** *108*, 159.

[218] Pachulski, A.; Schoedel, R.; Claus, P. *Appl. Catal. A-Gen.* **2011** *400*, 14.

[219] Jin, Y. M.; Datye, A. K.; Rightor, E.; Gulotty, R.; Waterman, W.; Smith, M.; Holbrook, M.; Maj, J.; Blackson, J. *J. Catal.* **2001** *203*, 292.

[220] Tiruppathi, P.; Low, J. J.; Chan, A. S. Y.; Bare, S. R.; Meyer, R. J. *Catal. Today* **2011** *165*, 106.

[221] López, N.; Nørskov, J. K. *Surf. Sci.* **2001** *477*, 59.

[222] Sitthisa, S.; Trung, P.; Prasomsri, T.; Sooknoi, T.; Mallinson, R. G.; Resasco, D. E. *J. Catal.* **2011** *280*, 17.

[223] Baber, A. E.; Tierney, H. L.; Lawton, T. J.; Sykes, E. C. H. *ChemCatChem* **2011** *3*, 607.

[224] Leviness, S.; Nair, V.; Weiss, A. H.; Schay, Z.; Guczi, L. *J. Mol. Catal.* **1984** *25*, 131.

[225] Maroun, F.; Ozanam, F.; Magnussen, O. M.; Behm, R. J. *Science* **2001** *293*, 1811.

[226] Kumar, D.; Chen, M. S.; Goodman, D. W. *Catal. Today* **2007** *123*, 77.

[227] Li, Z.; Gao, F.; Wang, Y.; Calaza, F.; Burkholder, L.; Tysoe, W. T. *Surf. Sci.* **2007** *601*, 1898.

[228] Li, Z.; Furlong, O.; Calaza, F.; Burkholder, L.; Poon, H. C.; Saldin, D.; Tysoe, W. T. *Surf. Sci.* **2008** *602*, 1084.

[229] Luo, K.; Wei, T.; Yi, C. W.; Axnanda, S.; Goodman, A. W. *J. Phys. Chem. B* **2005** *109*, 23517.

[230] Wei, T.; Wang, J.; Goodman, D. W. *J. Phys. Chem. C* **2007** *111*, 8781.

[231] Han, P.; Axnanda, S.; Lyubinetsky, I.; Goodman, D. W. *J. Am. Chem. Soc.* **2007** *129*, 14355.

[232] Gao, F.; Wang, Y.; Goodman, D. W. *J. Phys. Chem. C* **2009** *113*, 14993.

[233] Boscoboinik, J. A.; Plaisance, C.; Neurock, M.; Tysoe, W. T. *Phys. Rev. B* **2008** *77*, 045422.

[234] Boscoboinik, J. A.; Calaza, F. C.; Garvey, M. T.; Tysoe, W. T. *J. Phys. Chem. C* **2010** *114*, 1875.

[235] García-Mota, M.; López, N. *Phys. Rev. B* **2010** *82*, 7.

[236] Miura, H.; Terasaka, M.; Oki, K.; Matsuda, T. *Stud. Surf. Sci. Catal.* **1993** *75*, 2379.

[237] Sarkany, A.; Horvath, A.; Beck, A. *Appl. Catal. A-Gen.* **2002** *229*, 117.

[238] Sarkany, A.; Geszti, O.; Safran, G. *Appl. Catal. A-Gen.* **2008** *350*, 157.

[239] Choudhary, T. V.; Sivadinarayana, C.; Datye, A. K.; Kumar, D.; Goodman, D. W. *Catal. Lett.* **2003** *86*, 1.

[240] Hugon, A.; Delannoy, L.; Krafft, J.-M.; Louis, C. *J. Phys. Chem. C* **2010** *114*, 10823.

[241] Di Vece, M.; Bals, S.; Verbeeck, J.; Lievens, P.; Van Tendeloo, G. *Phys. Rev. B* **2009** *80*, 12.

[242] Gross, E.; Asscher, M. *Langmuir* **2010** *26*, 16226.

[243] Rodriguez, J. A. *J. Phys. Chem.* **1994** *98*, 5758.

[244] Tew, M. W.; Emerich, H.; van Bokhoven, J. A. *J. Phys. Chem. C* **2011** *115*, 8457.

[245] Sarkany, A.; Zsoldos, Z.; Furlong, B.; Hightower, J. W.; Guczi, L. *J. Catal.* **1993** *141*, 566.

[246] Wehner, P. S.; Gustafson, B. L. *J. Catal.* **1992** *135*, 420.

[247] Armbruester, M.; Wowsnick, G.; Friedrich, M.; Heggen, M.; Cardoso-Gil, R. *J. Am. Chem. Soc.* **2011** *133*, 9112.

[248] Ota, A.; Armbruester, M.; Behrens, M.; Rosenthal, D.; Friedrich, M.; Kasatkin, I.; Girgsdies, F.; Zhang, W.; Wagner, R.; Schlögl, R. *J. Phys. Chem. C* **2011** *115*, 1368.

[249] Armbruester, M.; Kovnir, K.; Behrens, M.; Teschner, D.; Grin, Y.; Schlögl, R. *J. Am. Chem. Soc.* **2010** *132*, 14745.

[250] Osswald, J.; Kovnir, K.; Armbruester, M.; Giedigleit, R.; Jentoft, R. E.; Wild, U.; Grin, Y.; Schlögl, R. *J. Catal.* **2008** *258*, 219.

[251] Armbruester, M.; Behrens, M.; Cinquini, F.; Foettinger, K.; Grin, Y.; Haghofer, A.; Kloetzer, B.; Knop-Gericke, A.; Lorenz, H.; Ota, A.; Penner, S.; Prinz, J.; Rameshan, C.; Revay, Z.; Rosenthal, D.; Rupprechter, N.; Sautet, P.; Schlögl, R.; Shao, L.; Szentmiklosi, L.; Teschner, D.; Torres, D.; Wagner, R.; Widmer, R.; Wowsnick, G. *ChemCatChem* **2012** *4*, 1048.

[252] Armbruester, M.; Borrmann, H.; Wedel, M.; Prots, Y.; Giedigkeit, R.; Gille, P. *Z. Krist.-New Cryst. Struct.* **2010** *225*, 617.

[253] Kovnir, K.; Schmidt, M.; Waurisch, C.; Armbruester, M.; Prots, Y.; Grin, Y. *Z. Krist.-New Cryst. Struct.* **2008** *223*, 7.

[254] Pattamakomsan, K.; Ehret, E.; Morfin, F.; Gelin, P.; Jugnet, Y.; Prakash, S.; Bertolini, J. C.; Panpranot, J.; Aires, F. J. C. S. *Catal. Today* **2011** *164*, 28.

[255] Choi, S. H.; Lee, J. S. *J. Catal.* **2000** *193*, 176.

[256] Breinlich, C.; Haubrich, J.; Becker, C.; Valcarcel, A.; Delbecq, F.; Wandelt, K. *J. Catal.* **2007** *251*, 123.

[257] Verdier, S.; Didillon, B.; Morin, S.; Uzio, D. *J. Catal.* **2003** *218*, 288.

[258] Sales, E. A.; Mendes, M. D.; Bozon-Verduraz, F. *J. Catal.* **2000** *195*, 96.

[259] Masai, M.; Honda, K.; Kubota, A.; Oohnaka, S.; Nishikawa, Y.; Nakahara, K.; Kishi, K.; Ikeda, S. *J. Catal.* **1977** *50*, 419.

[260] Hamm, G.; Schmidt, T.; Breitbach, J.; Franke, D.; Becker, C.; Wandelt, K. *Z. Phys. Chemie-Int. J. Res. Phys. Chem. Chem. Phys.* **2009** *223*, 209.

[261] Keresszegi, C.; Grunwaldt, J. D.; Mallat, T.; Baiker, A. *Chem. Commun.* **2003** *18*, 2304.

[262] Keresszegi, C.; Grunwaldt, J. D.; Mallat, T.; Baiker, A. *J. Catal.* **2004** *222*, 268.

[263] Kimura, H.; Kimura, A.; Kokubo, I.; Wakisaka, T.; Mitsuda, Y. *Appl. Catal. A-Gen.* **1993** *95*, 143.

[264] Sa, J.; Montero, J.; Duncan, E.; Anderson, J. A. *Appl. Catal. B-Environ.* **2007** *73*, 98.

[265] Anderson, J. A.; Mellor, J.; Wells, R. P. K. *J. Catal.* **2009** *261*, 208.

[266] Karski, S. *J. Mol. Catal. A-Chem.* **2006** *253*, 147.

[267] Soto-Verdugo, V.; Metiu, H. *Surf. Sci.* **2007** *601*, 5332.

[268] Albers, P. W.; Moebus, K.; Frost, C. D.; Parker, S. F. *J. Phys. Chem. C* **2011** *115*, 24485.

[269] Ulan, J. G.; Maier, W. F.; Smith, D. A. *J. Org. Chem.* **1987** *52*, 3132.

[270] Schlögl, R.; Noack, K.; Zbinden, H.; Reller, A. *Helv. Chim. Acta* **1987** *70*, 627.

[271] Ivanova, A. S.; Slavinskaya, E. M.; Gulyaev, R. V.; Zaikovskii, V. I.; Stonkus, O. A.; Danilova, I. G.; Plyasova, L. M.; Polukhina, I. A.; Boronin, A. I. *Appl. Catal. B-Environ.* **2010** *97*, 57.

[272] Greenwood, N. N.; Earnshaw, A. *Chemistry of the Elements, and references therein*, Elsevier Science & Technology Books, 2nd ed. **2008**.

[273] Knapton, A. G. *Platinum Met. Rev.* **1977** *21*, 44.

[274] Andersin, J.; López, N.; Honkala, K. *J. Phys. Chem. C* **2009** *113*, 8278.

[275] Andersin, J.; Honkala, K. *Surf. Sci.* **2010** *604*, 762.

[276] Nykanen, L.; Andersin, J.; Honkala, K. *Phys. Rev. B* **2010** *81*, 7.

[277] Seriani, N.; Mittendorfer, F.; Kresse, G. *J. Chem. Phys.* **2010** *132*, 2.

[278] Bond, G. C. *Metal-catalysed Reactions of Hydrocarbons* Fundamental and applied catalysis, Springer Science & Business Media, Incorporated **2005**.

[279] López, N.; Lodziana, Z.; Illas, F.; Salmeron, M. *Phys. Rev. Lett.* **2004** *93*, 14.

[280] Palczewska, I.; Ratajczykowa, W.; Szymerska, I.; Krawczyk, M. *In: Proceedings of the 8th International Congress on Catalysis* vol. 4, Berlin, **1984**.

[281] Brunauer, S.; Emmett, P. H.; Teller, E. *J. Am. Chem. Soc.* **1938** *60*, 309.

[282] Santarossa, G.; Iannuzzi, M.; Vargas, A.; Baiker, A. *ChemPhysChem* **2008** *9*, 401.

[283] Ulan, G. J.; Kuo, E.; Maier, W. F.; Rai, R. S.; Thomas, G. *J. Org. Chem.* **1986** *52*, 3126.

[284] Chen, M. S.; Kumar, D.; Yi, C. W.; Goodman, D. W. *Science* **2005** *310*, 291.

[285] García-Mota, M.; López, N. *J. Am. Chem. Soc.* **2008** *130*, 14406.

[286] Jia, J. F.; Haraki, K.; Kondo, J. N.; Domen, K.; Tamaru, K. *J. Phys. Chem. B* **2000** *104*, 11153.

[287] Studt, F.; Abild-Pedersen, F.; Bligaard, T.; Sorensen, R. Z.; Christensen, C. H.; Nørskov, J. K. *Angew. Chem.-Int. Edit.* **2008** *47*, 9299.